Microbial Methane Production in Oxic Lake Waters

Marco Günthel, M.Sci

Submitted to Swansea University in fulfilment of the requirements for the Degree of “Doctor of Philosophy”

Swansea University

September 2019

Summary

Microbial methane production is commonly believed to be an exclusively anaerobic process performed by methanogenic Archaea, but the recent discovery of methane production in oxygenated waters challenges this paradigm and demands re-assessments of the global methane cycle. There are important questions regarding this newly recognized methane source: What are the environmental controls? Who are the responsible organisms? What are the underlying pathways? Is this phenomenon of global relevance?

This thesis shows that oxic methane production was a recurring phenomenon in the seasonally stratified oxic water column of Lake Stechlin. Sunlight exposure and phosphorus limitation promoted oxic-water methane accumulations in situ. Bacteria (Cyanobacteria) and Algae (Diatoms, Green Algae, Cryptophytes) produced methane from ^{13}C-labelled bicarbonate in incubation experiments, indicating that oxic methane production was associated with autotrophic carbon fixation. Further, correlations between water column methane concentrations and phytoplankton pigments were observed on the diurnal and seasonal scales. Together, these findings suggest that oxic methane production is a common feature of phytoplankton and likely relevant for limnic systems in general. Balancing the system-wide methane sources and sinks of Lake Stechlin's surface mixed layer shows the oxic methane source was a substantial contributor to atmospheric methane emission with pronounced short-term dynamics. In addition, empirical modelling based on results presented here and available literature data reveals that oxic methane production in lake waters has global implications: The oxic methane source is predicted to be the primary source of atmospheric methane emission from the mid-water column in lakes larger than 1 km^2.

Furthermore, the explanatory power of the widely used wind-based models for estimating water-to-air gas emission was much improved by incorporating water- and air temperatures as additional proxy parameters.

This thesis shows that oxic methane production is important to lake methane cycling, and global assessments like the upcoming IPCC report should acknowledge the oxic methane source.

Declaration & Statements

Declaration. This work has not previously been accepted in substance for any degree and is not being concurrently submitted in candidature for any degree.

Signed ..... (candidate)

Date .....

Statement 1. This thesis is the result of my own investigations, except where otherwise stated. Where correction services have been used, the extent and nature of the correction are clearly marked.

Other sources are acknowledged by giving explicit references. A bibliography is appended.

Signed ..... (candidate)

Date .....

Statement 2. I hereby give consent for my thesis, if accepted, to be available for photocopying and for inter-library loan, and for the title and summary to be made available to outside organisations.

Signed ..... (candidate)

Date .....

Table of Contents

Acknowledgements

The studies leading to this thesis were supported by several people with various backgrounds engaging with critical scientific discussions, providing technical equipment or human resources, giving access to data, or providing a friendly and motivating working environment.

Particularly Prof Kam W. Tang at the Swansea University is acknowledged for supervising this thesis. He provided not only important scientific and administrative care but also gave valuable ethical guidance for becoming an appreciated member of the scientific and academic community.

Further, Prof Hans-Peter Grossart, his research group 'Experimental Limnology' as well as the lake lab and technician team (Uta Mallok, Armin Penske, Michael Sachtleben) and Dr Peter Casper and his research group at the Leibniz Institute for Freshwater Ecology and Inland Fishery in Germany, are acknowledged for close collaboration and valuable scientific/technical input. Likewise, Prof Daniel F. McGinnis and his group members in the Aquatic Physics Group at the University of Geneva, are acknowledged for sharing their professional expertise and close collaboration.

Anke Penzlin and Marcus Wallasch at the German Federal Office for Environment are acknowledged for giving access to weather data recorded by the Neuglobsow weather station.

"I am grateful that I had the opportunity to become a part of a large network of scientists with different backgrounds participating in interdisciplinary debates and stimulating new ideas and each other's work. The nice working environment created by my colleagues – many of them being friends now – was a daily motivation for my work."

– The Author –

Financial support was provided by a Swansea University postgraduate research studentship.

List of Figures

List of Tables

Symbols & Abbreviations

Symbol	Unit	Description
α	[ ]	Carbon isotope fractionation factor
a	[%]	Regression constant
A_{global}	[m^2]	Earth's total lake surface area
A_{class}, A_{mean}	[m^2]	Lake size class area; class refers to the range of the lake size class (max/min) and mean refers to the mean of the max/min size of a lake size class
A_p	[m^2]	Planar area
A_{sed}	[m^2]	(littoral) sediment area
A_{th}	[m^2]	Thermocline area (planar)
A_{tot}	[m^2]	Lake surface area
β	[s^{-1}]	Buoyancy frequency
b	[km^2]	Regression constant
C_C, C_R	[mol m^{-3}]	Concentration in outflowing (R) or inflowing (C) water
^{13}C atom% excess	[%]	Increasing enrichment of ^{13}C during reaction
^{13}C atom% (t_0)	[%]	Percentage ^{13}C in the sample at time point 0
^{13}C atom% (t_n)	[%]	Percentage ^{13}C in the sample at time point n
C_{DIC}, $C_{CH4,\ total}$	[mol m^{-3}]	Overall concentration of the dissolved inorganic carbon or methane pool
CH_4 Oxidation, MOx	[mol m^{-3} s^{-1}]	Consumption of methane
CH_4 Production	[mol m^{-3} s^{-1}]	Production of methane
$CH4_{\ substrate\ label}$	[%]	Abundance of ^{13}C-isotopologue in the methane pool
conc	[mol m^{-3}]	Concentration
$DIC_{\ substrate\ label}$	[%]	Abundance of ^{13}C-isotopologue in the dissolved inorganic carbon pool
ε	[m^2 s^{-3}]	Turbulence, TKE dissipation
$\delta^{13}C$	[‰]	Carbon isotope signature relative to Vienna-PeeDee-Belemnite
D_{CH4}	[m^2 s^{-1}]	Diffusion coefficient of methane in water
fetch	[m]	Wind fetch
F_{eb}	[mol m^{-2} s^{-1}]	Ebullitive methane flux
F_L	[mol m^{-2} s^{-1}]	Littoral methane flux at the sediment-water interface
F_R	[mol m^{-2} s^{-1}]	Methane flux from river into lake
F_S, F_{CH4}	[mol m^{-2} s^{-1}]	Surface methane emission (water-to-air flux)
F_z	[mol m^{-2} s^{-1}]	Depth-dependent turbulent diffusive methane flux
γ, γ_{class}, γ_{global}	[%]	Contribution to a lake size class (class) or to the global lake inventory (global)
k, k_{CH4}, k_{600}	[m s^{-1}]	Gas transfer constant; indices CH4 and 600 refer to methane at ambient temperature or carbon at 20°C
K_z	[m^2 s^{-1}]	Depth-dependent basin-scale diffusivities

λ	[radians]	longitude
μ		Mean value
m	[cm s h^{-1} m^{-1}]	Regression constant
m/z	[ ]	Mass/charge ration
ν	[m^2 s^{-1}]	Kinematic viscosity
n	[cm h^{-1}]	Regression constant
nat.^{13}C ratio	[ ]	Ratio of naturally occurring ^{13}C in the sample
n_{CH4}	[ ]	Methane mole fraction
N_1, N_2	[g]	Biomass, 1 and 2 denote initial and final time point
OMC, OMC_{class}, OMC_{global}	[%]	Contribution of the oxic methane source to surface emission, indices class and global refer to a lake size class of earth's lake inventory, or global lake size area
φ	[radians]	Latitude
Φ	[ ]	Porosity
P_{net}	[mol m^{-3} s^{-1}]	Methane production rate
q	[ ]	Dimensionless conversion factor for transforming different gas transfer constants into each other (e.g. k_{600}, k_{CH4}); c = -2/3 at wind speed <3.7 m s^{-1}, c = -1/2 at wind speed >3.7 m s^{-1}
Q, Q_C, Q_R	[m^3 s^{-1}]	Flow rate, C and R denote out-/inflow
ρ	[bar]	Pressure
rad_{earth}	[km]	Earth's radius
R	[kg m^2 s^{-2} mol^{-1} K^{-1}]	Gas constant
Ra	[km]	Equivalence radius
σ		Standard deviation (SD)
Sc, Sc_{CH4}	[ ]	Schmidt number, CH4 refers to methane at ambient temperature
t, t_0, t_n	[s]	Time; 0 and n refer to starting and end time
θ	[ ]	Tortuosity
T, T_{air}, T_{SW}	[°C]	Temperature; indices air and SW refer to atmospheric temperature and temperature of surface water
TP	[µg l^{-1}]	Total phosphorus
U, U_{10}	[m s^{-1}]	Wind speed, 10 denotes the height in [m] above surface
V	[m^3]	Surface mixed layer volume
V	[m^3]	Volume
x_{CH4}	[ ]	Methane mixing ratio
Y	[g s^{-1}]	Biomass yield rate
z, z_{SML}	[m]	Depth; SML symbolizes surface mixed layer

ADCP	Acoustic doppler currency profiler
CF-IRMS	Continuous-flow isotope ratio mass spectrometry
conc	Concentration
CR	Central reservoir
DIC, $DI^{13}C$	Dissolved inorganic carbon, 13 denotes DIC carrying the heavy carbon isotope ^{13}C
E1, E13	Experimental enclosure 1 or 13
GC	Gas chromatography
GC/FID	Gas chromatography/Flame ionisation detector
GC-IRMS	Gas chromatography Isotope ratio mass spectrometry
GLM	General linear model
LM	Linear model
MIMS	Membrane inlet mass spectrometry
NE	Northeast basin
PAR	Photo active radiation
S	South basin
SD	Standard deviation
SE	Standard error
SML	Surface mixed layer (epilimnion)
SRP	Soluble reactive phosphorus

Chapter 1: Introduction

1.1 Methane Cycling

After carbon dioxide, methane is the second most important carbon-based greenhouse gas with a global warming potential 25-28 times that of carbon dioxide (Myhre et al. 2013, IPCC 2014, Allen et al. 2018). Methane cycling connects the organic and inorganic carbon pool (Figure 1.1) (Falkowski et al. 2008, Dean et al. 2018) and, accordingly, is an important part of the global carbon cycle, forming a bridge between the atmosphere, hydrosphere, terrestrial biosphere and geosphere.

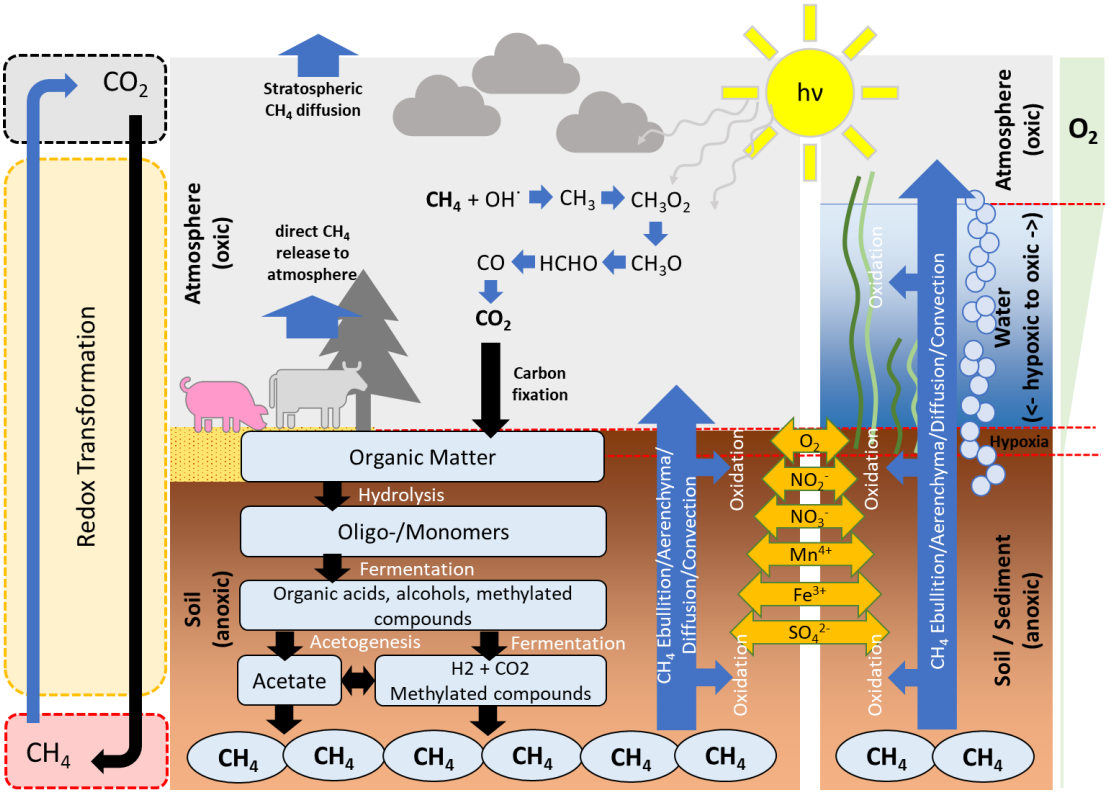

Figure 1.1: Methane cycling. *Atmospheric carbon dioxide is fixed by autotrophic organisms and incorporated into organic matter (oxic environment). Organic matter is transformed into carbon dioxide and methane by a multistep transformation cascade involving Bacteria and methanogenic Archaea (anoxic environment). Alternatively, the methane pool can originate from thermogenic or pyrogenic sources. Methane oxidation in anoxic and oxic zones convert methane back to carbon dioxide closing the methane cycle. Physical transport processes enable carbon dioxide, methane and intermediate meta- and catabolites to migrate between the oxic and anoxic environments. The figure was created based on Monks (2003), Conrad (2009) and Dean et al. (2018).*

Methane sources can be of biogenic, thermogenic or pyrogenic nature (Kirschke et al. 2013, Saunois et al. 2016a): Atmospheric carbon dioxide is fixed via biochemical processes into organic matter, which is subsequently decomposed to (biogenic) methane.

Thermogenic methane is the result of organic matter being exposed to intense heat and pressure in the earth's crust over millions of years. And, pyrogenic methane is produced during incomplete combustion of biomass/soil carbon/bio-/fossil fuels. Methane sinks, on the other hand, are methanotrophic organisms transforming methane enzymatically, and atmospheric radical photochemistry both converting methane back into carbon dioxide. Meanwhile, physical transport processes allow methane, carbon dioxide and intermediate compounds to cycle between the anoxic and oxic environments (Figure 1.1).

Accurate quantification of global methane production and consumption is important for i) accounting for its role in the carbon cycle, ii) understanding climate feedbacks, iii) examining ecological interrelationships and iv) predicting future climate change scenarios (Dean et al. 2018). Many environments emit methane to the atmosphere, such as wetlands (e.g. swamps, mangroves), waterbodies (marine, freshwater systems), permafrost (e.g. boreal, alpine, arctic zones), animal intestines (e.g. termites, wild animals), farm lands (e.g. grazing pastures, rice paddies) as well as bio- and fossil fuel combustion sites (Kirschke et al. 2013, Saunois et al. 2016a, Dean et al. 2018). The clathrate-bound methane pool (methane stabilized in water cages under high pressure) is an additional geological source that can leak into the atmosphere (Buffett and Archer 2004, Hester and Brewer 2009). Natural and anthropogenic sources of atmospheric methane emission are each estimated to cause about half of the global methane emission (Figure 1.2) (Saunois et al. 2016a). Wetlands and freshwaters dominate the natural methane emission (Bousquet et al. 2006, Kirschke et al. 2013, Saunois et al. 2016a). On the side of the anthropogenic emission, enteric fermentation, usage of fertilizer/gas/oil and industrial activities are the main sources (Kirschke et al. 2013, Saunois et al. 2016a). Combined, the natural and anthropogenic methane emission exceed the sinks (tropospheric photochemistry, stratospheric loss, soil storage) by ca. 10 Tg yr^{-1} leading to a continuous increase of the atmospheric methane content (Saunois et al. 2016a). The radiative forcing associated with atmospheric methane subsequently promotes global warming (IPCC 2007, IPCC 2014).

Assessments of the global methane budget are marred by high uncertainties as indicated by bottom-up and top-down budgets not matching each other (Figure 1.2; Kirschke et al. 2013, Saunois et al. 2016a). Freshwater systems estimations have the proportionally highest uncertainty (error bars in Figure 1.2) due to highly variable methane density fluxes within and across systems (Cole et al. 2007, Natchimuthu et al.

2015, Wik et al. 2016a, Sabrekov et al. 2017, Xiao et al. 2017), uncertain estimation of global freshwater system surface areas (Allen and Pavelsky 2016, Thornton et al. 2016) and the lack of long-term data (Saunois et al. 2016). To improve global assessments, a better understanding of methane production, consumption and transport processes is needed. In the light of the large contribution of freshwater systems to the global methane emission, this thesis is focussing on lake systems.

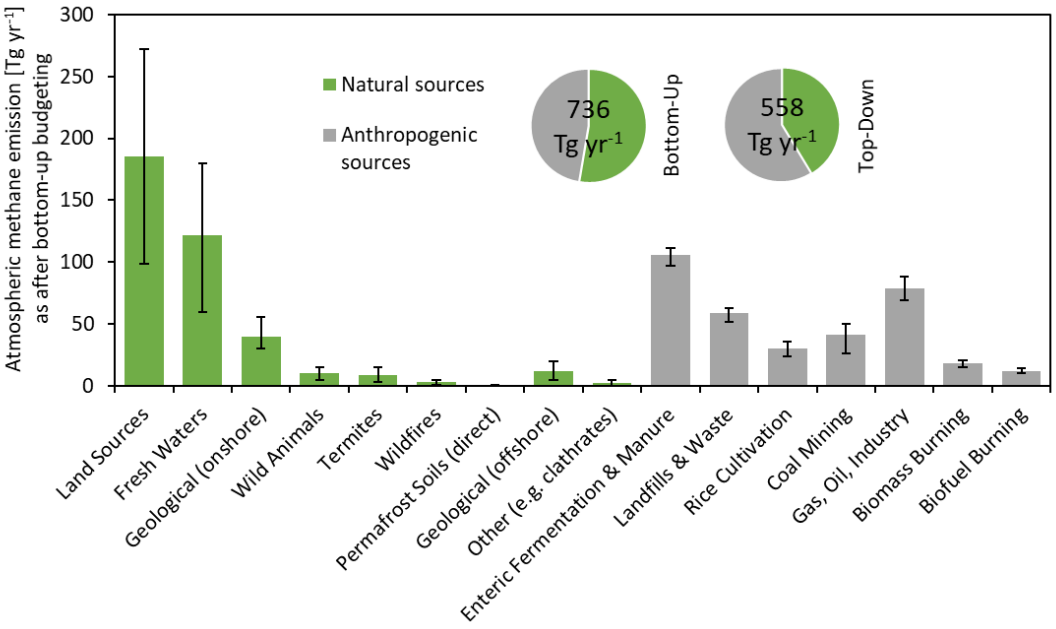

Figure 1.2: Sources of atmospheric methane emission 2003-2012. *Bottom-Up budgets account for methane density fluxes from individual source-sink nexuses. Top-Down budgets are generally seen to be more precise as they are based on the atmospheric burden. The total atmospheric methane input varies between both budgeting types (736 Tg yr^{-1} in Bottom-Up budget versus 558 Tg yr^{-1} in Top-Down budget). Nevertheless, natural and anthropogenic sources each contribute approximately half to the total atmospheric methane emission. Estimations of natural emissions are connected to large uncertainties; freshwater emission has proportionally the highest uncertainty (Kirschke et al. 2013, Saunois et al. 2016a). Error bars indicate a minimum-maximum uncertainty range. Data were taken from Saunois et al. 2016a.*

1.2 Methane Production

Depending on the substrate (organic or inorganic) and process (biodegradation or thermochemical mechanisms), methane can be grouped into biogenic/biological (methanogenesis), pyrolytic and abiogenic (synthesis) (Strapoc 2017). The following focusses on biological methanogenesis as this type of methane is most relevant when methane production is investigated in lakes.

Biological methane production. Methanogens, a subgroup of the Archaebacteria kingdom (Archaea domain), are responsible for biogenic methane production (i.e. Thauer 1998, Ferry and Kastead 2007). Since their discovery in aquatic sediments in 1777 (Volta 1777), research focusses on these organisms as biological methane source. There are seven orders of Euryarchaeota (Methanomassiliicoccales, Methanomicrobiales, Methanococcales, Methanosarcinales, Methanobacteriales, Methanocellales, Methanopyrales), all of which conduct methanogenesis as basic energy metabolism (Thauer 1998, Pace 2009, Dean et al. 2018). More recently, additional taxa (*Bathyarchaeota, Verstraetearchaeota*) have been discovered (Lang et al. 2015, Evans et al. 2016, Vanwonterghemet al. 2016). Methanogenesis is known to take different pathways: Acetoclastic methanogenesis reduces acetic acid under disproportionation to carbon dioxide and methane ($CH_3COOH \rightarrow CH_4 + CO_2$); hydrogenotrophic methanogenesis involves hydrogen metabolism and carbon dioxide reduction ($CO_2 + 4H_2 \rightarrow CH_4 + 2\ H_2O$); and methylotrophic methanogenesis reduces methylated single- or multi-carbon precursors (Thauer 1998, Dean et al. 2018) for methane generation. Typical methylated precursor molecules are methanol, formate, alcohols, methylated amines and sulphides (Whiteman et al. 2006, Strapoc 2017); even carbon dioxide (Moran et al. 2008) and methoxylated aromatic compounds (Mayumi et al. 2016) have been reported to serve as precursor compound. Most methanogens can either convert carbon dioxide or methylated molecules to methane (using hydrogen as e- donor) (Fricke et al. 2006, Dridi et al. 2012, Lang et al. 2015, Dean et al. 2018). While some methanogens specialized on single pathways of methane formation (e.g. *Methanosaeta*, Strapoc 2017), others can perform several pathways that are favoured by different environmental settings (e.g. *Methanosarcinales*, Kendall & Boone, 2006). In many ecosystems, methanogens form syntrophic communities with Bacteria. Methanogens benefit from access to organic methane precursors, and in turn, the removal of bacterial products promotes bacterial growth (Strapoc 2017). This syntrophy can even extend to electron

transfer from Bacteria to methanogen (Rotaru et al. 2014, Kouzuma et al. 2015). Alternatively, inorganic precursors for methanogenesis may originate from processes like water radiolysis or carbonate thermolysis (Blair et al. 2007), olivine serpentinization (Sleep et al. 2004) or water-mineral reactions (Mayhew et al. 2013), as summarised in Strapoc (2017).

The enzymatic reactions of methanogenesis can be divided into the oxidative and the reductive part (Thauer et al. 1998): During the oxidative part methyl-coenzyme M (CH_3-S-CoM) is formed from coenzyme M (H-S-CoM) and the pathway-related methane-precursor molecule (e.g. acetate, carbon dioxide, etc.). Among the different methanogenesis pathways, various intermediates are involved in the methylation of coenzyme M (e.g. transfer from methyltetrahydromethanopterin or methyltetrahydrosarcinapterin). Subsequently, methyl-coenzyme M is oxidised with coenzyme B (H-S-CoB) to a heterodisulphide of both coenzymes (CoM-S-S-CoB). This process is catalysed by the enzyme methyl-coenzyme M reductase and releases methane (CH_3-S-CoM + H-S-CoM → CoM-S-S-CoB + CH_4). During the reductive part, the heterodisulphide undergoes reduction that is coupled with ADP phosphorylation conserving energy. The activation of the reductive process (electron supply) is pathway specific. For example, oxidation of hydrogen, formate or ethanol can provide the necessary electrons. Coenzyme M, as well as methyl-coenzyme M have not yet been detected in other organisms. Therefore, these enzymes are targeted when identifying methanogens in complex microbiomes.

Archaeal methanogenesis is connected to three basic requirements (Strapoc 2017): i) anoxia (oxygen low or absent) (IPCC 1990, IPCC 2013) due to the involved enzyme machinery being oxygen-sensitive (Schönheit et al. 1981, Jarrell 1985, Ragsdale and Kumar 1996), ii) low abundance of competitive electron acceptors (oxidisers) like nitrate, sulphate or multivalent metals, and iii) substrate availability. Also, the content and quality of organic matter, as well as temperature are controlling factors over methanogenesis production rates (Borrel et al. 2011). Many environments satisfy these requirements and are inhabited by methanogenic Archaea: these include rice paddies, wetlands, freshwater and marine sediments, soils, animal intestines and even extreme environments with high salt contents (Paterek and Smith 1988) or temperatures up to 122°C (Takai et al. 2008, Strapoc 2017).

Thermochemical methane production. Beside biological processes, thermochemical processes can also transform organic molecules into methane under certain environmental conditions. Thermal composition (pyrolysis), hydrothermal/metamorphic methane-synthesizing mineral-fluids (Sherwood Lollar 1993), or the Fischer-Tropsch reactions at high temperature and pressure conditions (Horita and Berndt 1999) can lead to natural methane formation (Strapoc 2017). Additionally, methane can be synthesized artificially using photochemical methods (Rao et al. 2017, Strapoc 2017, Zhang et al. 2017).

1.3 Methane Consumption

Methane is converted back to carbon dioxide via microbial and photochemical oxidation (Figure 1.1). Microbial methane oxidation (methanotrophy) is performed either aerobically or anaerobically before methane emission to the atmosphere. Methanotrophy can remove a substantial part of the methane during movement from anoxic zones to the oxic atmosphere (ca. 60 %, Reeburgh 2007). Once in the troposphere, photochemical processes govern the conversion of methane, oxidizing about 90 % of the remaining methane pool (Dean et al. 2018).

Aerobic methanotrophy. Methanotrophic Bacteria are responsible for methane oxidation in oxygenated environments. They have been known since the early 20th century (Söhngen 1906) and are represented by the taxa Alphaproteobacteria (*Beijerinckiaceae* – ubiquitous), Gammaproteobacteria (*Methylococcaceae*, *Methylocystaceae* – ubiquitous) and Verrucomicrobia (*Methylacidiphilaceae* – high temperature, low pH environments habitats) (Borrel et al. 2011, Dean et al. 2018). The pathway of methane oxidation is sequential oxidation of methane to methanol, formaldehyde, formate and finally carbon dioxide (Semrau et al. 2010, Borrel et al. 2011). Aerobic oxidisers are equipped with the key enzyme methane monooxygenase which exists in cytoplasmic-soluble and (mainly) membrane-bound forms. This enzyme catalyses the first step of methane oxidation under oxygen consumption (Hanson and Hanson 1996, Borrel et al. 2011, Dean et al. 2018). Aerobic methanotrophs depend on the availability of methane and oxygen, which is why they are normally found at the interface between oxic and anoxic zones such as the upper layers of sediments or at the oxycline in stratified lakes (Borrel et al. 2011). It has long been believed that

methanotrophic Bacteria are obligate methylotrophic; however, recent findings showed that they could also use acetate as an energy source (Dedysh et al. 2005, Conrad 2009). Aerobic methane oxidation rates are modulated by temperature (Borrel et al. 2011), ammonium (inhibits the activity of methane monooxygenase; Murase and Sugimoto 2005) and food-web interrelations with other members of the microbiome (e.g. planktonic organisms; Borrel et al. 2011).

Anaerobic methanotrophy. Methane is thermodynamically very stable; therefore, oxygen was initially believed to be the only electron acceptor for methane oxidation (Dean et al. 2018). However, sulphate has been identified as electron acceptor for this reaction (Reeburgh 1976, Panganiban 1979) in anaerobic methanotrophic Archaea (e.g. *Methanosarcinales*) and sulphate-reducing Bacteria (e.g. *Desulfococcus*) (Conrad et al. 2009, Dean et al. 2018). Corresponding Archaea are related to methanogens and have methanogenesis-like enzyme machineries (methyl-Coenzyme M reductase homologue) running in reverse order (Conrad 2009, Dean et al. 2018). The reducing equivalents (originating from methane oxidation) are subsequently transferred to sulphate reducing bacteria (Krüger et al. 2003).

Similarly, nitrogen oxides can act as an electron acceptor for methane oxidation in the Bacteria *Methylomirabilis oxyfera* and the Archaea *Methanoperedens nitroreducens* using the same strategy of inversely running methanogenesis enzyme reactions (Haroon et al. 2013, Dean et al. 2018).

Photochemical methane transformation. Tropospheric methane oxidation to carbon dioxide is a highly complex network of radical reactions (Monks 2003). Here, the photon-triggered conversion of methane to carbon dioxide is explained in brief.

The capacity of tropospheric methane photo-oxidation relates to the content of ozone, hydroxy radicals, and hydrogen peroxide (Thompson 1992). Tropospheric ozone is converted to hydroxyl radicals by UV light under the presence of water vapor. The highly reactive hydroxyl radical is the initial reaction partner for methane leading to the formation of peroxy radicals (e.g. HO_2, CH_3O_2) followed by production of peroxy hydroperoxides, methoxy radicals, formaldehyde and hydroperoxyl. In the final reaction, hydroperoxyl reacts with carbon monoxide (originating from formaldehyde conversion) to form carbon dioxide. The overall net reaction of this photolytic methane turnover can

be formulated as $CH_4 + O_2 \rightarrow CO_2 + 2H_2$ (Monks 2003). It has been estimated that about 90 % of tropospheric methane is oxidised by photochemical pathways (Dean et a. 2018).

1.4 Methane Dynamics in Lakes

General background. Lakes are enclosed water bodies cut-off from marine systems that originated from various geological processes (Meybeck 1995). They comprise typically fresh water and may have water in-/outflows. Lake water physics, chemistry and biology are modulated by many factors such as meteorological variability among climate zones and groundwater input. Consequently, lakes can be classified according to their geological origin (Meybeck 1995), trophic state or thermal lake structures. The classification of trophic state was introduced by Thienemann and Nauman (1925-1932), which is based on nutrient conditions and the corresponding autotrophic production rates. Based on phosphorus, oxygen, chlorophyll content and water transparency lakes are divided into oligo-, meso-, eu- and hypereutrophic systems with increasing nutrient content and primary production in the given order (Hakanson and Jansson 1983). Lake water absorbs solar radiation; the associated processes of heating (and convective cooling) can lead to the development of density gradients throughout the water columns as reflected by temperature profiles. This layering process is called stratification. In most cases of stratification, three water layers (strata) are apparent: Warm near-surface water, referred to as epilimnion (lowest water density), cold water remote from surface and sunlight, referred to as hypolimnion (highest water density), and the transition zone between epilimnion and hypolimnion that is defined as metalimnion or also called thermocline (steepest temperature and density gradient). Driven by various climate conditions, stratification patterns are commonly classified into dimictic, cold-/warm monomictic, polymictic, oligomictic and amictic (Hakanson and Jansson 1983).

Methane cycling in lakes is a complex network of transformation, transport and storage processes affected by numerous environmental parameters. The complexity of the involved processes leads to substantial spatial and temporal variability of methane emission at the water-air interface within and across lake types (e.g. Wik et al. 2016a, Sanches et al. 2019), which makes it hard to accurately quantify overall methane emission in global assessments (Kirschke et al. 2013, Saunois et al. 2016a).

Sediments. According to the conventional understanding, microbial methane production in lakes occurs exclusively under anoxic conditions via methanogenic Archaea (Thauer et al. 1998, Ferry and Kastead 2007). The amount of methane that is released from lake sediments into the water column depends on sediment type/structure (e.g. sand/clay/silt) (Liu et al. 2016), the interactions between methanogenic and methanotrophic microorganisms (Reeburgh et al. 1991), substrate availabilities and quality (Borrel et al. 2011), temperature conditions (Duc et al. 2010) and transport mechanisms (Sanches et al. 2019). Different methanogens utilise different pathways and precursors for methane generation (section 1.2) at different production rates. For example, acetoclastic and hydrogenotrophic methanogenesis can both be found in lake sediments in equal proportion (Whiticar et al. 1986, Murase et Sugimoto 2002). The organic material that is used for methanogenesis originates either from lake internal cycling, atmospheric carbon fixation (autochthonous feed), e.g. photosynthesis by phytoplankton or vegetation in the littoral zone, or external feeds via groundwater or river input (allochthonous feed). After its decomposition, this organic material is utilised for sediment methanogenesis. Once the methane has been generated, it migrates towards water surface via diffusion, ebullition or plant-mediated transport (through aerenchyma). Alongside diffusive transport, methane is consumed by methanotrophic microorganisms (Figure 1.1). The sediment-water interface is a hotspot for methane oxidation activity as here methane and oxygen come together in a niche environment. Most of the diffusing sediment methane is oxidised here before it enters the water column (66-95 %; Frenzel et al. 1990, Bosse et al. 1993, Liikanen et al. 2002). Ebullition, on the other hand, is a spontaneous transport process that largely escapes methane oxidation and can release methane gas bubbles quickly into the water column (Borrel et al. 2011). While methane gas bubbles migrate towards the water surface, they exchange gas content with the surrounding water column (e.g. following the partial pressure gradients methane is exchanged with oxygen, carbon dioxide, nitrogen and other gases). In case the water table and the vertical transport distance are short (≤20 m), gas bubbles transport methane directly to the atmosphere; otherwise the methane is mainly stored in the dissolved form inside the water column (Tang et al. 2014). In the littoral zone, vegetation can constitute another efficient way for methane emission (e.g. Shannon et al. 1996). Methane migrates through aerenchyma of vascular plants via molecular diffusion and is directly released to the atmosphere. This gas transport is fuelled by concentration gradients, and as such, other gases are also transported. Oxygen for instance also passes through the aerenchyma

but in the opposite direction into the sediments where it can stimulate higher methane oxidation rates and reduce methane diffusion at the sediment-water interface (Shannon et al. 1996).

As a result of various parameters modulating the sediment methane inventory, different methane production rates have been reported for sediments (e.g. Murase and Sugimoto 2002, Fuchs et al. 2016), as well as different methane fluxes can be observed at the sediment-water interface. For example, in oligotrophic lake systems sediment-water methane fluxes of 0.2 mmol m^{-2} d^{-1} have been recorded, whereas eutrophic systems showed up to 5.2 mmol m^{-2} d^{-1} (Adams 2005). Sediments in the littoral zone typically account for higher methane fluxes compared to the profundal zone (Babenzien and Babenzien 1985, Murase and Sugimoto 2001) because here is a hotspot for organic matter turnover (e.g. lake vegetation/surrounding forests). Furthermore, littoral sediments are exposed to sunshine, and associated heating accelerates methanogenic methane production. The temperature dependence of sediment methanogenesis is often described by the Arrhenius-Boltzmann equation (Burdige et al. 2011, Aben et al. 2017, Peeters et al. 2019), or sometimes using the Ratkowsky formula (Ratkowsky et al. 1982).

Water Column. Methane that is not transported to the atmosphere via ebullition or plants migrates by diffusion through the water column. Inside the water column, diffusion is governed by concentration gradients and internal turbulences (MacIntyre et al. 2010). Closer to the surface where water layers are exposed to heating and cooling effects, methane transport may also take place via convection (Bouffard and Wüest 2019). Generally, the transport of dissolved methane takes place vertically (e.g. from sediment to water surface) and horizontally (e.g. from shore to mid-water) distributing the dissolved methane all over the water table. Typically for oxic watercolumns, more methane accumulates in the epilimnion compared to the hypolimnion and a peak is apparent at thermocline depth. This pattern is displayed in Figure 1.3, showing the methane concentration profile of the mid-water column in a stratified lake.

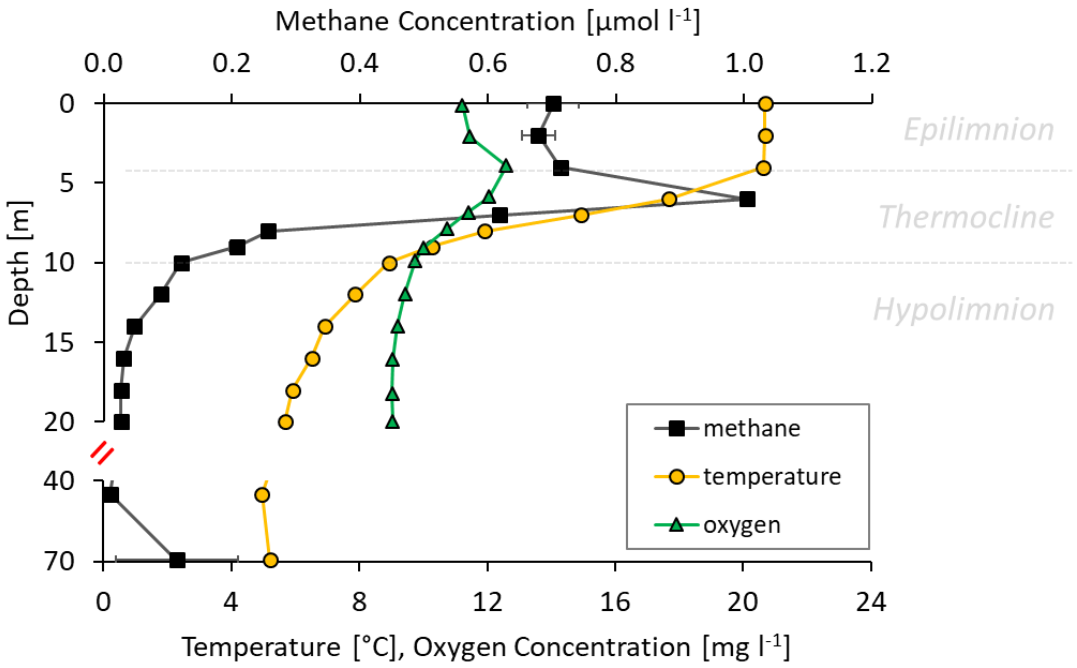

Figure 1.3: Methane, temperature and oxygen profile of the mid-water column in temperate Lake Stechlin during the stratified period (NE Germany). *Water samples were taken at the deepest point of Lake Stechlin (max. 69.5 m deep) on 20th June 2016. Samples were collected using a Limnos Water Sampler, transferred to serum bottles, 3x times flushed and crimp-closed. Methane concentrations were measured by headspace replacement technique and GC/FID analysis. Temperature and oxygen concentration were recorded with a YSI probe. Methane data depict a typical water column profile with high methane content in epilimnic water, a sharp maximum in the thermocline and low methane content in the hypolimnion. At the sediment-water interface, a slight increase in methane concentration was recorded (0.12 µmol l^{-1}; 5.2 °C). High methane concentrations in lakes often coincide with high oxygen concentration reaching oversaturation-values (>9 mg ml^{-1} O_2 at 20°C). In Lake Stechlin the entire water column never turns anoxic.*

The shape of the profile is controlled by various biological and physical processes. Murase et al. (2005) summarised that the horizontal feed of dissolved methane from littoral sediments and rivers are a significant source of epilimnic and thermocline methane, as well as wave-induced methane release from littoral and sub-littoral sediments (Murase et al. 2005, Hofmann et al. 2010) (Figure 1.4).

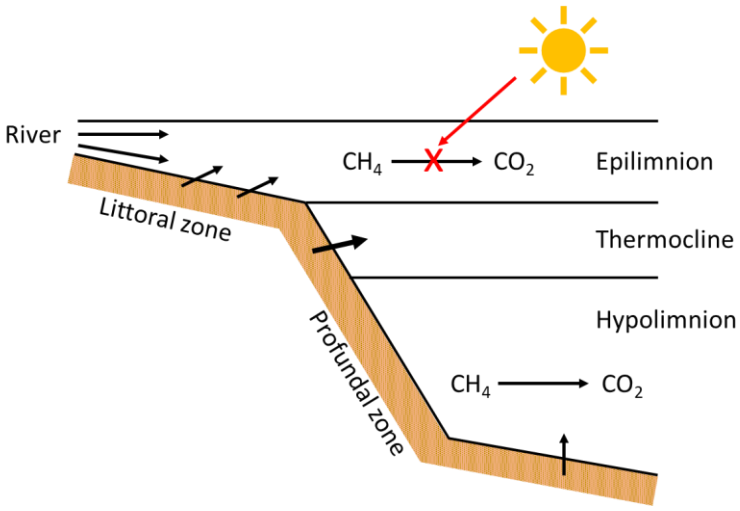

Figure 1.4: Schematic illustration of methane fluxes in lake Biwa. *The strength of methane sources (littoral/profundal sediments, rivers) is displayed by arrow size. Inside the hypolimnion, methane is oxidised but not inside the epilimnion due to light inhibition of methane oxidation (Murase and Sugimoto 2005). Picture drafted after Murase et al. (2005).*

Sediments in the profundal zone are considered to be a minor methane source for surface emission compared to the littoral because most of the methane is oxidised at the sediment-water interface (Frenzel et al. 1990, Bosse et al. 1993, Liikanen et al. 2002) or inside the hypolimnion (Bastviken et al. 2008, Donis et al. 2017), and littoral sediments typically have higher methane production rates (Babenzien and Babenzien 1985, Murase and Sugimoto 2001). Oxygen availability is a determining factor for methane oxidation rates in the water. Close to the surface, lake water is rich in oxygen, but eutrophic (Thomas et al. 1996) and especially deep lakes (Müller et al. 2012) can develop hypoxia/anoxia inside the hypolimnion limiting methane oxidation. Recent studies suggest that water-column methane oxidation can remove 45-100 % of methane (Bastviken et al. 2002) and is inhibited by light (Murase and Sugimoto 2005) which might additionally contribute to shaping the methane profile.

There are several hypotheses to explain the methane peak inside the thermocline. The epilimnion is a layer of mixed water due to convection (mixing based on daytime heating and nighttime cooling) and turbulent flux (e.g. wind/river induced turbulence). Dissolved methane inside this surface-mixed layer, therefore, will distribute vertically and horizontally. In fact, a recent study has shown that the horizontal transport of dissolved methane follows a predictive function up to 2 km offshore (DelSontro et al. 2018). If dissolved methane inside the epilimnion was to be assumed homogenous,

diffusive loss to the atmosphere would create a concentration gradient with higher methane surface concentration in proximity to the shore compared to mid-waters. Additionally, waves might release methane from sub-littoral sediments creating a substantial source of dissolved methane in thermocline depth (Murase et al. 2005). Further, different mechanisms can transport methane horizontally to mid-water at thermocline depth: transport with cold groundwater following the density gradient, thermocline jets/currents or differential cooling effects (e.g. quicker nighttime cooling of shallow waters) (Bouffard and Wüest 2019, personal communication[1]). The thermocline separates warm water of the epilimnion from cold water in the hypolimnion. As methane is a sparsely soluble gas, and gas solubility generally decreases with increasing temperature, the temperature gradient between epilimnion and hypolimnion might be responsible for the methane thermocline peak (Wilkinson et al. 2015). These hypotheses attempt to explain the phenomenon of thermocline methane peaks in lakes that align with the dogma of microbial methane production being an anoxic process.

Water Surface. In shallow waters, especially in littoral zones ebullition (Aben et al. 2017, Sanches et al. 2019) and plants (Milberg et al. 2017) might be the dominant ways for atmospheric methane emission. The importance of diffusion and convection for surface methane emission, however, increases together with water column depth and shore distance. For example, typically 4-6 mm seized natural methane bubbles (Ostrovsky et al. 2008, Maeck et al. 2013) released from 20 m deep sediments lose about 60-80 % of their methane content to surrounding water on their way to the surface, while they lose >98 % when released from 70 m depth (Tang et al. 2014). Generally, gas transfer from water to air depends on the partial pressure gradient, the condition of the water-air interface and the gas mobility. Wind forcing (MacIntyre et al. 2010), precipitation (Ho et al. 1997/2007), tidal currents (Borges et al. 2004, Zappa et al. 2007), wave breaking (Zappa et al. 2004), as well as thermal convection (MacIntyre et al. 1995) induce turbulence and, therefore, are driving forces of the water-air transfer. Also, other parameters such as surfactants (reduce the gas exchange rate; Frew et al. 1990, McKenna and McGillis 2004), particulate matter (reduces the gas exchange rate; Abril et al. 2009, Calleja et al. 2009) and microbubbles (enhance the gas exchange rate, McGinnis et al.

[1] Personal communication with Prof Hans-Peter Grossart, Dr Danny Ionescu, Dr Georgiy Kirillin (Leibniz Institute for Freshwater Ecology and Inland Fisheries - IGB Berlin, Germany) and Dr Ilia Ostrovsky (Israel Oceanographic and Limnological Research, Israel)

2015) have been noted as modulating factors. The complexity of gas exchange creates high spatial and temporal variability within and across lakes' surface emission (Blees et al. 2015, Natchimuthu et al. 2015, Wik et al. 2016a). Figure 1.5 shows an example surface methane emission and corresponding methane profiles in surface water taken on a transect in a stratified lake. The interplay between storage and emission is apparent when methane surface-water concentrations and emission of different transect sites are compared with each other.

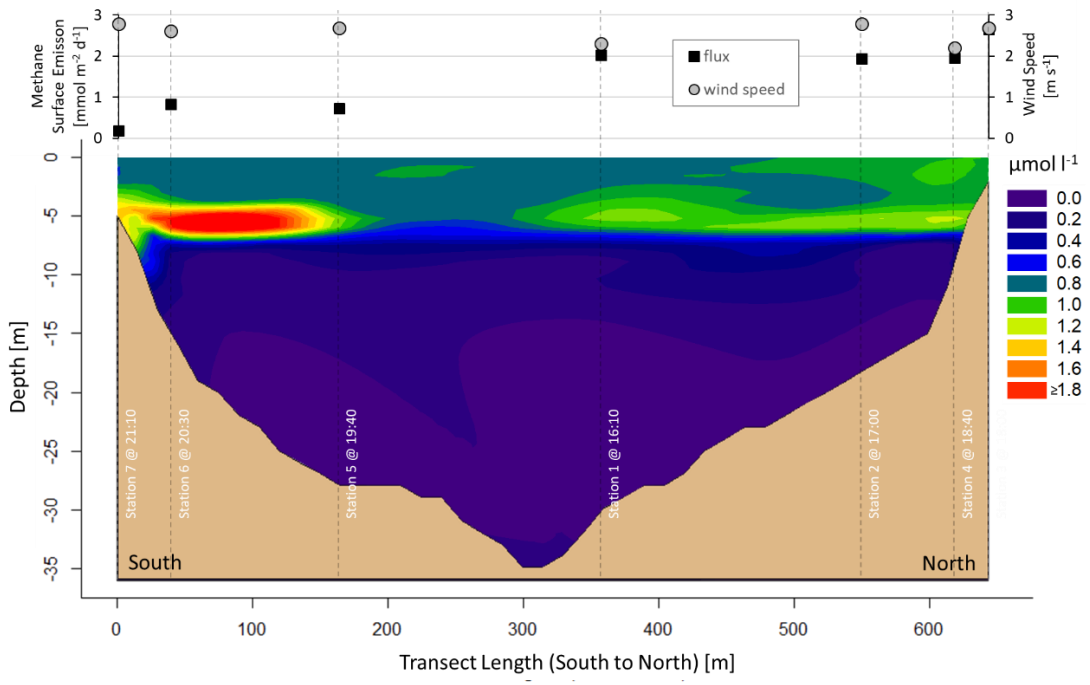

Figure 1.5: Surface water methane heterogeneity along transect measurements in the South basin of stratified Lake Stechlin (temperate region in North-East Germany). *The heatmap illustrates surface methane concentration [µmol l^{-1}] in 0-12 m depth and the scatterplot corresponding methane surface emission [mmol m^{-2} d^{-1}] and wind speed in 10 m height [m s^{-1}]. Water samples have been taken at station 1-7 during the stratified season on 16th June 2017 between 16^{00}-21^{30} (local time) from a boat using a Limnos Water Sampler. Water was transferred into serum bottles, 3x flushed and crimp-closed without gas enclosure. Methane content was determined by headspace replacement technique and GC/FID analysis (duplicate measurements). Surface methane emission was recorded simultaneously by deploying a flux chamber and Los Gatos GHG analyzer. The increasing methane content in the flux chamber was regressed over time (ca. 10 min with a 1-second resolution) giving the surface methane emission. Wind speed was provided by the Umweltbundesamt (Neuglobsow weather station, 600-900 m away from sampling locations). Coordinates of sampling stations were recorded with a GPS tracker and aligned with the lake's depth profile (extracted from bathymetry data). Note, this plot illustrates the heterogeneity of surface water methane (0-12 m depth) and surface fluxes relative to shore distance and water-column-depth; increased methane content at the sediment-water interface is neglected. SigmaPlot (v.12.0), R (v.3.3.1, raster/marmab package), RStudio (v.1.0.153) and MS Office (v.365ProPlus) were used to draft this figure.*

The surface-emission can be directly measured by the floating chamber method or predicted from proxy parameters such as wind speed, temperature, water-air concentration gradient, turbulence etc. Accurate estimation of surface methane emission is crucial for regional and global methane budgets, as well as predicting future climate change scenarios.

1.5 The Methane Paradox and the Oxic Methane Production

The Paradox. Methane is the most reduced hydrocarbon. Since the discovery of microbial methanogenesis in sediments during the 17th century (Volta 1777), it is commonly believed that this process is exclusive to anoxic zones (Reeburgh 2007, Thauer et al. 2008). Also, many of Archaeas' enzyme machineries responsible for reducing precursors to methane have been found to be highly oxygen-sensitive (Schönheit et al. 1981, Jarrell 1985, Ragsdale and Kumar 1996). Notwithstanding, methane oversaturation (relative to atmospheric methane content) has been frequently observed in oxic sea and lake water remote from anoxic sediments (e.g. in marine systems: Conrad and Seiler 1988, Watanabe et al. 1995, Jayakumar et al. 2001, McGinnis et al. 2006, Sasakawa et al. 2008, Vagle et al. 2010; in limnic systems: Rudd et al. 1976, Bedard and Knowles 1997, Bastviken et al. 2008, Juutinen et al. 2009). Figure 1.3 showed a more detailed example of mid-water methane oversaturation coinciding oxygen oversaturation in a stratified lake. This phenomenon, dubbed 'the methane paradox', requires an explanation. As discussed earlier, the entire methane inventory in oxic waters is commonly assumed to be the result of horizontal and vertical transport from the anoxic methane sources, especially littoral sediment methanogenesis (e.g. Murase et al. 2005, Hofmann et al. 2010,). Studies specifically designed to quantify the contribution of anoxic sources to mid-water methane oversaturation, however, found that an internal source is needed (besides physical transport from anoxic zones) to fully explain the paradox (marine: Scranton and Brewer 1977, Sparrow et al. 2018,; limnic: Bogard et al. 2014, Donis et al. 2017). A recent study found that when oxic water was incubated in serum bottles, the methane concentration increased over time (Grossart et al. 2011). Nevertheless, some researchers suggest the presence of micro-anoxic zones that are responsible for active methane production in oxic waters (e.g. Reeburgh 2007). As described by Murase et al. (2005), several anoxic sources potentially contribute to the

paradoxical methane accumulation, such as: anaerobic production in the guts of zooplankton and fish (Sieburth 1987, de Angelis and Lee 1994, Schmale et al. 2017, Stawiarski et al. 2019), anaerobic production in particulate organic matter such as faecal pellets (Karl and Tilbrook 1994, van der Maarel et al. 1999), submarine groundwater discharge (Bussmann and Suess 1998, Corbett et al. 2000) and groundwater inflow in lakes (Taniguchi 2001, Murase et al. 2005).

Oxic Methane Production. While some researchers attribute oxic-water methane oversaturation entirely to anaerobic methane production via methanogenic Archaea and physical transport, recent studies have begun to consider the alternative explanation of microbial methane production under oxic condition. Tang et al. 2016 reviewed the discovery of methane production in oxic environments, a phenomenon termed 'oxic or aerobic methane production' to distinguish it from the conventionally accepted anaerobic production pathway (Liu et al. 2015). The following passages summarise this discovery and the current knowledge and ideas on the mechanisms that potentially explain paradoxical methane accumulation in aquatic systems.

Oxic methane production might be explained by 1) the responsible enzyme machinery of 'conventional' methanogenesis being oxygen-tolerant, 2) oxygen detoxifying processes such as catalase activity (Angel et al. 2011), or 3) novel pathways by known/yet to be identified organisms. Oxygen-tolerant enzyme machineries might be an evolutionary artefact of anaerobic microbes adapting to increasingly oxic environment throughout earth's history (Tang et al. 2016). Some studies indicate the presence (Grossart et al. 2011, Bogard et al. 2014) and activity (Angel et al. 2011, Angle et al. 2017) of methanogenic Archaea in oxic zones and oxygen-tolerance of some enzymes (Jarrell 1985). Further, some Archaea (*Methanosarcina, Methanocella*) have been found to biochemically eliminate toxic reactive oxygen species with the enzyme catalase, allowing them to produce methane under oxic conditions (Angel et al. 2011). Evidence for an alternative pathway was first reported by Keppler and colleagues in 2006 when they showed that intact plants and detached leaves produced methane at substantial rates under oxic conditions. The underlying process was later proposed to involve radicals (non-catalytic, chemical): UV-radiation generates reactive oxygen species (ROS) that subsequently form methane from the cell wall component pectin (McLeod et al. 2008, Messenger et al. 2009, Nisbet et al. 2009). The existence and significance of this oxically produced methane has been debated rigorously (Kirschbaum et al. 2006, Dueck et al.

2007). Chemical pathways of oxic methane production were subsequently described for other eukaryotic organisms - fungi and animals - and were considered a stress response (Ghyczy et al. 2008, Wang et al. 2013, Liu et al. 2015). Fungi, for example, have been shown to produce methane (Lenhart et al. 2012).

In the aquatic environments, oxic methane production via (methyl) phosphonate metabolism by marine microbes was first proposed by Karl et al. (2008). This biocatalytical mechanism of methane production has been shown in various organisms: Alphaproteobacteria (sea: Carini et al. 2014; lake: Yao et al. 2016), Gammaproteobacteria (sea: Repeta et al. 2016; lake: Wang et al. 2017), Haptophyta (sea: Lenhart et al. 2016) and Cyanobacteria (sea: Beversdorf et al. 2010, Teikari et al. 2018; predicted in lakes: Yao et al. 2016). Here, methylphosphonate metabolism producing methane as a by-product is thought to be an alternative way for phosphorus acquisition when inorganic phosphorus is limited (Carini et al. 2014). It is known that phosphonates can be produced by Eukaryotes and Bacteria (Yu et al. 2013, Ju et al. 2015) but biogenic methylphosphonate formation has so far only been associated with *Thaumarchaeota* in marine and freshwater (Metcalf et al. 2012, Callieri et al. 2016). This spatially separates the synthesis of methylated precursor and the process of final reduction to methane to two different organisms. For example, high methane oversaturation in surface-water in Lake Stechlin (Grossart et al. 2011) might be explained by methylphosphonate generation by Actinobacteria (Tang et al. 2016) and subsequent reduction to methane by Cyanobacteria (Yao et al. 2016). While the majority of studies describes methylphosphonate degradation to be a two-organism process, there is growing evidence that autotrophic organisms can produce methane in oxic environments independently (Lenhart et al. 2016, Klintzsch et al. 2019). Independent production pathways have been speculated to be based on unknown Coenzyme-M homologues and unknown methyl reductases (Tang et al. 2016). The reducing energy that is required for methyl reduction could alternatively originate from photosystems/proteorhodopsin under a nutrient limitation or energy conservation from electron bifurcation (Buckel et al. 2013). It is also reasonable to assume that other compounds also can serve as methyl donor for methane generation beside methylphosphonates, for example, thioethers and corresponding sulphoxides (DMSO etc.), methionine (Althoff et al. 2014, Damm et al. 2015/2010, Klintzsch et al. 2019) or methylated nitrogen molecules (Ghyczy et al. 2003, Tang et al. 2016). Bizic-Ionescu et al. (2018) (with M. Günthel as co-author), for instance, found

that trimethyl amine stimulated oxic-water methane production, identifying the first non-phosphonate related precursor for the process. Another recent study showed a similar process via breaking down sulphur-methyl bonds homolytically catalysed by nonheme oxo iron (Klintzsch et al. 2019). Other studies investigating oxic methane production based on demethylation did not yield conclusive results. For instance, sea and freshwater enriched with methylated precursor failed to increase methane production (Grossart et al. 2011, Borges et al. 2018). It is likely that methane production in oxygenated water operates via different pathways, not all of them being dependent on availability of methylated precursor molecules (Bizic-Ionescu et al. 2018).

Another possible source for oxically produced methane is nitrogenase enzymes. It has been recently shown, that a biotechnologically modified nitrogenase enzyme of the alphaproteobacterium *Rhodopseudomonas palustris* was capable of transforming carbon dioxide to methane (Fixen et al. 2016). Subsequent work showed that a wild-type iron-only nitrogenase derivate of the same organism could catalyse the same reaction (Zheng et al. 2018). It is, however, unclear, if this mechanism is performed by microbes in oxic waters.

Environmental Significance. Methane production in anoxic lake sediments must be transported prior to release to the atmosphere and in this regard, will be modulated by biological (e.g. oxidisation) and physical processes (e.g. storage). In contrast, methane production in the oxic upper layer of a lake places the methane source closer to the atmosphere, and therefore, its contribution to atmospheric emission can be significant (Tang et al. 2016, Donis et al. 2017). Methane emission from lakes has been measured for many years. As the entire methane inventory in lakes is commonly attributed to only anoxic sources, we currently lack the understanding of how much the oxic methane sources contribute to atmospheric methane emission. DelSontro and colleagues (2018) developed a model describing distribution patterns of dissolved methane in lakes alongside transport from shore to mid-water. Their study revealed that biological moderation during this transport could result in a net decrease (oxic source outbalanced by oxidation) or a net increase of surface water methane (oxidation outbalanced by oxic source). Two independent recent studies in two different lakes suggest that a substantial amount (ca. 20-90 %) of the mid-water diffusive methane flux to the atmosphere might originate from oxic sources (Bogard et al. 2014, Donis et al. 2017). Whether this is a common phenomenon in lakes and of global relevance for the

atmospheric methane burden is currently unknown. There is an urgent need to investigate the underlying biological pathways, as well as regional and global relevance of this phenomenon, not only for a more accurate assessment of the global methane budget but also to understand its response to environmental changes. For example, widespread lake eutrophication leading to more pronounced phytoplankton blooms worldwide (Paerl and Huisman 2009, Visser et al. 2016, Huisman et al. 2018) may increase atmospheric methane emission at the lake-air interface via increased oxic methane production. In the light of global warming, mean lake water temperature will increase (Kundzewicz et al. 2007, Czernecki and Ptak 2018) and stratification periods will extend (Peeters et al. 2007, De Stasio Jr. et al. 1996); understanding global warming feedbacks on oxic methane production will help to predict future scenarios in a warmer world.

There is growing evidence that methane production is a common feature of organisms, not only in the domain of Archaea but also in the domains of Prokaryotes and Eukaryotes via various mechanisms. Recent reviews on biogenic methane formation (e.g. Dean et al. 2018) and current assessments of regional (Fernandez et al. 2016, Peeters et al. 2019) and global methane budgets (IPCC 2007, IPCC 2013) still fail to consider oxic methane production as a relevant methane source. Global assessments are hampered by large uncertainties in freshwater methane emissions (Figure 1.1). Better measurements of the oxic methane source and the related processes will help to reduce these uncertainties.

Challenges and Opportunities. Methane cycling in aquatic systems has been researched for many years. The conventional understanding of strictly anoxic microbial methane production, however, has led to biased attribution of the total methane inventory to anoxic sources and to disregarding the oxic sources. There are many open questions; e.g. which organisms can produce methane under oxic conditions, what are the molecular pathways, under what physiological/ecological/environmental conditions does it happen, and how important is this process on a regional and global scale?

Numerous biochemical and physical processes affect methane cycling in limnic systems simultaneously. The methane production/consumption rate, for instance, is influenced by the microbiome, sediment composition/thickness or ground water feed. Morphological properties (size, aspect-ratio, water depth, steepness etc.) modulate transport patterns inside the water column and at the water-air boundary (DelSontro et

al. 2018). Meteorological diversity affects methanogenesis turnover (driven by different temperature regimes in different climate zones) and methane surface emission (driven by different wind and precipitation regimes). Also, lake physics regulates transport and emission processes (e.g. through stratification patterns, seiches, water in-/outflow, internal turbulence). The complex network of parameters controlling methane production/consumption/storage/transport/emission creates large heterogeneity within and across systems (e.g. Blees et al. 2015, Natchimuthu et al. 2015, Wik et al. 2016a). To that end, the proper distinction between oxically and anoxically produced methane is a major challenge in this new field of research. Accordingly, methodological approaches also have to be evaluated carefully. For example, changing methane concentration in bottle incubation of oxic lake water not only is the result of methane oxidation but a mixed dynamic of oxidation and production (Murase and Sugimoto 2005). Furthermore, some processes are still poorly understood, such as the ecological regulation of methane emissions through trophic cascade (fish-zooplankton-methane oxidisers/producers-interactions; Devlin et al. 2015), and physical distribution processes like differential cooling (Bouffard and Wüest 2019). As such, it remains challenging to incorporate all parameters affecting methane cycling into climate models (McKay et al. 2009).

1.6 Lake Stechlin

The methane paradox is a phenomenon that can be observed in oceans and lakes (Tang et al. 2016). Lakes, however, have been reported to be more important for the atmospheric methane burden: Lakes contribute about five times more methane to the atmosphere compared to oceans (76 Tg yr^{-1} versus 14 Tg yr^{-1}) (Saunois et al. 2016a); nevertheless, lakes cover only 1 % (Cael et al. 2017) and oceans 70 % (Tang et al. 2016) of earth's surface. This and the fact that methane concentrations in oxic freshwaters are nearly 1000x higher than in oxic-seawater (Tang et al. 2016) might indicate that the oxic methane sources of both system types are equally important on a global scale.

This thesis is focused on investigating the phenomenon of microbial methane production in oxic waters in Lake Stechlin. Oxic methane production in lake water was discovered in the very same lake and has been repeatedly observed since that time with oxic-methane peak concentrations up to 1.4 µmol l^{-1} (Grossart et al. 2011, Tang et al. 2014). Methanogenesis activity in Stechlin's sediments is low, mainly taking place below

20 cm (Casper 1996, Casper et al. 2003, Casper et al. 2005, Conrad et al. 2007). As a dimictic lake in the temperate region in North-East Germany (53°09'06.5"N 13°01'40.5"E) Lake Stechlin is thoroughly mixed during winter, stratifies during May and remains stratified until September or October. With 4.25 km^2 this glacial lake is medium-sized and with a maximum depth of 69.5 m (average depth of 22.7 m) it belongs to the deepest clear-water lakes in Germany. Its water column never turns anoxic, and the water has a residence time above 60 years (Holzbecher et al. 1999). The lake has a low overall phosphorus input and is often referred to as an oligotrophic system (e.g. Casper 1985), however, due to eutrophication the lake is now at the verge of becoming mesotrophic (personal communication[2]).

In the 1960s a nuclear power plant was built next to Stechlin, and for about 25 years the power plant used water from the neighbouring Lake Nehmitz for cooling down the reactor and fed the approx. 10 °C warmer water into Lake Stechlin (Koschel and Casper 1986). To investigate the ecological consequences of this thermal pollution, a limnological research facility was created at Stechlin's shoreline. Today, Lake Stechlin belongs to the best-investigated inland waters worldwide (Casper 1985). The Lake has no river in- nor outflow, only an artificial channel that allowed water circulation with Lake Nehmitz during times when the nuclear power plant was active. The Leibniz-Institute for Freshwater Ecology and Inland Fisheries (IGB Berlin) constructed a lake lab facility in Lake Stechlin containing one central reservoir (30 m diameter, 14,000 m^3) and 24 mesocosm enclosures (9 m diameter, 1,200 m^3) (IGB webpages[3]). Since 2011, these enclosures have been frequently used for experiments to study how lakes respond to changing environmental conditions. Lake Stechlin's location, bathymetry and the facilitated lake lab are illustrated in Figure 1.6.

[2] Personal communication with Prof Hans-Peter Grossart at the Leibniz-Institute for Freshwater Ecology and Inland Fisheries; institute-internal data.

[3] Homepage of the Leibniz-Institute of Freshwater Ecology and Inland Fisheries (IGB Berlin) (www.igb-berlin.de/en) and webpage of the lake lab facility (www.lake-lab.de).

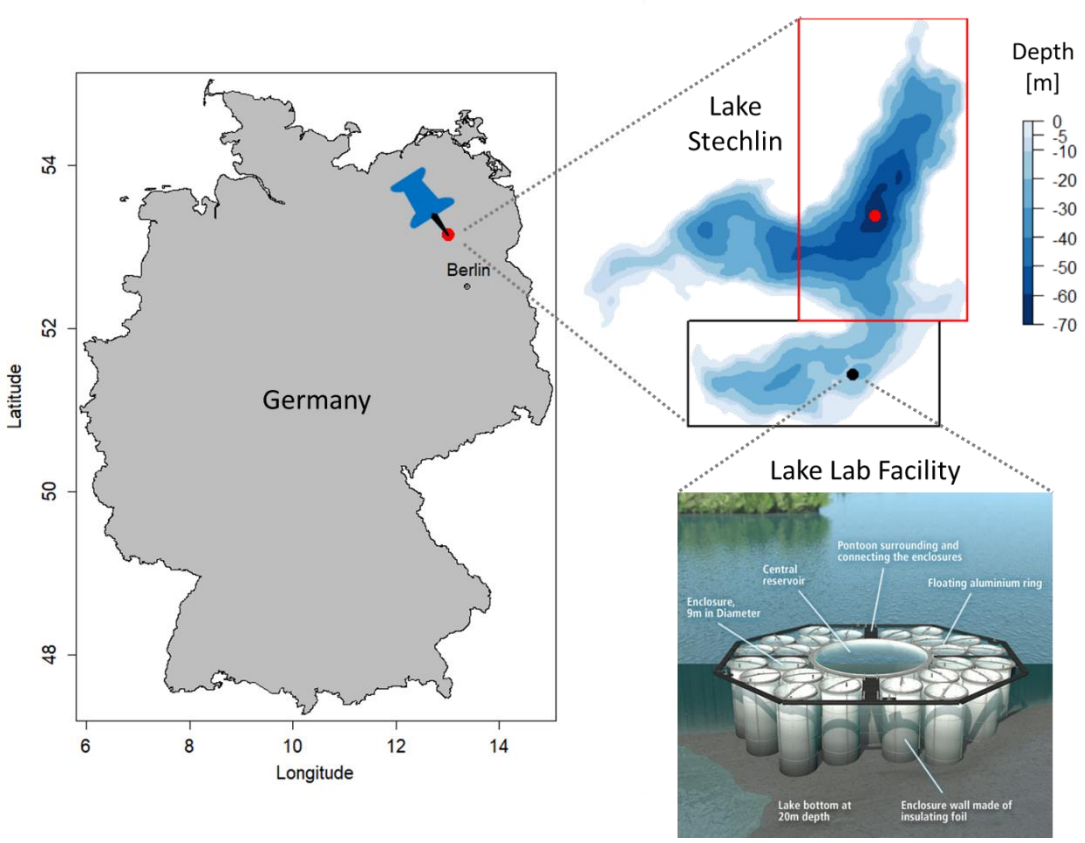

Figure 1.6: Lake Stechlin – location, depth profile and the lake lab facility. *The map of Germany illustrates the lakes' location in the geographical coordinate system. Stechlin's depth profile was plotted from bathymetry data. The lake consists of three basins: 2.01 km^2 sized Northeast basin, 1.12 km^2 sized South basin and the 1.12 km^2 seized Northwest basin. Frames display the main sampling locations in the Northeast basin (red) and the South basin (black). The dots indicate the deepest point (red; 69.5 m deep) and the location of the lake lab facility (black; approx. 20 m deep). The sketch of the lake lab facility was taken from the homepage of the Leibniz-Institute for freshwater ecology and inland fisheries (www.lake-lab.de). R (v.3.3.1, raster/marmab/maps/mapdata package), RStudio (v.1.0.153) and MS Office (v.365 ProPlus) were deployed to create this figure.*

1.7 Thesis Objectives

This thesis aims to produce a better understanding of i) what are the environmental conditions triggering methane production in oxic lake waters, ii) what microbes are capable of oxic methane production, and iii) the local and global relevance of this phenomenon for lake-methane assessments. The following sections highlight the objectives of individual chapters.

Chapter 2: The existence of oxic-water methane production has been demonstrated in marine (Karl et al. 2008) and limnic systems (Grossart et al. 2011). However, it is unclear what environmental conditions trigger this phenomenon. The association of methane production with phytoplankton (Grossart et al. 2011, Lenhart et al. 2016, Yao et al. 2016, Teikari et al. 2018) and methyl phosphonate (Carini et al. 2014, Wang et al. 2017, Bizic-Ionescu et al. 2018, Teikari et al. 2018) suggests that light and inorganic phosphorus availability could be key factors in oxic lake water methane production. A high-resolution field campaign was conducted recording water column-methane, corresponding ^{13}C-signatures together with a series of environmental parameters on a seasonal (weekly sampling) and diurnal scale (6 h interval). The comprehensive dataset was analysed to investigate what major phytoplankton groups were associated with methane formation and whether light exposure and phosphorus limitation promoted methane formation. A variety of bottle incubation experiments were conducted to compliment the field sampling. Furthermore, an earlier study (Tang et al. 2014) speculated that the reductive power necessary for methane formation in oxygenated environments could originate from photosynthesis. To test whether photosynthesis was involved in oxic methane formation, an isotope-labelling experiment was conducted adding ^{13}C-bicarbonate to lake water microbiome and monitoring the incorporation of the ^{13}C-label into the methane pool.

Mid-water methane emission in lakes is commonly attributed to physical transport processes from anoxic zones (Murase et al. 2005, Fernandez et al. 2016, Peeters et al. 2019). To quantify the contribution of the oxic methane source to mid-water emission, oxic methane production rates were determined by bottle incubations experiments, and the results were compared to surface emission recorded in the field.

Chapter 3: Cyanobacteria are ubiquitous organisms thriving in nearly all ecosystems worldwide, and there are earlier reports of methane production in association with Cyanobacteria (Yao et al. 2016, Bizic-Ioescu et al. 2018, Teikari et al. 2018). Therefore, the ability of methane formation by various Cyanobacteria isolates originating from freshwaters, oceans and deserts was examined in this chapter. Two different approaches were used: incubation experiments coupled with either membrane inlet mass spectrometry (MIMS) or isotope analysis (GC-IRMS). Both methods were set up to investigate methane production with underlying mechanisms other than phosphorus demethylation. Building upon Chapter 2, Cyanobacteria cultures were incubated with

^{13}C-labelled bicarbonate, and its transformation into methane was monitored providing evidence for oxic methane production being connected to autotrophic carbon fixation.

Chapter 4: Methane production in oxic lake-surface waters is a very recent discovery (Grossart et al. 2011). Therefore, it is not surprising that only three studies are available in the literature describing oxic production rates and the contribution of the oxic methane source to atmospheric emission (Grossart et al. 2011, Bogard et al. 2014, Donis et al. 2017). These studies are based on discrete measurements, not allowing detailed examination of the temporal dynamics of oxic methane production. To address this knowledge gap, a high-resolution field campaign was conducted recording near-surface water methane, methane ^{13}C-signatures, surface emission and environmental parameters over the diurnal cycle of 11 consecutive days (4 h-interval, automatized approach) in order to obtain a better understanding of the temporal variabilities of the oxic methane source. Subsequently, the system-wide sources and sinks of surface mixed layer methane were compared, providing methane production rates and an overview of the short-term dynamics of oxic methane production in the field. The production rates and isotope signatures were further analysed in relation to phytoplankton abundance to examine if the photoautotrophic community was responsible for oxic-water methane production.

Chapter 5: Quantifying the gas emission at the water-air interface is a key step in assessing greenhouse gas budgets. The emission can be directly measured by using the floating chamber approach combined with chromatographic techniques. This method, however, is time consuming and impractical for large-scale studies. As an alternative, it is far more common that emission is estimated from proxy parameters such as wind speed or the concentration gradients across the water-air interface based on empirically derived wind-based models (e.g. Lana et al. 2011, Bade 2009, Lopez Bellido et al. 2009, Takahashi et al. 2009, Wanninkhof 2014).

Especially in lakes, heterogeneous water column physics can lead to substantially different emission estimates between the different methods (Duchemin et al. 1999, Matthews et al. 2003, Dugan et al. 2015, Erkkilä et al. 2018). In this chapter, wind-based methane emission predictions, as well as emission predictions deduced from near-surface turbulence, were compared to floating chamber measurements. The objective was to identify the environmental conditions leading to deviation in emission predictions.

It has been suggested that the incorporation of additional proxy-parameters into empirical wind-models can improve emission predictions (MacIntyre et al. 2010, Vachon and Prairie 2013). As such, this chapter also tested the addition of water and air temperatures (two parameters recorded throughout routine measurements worldwide) to a wind-based model to improve methane emission estimation in comparison to the flux chamber method.

Chapter 6: Global assessments of freshwater methane emissions are marred by large uncertainty (Figure 1.2; Kirschke et al. 2013, Saunois et al. 2016a). This uncertainty is caused by heterogeneous methane density fluxes within and across systems (Natchimuthu 2015, Wik et al. 2016a, Sabrekov et al. 2017, Xiao et al. 2017), uncertainty in global freshwater surface area estimates (Allen and Pavelsky 2016; Thornton et al. 2016; Cael et al. 2017) and the lack of long-term data (Kirschke et al. 2013, Saunois et al. 2016a). Oxic methane production is currently not acknowledged in global assessments (IPCC 2007, IPCC 2013, Kirschke et al. 2013, Saunois et al. 2016a) despite its potential to explain variable density fluxes.

The contribution of oxic methane production to the system-wide surface emission in lakes has been reported only for three lakes. Accordingly, it is unknown whether oxic lake water methane production is of global significance. Here, the system-wide methane sources and sinks in the surface mixed layer of two basins of Lake Stechlin were compared providing the contribution of oxic methane production to surface emission on a seasonal scale (for the first time showing the transition from mixed to stratified period). These results were then combined with literature values and additional lake estimates (computed from literature data) to develop a model predicting the contribution of oxic methane production to surface emission in relation to lake morphology. Finally, the predictive model was applied to the global lake inventory data to derive a first estimate of the importance of oxic methane production for lake water methane emission on a global scale.

1.8 Contributions & Publishing Information

Contributions. The thesis introduction (Chapter 1) and general discussion and conclusion (Chapter 7) has been entirely composed by me. Other chapters include contributions by other researchers as laid out in the following.

Chapter 2: Together with Kam W. Tang and Hans-Peter Grossart I conceived the study. I collected field data on a weekly basis supported by Isabell Klawonn, Jason Woodhouse, Danny Ionescu, Lars Ganzert, Mina Bizic-Ionescu or Luca Zoccarato (concurrent measurement and local safety regulation required two people). Experiments (size fractionation, depth-specific methane production, ^{13}C-labeling experiment, light-dark incubation) were designed, conducted and analysed by me with help from Isabell Klawonn and Jason Woodhouse (size fractionation, ^{13}C-labeling experiment). MIMS experiments were designed, conducted and analysed by Danny Ionescu and Mina Bizic-Ionescu. I determined field ^{13}C isotope signatures with support from Steffen Kümmel and Ivonne Nijenhuis (provided method and IRMS). I conducted statistical analysis of all field data, synthesized field and lab data and illustrated all data other than MIMS data. The manuscript was written by me and Kam W. Tang with input from the collaborators.

Chapter 3: Mina Bizic-Ionescu, Thomas Klintzsch, Danny Ionescu, Frank Keppler and Hans-Peter Grossart conceived the study and designed the experimental design. MIMS experiments, in situ measurements and corresponding data analysis were performed by Mina Bizic-Ionescu, Danny Ionescu, Muna Y. Hindiyeh, me, Alicia M. Muro-Pastor and Werner Eckert. Thomas Klintzsch conducted stable isotope measurements, and together with Frank Keppler he analysed the corresponding data. Transcriptomic experiments and microbial community analyses were done by Mina Bizic-Ionescu and Danny Ionescu. qPCR analysis was performed by Tim Urich. All collaborators discussed the results and wrote the manuscript. In particular, my contribution included initial MIMS measurements, in situ measurements and manuscript preparation.

Chapter 4: The study was planned by Jan F. Hartmann, me, Thomas Klintzsch, Hans-Peter Grossart, Frank Keppler and Margot Isenbeck-Schröter. Field measurements and corresponding data analysis was performed by Jan F. Hartmann, me, Thomas

Klintzsch, Hans-Peter Grossart and Georgiy Kirillin. Thomas Klintzsch conducted in-lab phytoplankton experiments, and together with Frank Keppler he analysed the corresponding data. All collaborators discussed the results and wrote the manuscript. In detail, I contributed to the study design, field measurements (in situ methane, surface emission, probe measurements) and their automation, flux parameterisation, mass balance analysis, statistical field data analysis and manuscript preparation.

Chapter 5: This study was entirely conceived by me. Raw data were taken from Chapter 4. I conducted the data analysis, illustration and interpretation. I wrote the chapter. Together with Kam W. Tang and Georgiy Kirillin, I currently prepare a manuscript on the basis of Chapter 5.

Chapter 6: The study was designed by me, Hans-Peter Grossart, Kam W. Tang, Daniel F. McGinnis, Daphne Donis and Georgiy Kirillin. I collected the field data (2016, 2018) with support from Hans-Peter Grossart (2016), Danny Ionescu (2014) and Mina Bizic-Ionescu (2014). I analysed all data with input from Daniel F. McGinnis and Daphne Donis (mass balance parameterisation, Lake Hallwil analysis) and Georgiy Kirillin (provided diffusivities). I illustrated the data and, together with Kam W. Tang and input from the other collaborators, I wrote the manuscript.

Table 1.1 summarises the contribution of all authors on manuscripts related to the different thesis chapters.

Publishing Information. Several chapters of the thesis have been modified into manuscripts intended for publication (author ranking as stated on published/submitted/to be submitted manuscripts):

Chapter 2: Günthel, M., Klawonn, I., Woodhouse, J., Bizic M., Ionescu, D., Ganzert, L., Kümmel, S., Nijenhuis, I., Zoccarato, L., Grossart, H.-P., Tang, K. W. Photosynthesis-driven methane production in oxic lake water as an important contributor to methane emission. (submitted: *Limnol. Oceanogr.*)

Chapter 3: Bizic-Ionescu, M., Klintzsch, T., Ionescu, D., Hindiyeh, M. Y., Günthel, M., Muro-Pastor, A. M., Eckert, W., Urich, T., Keppler, F., Grossart, H.-P. Aqautic and terrestrial Cyanobacteria produce methane. (published: *Sci. Adv.* 6, eaax5343 (2020))

Table 1.1: Contributors.

Chapter	Original idea	Data collection	Data analysis	Manuscript preparation
2	**GM**, GHP, TKW	**GM**, BIM, ID, KI, KS, NI, WJ (GL, ZL)	**GM** (KI)	**GM**, TKW (BIM, GHP, GL, ID, KI, KS, NI, WJ)
3	BIM, GHP, ID, KF, KT	**GM**, BIM, EW, HMY, ID, KT, MPAM	BIM EW, HMY, ID, KF, KT, MPAM,	**GM**, BIM, EW, GHP, HMY, ID, KF, KT, MPAM, UT
4	**GM**, GHP, JFH, KF, MIS, TK	**GM**, HJF, KG, KT (GHP)	**GM**, HJF, KF KG, KT (GHP)	**GM**, GHP, HJF, ISM, KF, KG, KT
5	**GM**		**GM**	**GM** (TKW, KG)
6	**GM**, DD, GDF, GHP, KG, TKW	**GM**, BIM, GHP, ID,	**GM** (DD, GDF, KG)	**GM**, BIM, TKW (DD, GDF, GHP, ID, KG)

Günthel, Marco (**GM**); Bizic-Ionescu, Mina, Leibniz-Institute for Freshwater Ecology and Inland Fisheries, Germany (BIM); Donis, Daphne, University of Geneva, Switzerland (DD); Eckert, Werner, Israel Oceanographic and Limnological Research, Israel (EW); Ganzert, Lars, Helmholtz-Centre Potsdam, Germany (GL; Grossart, Hans-Peter, Leibniz-Institute for Freshwater Ecology and Inland Fisheries, Germany (GHP); Hartmann, Jan F., Heidelberg University, Germany (HJF); Hindiyeh, Muna Y., German Jordanian University, Jordan (HMY); Ionescu, Danny, Leibniz-Institute for Freshwater Ecology and Inland Fisheries, Germany (ID), Isenbeck-Schröter, Margot, Heidelberg University, Germany (ISM); Keppler, Frank, Heidelberg University, Germany (KF); Kirillin, Georgiy, Leibniz-Institute for Freshwater Ecology and Inland Fisheries, Germany (KG); Klawonn, Isabell, Leibniz-Institute for Freshwater Ecology and Inland Fisheries, Germany (KI); Klintzsch, Thomas, Heidelberg University, Germany (KT); Kümmel, Steffen, Helmholtz-Centre Leipzig, Germany (KS); McGinnis, Daniel F., University of Geneva, Switzerland (GDF); Muro-Pastor, Alicia M., University of Seville, Spain (MPAM); Nijenhuis, Ivonne, Helmholtz-Centre Leipzig, Germany (NI); Tang, Kam W., Swansea University, UK (TKW), Urich, Tim, University of Greifswald, Germany (UT); Woodhouse, Jason, Leibniz-Institute for Freshwater Ecology and Inland Fisheries, Germany (WJ); Zoccarato, Luca, Leibniz-Institute for Freshwater Ecology and Inland Fisheries, Germany (ZL); initials in parentheses indicate minor contribution.

Chapter 4: Hartmann, J. F., Günthel, M., Klintzsch, T., Kirillin, G., Grossart, H.-P., Keppler, F., Isenbeck-Schröter, M. High spatio-temporal dynamics of production and emission of methane in oxic surface water. (in press: *Environ. Sci. Technol.*)

Chapter 5: Günthel, M., Kirillin, G., Tang, K. W. Comparing wind-based models and the surface renewal model with the flux chamber method for estimating greenhouse gas emission at the water-air interface. (*Manuscript in preparation*)

Chapter 6: Günthel, M., Donis, D., Kirillin, G., Ionescu, D., Bizic-Ionescu, M., McGinnis, D. F., Grossart, H.-P., Tang, K. W. Contribution of oxic methane production to surface methane emission in lakes and its global importance. (published: *Nat. Commun.* 10, 5497 (2019) doi:10.1038/s41467-019-13320-0)

Chapter 2: Photosynthesis-driven Methane Production in Oxic Lake Water as an Important Contributor to Methane Emission

A diversion of this chapter has been submitted to Limnology and Oceanography and is currently under consideration: **M. Günthel**, I. Klawonn, J. Woodhouse, M. Bizic, D. Ionescu, L. Ganzert, S. Kümmel, I. Nijenhuis, L. Zoccarato, H.-P. Grossart, K. W. Tang. Photosynthesis-driven methane production in oxic lake water as an important contributor to methane emission. Limnology and Oceanography Wiley, John Wiley & Sons Limited.

2.1 Abstract

Recent discovery of methane production in oxic waters challenges the conventional understanding of strict anoxic requirement for biological methane production. High-resolution field measurements in Lake Stechlin, as well as incubation experiments, suggested that oxic-water methane production was associated with phytoplankton especially Cyanobacteria, Green Algae and Diatoms. In situ concentration and $\delta^{13}C$ of methane within the oxic layer negatively correlated with soluble reactive phosphorus concentration. Incubations of lake water with ^{13}C-labelled bicarbonate resulted in ^{13}C enrichment in the methane pool. Methane production exceeded oxidation at day but was comparable at night. These experimental data, along with complementary field observations, indicate a link between photosynthesis and methane production-consumption balance in phosphorus-limited epilimnic waters. Comparison between surface methane emission data and experimental methane production rates suggests that about 18 % of the surface flux in Lake Stechlin could be attributed to oxic methane production.

Chapter 3: Aquatic and Terrestrial Cyanobacteria Produce Methane

From M. Bižić, T. Klintzsch, D. Ionescu, M. Y. Hindiyeh, **M. Günthel**, A. M. Muro-Pastor, W. Eckert, T. Urich, F. Keppler, H.-P. Grossart. Aquatic and terrestrial Cyanobacteria produce methane. Science Advances 6, eaax5343 (2020) (doi: 10.1126/sciadv.aax5343). Reprinted with permission from AAAS.

3.1 Abstract

Evidence is accumulating to challenge the paradigm that biogenic methanogenesis, considered a strictly anaerobic process, is exclusive to Archaea. Here, Cyanobacteria from marine, freshwater and terrestrial environments are demonstrated to produce methane at substantial rates under light, dark, oxic and anoxic conditions. These findings link methane production with light-driven primary productivity in a globally relevant and ancient group of photoautotrophs. Methane production, attributed to Cyanobacteria using stable isotope labelling techniques, was enhanced during oxygenic photosynthesis. Methane formation by Cyanobacteria may contribute to methane accumulation in oxygen-saturated marine and limnic surface waters. In these environments, frequent cyanobacterial blooms are predicted to further increase due to global warming, potentially having a direct positive feedback on climate change. Cyanobacterial methane formation likely contributed to the natural methane budget since Cyanobacteria first evolved on Earth.

3.2 Introduction

Methane is the second most important anthropogenic greenhouse gas after carbon dioxide and is estimated to have 25-28 times higher warming effect than the latter (Myhre et al. 2013, IPCC 2014, Allen et al. 2018). The mixing ratio of methane in the troposphere has increased from 715 ppbv in the preindustrial era to currently 1,865 ppbv (Feb. 2019 NOAA/ESRL[4]). Estimated global methane emissions to the atmosphere average at ca. 560 Tg year (1 Tg = 10^{12} g) exceeding the currently estimated sinks by ca. 13 Tg per year (Saunois et al. 2016a). Thus, to mitigate the constant increase in atmospheric methane, a comprehensive understanding of global methane sources and the environmental parameters that affect them is necessary.

Traditionally, biogenic methanogenesis is the formation of methane under strictly anoxic conditions by microbes from the domain Archaea (phylogenetically distinct from both eukaryotes and Bacteria). However, in the past decade there has been growing evidence that also eukaryotes such as algae (Lenhart et al. 2016), plants (Keppler et al.

[4] NOAA/ESRL, Ed Dlugokencky, NOAA/ESRL (National Oceanic and Atmospheric Administration/Earth System Research Laboratory/Global Monitoring Division; www.esrl.noaa.gov/)

2006), animals (Tuboly et al. 2013), fungi (Lenhart et al. 2012) and probably humans (Keppler et al. 2016) produce methane under oxic conditions albeit at considerably lower rates. These recent findings suggest that the phenomenon may not be solely limited to methanogenic Archaea and could include new metabolic pathways. For example, the conversion of methylated substrates such as methylphosphonates to methane by Bacteria has been extensively addressed in recent years with regards to the "methane paradox" (Repeta et al. 2016, Wang et al. 2017). Recently, Zheng et al. (2018) have shown methane formation by *Rhodopseudomonas palustris* during nitrogen fixation. Methane emission was also detected from photoautotrophic communities on plant, rock and soil surfaces (cryptogamic covers) (Lenhart et al. 2015).

Accumulation of methane in oxygenated freshwater environments has been repeatedly associated with the presence of Cyanobacteria (Figure 3.1). Methane production by Cyanobacteria has been attributed to either demethylation of methylphosphonates (Beversdorf et al. 2010, Gomez-Garcia et al. 2011, Yao et al. 2016) or to the association of filamentous Cyanobacteria with methanogenic Archaea, providing the latter with the necessary hydrogen for methane production (Berg et al. 2014). Cyanobacteria are ubiquitous, found literally in any illuminated environment as well as unexpectedly in some dark subsurface ones as well (Hubalek et al. 2016, Puente-Sanchez et al. 2018). Furthermore, this phylum predominated Earth whilst the environment was still reductive and ca. 1.3 billion years prior to the great oxygenation event, which occurred 2.4 billion years ago (Gumsley et al. 2017). Therefore, it was tested whether this phylum contributes to the global methane budget independent of naturally occurring, extra-cellular precursor substances or the presence of methanogenic Archaea. If so, their ubiquitous nature, their expected future increase in abundance (Visser et al. 2016, Huisman et al. 2018) and their proximity to the interface with the atmosphere make them potential key players in the global methane cycle.

Unicellular as well as filamentous, freshwater, marine and terrestrial members of the prominent and ubiquitous phylum Cyanobacteria – a member of the domain Prokaryote – are demonstrated to produce methane at substantial rates under light and dark as well as oxic and anoxic conditions.

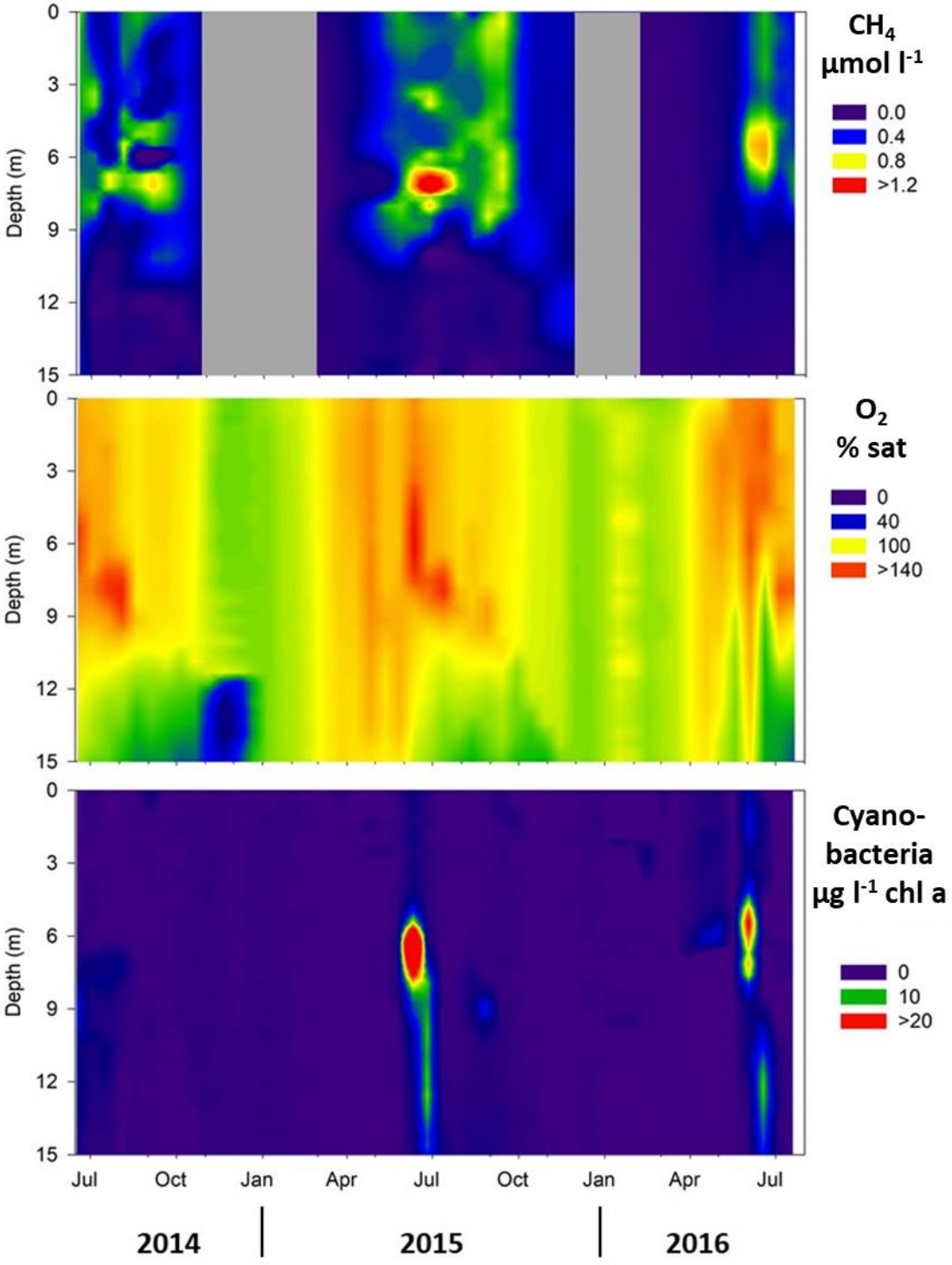

Figure 3.1: Temporal profiles of methane, oxygen and cyanobacterial derived chlorophyll a in Lake Stechlin (2014 to 2016). *The methane data was measured every 1 - 4 weeks depending on the season using a GC/FID as described in Grossart et al. (2011). Oxygen and chlorophyll a were measured hourly using a YSI and a BBE probe (see www.lake-lab.de), respectively. This figure was drafted by collaborators and was modified to fit the thesis layout.*

3.3 Methods

Experiments and analyses performed by collaborators are marked with * and have been included in the thesis to enhance the discussion.

Lake water characterization. As part of the routine monitoring at Lake Stechlin a YSI probe Model 6600V2 was deployed to record dissolved oxygen and other physico-chemical parameters which are not displayed here. Concentrations of taxon-specific phytoplankton pigments were measured by a BBE Moldaenke Fluoroprobe. Methane Concentrations in the Lake Stechlin were determined as follows. Water was transferred from a Limnos Water Sampler to 60 ml serum bottles (clear borosilicate glass, ≥ 88 % transmission of PAR spectrum), 3 times flushed and crimp-closed (PTFE-butyl septa, aluminium caps) without gas bubbles. Dissolved methane was extracted using headspace displacement method and measured by a Shimadzu 14A GC/FID (35 °C Permabond FFAP column running on nitrogen, split-less injection and detection at 140 °C). Headspace methane was converted to dissolved methane concentrations based on Henry's Law and standard conditions.

Cyanobacterial cultures. Seventeen different cyanobacterial cultures were obtained from various sources and grown using the media described in Table 3.1 below. All the cultures were used for Membrane Inlet Mass Spectrometry (MIMS) measurements, while 13 cultures were used for stable isotope labelling experiments.

Table 3.1: Cyanobacterial cultures used in Chapter 3 and their growth conditions.

Strain	N_2	Source	Morphology	Medium	T [°C]
Dolichospermum sp. PCC7120*	+	IBVF	Filamentous	BG11	30
Dolichospermum cylindrica ATCC29414	+	IBVF	Filamentous	BG11	30
Dolichospermum borealis	+	CCALA	Filamentous	BG11	30
Scytonema hofmanni PCC7110	+	IBVF	Filamentous	BG11	30
Leptolyngbya sp. (desert crust)	?	HUJI	Filamentous	BG11	30
Phormidium persicinum	?	IBVF	Filamentous	f/2	26
Trichodesmium erythraeum	+	MPI-MM	Filamentous	YBCII	26
Nodularia spumigena	+	IOW	Filamentous	f/2 (8 psu)	20
Chroococcidiopsis sp. PCC9317	+	IBVF	Unicellular	BG11	30
Microcystis aeruginosa PCC7806	-	IGB	Unicellular	BG11	30
Prochlorococcus sp. MIT9313	-	Uni Freiburg	Unicellular	AMP1	22
Prochlorococcus sp. MIT9312*	-	Haifa Uni	Unicellular	ASW-Pro99	22
Prochlorococcus sp. MIT0604*	-	Haifa Uni	Unicellular	FSW-Pro99	22
Prochlorococcus sp. NATL2A*	-	Haifa Uni	Unicellular	ASW-Pro99	22
Prochlorococcus sp. MED4*	-	Haifa Uni	Unicellular	ASW-Pro99	22
Synechococcus sp. WH7803*	-	Haifa Uni	Unicellular	ASW-Pro99	22
Synechococcus sp. WH8102*	-	Haifa Uni	Unicellular	ASW-Pro99	22

Asterisk-marked cultures are fully axenic while others are mono-algal. The ability (inability) of nitrogen fixation (N_2) is indicated by + (-). ? shows that the ability of nitrogen fixation still has to be clarified. Sources abbreviations: IBVF: Culture collection of the Institute for Plant Biochemistry and Photosynthesis, Sevilla Spain; CCALA: Culture collection of autotrophic organisms; HUJI: Laboratory of Aaron Kaplan, Hebrew University of Jerusalem, Jerusalem Israel; IOW: Laboratory of Falk Pollehne, Leibniz Institute for Baltic Sea research, Warnemünde, Germany; MPI-MM: Max Planck Institute for Marine Microbiology, Bremen, Germany; IGB: Leibniz Institute of Freshwater Ecology and Inland Fisheries, Neuglobsow, Germany; Uni. Freiburg, Laboratory of Claudia Steglich, Freiburg University, Freiburg, Germany. Haifa University, Laboratory of Daniel Sher. Media source: BG11 (Rippka et al. 1979); f/2 (Guillard and Ryther 1962); YBCII (Chen et al. 1996); AMP1 (Moore et al. 2007); Filtered sea water (FSW)/Artificial sea water Pro99 (Moore et al. 2007).

***Stable isotope labelling experiments.** *Culturing and treatments:* To investigate the production of Cyanobacteria-derived methane, 60 ml vials with 40 ml liquid and 20 ml headspace volume (laboratory air) were used and sealed with septa suitable for gas sampling. For the ^{13}C labelling experiments ^{13}C-bicarbonate (99 % purity, Sigma-Aldrich, Germany) was added amounting to 10 % of the initial dissolved inorganic carbon (DIC) in BG11 (Rippka et al. 1979) (DIC = 0.4 mM, enriched by added $NaHCO_3$; pH ≈ 7.0) and 4.5 % of the DIC in f/2 medium (Guillard and Ryther 1962) (DIC = 2.01

mM; pH ≈ 8.2) and 1 % of the DIC in the Pro99 (Moore et al. 2007) based medium used for axenic *Synechococcus* and *Prochlorococcus* cultures. Four different examination groups were used: (1) Sterile medium; (2) Sterile medium with ^{13}C-bicarbonate; (3) Sterile medium with culture; (4) Sterile medium with culture and ^{13}C-bicarbonate; Four replicates of each cyanobacteria culture (n = 4). The cultures were grown under a light–dark cycle of 16 and 8 hours at 22.5 °C at a light intensity of ≈ 30 µmol photons m^{-2} s^{-1} for a total period of 3 days. *Continuous-flow isotope ratio mass spectrometry (CF-IRMS):* CF-IRMS was employed for measurement of the δ^{13}C-methane values in the headspace gas above the cultures. Headspace gas from exetainers was transferred to an evacuated sample loop (40 mL), and interfering compounds were then separated by GC and methane trapped on Hayesep D. The sample was then transferred to the IRMS system (ThermoFinniganDeltaplus XL, Thermo Finnigan, Bremen, Germany) via an open split. The working reference gas was carbon dioxide of high purity (carbon dioxide 4.5, Messer Griesheim, Frankfurt, Germany) with a known δ^{13}C value of -23.64 ‰ relative to Vienna Pee Dee Belemnite (VPDB). All δ^{13}C-methane values were corrected using three methane working standards (isometric instruments, Victoria, Canada) calibrated against IAEA and NIST reference substances. The calibrated δ^{13}C-methane values of the three working standards were -23.9 ± 0.2 ‰, -38.3 ± 0.2 ‰, and -54.5 ± 0.2 ‰. The average standard deviations (n = 3) of the CF-IRMS measurements were in the range of 0.1 to 0.3 ‰. All ^{13}C/^{12}C-isotope ratios are expressed in the conventional δ notation in per mille (‰) vs. VPDB, using the following equation:

$$\delta = \left[\frac{\left({}^{13}_{1}C/{}^{12}_{1}C\right)_{sample}}{\left({}^{13}_{1}C/{}^{12}_{1}C\right)_{standard}}\right] - 1 \qquad (3.1)$$

Membrane inlet mass spectrometer experiments. Experiments were conducted using a Bay Instruments (MD, USA) Membrane Inlet Mass Spectrometer (MIMS) consisting of a Pfeiffer Vacuum HiCube 80 Eco turbo pumping station connected to a QMG 220 M1, PrismaPlus®, C-SEM, 1-100 amu, Crossbeam ion source mass spectrometer (Pfeiffer Vacuum, Germany). Culture samples were pumped (Minipuls3, peristaltic pump, Gilson) through a capillary stainless tubing connected to Viton® pump tubing as described in Kana et al. (2006). The coiled stainless-steel tubing was immersed in a water bath to stabilize the sample temperature. Temperatures were set according to the growth conditions of the different cultures. Inside the vacuum inlet, the

sample passed through an 8 mm long semipermeable microbore silicone membrane (Silastic®, DuPont) before exiting the vacuum and returning to the culture chamber forming a closed system with respect to liquids. This required a 3.5 ml experimental chamber which consisted of an inner chamber where cultures were placed, and an isolated outer chamber connected to a water bath to maintain the culture at a constant temperature. The experimental chamber was placed on a magnetic stirrer, and the cultures were continuously stirred for the duration of the experiments to prevent the formation of concentration gradients.

Cultures were transferred to a fresh medium before the onset of each experiment after which 3.5 ml of the culture were transferred to the experimental chamber, and an equal volume was used for determination of cell counts or dry weight. The latter was determined by filtering the samples on pre-weighed combusted GFF filters (Millipore) and drying at 105 °C for 48 h. In the case of non-homogenous cultures, the biomass from the experimental chamber was used at the end of the experiment for the determination of dry weight. Marine Picophytoplankton cultures were normalized by cell counting using a FACSAria II flow cytometer (BD Biosciences, Heidelberg, Germany) at a flow rate of 23.5 µl / min for 2.5 min. Autofluorescence was used to separate cells from salt precipitates in the medium. Cells for counting were collected from the same batch used in the experimental chamber.

The light regime for the experiments was as follows: dark from 19:30 to 09:00 then light intensity was programmed to increase to 60, 120, 180, 400 µmol photons m^{-2} s^{-1} with a hold time of 1.5 h at each intensity. After maximum light, the intensity was programmed to decrease in reverse order with the same hold times until complete darkness again at 19:30. Experiments lasted a minimum of 48 h with at least one replicate longer than 72 h. A minimum of 3 replicate experiments were conducted for each culture.

As negative controls, ultrapure water, as well as autoclaved cyanobacterial biomass, were measured to test for non-biogenic methane production by the experimental system.

***Experiments using photosynthesis inhibitors.** Three photosynthesis inhibitors were used to observe their effect on methane production by Cyanobacteria. All three were dissolved in water rather than ethanol as the latter results has an ionisation pattern masking that of methane. Atrazine (Cat: 45330-250MG-R, Sigma-Aldrich) has a

solubility of 33 mg l^{-1} (153 µmol l^{-1}) in water and was used at final concentrations of 5 and 10 µmol l^{-1}. DBMIB (2,5-Dibromo-6-isopropyl-3-methyl-1,4-benzoquinone) (Cat: 271993-250MG, Sigma-Aldrich) has a solubility 132 mg l^{-1} (410 µmol l^{-1}) and was used at final concentrations of 5, 10 and 40 µmol l^{-1}. HQNO (2-n-Heptyl-4-hydroxyquinoline N-oxide) (Cat: sc-202654A, Santa Cruz Biotechnology) is described as only very slightly soluble in water without any numerical information. 0.1 mg ml^{-1} culture were used, and it has been noticed that the powder grains remained nearly intact. However, in the light of the observed effect on the culture, some material must have dissolved into culture media. For the experiments, cultures of *Dolichospermum sp.* PCC 7120 were concentrated and resuspended in fresh BG11 medium and incubated in a 10 ml analysis chamber connected via circular flow to the MIMS. Inhibitors were introduced via injection of a concentrated solution at 11:00 after 24 h from the experiment start to allow the culture to acclimate. The light regime used was the same as described above.

Methane calculations. Methane (and oxygen) concentrations were calculated using the ratio relative to the inert gas argon (m/z 40). Methane concentration was deduced from mass 15 (ionisation pattern of methane is visible in Supplementary Figure S3.1), which does not overlap with other gases in the sample (Schlüter et al. 2008). The methane, oxygen and argon concentration in the different media were calculated based on known solubility constants (Powell 1972) and were calibrated to the measured signals in MilliQ water and growth media at different temperatures. To further calibrate the methane (m/z 15) to argon ratio, measurements were conducted on air-saturated water at different salinities (Supplementary Figure S3.2).

Methane production rates were calculated as 1st derivative of the Savizky-Golay (Savitzky and Golay 1964) smoothed data using the sgolay function in the R package signal[5]. To account for the continuous degassing from the methane supersaturation experimental chamber, the degassing rate was determined experimentally using rapid heating of air-saturated water from 18 to 30 °C leading to an instant (super)saturation of 127 % and 130 % for methane and argon, respectively. This procedure was repeated under two mixing conditions: I) mixing was applied via magnetic stirring as conducted for most cultures; II) mixing occurred only via the cyclic pumping of the sample through the MIMS membrane as applied to *Synechococcus* and *Prochlorococcus* cultures. The

[5] http://r-forge.r-project.org/projects/signal/

change in concentration of methane was monitored, and a linear (R^2 = 0.95) saturation degree dependent rate was determined. The determined rate is given in Equations 3.2 and 3.3 for type I and type II mixing, respectively, was similar to that determined by comparing the most negative slopes of the culture experiments, when cyanobacterial production rates are expected to be minimal or zero, and the supersaturation state of the culture. Final rates were calculated by adding the absolute values of the local methane slope (1st derivative) and the local degassing rate (Equations 3.2 and 3.3).

$$R_{degassing} = -2.2365 * 10^{-12} * Sat_{CH4} + 2.12656 * 10^{-12} \quad (3.2)$$

$$R_{degassing} = -8.8628 * 10^{-14} * Sat_{CH4} + 3.5819 * 10^{-14} \quad (3.3)$$

Here $R_{degassing}$ is the degassing rate in mol methane per second, and Sat_{CH4} is the fraction methane saturation state >1 (and <1.3) determined by measured concentration versus calculated solubility.

***Exclusion of archaeal methanogenesis.** Collaborators of this study conducted molecular biological analyses showing that observed methane production in used Cyanobacteria cultures is not the result of contamination with methanogenic Archaea (Supplementary Note 3.1).

3.4 Results & Discussion

To test the hypothesis that Cyanobacteria produce methane independently of known methylated precursors (e.g. methylphosphonates) in ambient water, thirteen different filamentous and unicellular cyanobacterial cultures (for details of chosen cultures see Table 3.1) that are known to grow in marine, freshwater and terrestrial environments were incubated under sterile conditions with ^{13}C labelled sodium hydrogen carbonate as carbon source. All investigated cyanobacterial cultures showed methane production with increasing stable isotope values ($\delta^{13}C$-methane values) clearly indicating that ^{13}C carbon was incorporated into methane, whereas no ^{13}C enrichment occurred in the control experiments (Figure 3.2).

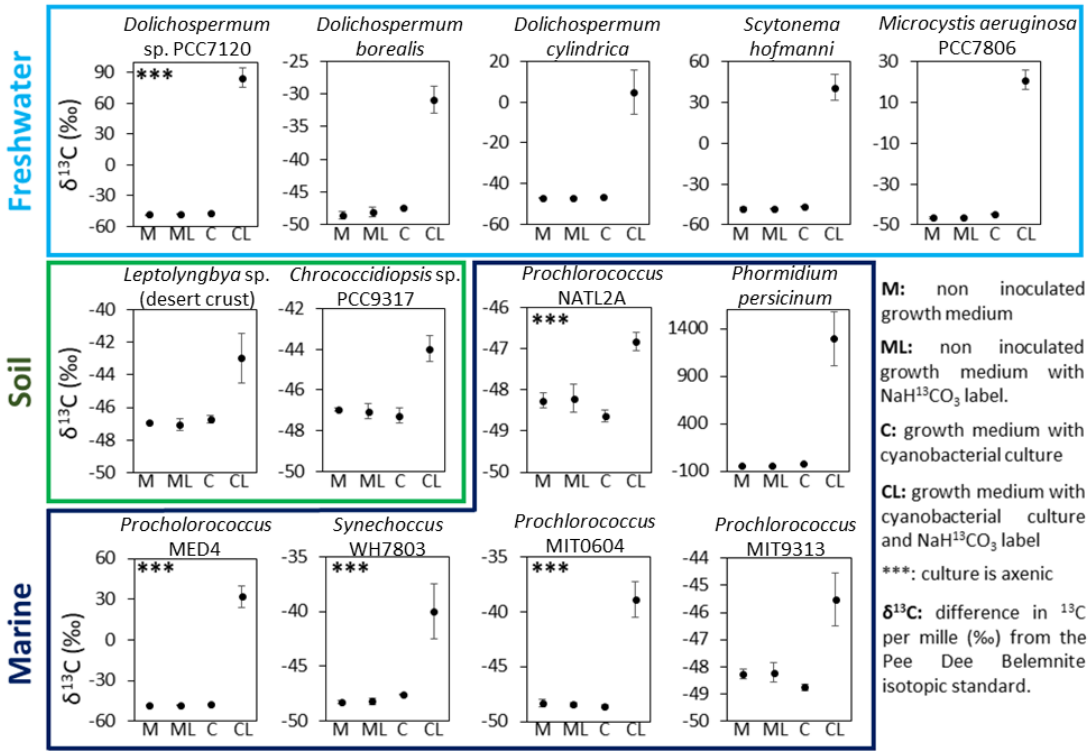

Figure 3.2: Isotope evidence for the conversion of bicarbonate to methane by Cyanobacteria. *δ^{13}C-methane values measured during incubation experiments of thirteen different filamentous and unicellular freshwater, soil and marine cyanobacterial cultures with and without ^{13}C-bicarbonate supplementation. All cyanobacterial cultures produced methane. Using ^{13}C-bicarbonate as carbon source (CL) resulted in increasing stable δ^{13}C-methane values as compared to the starting condition. This establishes the direct link between carbon fixation and methane production. The ^{13}C enrichment is not quantitative and thus not comparable between cultures. Error bars represent standard deviation (n = 4). Figure drafted by collaborators.*

These results unambiguously show that Cyanobacteria produce methane per se and that the process is most likely linked to general cell metabolism such as photoautotrophic carbon fixation. The different enrichment of ^{13}C indicated by δ^{13}C-methane values ranging from 1.71 to 1337 ‰ observed in the different cultures is a result of different production rates as well as differences in biomass. The involvement of methanogenic Archaea in this process can be ruled out. First, five of the cultures were axenic. Second, the oxygen concentrations during methane production were in most cases above the saturation level as Figure 3.3 shows exemplarily for two cyanobacterial cultures (data for all Cyanobacteria strains is given by Supplementary Figure S3.4). While methanogenic Archaea were recently reported in oxic environments (Angle et al. 2017), their activity is attributed to anoxic micro-niches. Peters and Conrad (1995) have

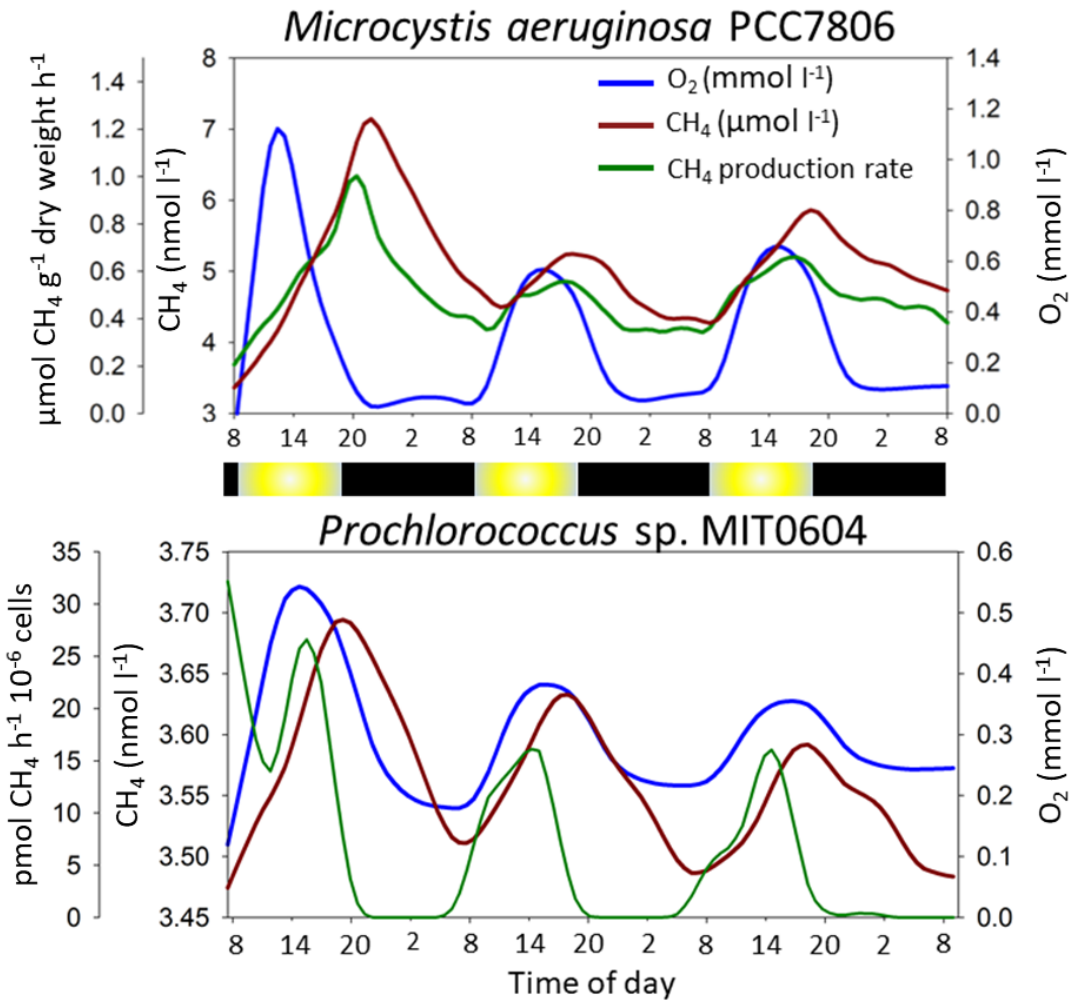

Figure 3.3: Continuous measurements of methane and oxygen during incubation of Cyanobacteria cultures. *Measurements were done throughout consecutive light-dark cycles using a Membrane Inlet Mass Spectrometer (MIMS). Examples are shown for two cultures. Data for other cultures can be found in Supplementary Figure S3.4. A decrease in methane concentration is a result of either reduced, or no, production coupled with degassing from the supersaturated, continuously-mixing, semi-open incubation chamber towards equilibrium with atmospheric methane (2.5 nmol l^{-1} and 2.1 nmol l^{-1} for freshwater and seawater, respectively). Calculated methane production rates account for the continuous emission of methane from the incubation chamber for as long as the methane concentrations are supersaturated. The light regime for the experiments was as follows: dark (black bar) from 19:30 to 09:00 then light intensity (yellow bar) was programmed to increase to 60, 120, 180, 400 µmol photons m^{-2} s^{-1} with a hold time of 1.5 h at each light intensity. After the maximum light period, the light intensity was programmed to decrease in reversed order with the same hold times until complete darkness again at 19:30. Temperature was set to 30 °C (Microcystis aeruginosa PCC7806) or 22 °C (Prochlorococcus sp. MIT0604). Collaborators drafted this figure.*

additionally shown that while methanogens are abundant in oxic environments, methanogenesis remains inactive. Furthermore, our transcriptomic data from two

experiments were conducted over the course of 24 h with non-axenic cultures of *Dolichospermum sp.* PCC 7120 and *Microcystis sp.* PCC 7806 have revealed no expression of genes known to be related to the classical methanogenic activity. Third, our sequencing analysis of non-axenic cultures and quantitative real-time PCR of the methyl coenzyme M reductase gene (*mcrA*) showed that methanogenic Archaea were either absent or present in negligible numbers (Supplementary Figure S3.3).

Furthermore, for the following reasons demethylation of methylphosphonates from the spent growth medium is unlikely to be the mechanism involved in this instance even though some Cyanobacteria do possess the necessary enzymatic machinery (Beversdorf et al. 2010, Gomez-Garcia et al. 2011). First, thus far, demethylation of methylphosphonates has been shown to occur only under phosphorus starvation, which was highly unlikely in this study since the culture medium contained ca. 200 µmol phosphorus l^{-1}. Publicly available transcriptomic data for *Dolichospermum sp.* PCC 7120 (Flaherty et al. 2011, Mitschke et al. 2011) and *Trichodesmium erythraeum* (Pfreundt et al. 2014) show that the phosphonate C-P lyase genes are not expressed under standard (phosphorus-rich) culture conditions. This was further corroborated by transcriptomes of cultures of *Dolichospermum sp.* PCC 7120 and *Microcystis sp.* PCC 7806, where no expression of the C-P lyase genes was detected by the Cyanobacteria or the accompanying microorganisms. Second, some of the Cyanobacteria used in this study (i.e. *Microcystis aeruginosa* PCC 7806, *Synechococcus* WH7803 and WH8102, as well as all sequenced species of *Chroococcidiopsis sp.*, *Leptolyngbya sp.*, *Phormidium sp.* and *Prochlorococcus sp.*) do not possess the known C-P lyase genes necessary for the conversion of methylphosphonates to methane. The lack of the C-P lyase genes, responsible for conversion of methylphosphonates to methane, was demonstrated to be a common feature of the genus *Prochlorococcus* (Luo and Konstantinidis 2011). A recent study looking at the processing of methylphosphonates by *Prochlorococcus* (Sosa et al. 2019) revealed an alternative pathway where methylphosphonates are oxidised to formate. *T. erythraeum* was shown to internally produce phosphonates as phosphorus storage later to be freed by demethylation (Dyhrman et al. 2009), a process that is likely to release methane. Nevertheless, the same study shows, though not focusing on Cyanobacteria alone, that marine unicellular organisms such as *Synechococcus* and *Crocosphaera* do not contain any detectable phosphonate storage.

Rhodopseudomonas palustris has recently been found to produce methane during nitrogen fixation (Zheng et al. 2018). This pathway is unlikely to be the underlying mechanism in this study: First, most Cyanobacteria used in this study are unable (e.g. marine *Synechococcus*, *Prochlorococcus*, *Microcystis aeruginosa*) or unknown (*Leptolyngbya sp.*, *Phormidium persicinum*) to fix nitrogen. Second, all experiments were conducted in nitrate or ammonium rich, fresh, media, and therefore nitrogen fixation in capable Cyanobacteria is likely to be inhibited to a certain degree (Knapp 2012). Thus, given the rapid and tight response of methane production with the onset of light, the mechanism by which Cyanobacteria readily convert fixed carbon dioxide to methane under light conditions likely revolves around the photosynthesis process. Inhibitors of photosynthesis such as Atrazine, DBMIB (2,5-Dibromo-6-isopropyl-3-methyl-1,4-benzoquinone) and HQNO (N-oxo-2-heptyl-4-Hydroxyquinoline) inhibited the methane production under light conditions (Figure 3.4) and suggest a connection to the photosynthetic electron transfer chain. However, the exact biochemical pathway(s) involved in light-driven Cyanobacteria-derived methane formation remains so far unknown and thus requires further investigation.

Methane production rates. Patterns and rates of methane production were investigated in seventeen cultures (the above mentioned 13 and additional 4) over several days of continuous methane using a Membrane Inlet Mass Spectrometry system (MIMS). The measurements, lasting 2-5 days, showed that methane production occurs both under light and dark conditions (Figure 3.3, Supplementary Figure S3.4). This is evident by a positive production rate at almost all times in all experiments. Replicate experiments revealed that, while Cyanobacteria repeatedly produced methane, rates and patterns were not consistent, particularly so for the production during dark periods. Often, a period with lower methane production rates was observed between light and dark phases (Figure 3.3, Supplementary Figure S3.4). The latter is evidenced as a decrease in methane concentration resulting from degassing of the incubation system. These observations suggest that different mechanisms may be involved in methane production under light and dark conditions, presumably dependent on freshly generated photosynthetic products during light and on storage compounds during dark periods. Fermentation of storage compounds by Cyanobacteria has been previously described and known to produce, among other compounds, acetate and hydrogen, which are known precursors of acetoclastic methane formation (Stal and Moezelaar 1997). Interestingly, most of the

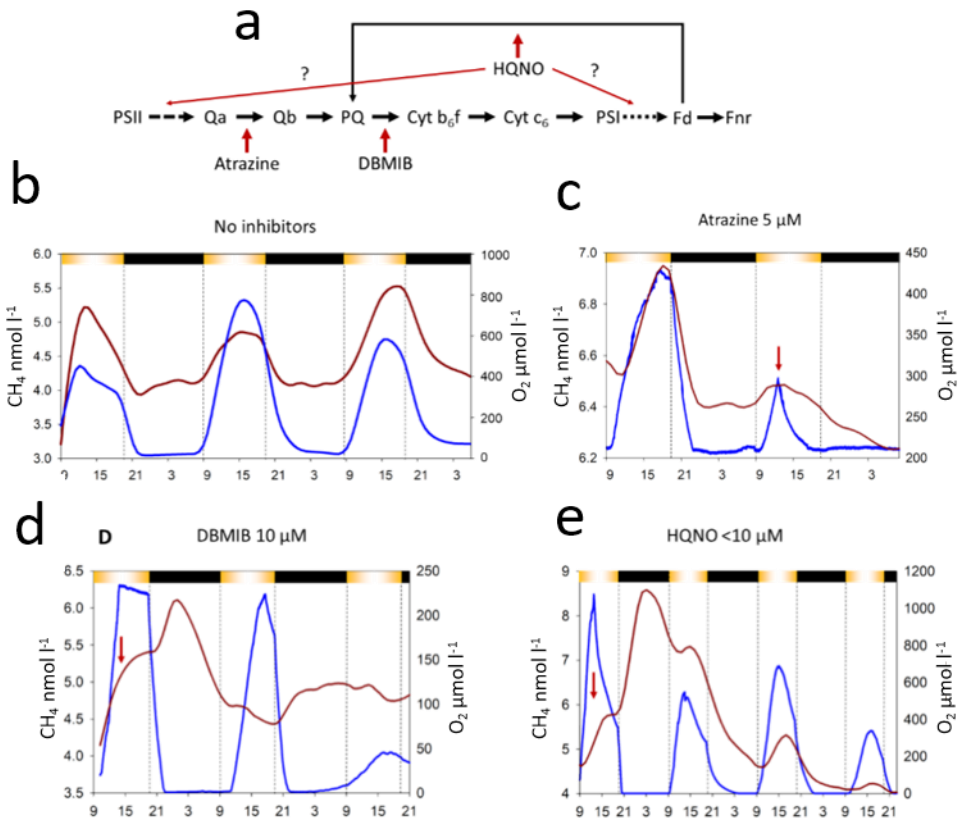

Figure 3.4: Effect of photosynthesis-inhibitors on cyanobacterial methane production. *Atrazine, DBIMB (2,5-dibromo-3-methyl-6-isopropylbenzoquinone) and HQNO (2-Heptyl-4-hydroxyquinoline n-oxide) were used as photosynthesis inhibitors and applied to a culture of Dolichospermum sp. PCC7120. Panel (**a**) displays where the inhibitors affect the photosynthesis reaction chain. The inhibitors were added at 11:00 am (red arrows) after the culture was exposed for 2 h to illumination, and the expected increase in methane concentration was observed. Panel (**b**) shows the diurnal methane (red lines) and oxygen (blue lines) profiles without inhibitor application. Panel (**c**) illustrates the Atrazine treatment: methane and oxygen generation were blocked immediately leading to the subsequent death of the culture. Panel (**d**) lays out the DBIMB treatment: the methane production rate decreased immediately under oxic conditions and a burst in methane production was observed when the culture turned anoxic. In subsequent days a decrease in methane concentration was observed immediately upon illumination. This was a result of ceased production coupled with methane degassing from the semi-open experimental system. Since DBMIB can be reduced and it's blocking site bypassed, the culture resumes normal activity within a few days. Panel (**e**) is the treatment with HQNO application: A similar effect to DBMIB was observed in the dark anoxic culture. Upon re-illumination methane production was delayed until stronger light intensities were applied. This figure has been drafted by collaborators. Note, the original figure has been modified to fit the thesis layout.*

genes required for methanogenesis are present in non-methanogenic organisms, including Cyanobacteria. Nevertheless, in this instance, since the methyl-coenzyme reductase gene is absent, this would suggest that if Cyanobacteria produce methane via

conventional pathways, an ortholog to the methyl-coenzyme reductase gene exists, a rather unlikely option considering current knowledge from cyanobacterial genomes.

Methane production rates (Figure 3.5) were calculated using the slope of methane profiles and were normalized to cyanobacterial biomass dry weight for larger Cyanobacteria or to cell counts for small-celled marine picophytoplankton. The latter was used to obtain high accuracy for the small-cell-sized picophytoplankton, *Synechococcus* and *Prochlorococcus*. Hourly methane production rates across cultures of larger Cyanobacteria were in the range of 0.1 to 3.4 µmol g^{-1} h^{-1} in individual experiments and showed aa overall mean of 0.51 ± 0.26 µmol g^{-1} h^{-1}. Among the marine

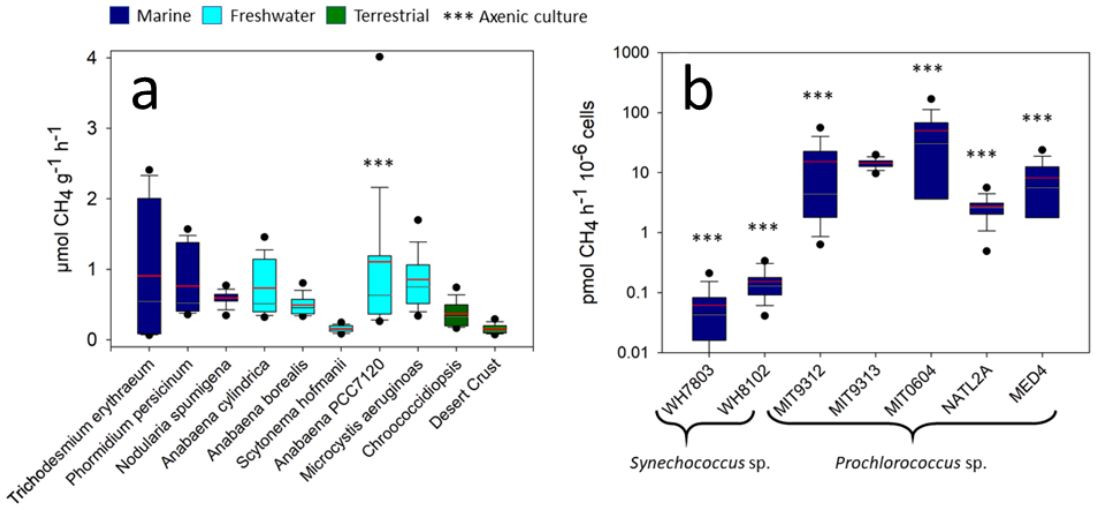

Figure 3.5: Average oxic methane production rates observed throughout 2-5 day-incubation of various cyanobacterial cultures using MIMS. *The rates are designated by colour according to the environment from which the Cyanobacteria were originally isolated; dark blue, light blue and green for marine, freshwater and soil environments, respectively. Grey and red lines represent median and mean values, respectively. Rates for larger Cyanobacteria in panel (**a**) are relative to dry weight, and rates for the picocyanobacterial (**b**) are relative to cell counts. Note, that y-axis is linearly scaled in panel (a) but log-scaled in panel (b). This figure was drafted by collaborators and subsequently modified.*

picophytoplankton, *Synechococcus sp.* exhibited low production rates ranging between 0.01 and 0.6 pmol methane per 10^6 cells h^{-1}, while *Prochlorococcus* cultures produced methane at rates ranging from 0.8 to 110 pmol methane per 10^6 cells h^{-1}. When compared to production rates of typical methanogenic Archaea, methane production rates of freshwater, soil and large marine cyanobacteria are three to four orders of magnitude lower than the methane production rates noted for typical methanogenic Archaea in culture under optimal conditions (oxygen-free), but one to three orders of magnitude

higher than rates observed in eukaryotes (Figure 3.6). In own experiments, *Prochlorococcus* and *Synechococcus* cultures produced methane only at light intensities above 20 µmol photons m^{-2} s^{-1} and therefore, it is likely that only *Procholorococcus* and *Synechococcus* communities in the upper water layers contribute to the oceanic methane flux to the atmosphere.

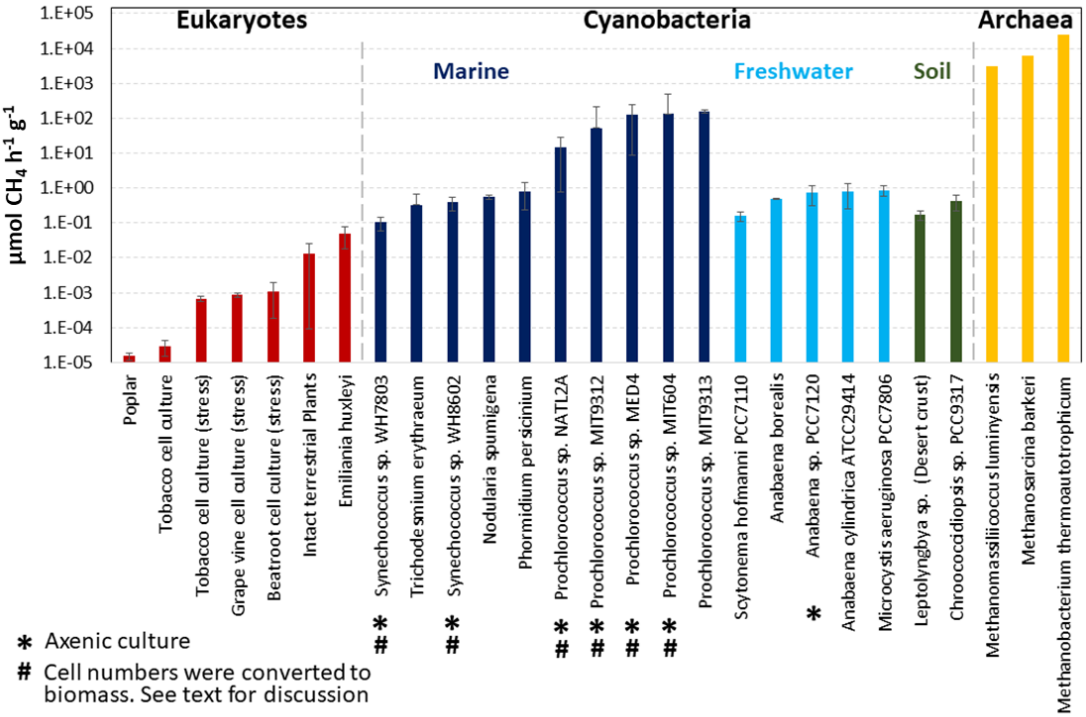

Figure 3.6: Comparison of methane production rates by Cyanobacteria, eukaryotes and Archaea. *Cyanobacterial methane production rates were obtained from multiple long-term measurements (2-5 days) using MIMS. Bar colours of Cyanobacteria refer to the environment they were originally isolated from: Dark blue, light blue and green for marine, freshwater and soil environments, respectively. Methane production rates of 3 Archaea were taken from the literature: Mountfort and Asher (1979), Gerhard et al. (1993), and Kröninger et al. (2017). Eukaryotic production rates including marine algae and terrestrial plants were taken from Keppler et al. (2006), Brüggemann et al. (2009), Qaderi and Reid (2009), Wishkermann et al. (2011), and Lenhart et al. (2016). Note, production rates are presented relative to dry weight. No emission rates (based on dry weight) were available for fungi and animals. The figure was drafted by collaborators.*

Methane production in oxic soils has been previously discussed and attributed mainly to abiotic factors (Jugold et al. 2012) or methanogenic Archaea (Hao et al. 1988), although the latter was thought unlikely (Kammamm et al. 2009, Jugold et al. 2012). A typical desert crust Cyanobacterium (identified in this study as *Leptolyngbya sp.*), as well as the most common endolithic Cyanobacterium *Chroococcidiopsis* (Garcia-Pichel et al.

2003) were found to produce methane both under light and dark conditions (Figure 3.3 and Supplementary Figure S3.4), thus inferring a new but, yet unknown and unaccounted methane source in oxic soils.

Cyanobacterial methane production in aquatic systems. Cyanobacteria are ubiquitous in nature, and their presence in aquatic systems is expected to increase with eutrophication and rising global temperatures (Visser et al. 2016). The "methane paradox" describing the production of methane in oxic water layers has been known for four decades (Scranton and Farrington 1977). Though values may vary between water bodies, a recent study suggests that up to 90 % of methane emitted from freshwater lakes can be produced in the oxic layer (Donis et al. 2017) with Cyanobacteria often being associated with elevated methane concentration in oxygen supersaturated freshwater systems (Grossart et al. 2011). In open oceanic environments, distant from any coast, the contribution of lateral transport from anoxic environments is expected to be absent. Nevertheless, based on the emission rates observed in laboratory studies, it is difficult to extrapolate the contribution of Cyanobacteria to marine, freshwater, terrestrial, and finally to the global methane budget. First, only one attempt has been performed to estimate the global cyanobacterial biomass (Garcia-Pichel et al. 2003). That study does not account for the increase in blooms of toxic and non-toxic Cyanobacteria in freshwater systems (Paerl and Huisman 2009, Glibert et al. 2014, Bowling et al. 2015, Visser et al. 2016, Huisman et al. 2018), nor for less monitored cyanobacterial environments such as those under the ice-cover of frozen lakes (Bizic-Ionescu et al. 2014). Recent estimations of *Prochlorococcus* (Lange et al. 2018) suggest a global biomass of 3.4×10^{27} cells globally, larger by 33 % than estimated in 2003 by Garcia-Pichel et al. (2003). Second, while own experiments demonstrate unambiguously the ability of all investigated Cyanobacteria to produce methane, the experimental setup did not account for the effect of nutrient concentrations and environmental factors such as light and temperature to control emissions in the natural environment. Temperature alone was shown to have a major effect on the *Prochlorococcus* growth rates (Ribalet et al. 2015). Nevertheless, considering the combined day and night average methane production rates of high and low light *Prochlorococcus* species (~9 pmol methane h^{-1} 10^{-6} cells) which prevail in the upper 100 m of the oceans, and an average abundance of 10^8 cells l^{-1}, the gross daily methane production by *Prochlorococcus* is ~22 nmol l^{-1}. The daily produced amount of methane is around one order of magnitude higher than concentrations of methane found

in seawater that is at atmospheric equilibrium (~2 nmol l^{-1}). However, methane in the mean mixed layer of the Atlantic Ocean and surface waters of the Mediterranean Sea have been reported to be often supersaturated reaching maximum methane values up to 7 and 25 nmol l^{-1}, respectively (Forster et al. 2009, Grilli et al. 2018). This simplified calculation demonstrates that *Prochlorococcus* alone (aside from other marine Cyanobacteria) might contribute substantially to the observed oceanic methane supersaturation.

Consider cyanobacterial methane production. In this study, we showed that Cyanobacteria can readily convert fixed inorganic carbon directly to methane and emit the potent greenhouse gas under both light and dark conditions. This is in addition to the already established ability of Cyanobacteria to produce methane by the demethylation of methylphosphonates (Beversdorf et al. 2010, Gomez-Garcia et al. 2011). Cyanobacteria as a phylum are the most ubiquitous group of organisms on Earth, thriving in most, naturally and artificially, illuminated environments almost regardless of temperatures, salinity and nutrient concentrations. Accordingly, their ability to produce methane via different pathways, likely related to their surroundings, makes them important to the present and future global methane cycle and budget. Even more so, as blooms of Cyanobacteria are increasing with eutrophication and rising global temperatures (Visser et al. 2016, Huisman et al. 2018). A recent study, independently predicts that eutrophication resulting in a strong increase in photoautotrophs in the water column (chlorophyll a), will increase freshwater methane emission by 30-90 % (Beaulieu et al. 2019). According to Fletcher and Schafer (2019) the drastic increase in atmospheric methane concentrations since 2007 coupled to the decrease in δ^{13}C-methane values presumable caused by the increase in ^{12}C-enriched biogenic methane sources is difficult to explain with the current understanding of known methane sources and sinks of the global methane budget. This further highlights the need to fully understand the cyanobacterial contribution to the global methane budget and to identify the isotopic signatures of the various methane production pathways they might harbour. Additionally, as phototrophic prokaryotes such as Cyanobacteria have been inhabiting Earth for more than 3.5 billion years (Falcon et al. 2010, Frei et al. 2016) they may have had a major contribution to Earth's methane cycle such as during the great oxygenation event or even earlier when the conditions on Earth were more reductive favouring methane production.

Further research will elucidate the biochemical pathways of methane formation in Cyanobacteria and fully assess the environmental factors affecting it, clarifying its relevance for ecology and the global methane budget throughout Earth history, how it might change in the future, and how this methane source can be mitigated.

Chapter 4: High Spatio-Temporal Dynamics of Production and Emission of Methane in Oxic Surface Water

From J. F. Hartmann, **M. Günthel**, T. Klintzsch, G. Kirillin, H.-P. Grossart, F. Keppler and M. Isenbeck-Schröter. High Spatio-Temporal Dynamics of Methane Production and Emission in Oxic Surface Water. Environmental Science & Technology XXXX, XXX, XXX-XXX (2020) (just accepted manuscript) (doi:10.1021/acs.est.9b03182). Reproduced in part with permission from Environmental Science & Technology, in press.

4.1 Abstract

The discovery of methane accumulation in oxic marine and limnic waters led to re-defining the role of aquatic environments in the regional methane cycle. Although methane accumulation in oxic surface waters became apparent over recent years, the sources are still subject to controversial discussions. This study presents high-resolution in situ measurements of methane concentration and its stable isotope composition in a stratified oligo-mesotrophic lake. Aquatic surface water methane accumulation is shown to originate from a highly dynamic interplay between (oxic) methane production and surface emission. Laboratory incubations of different phytoplankton types and application of stable isotope techniques provide the first unambiguous evidence that major phytoplankton classes in Lake Stechlin per se produce methane under oxic conditions. Combined field and lab results show that the photoautotrophic community is an important driver for methane production and its highly dynamic accumulation in oxic surface waters.

Chapter 5: Comparing Wind-based Models and the Surface Renewal Model with the Flux Chamber Method for Estimating Greenhouse Gas Emission at the Water-air Interface

5.1 Abstract

Reliable estimates of greenhouse gas emission at the water-air interface are important for understanding and quantifying global cycling. Wind-based models, the surface renewal model and flux chamber measurements are different classes for estimating water-air gas transfer. Global assessments mainly rely on wind-based emission models as these empirical models are cheap, simple and use easily obtained wind speed as proxy parameter. A series of wind-based models and the surface renewal model are here compared to flux chamber measurements regarding their ability to provide reliable greenhouse gas emission estimates from a stratified lake in the temperate region. Surface renewal emission estimates generally agreed better with flux chamber measurements versus wind-based models using wind speed only as a proxy. The best agreement with the surface renewal model was found at 3 m s^{-1} wind speed; at lower wind speeds, the surface renewal overestimated the emission whereas at higher wind speeds underestimation was observed. Applied to the here presented dataset, wind-based models predicted mean emission values with up to 52 % deviation compared to flux chamber measurements. When wind-based models are applied to datasets where wind is absent or strong wind only, the deviation is expected to exceed 100 % easily or even 200 %. Best emission prediction was observed when the temperature gradient across the water-air interface was incorporated into a wind-based emission model. Regional and global emission assessments will benefit from including water and air temperature as additional proxy parameter beside wind speed.

5.2 Introduction

Gas transfer at the water-air interface is an important part of greenhouse gas cycling connecting global sources and sinks. For instance, methane efflux from lakes is estimated to account for ca. 20 % of methane emissions to the atmospheric burden (Saunois et al. 2016a). Highly variable methane density fluxes within and across systems introduce large uncertainty in this global estimate (Natchimuthu 2015, Wik et al. 2016a, Sabrekov et al. 2017, Xiao et al. 2017). It is, therefore, crucial that underlying methane density flux estimations are reliable.

General gas transfer. Accurate flux estimation is not trivial as there is a variety of emission classes that can lead to different results (e.g. Duchemin et al. 1999, Kremer

et al. 2003a, Matthews et al. 2003, Dugan et al. 2015, Erkkilä et al. 2018), also the way how measurements are conducted may affect the results (Lorke et al. 2015).

The gas emission from the water-air interface is commonly described by the general gas transfer equation (Tang et al. 2016):

$$F = k * (gas_{water} - gas_{air}) \quad (5.1)$$

Here, F is the gas emission [mmol m^{-2} d^{-1}], k [cm h^{-1}] is the gas transfer constant, and gas_{water} and gas_{air} [mol m^{-3}] refer to gas concentration in the water and atmospheric saturation concentration, respectively. Accordingly, the dimension of the gas emission is controlled by the concentration gradient across the water-air interface and the gas transfer constant. Water- and airside gas concentrations can be measured for example, by deploying gas chromatographic methodologies. Different emission model classes determine different variables within this equation: While the flux chamber approach directly measures the gas emission (F), wind-based models and the surface renewal model estimate the gas transfer constant (k). By knowing k and the concentration gradient, the gas emission can be computed after Equation 5.1.

It is crucial to recognize that gas transfer constants vary among gas types and temperatures. That is why gas transfer constants are typically expressed in standardized notation relative to carbon dioxide at 20 °C (k_{600}) (= oxygen transfer constant at 17.5°C). This study uses methane emission as an example of greenhouse gas emission. The standardized gas transfer constant (k_{600}) and the gas transfer constant for methane at individual temperatures (k_{CH4}) can be transformed into each other using the following formula:

$$k_{CH4} = \frac{k_{600}}{(\frac{Sc}{600})^q} \quad (5.2)$$

The exponent q is a conversion factor dependent on the wind speed (U_{10}) (Jähne et al. 1987): q = -2/3 for U_{10} < 3.7 m s^{-1} and q = -1/2 for U_{10} ≥ 3.7 m s^{-1}. As summarised by Raymond et al. (2012), Schmidt numbers (Sc) for various gases can be reliably estimated by empirically derived temperature formulas (see methods).

Standardized gas transfer constants (k_{600}) are commonly examined when different emission models or model classes are compared to each other.

Flux chamber approach. The flux (or floating-) chamber approach is an emission model class and inexpensive methodology for estimating gas transfer across the water-air interface. This technique deploys a floating chamber on the water surface accumulating emitted gases such as methane over time. Depending on the concentration gradient across the interface, gases also can migrate from the air-phase into the water-phase. The changing gas content over time is quantified via a directly attached Los Gatos GHG analyzer or by drawing gas samples with syringes and remote analysis (e.g. gas chromatography). By knowing the chamber volume and covered water surface area, the methane emission is finally computed via timely regression.

If the concentration gradient across the water air interface is determined in addition to gas emission, gas transfer constants can be computed applying Equation 5.1 and 5.2.

Wind-based models. Wind-based models are a class of emission models predicting k_{600} from empirical equations. Wind speed is the most commonly deployed proxy parameter. These empirical models are typically shaped as follows:

$$k_{600} = n + \mathrm{m} * \mathrm{U}_{10} \tag{5.3}$$

U_{10} [m s^{-1}] is the wind speed at the height of 10 m, and m and n are regression constants. Wind-based models are also commonly expressed as power-law or exponent functions throughout the literature. Deploying these empirical trendline functions allow investigators to estimate gas emission without actually measuring the emission.

The first step for developing wind-based models is gas emission estimation. There is a number of model classes available for estimating gas transfer across the water-air interface. In practice the main methodologies are the flux chamber approach as described above (e.g. Repo et al. 2007, Beaulieu et al. 2012), tracer experiments typically using SF_6 (e.g. Frost and Upstill-Goddard 2002, Matthews et al. 2003), the surface renewal model that requires measurements of turbulence (MacIntyre et al. 2010, Vachon and Prairie 2013), the eddy covariance method (Guerin et al. 2007, Johnsson et al. 2008), and the actively controlled flux technique using heat flux as a proxy (Haußecker and Jähne 1995, Haußecker et al. 1995). The obtained emission, together with measured concentration gradient, is then applied to Equation 5.1 to compute k and subsequently standardized k_{600} (Equation 5.2). Finally, k_{600} is regressed over wind speed, and the hereby obtained trendline function resembles the wind-based model (Equation 5.3).

Investigators are now able to derive the gas emission by measuring wind speed and the concentration gradient and solving Equation 5.1-5.3 in reverse order. This exercise can be even more simplified when average concentration gradients are assumed across systems.

Wind-speed is an easily obtained proxy parameter. This makes wind-based emission models a simple, cheap and time-saving solution for estimating gas emission across systems. Especially studies investigating emission on a regional or global scale make use of wind-based emission models (Bade 2009, Lopez Bellido et al. 2009, Takahashi et al. 2009, Lana et al. 2011, Wanninkhof 2014).

For limnic systems, there are numerous wind-based models available in the literature that were developed by different investigators in different lakes. Figure 5.1 shows an initial comparison of k_{600} values predicted by 9 different wind-based models

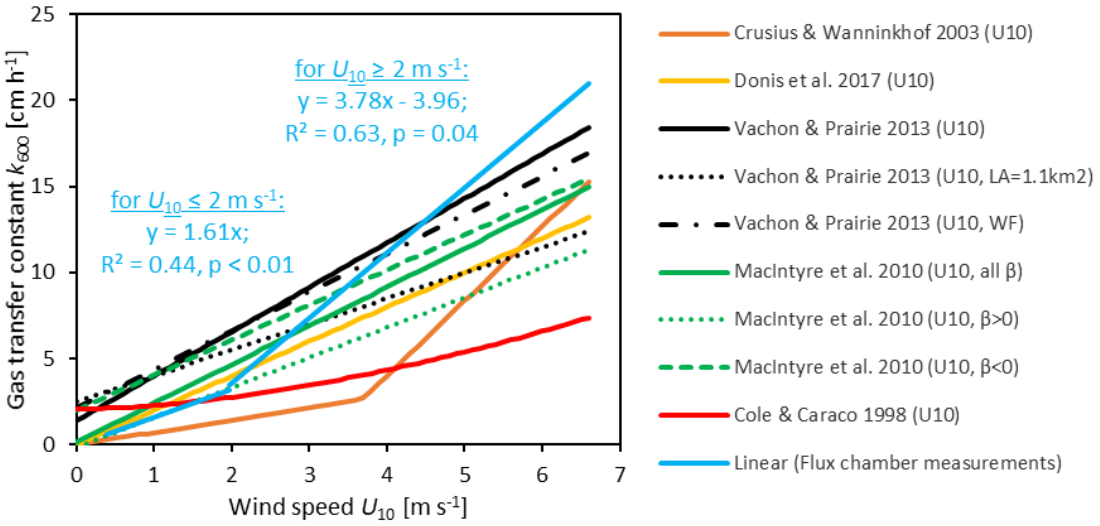

Figure 5.1: Comparison of gas transfer constants (k_{600}) retrieved from various wind-based model predictions and actual flux chamber measurements deploying a floating chamber. Gas transfer constants *predictions used wind-based emission models presented by Cole and Caraco 1998, Crusius and Wanninkhof 2003, MacIntyre et al. 2010, Vachon and Prairie 2013 and Donis et al. 2017. The corresponding wind-based models deploy wind speed, buoyancy flux (MacIntyre et al. 2010), lake area (Vachon and Prairie 2013) and wind fetch (Vachon and Prairie 2013) as a proxy. Applicable proxy and conditions are stated in brackets in the figure legend (U10 - wind speed, LA - lake area, WF – wind fetch). Note, Lake Stechlin accounts for a total lake area of 4.25 km^2 (1.12 km^2 basin), assuming west wind the wind fetch for the location of the flux chamber measurements was about 1.2 km. Flux chamber measurements were done in Lake Stechlin (4.25 km^2) (blue) during summer 2017.*

and k_{600} values computed from actual flux chamber measurements conducted in Lake Stechlin (2017 methane dataset; blue trendline).

The results showed that k_{600} values deviated substantially from each other. Especially the absence of wind and at high wind speeds, k_{600} predictions vary up to a factor of 3. The same deviation is found when k_{600} are translated to emission values (Equation 5.1).

Wind speed is an easily obtained proxy parameter. The gas transfer constant, however, does not depend on wind speed alone. Turbulence in the surface water is the driving force for the transfer of poorly soluble gases such as methane (MacIntyre et al. 1995), which is predominantly modulated by wind forcing and thermal convection from heat loss (Imberger 1985, Schladow et al. 2002, Eugster et al. 2003, McGillis et al. 2004). In fact, heat loss across the water-air interface (which is not accounted for in common wind-based models) can be the dominant driver of turbulence as it has been reported for small and tropical lakes before (MacIntyre and Melack 2009, MacIntyre et al. 2010). While heat loss is driven by the temperature gradient across the water-air interface, wind forcing changes depending on wind speed, wind fetch and wave height (Vachon and Prairie 2013). As summarised in Vachon et Prairie (2010), further parameters have been reported to significantly affect the gas transfer by modulating the near-surface turbulence, such as rainfall (Ho et al. 1997/2007), particulate matter (Abril et al. 2009, Calleja et al. 2009), wave breaking (Zappa et al. 2004), surfactants (Frew et al. 1990, McKenna and McGillis 2004), tidal currents (Borges et al. 2004, Zappa et al. 2007) and microbubbles (McGinnis et al. 2015) and others.

To improve k_{600} predictions, recently developed wind-based models incorporated additional proxy parameters (e.g. lake area and wind fetch; Vachon et al. 2013) and also started to restrict the application of the wind-based models to specific environmental conditions (e.g. positive or negative buoyancy flux β; MacIntyre et al. 2010).

Surface renewal model. An alternative approach to estimate the gas transfer at the water-air-interface is the surface renewal model. Instead of wind speed, this model uses turbulence (TKE dissipation), kinematic viscosity and the Schmidt number as a proxy to compute the gas transfer constant. The connection between gas transfer constant and near-surface turbulence was first described by Dankwerts (1951) and Lamont and

Scott (1970). In this study, the surface renewal model has been parametrised according to Vachon et al. 2010:

$$k = Sc^{-1/2} * (\varepsilon\nu)^{1/4} \quad (5.4)$$

Here ε symbolizes the turbulence (TKE dissipation) [m^2 s^{-3}] which can be determined using, for instance, an acoustic doppler current profiler (ADCP); ν is the kinematic viscosity [m^2 s^{-1}]. The kinematic viscosity can be retrieved from viscosimeter measurements or modelled by empirical temperature equations (Raymond et al. 2012).

Like wind-based models, the k_{600} obtained by the surface renewal model is subsequently used to compute the emission deploying Equation 5.1 and 5.2 what additionally requires the knowledge of the gas concentration gradient across water and air phase.

In contrast to wind-based models, the surface renewal model predicts k_{600} from turbulence which is the driving force of gas transfer across the water-air interface (MacIntyre et al. 1995). As mentioned earlier, wind speed is only one factor affecting the turbulence condition. Using the surface renewal model, therefore, can lead to more reliable emission estimates compared to wind-based models. Despite its potential for reliable emission estimates, the surface renewal model is rarely applied for field measurements (MacIntyre et al. 2010).

Aim. The discrepancy between wind-based models and other wind-based models (e.g. Kremer et al. 2003b, Dugan et al. 2015,) and the discrepancy between wind-based models and the flux chamber approach (Matthews et al. 2003, Erkkilä et al. 2018) has been reported before. Though global assessments depend on these empirical models as mechanistic modelling of every single aquatic system is not possible. In this study, the deviation between the flux chamber approach and wind-based models is determined for a methane dataset in stratified Lake Stechlin; and the deviation is subsequently analysed in regard to what are the environmental conditions leading to high deviation. This analysis will help future studies to estimate gas emission more reliably. Recently developed wind-based models by Vachon and Prairie (2013) incorporate lake area, and wind fetch as an additional proxy parameter to improve the emission prediction. Likewise, MacIntyre et al. (2010) developed wind-based models which are applicable to specific buoyancy flux (β) conditions. Turbulence can be induced by heat loss when the

buoyancy flux β is negative (MacIntyre et al. 2010). However, the calculation of effective heat flux and buoyancy flux requires knowledge of shortwave radiation, visible radiation, net longwave radiation and diffuse attenuation factor (MacIntyre et al. 2010). All these parameters, however, are not commonly recorded throughout routine measurements. Therefore, this chapter investigates if the temperature gradient across the water-air interface (water- and air temperature are routinely measured) can be used to improve emission estimates by wind-based models instead of computing the buoyancy flux.

The deviation between surface renewal predictions and flux chamber measurements has also been reported before (e.g. Vachon et al. 2010). Analog to wind-based models, the deviation between both methodologies is analysed, and environmental conditions leading to high deviation are identified. The obtained relationships between deviation and environmental parameters can be used to correct emission predictions in future studies.

5.3 Methods

This chapter makes use of data collected during the previous study presented in Chapter 4. Methods explained throughout Chapter 4 are briefly described here, for details the reader is forwarded to the corresponding method section of Chapter 4. Methodologies not previously mentioned are fully explained in the following.

Study site. This case study was conducted in the South basin (1.12 km^2) of Lake Stechlin, a meso-oligotrophic lake in the temperate region (NE Germany). Methane in this 4.25 km^2 sized lake has been subject to earlier studies and concentrations up to 1.4 µmol l^{-1} have been observed in the ca. 6.5 m deep epilimnion (Grossart et al. 2011, Tang et al. 2014, McGinnis et al. 2015). Lake Stechlin has a mean depth of ca. 22.7 m and has no river in-/outflow. The measurements were carried out in the South basin of Lake Stechlin at 53°08'36.6"N 13°01'39.5"E throughout the diurnal cycle (every 4h: ca. 03:20/07:20/11:20/15:20/19:20/23:20 local time) from 15th to 25th June 2017.

In situ methane. In situ surface water methane concentration at 0.5 m depth was recorded using an M-CRDS unit that has been previously reported to give reliable results (Hartmann et al. 2018). Continuous measurements over 20 min at a flow rate of 500±5 ml min^{-1} were averaged. The sampling has been automatized by attaching the M-CRDS

tubing to an automatic winch. Methane surface emission was estimated using two approaches.

Flux chamber measurements. Direct measurement of the methane emission (F_{meas}) was done by the floating chamber approach: A freely floating chamber (16.76 l volume; 0.1256 m^2 water surface covered; approx. 2 cm submerged at the perimeter) was deployed on the water surface for approx. 15-20 min. A Los Gatos GHG analyzer (LGR, USA) connected via Tygon 2375-tubings recorded the methane content inside the chamber in a 1 s-interval. The concentration records were linearly regressed over time when the methane content increase was steady (ca. first 10 min) as is described elsewhere (e.g. McGinnis et al. 2015). Flux chamber measurements were done in triplicates (within ca. 45 min) and averaged. The Los Gatos GHG analyzer was also used to determine methane content in the air directly above the water surface. For this purpose, the chamber was kept about 0.5 m above water surface until the air-side methane concentration was stable for about 3 min, and the methane concentration was finally averaged over this time period.

Environmental Parameters. Water temperature was recorded deploying a YSI probe that was attached to an automatic winch and made concurrent measurements with the M-CRDS unit. Air temperature in 21 m height, wind speed in 10 m height, and wind angle were retrieved in hourly intervals from the Umweltbundesamt (Neuglobsow weather station). Using linear regression, the time schedule of provided data was adjusted to times of flux chamber measurements.

Wind-based models. The following wind-based models have been taken from the literature and deployed to estimate the methane surface emission:

Table 5.1: Wind-based models for estimating the gas transfer constants. *Note, in k_{600} notation the gas transfer constant refers to carbon dioxide at 20 °C. For consideration of methane gas exchange, this gas transfer constant must be converted to the methane-based gas transfer constant (k_{CH4}) and ambient temperature.*

Model	Basis	Reference
$k_{600} = 2*U_{10}$	Flux chamber	Donis et al. 2017
$k_{600} = 2.07+0.215*U_{10}^{1.7}$	Tracer	Cole and Caraco 1998
$k_{600} = 0.72*U_{10}$ ($U_{10} < 3.7$ m s^{-1})	Tracer	Crusius and Wanninkhof 2003
$k_{600} = 4.33*U_{10}-13.3$ ($U_{10} \geq 3.7$ m s^{-1})		
$k_{600} = 2.0+2.04*U_{10}$ ($\beta < 0$)	Turbulence	MacIntyre et al. 2010
$k_{600} = -0.15+1.74*U_{10}$ ($\beta > 0$)	Turbulence	MacIntyre et al. 2010
$k_{600} = 0.16+2.25*U_{10}$ (all β)	Turbulence	MacIntyre et al. 2010
$k_{600} = 1.41+2.58*U_{10}$	Turbulence	Vachon and Prairie 2013
$k_{600} = 2.51+1.48*U_{10}+0.39*U_{10}*(\log10\ LA)$	Turbulence	Vachon and Prairie 2013
$k_{600} = 2.13+2.18*U_{10}+0.82*U_{10}*(\log10\ Fetch)$	Turbulence	Vachon and Prairie 2013

k_{600} – gas transfer constant normalized to carbon dioxide at 20 °C [cm h^{-1}]; U_{10} – wind speed in 10 m height [m s^{-1}]; β – buoyancy flux; LA – lake area [km^2]; Fetch – wind fetch [km].

Wind-based models provide standardized gas transfer constants (referring to carbon dioxide at 20 °C) using wind speed and other proxy parameters. To compute actual methane emission values, predicted k_{600} values were transformed to methane-based gas transfer constants at ambient temperature (k_{CH4}) using Equation 5.2.

The wind-based models presented by Vachon and Prairie (2013) use lake area and wind fetch as additional proxy parameters beside wind speed. Lake area was extracted from bathymetry data. Wind fetch was estimated graphically. Cardinal directions have been divided into 16 segments, each being a 22.5° interval (0 + n*22.5°). For each segment, the average distance between shoreline and sampling locations has been determined by comparing corresponding GPS locations using the haversine function (assuming spherical earth with a mean radius rad_{earth} = 6371 km) using the following equations[6]:

$$fetch = rad_{earth} * [2\ \text{atan2}\left(\sqrt{m}, \sqrt{1-m}\right)], \tag{5.5}$$

$$m = sin^2\left(\frac{\Delta\varphi}{2}\right) + \cos(\varphi_1) * \cos(\varphi_2) * sin^2\left(\frac{\Delta\lambda}{2}\right), \tag{5.6}$$

where φ and λ is latitude and longitude coordinate respectively (radians format). Wind fetches are summarised by the following table:

[6] A script for automated computation of distances between GPS coordinates was written by Chris Veness and is available online via https://www.movable-type.co.uk/scripts/latlong.html.

Table 5.2: Average wind fetch during flux chamber measurements in the South basin of Lake Stechlin in summer 2017 at different wind angles. *Wind angle data were provided by the Umweltbundesamt (Neuglobsow weather station next to the Lake Stechlin).*

Wind angle [°]	Average wind fetch [km]	Wind angle [°]	Average wind fetch [km]
0-22.5	2.49	180-202.5	0.38
22.5-45	1.28	202.5-225	0.48
45-67.5	1.02	225-247.5	0.67
67.5-90	0.52	247.5-270	1.10
90-112.5	0.29	270-292.5	1.01
112.5-135	0.25	292.5-315	0.60
135-157.5	0.25	315-337.5	0.45
157.5-180	0.28	337.5-360	0.39

The wind-based models developed by MacIntyre et al. 2010 are applied to different buoyancy flux (β) conditions. The authors concluded that three models were applicable when β is negative or positive or the data set contains both, positive and negative β values. When β is negative, heat loss increases near-surface turbulence and modulates the surface emission. In this chapter, the temperature gradient between air and water (T_{air} - T_{WS}) is tested if it can substitute the buoyancy flux condition to improve wind-based model predictions. Accordingly, the wind-based model for negative β is applied to the data set when the temperature gradient is negative. Likewise, the wind-based model for positive β is applied when the temperature gradient is positive. βind is used throughout this chapter, referring to this substitution.

Parameters necessary for transforming k_{600} to k_{CH4} and subsequent calculation of methane surface emission are summarised in Supplementary Table S5.5.

Surface renewal model. Current velocities were recorded by a pulse-coherent high-resolution acoustic doppler profiler HR Aquadopp (ADCP) from Nortek AS, Norway (2 cm-resolution at a 50 Hz frequency), and were transformed into turbulence TKE dissipation (Supplementary Note 6.2). The turbulence data were extracted in a 1 h-interval. Using $\log_{10}$-transformation and linear regression, the turbulence data was adapted to the time schedule of flux chamber measurements. Mean TKE dissipation values were retrieved by averaging $\log_{10}$-transformed values from 0.5 to 2.0 m depth (0.02 m intervals).

The kinematic viscosity ν [cm^2 s^{-1}] of water has been modelled using the following empirical function (Raymond et al. 2012) and feeding temperature T data [°C]:

$$\nu = [1.735 * (10^{-2})] - [5.023 * (10^{-4}) * T] + [8.598 * (10^{-6}) * T^2] + [8.598 * (10^{-8}) * T^3] \quad (5.7)$$

The dimensionless Schmidt number Sc is the ratio of kinematic viscosity ν and the diffusion coefficient D (Jähne et al. 1987) and, alternatively, can be computed using gas specific empirical equations (Wilke and Chang 1955, Wanninkhof 1992, Raymond et al. 2012), where T is temperature expressed in °C:

$$Sc = [1898] - [114.28 * T] + [3.29 * T^2] - [0.0391 * T^3] \quad (5.8)$$

TKE dissipation together with kinematic viscosity and Schmidt number was applied to the surface renewal model (Equation 5.4) to compute gas transfer constants. Methane emission was finally computed by applying gas transfer constants and the methane concentration gradient to Equation 5.1. Note, F_{calc} was used throughout this chapter to indicate methane emission computed from the surface renewal model.

Note, the different methods to estimate gas emission are compared by examining k_{600} values. k_{CH4} and k_{600} can be transformed into each via Equation 5.2.

Standard error. To evaluate the mean difference between k_{600} values estimated via different methods, the standard error (SE) was computed as after the following formula (a and b symbolize different methods and n is the number of data points):

$$SE = \left(\frac{\sum({k_{600}}^a - {k_{600}}^b)^2}{n-2}\right)^{1/2} \quad (5.9)$$

5.4 Results

Field observation. The field campaign in the South basin of Lake Stechlin from 15th to 25th June 2017 (ca. 20 m deep water column) was characterized by mainly calm weather conditions with wind speeds ranging from low values (0.4 m s^{-1}) to moderate wind speed regimes (6.6 m s^{-1}) for inland waters (Figure 5.2b) and low precipitation (occasional not intense rain, not recorded). Near-surface turbulence in the epilimnion, which was measured using an ADCP unit (here TKE dissipation or ε), followed the general trend of wind speed with less distinct peaks (in 0.5 to 2 m depth) (Figure 5.2a, g). Turbulence conditions in epilimnic water can be classified as low (log10 ε < -8), medium (-8 < $\log_{10}$ ε > -6) or high ($\log_{10}$ ε < -6). Following this classification, the near-surface turbulence condition was mainly in the middle range (mean -7.3 m^2 s^{-3}) but

occasionally reached low regime (down to -8.9 m^2 s^{-3}) and the border to highly turbulent condition (up to -6.0 m^2 s^{-3}). While air temperature varied throughout the diurnal cycle between 11 and 30 °C, the water surface temperature remained stable at mean±SD 21±2 °C (Figure 5.2b). Methane surface water concentrations recorded by an M-CRDS unit generally ranged from 0.4 to 0.7 µmol l-1 (Figure 5.2c). During the first half of the study period, the values were slightly lower (mean±SD 0.44±0.04 µmol l^{-1}) versus the second half (mean±SD 0.56±0.07 µmol l^{-1}). Air-side methane concentrations were measured with a Los Gatos GHG analyzer and scattered between 1.8 and 1.9 ppm (Figure 5.2c).

The surface methane emission retrieved from flux chamber measurement (F_{meas}) showed a similar pattern to wind speed (Figure 5.2d) with a mean±SD 0.95±0.81 mmol m^{-2} d^{-1}. By contrast, emission values retrieved the surface renewal model (F_{calc}) did not always follow the wind pattern and showed partially higher and lower values with mean±SD 0.90±0.32 mmol m^{-2} d^{-1} (Figure 5.2g). As indicated by the standard deviations, F_{calc} values scattered in a narrower range versus F_{meas}. When F_{meas} was in the range of 1 to 2 mmol m^{-2} d^{-1} F_{calc} had similar values, outside this range there was a positive and a negative deviation between both emission parameters. The wind-based models (Figure 5.2d-f) predicted methane emission also generally following the trend of wind with less distinct peak pattern. Wind-based models by Cole and Caraco (1998), Crusius and Wanninkhof (2003) predicted mainly lower effluxes compared to the flux chamber approach. The wind-based models after Vachon and Prairie (2013) and MacIntyre et al. (2010), as well as after Donis et al. (2017) predicted emission values mainly in the middle range compared to flux chamber measurements.

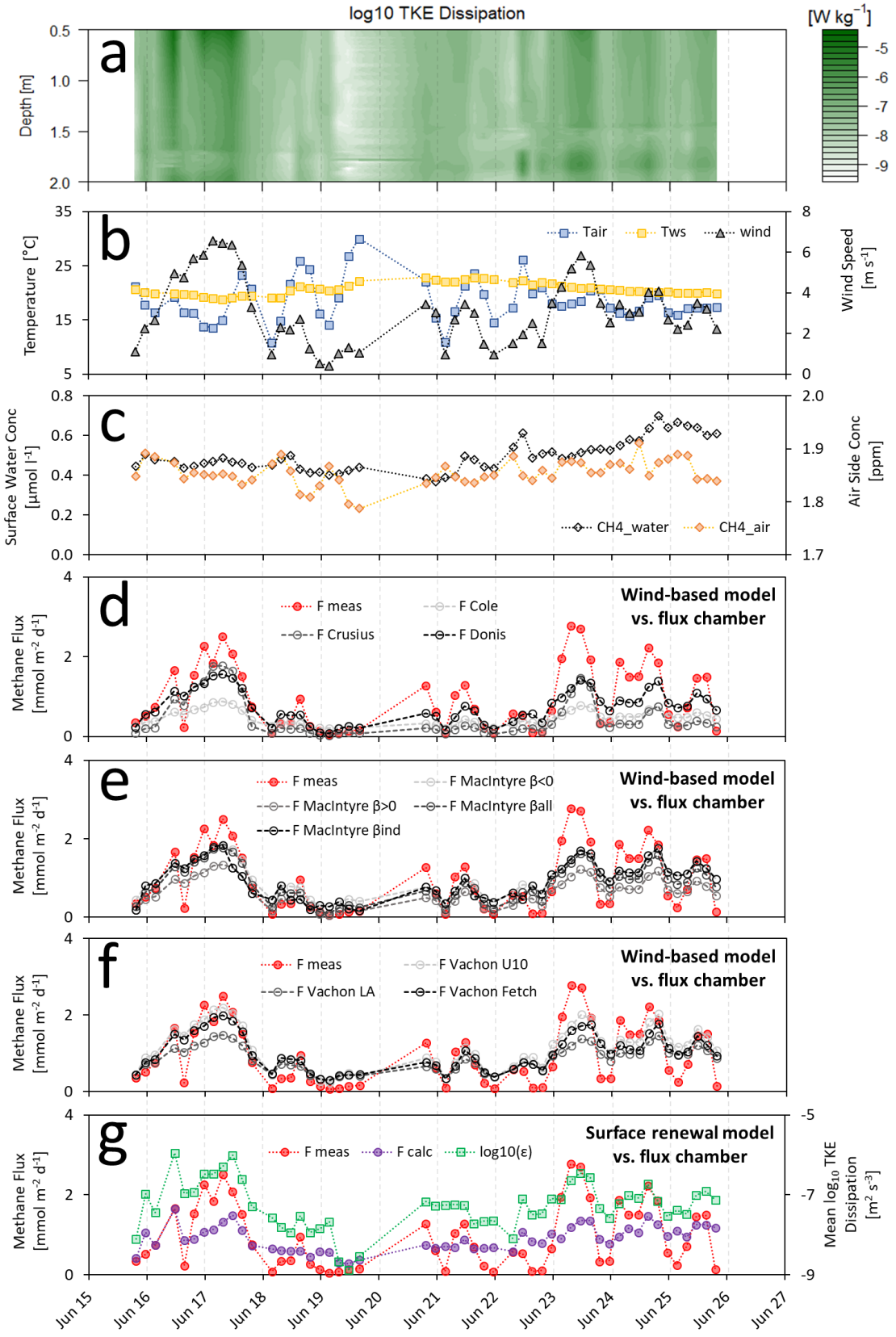

Figure 5.2: Parameter time series in Lake Stechlin of the 2017 summer field campaign in Lake Stechlin. *TKE dissipation is shown in panel (**a**) expressed as log_{10}. Values below -8 indicate low or no turbulence condition, between -8 and -6 is medium turbulence range, and above -6 the water column is highly turbulent. Temperature data for air (T_{air}) and surface water (T_{WS}), as well as wind speed, are displayed in*

*panel (**b**). Concurrently recorded methane content in the surface water (CH4_water) and in the air directly above the water surface (CH4_air) are depicted in panel (**c**). TKE dissipation values were averaged in log_{10} format. Methane emission estimated from wind-based models are compared to flux chamber emission values in panel **d-f**: F_{Cole} (Cole and Caraco 1998), $F_{Crusius}$ (Crusius and Wanninkhof 2003), F_{Donis} (Donis et al. 2017), $F_{MacIntyre\ B<0}$ (MacIntyre et al. 2010; negative buoyancy flux model applied to all data points), $F_{MacIntyre\ B>0}$ (MacIntyre et al. 2010; positive buoyancy flux model applied to all data points), $F_{MacIntyre\ Ball}$ (MacIntyre et al. 2010; any buoyancy flux model applied to all data points), $F_{MacIntyre\ Bind}$ (MacIntyre et al. 2010; individual application of models for positive/negative buoyancy flux), $F_{Vachon\ U10}$ (Vachon and Prairie 2013; only wind speed as proxy), $F_{Vachon\ LA}$ (Vachon and Prairie 2013; wind speed and basin size as proxy), $F_{Vachon\ Fetch}$ (Vachon and Prairie 2013; wind speed and wind fetch as proxy). The average TKE dissipation from 0.5 to 2.0 m depth is given together with methane surface emission measured by the floating chamber approach (F_{meas}) and estimated from the surface renewal model (F_{calc}) in panel (**g**). k_{600} predicted by wind-based models or the surface renewal model were used to subsequently compute methane emission (deploying the general gas transfer formula). Water temperature was recorded by a YSI probe, and air temperature was provided by the Umweltbundesamt together with wind speed. The data set contains 52 time points for each parameter. R (v.3.3.1), RStudio (v.1.0.153) and MS Office (v.365 ProPlus) have been used deployed to create the plots.*

Comparison of k_{600}. First, the k_{600} values were estimated via flux chamber measurements, wind-based models, and by the surface renewal model and subsequently averaged. Then, the deviation of wind-based mean k_{600} or surface renewal mean k_{600} from the flux chamber mean k_{600} was calculated. The results are given by Table 5.3. To additionally characterize the various k_{600} predictions, k_{600} values were linearly regressed, and statistical parameters were calculated (coefficient of determination, p-value, standard error) (Table 5.3). k_{600} predicted by all emission models showed significant correlation with flux chamber k_{600} values explaining 54 to 73 % of the variance, indicating that wind forcing was a major driving force for the methane transport across the water-air interface. The flux chamber measurements resulted in a mean k_{600} value of 7.93±6.65 cm h^{-1}. As suggested by the standard deviation, the flux chamber approach showed the highest range of k_{600} values; predictions of alternative emission models scattered in a smaller range.

Table 5.3: Comparison of k_{600} values obtained from flux chamber measurements with prediction by various wind-based models and k_{600} values obtained from the turbulence approach.

	Model	k_{600} mean±SD [cm h^{-1}]	Deviation [%]	R^2 [ ]	p [ ]	St. Error [cm h^{-1}]
	Flux Chamber	7.93±6.65				
wind-based models	Cole	3.78±1.46	(-) 52	0.72	<0.001	6.96
	Crusius	3.85±4.20	(-) 51	0.62	<0.001	5.95
	Donis	6.17±3.35	(-) 22	0.73	<0.001	4.57
	MacIntyre β<0	8.29±3.42	(+) 5	0.73	<0.001	4.18
	MacIntyre β>0	5.22±2.92	(-) 34	0.73	<0.001	5.25
	MacIntyre βall	7.10±3.77	(-) 10	0.73	<0.001	4.07
	MacIntyre βind	7.67±3.67	(-) 3	0.66	<0.001	4.28
	Vachon U_{10}	9.37±4.33	(+) 18	0.73	<0.001	4.02
	Vachon LA	7.13±2.51	(-) 10	0.73	<0.001	4.80
	Vachon Fetch	8.47±3.79	(+) 7	0.72	<0.001	4.07
	Surface renewal model	7.49±2.36	(-) 6	0.54	<0.001	5.25

Deviation indicates the percentage difference of the modelled k_{600} mean relative to the flux chamber k_{600} mean. Standard error was calculated as defined in the method section. If not other clarified the whole dataset was applied to the model (n = 52). Flux chamber – own flux chamber measurements; Cole – model described in Cole and Caraco(1998); - Crusius – model described in Crusius and Wanninkhof (2003); Donis – model described in Donis et al. (2017); MacIntyre – models described in MacIntyre et al. (2010); Vachon – models described in Vachon and Prairie (2013); Surface renewal model – refers to determining k_{600} from turbulence measurements combined with the surface renewal model. Note: MacIntyre models are differentiated by buoyancy flux (β) condition and all models have been applied to the full data set (n = 52). βind refers to differentiation of the buoyancy flux condition – when surface water temperature was higher than air temperature the β<0 model was deployed (n = 41) otherwise the β>0 model (n = 11). Models by Vachon and Prairie (2013) use wind speed (U_{10}) and additionally lake/basin area (LA) or wind fetch (Fetch) as proxy parameter. Wind data and air temperature was provided by the Umweltbundesamt. Water temperature was measured by a YSI probe and wind fetch was determined as described throughout the method section.

Wind-based models developed by Cole and Caraco (1998) and Crusius and Wanninkhof (2003) computed k_{600} means with substantial deviations of ca. 50 % versus flux chamber means. Also, these models showed the highest standard errors: In average, they predicted values that are 6 to 7 cm h^{-1} less the flux chamber values. All other models showed standard errors of ca. 4 to 5 cm h^{-1}. Best predictions of the mean k_{600} were obtained by MacIntyre et al. (2010) model βind when temperature gradient data was applied to the model prediction (only 3 % deviation). Also, the β<0 model (MacIntyre et al. 2010) resulted in good predictions with 5 % deviation. The wind-based model after Vachon and Prairie showed intermediate deviation of 18 %. Incorporating lake area or wind fetch improved the k_{600} predictions (10 or 7% deviation). The wind-based model developed by Donis et al. (2017) showed moderate deviation (22 %).

The surface renewal model provided good mean k_{600} estimations with only 6 % deviation albeit with a 5 cm h^{-1} standard error. Best predictions by wind-based models and predictions by the surface renewal model are very close to each other, but the surface renewal model had a ca. 25% higher standard error.

Error analysis. The various wind-based models and the surface renewal model use different proxy parameters: Wind speed (U_{10}), wind fetch (Fetch), buoyancy flux (β) (here the temperature gradient is used instead of β) and turbulence ($\log_{10}\varepsilon$).

While wind showed a strong linear correlation with the measured turbulence ($R^2 = 0.68$, $p < 0.001$, $n = 52$), temperature gradient only correlated at low wind speeds ($U_{10} \leq 1.3$ m s^{-1}) ($R^2 = 0.70$, $p = 0.003$, $n = 10$), and wind fetch did not show any significant correlation (tested for all data, low wind speed $U_{10} \leq 1.3$ m s^{-1} and high wind speed regime $U_{10} \geq 5.0$ m s^{-1}). To investigate under which condition the wind-based models and the surface renewal approach predicted lower or higher k_{600} values, the difference between k_{600} values was computed as k_{600}(model) – k_{600}(flux chamber) (in the following referred to as error). The error was subsequently correlated against the proxy parameters (Table 5.4), and significant correlations were plotted (Figure 5.3 and 5.4).

For all gas transfer models, the error has been found to be significant in relationship with wind speed which is underlined by the correlation with turbulence dissipation $\log_{10}(\varepsilon)$ resulting in very comparable regression statistics (Table 5.4). The explanatory power of wind speed scattered between 14 and 61 % (mainly between 20 and 30%) indicating that the different techniques capture wind forcing differently well. Wind fetch was only found in the wind-based model after Cole and Caraco (1998) and in the surface renewal approach to affect the error (6 – 9 % variance). The temperature gradient did not show any significant influence in the complete dataset. Only when low wind speed data points ($U_{10} \leq 1.3$ m s^{-1}; $n = 10$) were isolated, the temperature gradient explained the majority of variance (56 – 80 %) in the errors observed for the MacIntyre model βind and for the surface renewal approach.

Table 5.4: Influence of different environmental parameters on the discrepancy between k_{600} estimation by flux chamber measurements and wind-based models or the surface renewal model, respectively. *The difference between the k_{600} values was computed as k_{600}(model) – k_{600}(flux chamber) and correlated against wind speed (U_{10}), wind fetch (Fetch), temperature gradient and TKE dissipation ($\log_{10}(\varepsilon)$). Statistical parameters were computed after linear regression.*

Model	U_{10}		Fetch		T-gradient (all U_{10})		T-gradient ($U_{10} \leq 1.3$)		$\log_{10}(\varepsilon)$	
	R^2	p	R^2	p	R^2	p	R^2	p	R^2	p
Cole	0.61	<0.01	0.06	0.07	0.00	0.93	0.27	0.12	0.47	<0.01
Crusius	0.19	<0.01	0.00	0.94	0.00	0.99	0.22	0.17	0.18	<0.01
Donis	0.32	<0.01	0.03	0.19	0.00	0.81	0.06	0.51	0.27	<0.01
MacIntyre β<0	0.30	<0.01	0.03	0.20	0.00	0.81	0.05	0.52	0.26	<0.01
MacIntyre β>0	0.39	<0.01	0.04	0.13	0.00	0.82	0.09	0.41	0.32	<0.01
MacIntyre βall	0.24	<0.01	0.02	0.27	0.00	0.79	0.04	0.60	0.21	<0.01
MacIntyre βind	0.28	<0.01	0.04	0.15	0.03	0.21	0.56	0.01	0.20	<0.01
Vachon U_{10}	0.14	0.01	0.01	0.45	0.00	0.76	0.01	0.74	0.14	0.01
Vachon LA	0.46	<0.01	0.05	0.10	0.00	0.85	0.12	0.34	0.37	<0.01
Vachon Fetch	0.24	<0.01	0.00	0.68	0.00	0.76	0.05	0.54	0.22	<0.01
Surface renewal model	0.53	<0.01	0.09	0.03	0.00	0.66	0.80	<0.01	0.26	<0.01

Cole – model described in Cole and Caraco(1998); - Crusius – model described in Crusius and Wanninkhof (2003); Donis – model described in Donis et al. (2017); MacIntyre – models described in MacIntyre et al. (2010); Vachon – models described in Vachon and Prairie (2013); Surface renewal model – refers to determining k_{600} from turbulence measurements combined with the surface renewal model. The dataset contained n = 52 time points for all wind speeds or or n = 10 for $U_{10} \leq 1.3$ m s^{-1}. Note, temperature gradient (T-gradient) was computed as $T_{air} - T_{WS}$. Grey font indicates correlations with p values ≥0.10.

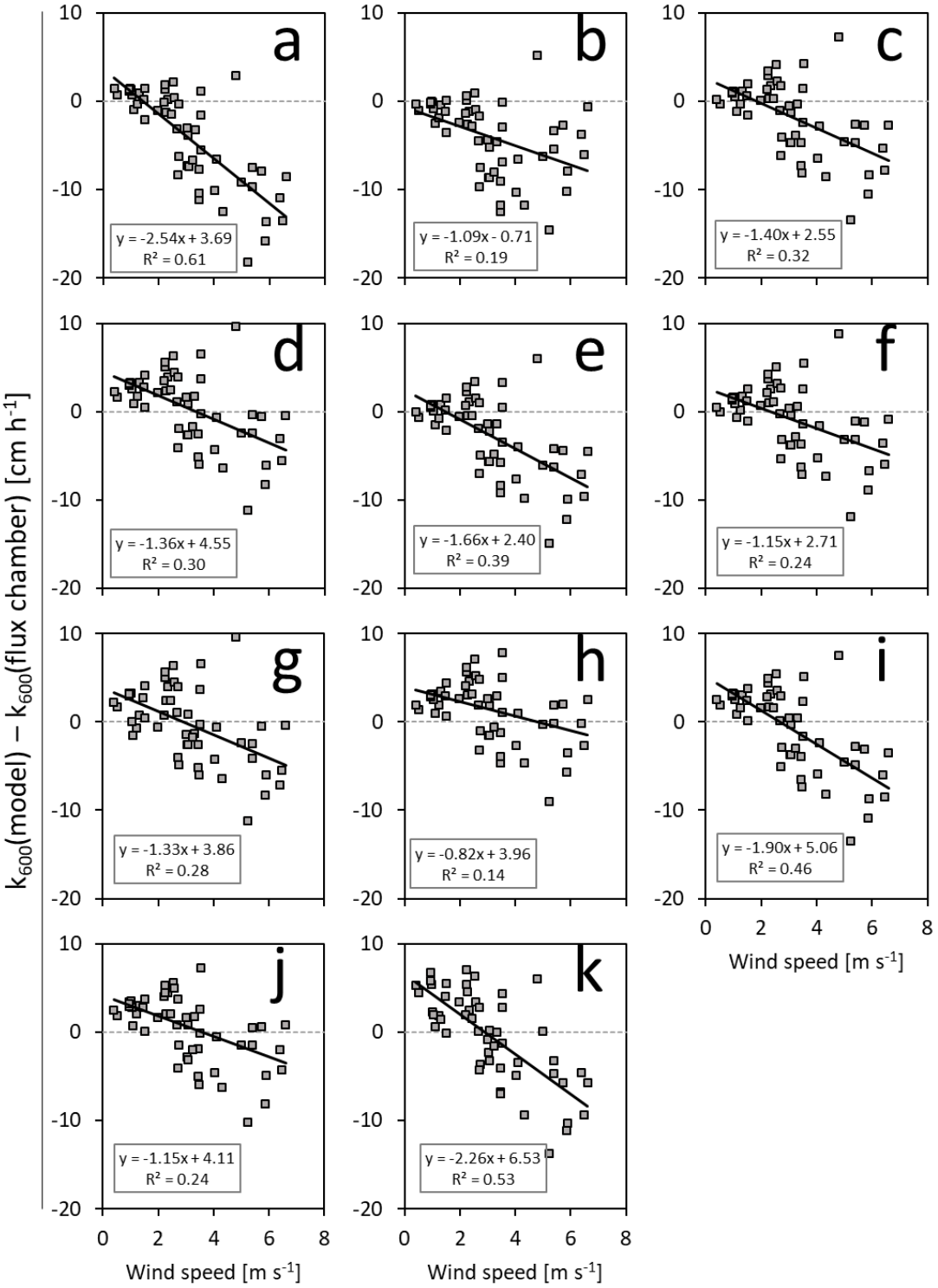

Figure 5.3: k_{600} deviation in relation to wind speed. *The different panels display k_{600} deviation of various wind-based models and the surface renewal approach relative to k_{600} values of flux chamber measurements conducted in Lake Stechlin (2017): Cole and Caraco 1998 (**a**), Crusius and Wanninkhof 2003 (**b**), Donis et al. 2017 (**c**), MacIntyre et al. 2010 – $B<0$ (**d**), MacIntyre et al. 2010 – $B>0$ (**e**), MacIntyre et al. 2010 – Ball (**f**), MacIntyre et al. 2010 – Bind (**g**), Vachon and Prairie 2013 – U_{10} (**h**), Vachon and Prairie 2013 – LA (**i**), Vachon and Prairie 2013 – Fetch (**j**),surface renewal model (**k**).*

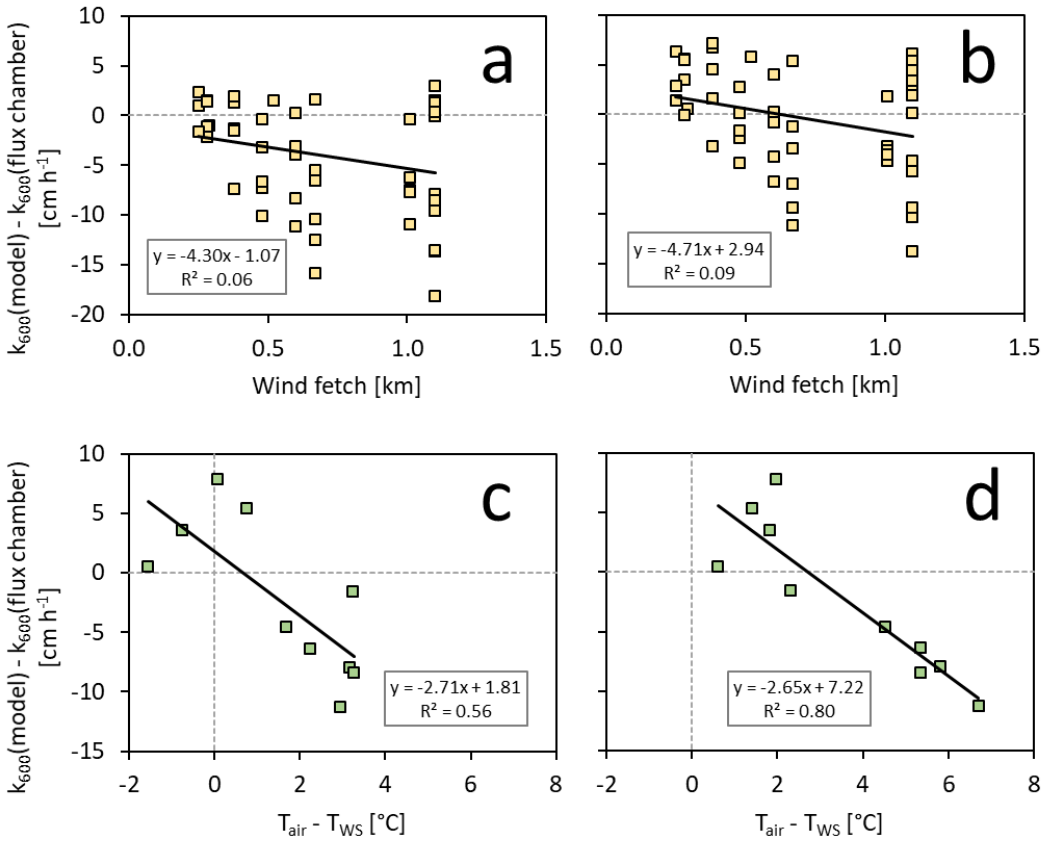

Figure 5.4: k_{600} deviation in relation to wind fetch and temperature gradient across the water-air interface. *The k_{600} deviation is plotted over wind fetch (n = 52) for the model by Cole and Caraco 1998 (**a**) and the surface renewal approach (**b**). Further, the deviation is plotted over air-water temperature gradient (n = 10) for the MacIntyre et al. 2010 – wind model (**c**) or the surface renewal approach (**d**). The temperature gradient was calculated as $T_{air} – T_{WS}$.*

The graphical illustration of the significant relationships (Figure 5.3) showed that the wind-based models by Cole and Caraco 1998 and Crusius and Wanninkhof 2003, as well as Donis et al. 2017, predicted low error k_{600} values in the low wind speed regime (< 3 m s^{-1}). Under high wind speed (> 3 m s^{-1}) they predict substantially smaller k_{600} values compared to flux chamber measurements. The wind-based models after MacIntyre et al. 2010 and Vachon et al. 2013, and the surface renewal model showed different trends: At wind speed of ca. 3 m s^{-1} the k_{600} estimation agreed very well with the flux chamber measurements; at lower wind speed the flux chamber values were smaller, and at wind speed above 3 m s^{-1} the flux chamber values were higher versus the other methods. Combining the corresponding trendline functions of all wind-based models by MacIntyre et al. 2010 and Vachon et al. 2013 showed small variation in the

regression constants (ca. 25 %): k_{600} error [cm h^{-1}] = -1.34(±0.36)*U_{10} [m s^{-1}] + 3.81(±0.95).

Wind fetch showed correlation with k_{600} error resulting from Cole and Caraco 1998 predictions and from surface renewal predictions (Figure 5.4). In both cases, higher wind fetch appeared underestimation of k_{600} values. Nevertheless, the intercept at error = 0 varied (ca. 0 or 0.5 km, which is about half of the total wind fetch range) and the explanatory power was low (<10 %).

At low wind speed regime (U_{10} ≤ 1.3 m s^{-1}) higher (more positive) temperature gradients caused underestimated k_{600} (Figure 5.4) and lower gradients led to overestimations in case of the wind-based model MacIntyre et al. 2010 – βind model, and in case of the surface renewal model. When the temperature gradient $T_{air} – T_{WS}$ was about 1 to 2 °C, the flux chamber k_{600} predictions agreed with the other two approaches (error approx. 0 cm h^{-1}). With 56 – 80 %, the temperature gradient seemed to cause most of the error variance at low wind speeds.

5.5 Discussion

In this chapter, a series of wind-based literature models and the surface renewal model were compared to actual flux chamber measurements regarding their potential to estimate reliable emission values (represented by gas transfer constants). The (standardized) gas transfer constant k_{600} is an important characteristic of the water-air gas transfer and (in addition to the concentration gradient) controls the gas transfer. Here presented k_{600} values are based on methane measurements conducted in 2017 in stratified Lake Stechlin, Germany. In general, the observed methane emission ranged from 0.05 to 2.77 mmol m^{-2} d^{-1} what is in the range that has been reported earlier for Lake Stechlin (up to 4.36 mmol m^{-2} d^{-1} at wind speed above 5 m s^{-1}; McGinnis et al. 2015).

While wind-based models developed by Cole and Caraco 1998, Crusius and Wanninkhof 2003, Donis et al. 2017 use wind speed only as proxy, models by Vachon and Prairie 2013 use wind speed and additionally lake area or wind fetch as a proxy parameters. MacIntyre et al., 2010 developed wind-based models for different buoyancy flux conditions. Here the temperature gradient across the water-air interface was tested regarding its potential to substitute the buoyancy flux and improve k_{600} predictions. In

contrast, the surface renewal model makes use of turbulence, Schmidt number and kinematic viscosity to predict k_{600} values.

The deviation of predicted k_{600} versus k_{600} retrieved from flux chamber measurements (referred to as error) was examined with respect to what are the environmental controls for the difference. In the light of highly variable greenhouse gas density fluxes from freshwater systems worldwide (e.g. methane: Natchimuthu 2015, Wik et al. 2016a, Sabrekov et al. 2017, Xiao et al. 2017), accurate estimations are important to properly parametrise global assessments such as the global methane cycle (Saunois et al. 2016a). Also, regional constraints (e.g. assessments of the oxic methane source in Lake Stechlin presented throughout previous chapters) depend on reliable gas flux determination.

Wind-based models. Wind-based models using wind speed as a proxy parameter are a popular choice for estimating k_{600} constants, for example, studies investigating gas transfer between the ocean and air (Takahashi et al. 2009, Lana et al. 2011, Wanninkhof 2014). When wind-based models are applied to other systems, the accuracy of predicted emission relates to how much turbulence is explained by the proxy parameter in the model system and in the target system, respectively. Especially in small and sheltered lakes physical condition can largely vary among and within the system (Vachon and Prairie 2013). Strictly speaking, if the physical condition of the sampling locations in the original lake and the target lake differ too much, the wind-based model will predict unreliable values. In this study all wind-based models predicted k_{600} values that are significantly related to k_{600} estimates from flux chamber measurements (Table 5.3). The trendline functions covered most of the variance (66 to73 %) between the datasets. While these parameters describe a similar trend, the absolute values showed substantial deviation as it was indicated by the mean values and the standard error (Table 5.3). The flux chamber measurements resulted in a mean k_{600} value of ca. 8 cm h^{-1}. In comparison, the wind-based models ranged between 4 and 9 cm h^{-1}, which renders deviations up to 52 %. Also, the standard error indicated that wind-based models vary strongly (4 to 7 cm h^{-1}). Comparable emission deviation has been reported earlier for aquatic systems even under the same wind speed condition and, when the same investigator is conducting the measurements: e.g. 30-50% (Marino and Howarth 1993, Kremer et al. 2003b).

The k_{600} errors recognized between the methods can have two types of causes: Systematic errors will emerge when the original study lake and the target lake differ in physical properties; further, every technique for estimating gas transfer is prone to individual bias introducing discrepancy and k_{600} error.

Lake area is a morphological characteristic substantially affecting the physical lake condition. With lake size affects a series of other parameters including effective wind forcing (wind speed, wind fetch; Vachon and Prairie 2013), depth of the surface mixed layer (MacIntyre et al. 2010), wave breaking (Zappa et al. 2004), tidal current (Borges et al. 2004, Zappa et al. 2007) and internal seiches (Kirillin et al. 2015). Vachon and Prairie (2013) investigated a series of lakes with different surface areas from 0.19 km^2 to 602 km^2, but mainly in the 602 km^2 sized hydroelectric reservoir (irregularly shaped; many islands). The authors found that k_{600} relates to lake size. This is reflected by the results presented here. When the corresponding wind-based model was applied to the Stechlin dataset, the mean k_{600} deviation was 18 % (R^2 = 0.73), and when lake size was additionally accounted beside wind speed, the deviation decreased to 10 % (R^2 = 0.73). In the same way, the deviation was smaller when the wind fetch was accounted for together with wind speed. k_{600} deviation, here, was only 7 % (R^2 = 0.72). Wind-based models presented in Cole and Caraco (1998) and Crusius and Wanninkof (2003) resulted in the highest deviation from own turbulence-based estimates (ca. 50 % each). These studies were conducted in two lakes of similar sizes. While Mirror lake in New Hampshire is 0.15 km^2 (10 m max depth) (Cole and Caraco 1998) and Lake 302N in Ontario is 0.13 km^2 (13.8 m max depth) (Brunskill and Schindler 1971), Lake Stechlin's South basin is about ten times larger (total: 4.25 km^2 with 69.5 m max depth; South basin: 1.12 km^2 with 34.5 m max depth). The comparable size of Mirrow Lake and Lake 302N might be responsible for similar mean k_{600} values. However, the size differences compared to Stechlin might have caused huge k_{600} deviation when applied to the Stechlin dataset. Likewise, the wind-based model of Donis et al. 2017 was developed in 10.2 km^2 sized Lake Hallwil, Switzerland, (1 basin) and, accordingly, the size difference might have caused the k_{600} prediction with intermediate deviation. Lake Meräsjarvi (3.8 km^2, 2 major embayments) which was investigated by MacIntyre and colleagues is closest to Lake Stechlin and its South basin regarding system size. Additionally, MacIntyre et al. differentiated buoyancy flux (β) conditions resulting in 3 different wind-based models for the conditions when β is negative, positive, or both conditions are included. In this

Chapter, the temperature gradient across the water-air interface was used as a proxy to identify account for turbulence induced by heat loss (occurs if β is negative). The temperature gradient was computed and depending on whether the value is positive or negative, a different wind-based model has been applied to the methane dataset. Application of the temperature gradient data resulted in the best k_{600} prediction of all models. This outcome suggests that using water and air temperature as additionally proxy parameters can improve emission predictions. This is a major advantage as temperature data is recorded throughout routine measurements.

At high wind speed regime, wind forcing-driven turbulence outweighs heat flux-driven turbulence whereas at low wind speed regime wind forcing is not the major turbulence control (Wanninkhof et al. 1987, MacIntyre et al. 2010). This might be the reason for temperature gradient being significantly correlated with only one literature model (MacIntyre βind) when wind speed was $U_{10} \leq 1.3$ m s^{-1}. Missing correlation between k_{600} and temperature gradients across the water-air interface has been noticed before (e.g. Cole and Caraco 1998). Nevertheless, the dataset showed that including the temperature gradient could improve k_{600} predictions. It is unclear if the studies Cole and Caraco (1998), Crusius and Wanninkhof (2003), Donis et al. (2017) and Vachon and Prairie (2013) investigated lakes with different temperature settings versus the Stechlin campaign (missing information). Surface water in the studies Crusius and Wanninkhof (2003) and Donis et al. (2017) showed a bigger temperature range compared to the 2017 Stechlin campaign, which might suggest different temperature gradients.

Wind fetch did not show any strong correlation with the k_{600} error of wind-based models. Only the Cole and Caraco (1998) model appeared to have a very weak correlation ($R^2 = 0.06$). Using wind fetch as second proxy parameter, however, improved the k_{600} prediction by the Vachon and Prairie model. The Stechlin dataset contains only a single sampling site in the lake's South basin (1.12 km^2). Depending on the wind angle, the wind fetches varied between 0.25 and 1.10 km. In contrast, Vachon and Prairie examined lakes with up to 602 km^2 surface area where wind fetch can vary within a considerably higher magnitude. Accordingly, wind fetch becomes a more important proxy when a range of lakes with different areas are investigated. It is, however, unclear to which extent lake surface area as proxy already covers the explanatory power of wind fetch. Wind fetch considerations may be more important when basin-central sites are compared with near-shore sites.

Wind-based models are easy in use as wind speed data are available. Nevertheless, lake physics is complex, and the explanatory power of wind speed for turbulence conditions varies among and within lake systems. Wind-based models will also be used for regional and global emission assessments in future studies. In this regard, an important question to ask is how much error is tolerated when these models are applied across the vast system heterogeneity of lakes. To reduce the error of wind-based models, it will be beneficial to restrict their applicability to systems with similar morphological properties (size, depth, aspect ratio, etc.). Clear systematics (e.g. lake size; Frost and Upstill-Goddard 2002, Vachon and Prairie 2013) and guidance under what meteorological conditions the models are applicable (e.g. buoyancy flux; MacIntyre et al. 2010) will help produce more reliable estimates of gas emission. For the case that wind-based models are applied globally to many lakes with different properties, classification after climate zones might improve emission predictions as turbulence modulating factors like precipitation (Ho et al. 2007/1997), and temperature settings (Duchemin et al. 1999, MacIntyre et al. 2010) are largely different among climate zones. For assessments of individual lakes, especially for comparing basin-central and near-shore sites, additional factors such as particulate matter (Abril et al. 2009, Calleja et al. 2009), wave breaking (Zappa et al. 2004), surfactants (Frew et al. 1990, McKenna and McGillis 2004), tidal currents (Borges et al. 2004, Zappa et al. 2007) and microbubbles (McGinnis et al. 2015) should be considered.

It might be questioned why some wind-based model predicted reliably the mean k_{600} despite high standard error. This observation can be explained by the data distribution over the wind speed spectrum: The wind-based models by MacIntyre et al. 2010 and Vachon and Prairie 2010 estimated lower k_{600} at low wind speed regime and higher k_{600} at high wind speed regime versus flux chamber measurements (Figure 5.4). This can be summarised by their average trend line function: k_{600} error [cm h^{-1}] = -1.34(±0.36)*U_{10} [m s^{-1}] + 3.81(±0.95). From this function it is apparent that the error is minimal at wind speeds around 3 m s^{-1}. When the wind speed data was binned and its distribution plotted over wind speed bins, the data showed a pattern similar to a normal distribution (Figure 5.5) with a mean value around 3 m s^{-1}. Additionally, the distribution was characterized by one elevated bin count (1-1.5 m s^{-1}) and a small tailing at the upper wind speed end. Accordingly, most data points accounted for low k_{600} errors around 3 m s^{-1} and the elevated bin count and tailing effect compensated each other. Taken all

together, this led to comparable mean k_{600} predictions. In contrast, the other wind-based models showed trend line functions not being symmetrically centred around 3 m s^{-1}. Here, the deviations of individual data points translated to substantially higher deviations in the k_{600} mean.

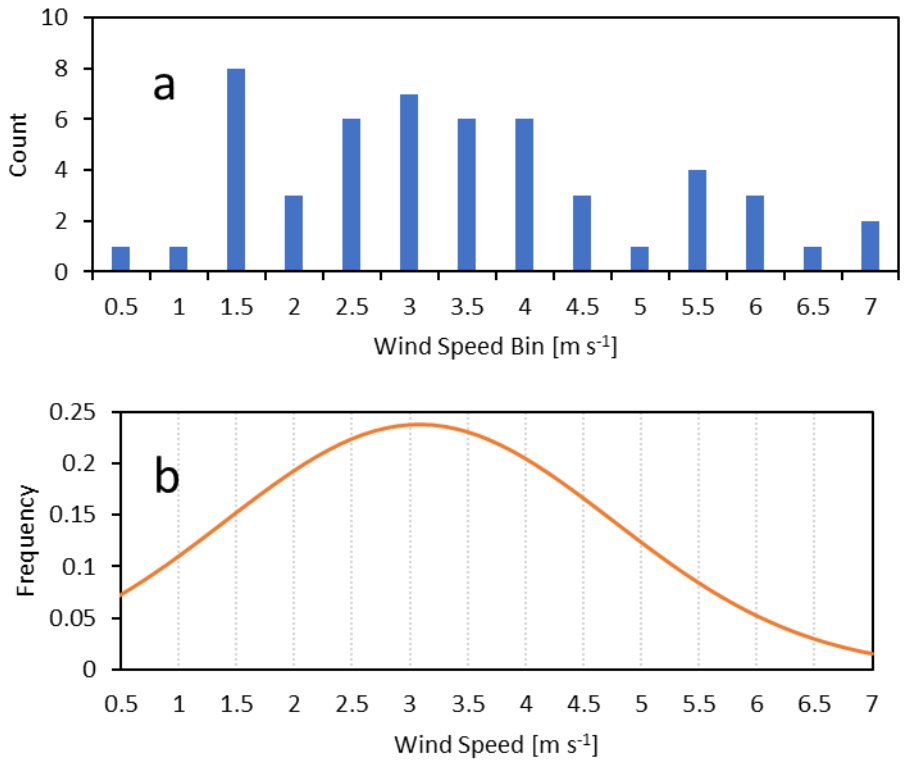

Figure 5.5: Wind data distribution for the 2017 field campaign in Lake Stechlin. *Counts plotted over wind speed bins (0.5 m s^{-1} intervals) (**a**); and normal distribution calculated from corresponding mean value and standard deviation (**b**).*

Surface renewal model. The surface renewal model predictions showed a (strong) correlation with wind speed (R^2 = 0.53, $p < 0.01$) and had the strongest correlation with temperature gradient at U_{10} below 1.3 m s^{-1} (R^2 = 0.80, $p < 0.01$). This observation underlines that wind forcing and heat flux are both important driving forces for gas emission in Lake Stechlin. The discrepancy between the surface renewal model and the floating chamber approach has been reported before (e.g. Eugster et al. 2003, Vachon et al. 2010) with values differing by a factor up to 2.4. In this chapter, flux chamber measurements deviated by a factor of 0.1 to 2.3 (combining over- and underestimation). This difference can have multiple methodological sources: The surface renewal model, as well as flux chamber measurements, are prone to their own biases. The surface renewal model was parametrised with turbulence recorded by an ADCP unit in 0.5 to 2.0 m depth. Currently, it is not well investigated which depth range of the

surface mixed layer best resembles the gas exchange factor. Measuring the turbulence in close proximity to the surface (few centimetres) is generally a methodological challenge but might improve future predictions by the surface renewal model (Tokoro et al. 2008, Vachon et al. 2010). The optimal working depth for turbulence measurements must be subject to future work. Turbulence is recorded multiple times per second by the ADCP unit. In contrast, the flux chamber approach took approximately 15-20 minutes. To make these measurements comparable, the turbulence measurements have been averaged hourly and adapted to the time frame of the floating chamber measurements. These transformations are another source of k_{600} bias. Furthermore, the Schmidt number and kinematic viscosity, which are used in the surface renewal model were determined from empirical temperature models (Raymond et al. 2012) potentially introducing further inaccuracies. Floating chambers can modulate the surface turbulence due to being submerged at the perimeter, especially at very calm (Vachon et al. 2010) and very turbulent surface conditions (Lorke et al. 2015). Also, the heat flux condition can be modulated by the flux chamber approach (Duchemin et al. 1999). To minimize these effects, swimming elements kept the floating chamber only 2 cm submerged at the perimeter during measurements, and the whole flux chamber was painted in white to avoid heating by sunlight. The floating chamber had a round profile and was freely floating to minimize bias (Lorke et al. 2015). Occasional rain also might have caused deviation between the two methods as the flux chamber mainly shields the investigated water surface from rain-induced turbulence (Ho et al. 1997/2007).

The surface renewal model is a useful alternative to flux chamber measurements. The only drawbacks of this methodology are the high acquisition costs and rather complicated calculations.

Gas transfer in Lake Stechlin. Lake Stechlin is an irregularly shaped lake and has three basins with surface areas between 1 and 2 km^2. Depending on the sampling conditions, other models can substitute floating chamber measurements to capture greenhouse gas emission. The wind-based model after Cole and Caraco (1998), Crusius and Wanninkhof (2003) and Donis et al. (2017) provided k_{600} estimates in the same dimension as provided by the floating chamber approach under low wind speeds (below 3 m s^{-1}). Under higher wind speed, these models should not be applied to Lake Stechlin data due to strong under-estimation of the k_{600}. The turbulence-based wind-based models after MacIntyre et al. (2010) and Vachon and Prairie 2013 provided reliable estimations

at wind speeds around 3 m s^{-1}. Additionally, these models are suitable for Lake Stechlin when measurements are done over a well-balanced wind speed range between 0 and 7 m s^{-1}. By being located in the temperate region, Lake Stechlin typically features low wind speed at midnight and high wind speed at noon. Therefore, these models should be considered when diurnal cycles are investigated. The same applies to the surface renewal model combined with ADCP-turbulence measurements: Measurements done throughout the day-night cycle will reduce the k_{600} error. The regression formulas presented throughout this chapter (Figure 5.3 and 5.4) might be used to eliminate a substantial deviation between the emission models.

In the previous Chapter 4 the system-wide sinks and sources of Lake Stechlin's epilimnion were balanced. The results indicated that a substantial amount of methane is unaccounted when only horizontal and vertical transport from anoxic zones are considered. Approximately 50-90 % (depending on parametrisation) of methane emitted at the water surface must have been produced in oxic epilimnic waters during the 2017 field campaign in Stechlin's South basin (Chapter 4). The mass balance was parametrised with flux chamber measurements and computed average oxic-water methane production rates of 168 nmol l^{-1} d^{-1}. If the mass balance were to be parametrised with the methane emission estimated here using the surface renewal model (6 % lower mean emission) slightly lower oxic production rates are computed (about 158 instead of 168 nmol l^{-1} d^{-1}). Both, parametrising the methane mass balance with flux chamber measurements and the methane emission retrieved from the surface renewal model, computed a substantial methane source is missing in the epilimnion. Accordingly, the unaccounted methane source calculated by the mass budgeting is not an inherited mistake from flux chamber errors and oxic production. Oxic methane production indeed, is a major methane source for the atmospheric methane emission in Lake Stechlin.

Choice of emission model. What is the best model to estimate gas emission? There is no straight answer to this question as each method and model comprises individual error and inaccuracies. It is good practice to conduct actual measurements, ideally via multiple different techniques, to quantify gas emission. On the one hand, flux chamber measurements are a cheap and time-efficient solution to record surface fluxes. Gathered emission values, may be prone to individual bias depending on the chamber structure and deployment (Vachon et al. 2010, Lorke et al. 2015). On the other hand, the application of the surface renewal model and turbulence measurements can give reliable

emission estimates. This method, however, is expensive. Also, the surface renewal model is prone to its own bias (e.g. depth of turbulence measurements, empirical parameters, etc.). In case actual measurements are not possible and wind-based models are used; the investigators should be aware of the huge variety of models (also including other proxy parameters) and that these models may relate to individual conditions of the sampling location (e.g. effective wind forcing influenced by wind fetch, wave height; Vachon and Prairie 2013). It is advised to confirm the applicability of specific wind-based models to specific sampling locations with other methodologies, or as the case may be, use personally developed prediction models for individual sampling locations. First, the physical condition of the target lake shall be considered. The wind-based model should be developed in a lake with similar morphological properties (e.g. lake size; Frost and Upstill-Goddard 2002, Vachon and Prairie 2013) and similar meteorological conditions (wind speed range, temperature gradient, precipitation, etc.). Measurements taken at the lake basin centre may improve emission estimates (Vachon and Prairie 2013). As indicated by the k_{600} error analysis (Figure 5.3 and 5.4), methodological deviation occurs under specific conditions. Therefore, if emission measurements are to be done under strong wind, absence of wind, high precipitation, strong tidal currents, extreme heat/cold, high surfactants or strong wave breaking, application of wind-based models should be avoided. Additionally, it should be noticed that the wind-based models investigated here capture diffusive (and partially convective) gas fluxes (MacIntyre et al. 2010). None of the models is applicable when ebullition contributes to surface evasion, especially when measurements are done close to the littoral zone of lakes.

Chapter 6: Contribution of Oxic Methane Production to Surface Methane Emission in Lakes – Local and Global Implications

From **M. Günthel,** D. Donis, G. Kirillin, D. Ionescu, M. Bizic, D. F. McGinnis, H.-P. Grossart and K. W. Tang. Contribution of oxic methane production to surface methane emission in lakes and its global importance. Nature Communications 10, 5497 (2019) (doi:10.1038/s41467-019-13320-0).

6.1 Abstract

Recent discovery of oxic methane production in sea and lake waters, as well as wetlands demands re-thinking of the global methane cycle and re-assessment of the contribution of oxic waters to atmospheric methane emission. Here the system-wide sources and sinks of surface-water methane (Figure 6.1) were analysed in two basins of a temperate lake. A mass balance analysis showed that internal methane production in well-oxygenated surface water was an important source for surface-water methane during the stratified period. Combining results presented here and literature reports, oxic methane contribution to emission follows a predictive function of littoral sediment area and surface mixed layer volume. The contribution of oxic methane source(s) is predicted to increase with lake size, accounting for the majority (>50 %) of surface methane emission for lakes with surface areas >1 km^2.

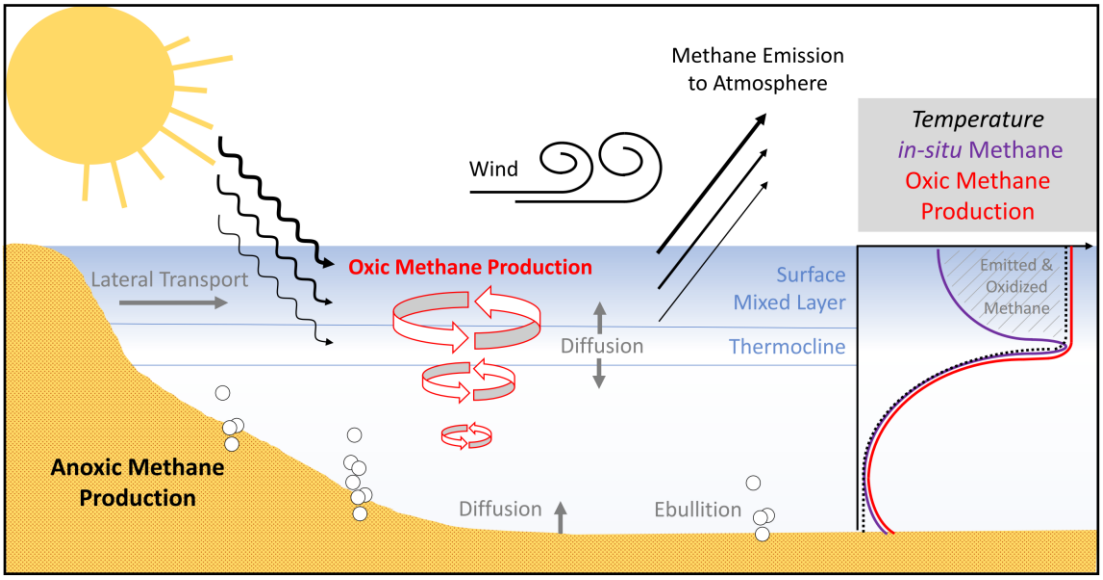

Figure 6.1: Abstract art of Chapter 6.

6.2 Introduction

After carbon dioxide, methane is the second most important carbon-based greenhouse gas (IPCC 2007, IPCC 2013) and its continuous increase in the atmosphere is a global climate threat (Saunois et al. 2016b, Fletcher and Schaefer 2019, Nisbet et al. 2019). A basic premise in methane biogeochemistry is that biological methane formation occurs exclusively under anoxic conditions (Thauer 1998, Ferry and Kastead 2007). Over the past several decades (Scranton & Brewer 1977) there have been multiple reports of

paradoxical methane oversaturation in oxic sea and lake waters (Tang et al. 2016 and references herein). This 'methane paradox' can be resolved by attributing the methane to conventional anoxic sources (Hofmann et al. 2010, Murase et al. 2005), or by additionally considering oxic-water methane production. The idea of oxic methane production goes against the long-standing paradigm in methane research, and despite the scepticism (Fernandez et al. 2016, Peeters et al. 2019), different investigators have confirmed repeatedly that methane production can and does occur under oxic condition in sea and lake waters (Karl et al. 2008, Grossart et al. 2011, Tang et al. 2014), and studies have begun to identify the responsible organisms (Chapter 3, Yao et al. 2016, Wang et al. 2017) and the underlying biochemical pathways (Carini et al. 2014, Yao et al. 2016). Unlike anoxic methane sources in sediments and bottom waters, methane production in the surface mixed layer places the methane source closer to the water-air interface, and therefore its contribution to surface emission can be significant (Tang et al. 2016, Donis et al. 2017).

Globally, it is estimated that freshwaters account for (SD ± minimum error range) 122±60 Tg yr^{-1} methane to the atmosphere (ca. 20 % of the total emission) (Saunois et al. 2016a). Such global constraints, however, are highly uncertain as it is indicated by the 100 % minimum uncertainty range (Saunois et al. 2016a) and bottom-up and top-down methane budgets not agreeing well with each other (Kirschke et al. 2013, Saunois et al. 2016a). The large uncertainty of freshwater emission during upscaling is commonly attributed to i) highly variable methane density fluxes within and across systems (Natchimuthu et al. 2015, Wik et al. 2016a, Sabrekov et al. 2017, Xiao et al. 2017), ii) scarce long-term data, which do not cover high ecosystem variability (Bastviken et al. 2004, Saunois et al. 2016a), or iii) uncertainties in global areas (Allen and Pavelsky 2016; Thornton et al. 2016; Cael et al. 2017). Oxic methane production has so far not been considered in global assessments including methane budgets (Kirschke et al. 2013, Saunois et al 2016a) and IPCC reports (IPCC 2007, IPCC 2013) despite its potential to cause highly variable methane density fluxes in freshwater systems (Grossart et al. 2011, Bogard et al. 2014, Donis et al. 2017). For more accurate modelling of freshwater emission and corresponding contribution to the global budget, a better understanding of internal production and distribution pathways is needed.

While methanogenic Archaea are largely responsible for anoxic methane production (Ferry and Kastead 2007, Dean et al. 2018), primary production has been

associated with the oxic source (e.g. Chapter 3, Chapter 4, Grossart et al. 2011, Bogard et al. 2014). Therefore, the oxic and anoxic source will react differently to environmental controls. Global methane budget assessments and future climate change predictions will benefit from proper distinction of oxic versus anoxic methane sources and identifying their individual contribution to the system-wide emission.

Bogard et al. (2014) conducted experiments in Lake Cromwell (Canada) and estimated that oxic methane production accounted for 20 % of the total surface emission, with the rest originating from anoxic sources. Likewise, Donis et al. (2017) estimated that oxic production was the main methane source in the surface mixed layer of Lake Hallwil (Switzerland) and accounted for 63–83 % of the surface emission (value updated, see Supplementary Note 6.1). While both studies demonstrate that oxic methane production can be an important source of methane emission, it is not clear if it is a general phenomenon in lakes and what may explain the different contribution patterns in different lakes.

Lake Stechlin is a medium-size (4.25 km^2) meso-oligotrophic lake with a mean depth of 22.7 m (max. 69.5 m) in North-eastern Germany (Figure 6.2a).

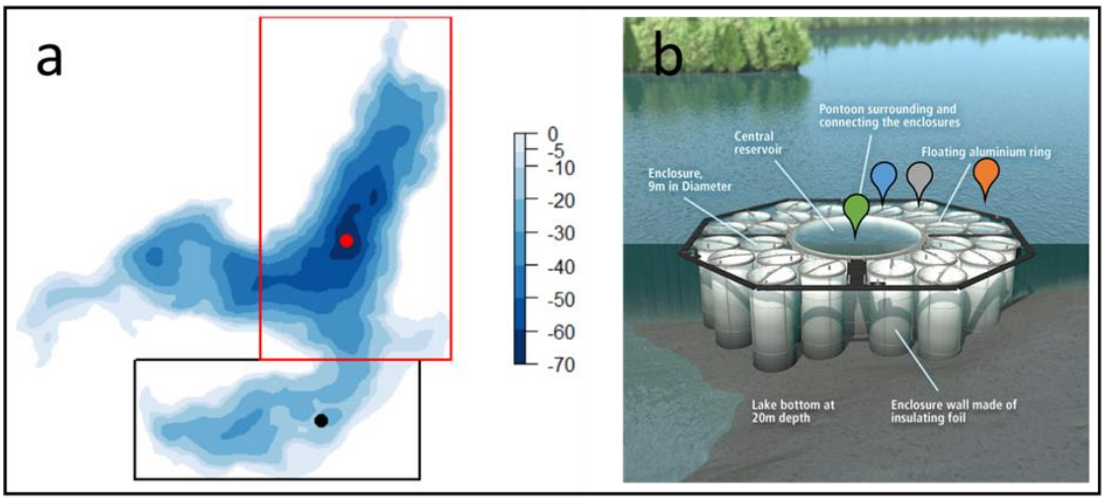

Figure 6.2: Illustration of the lake's bathymetry and sampling sites. *Panel (**a**) depicts the bathymetry of Lake Stechlin [m]. The lake has 3 basins: South (black frame), Northeast (red frame) and North-West basin. Seasonal methane measurements were done at the deepest point (69.5 m deep; red dot) and adjacent to the lake lab facility (20.5 m deep; black dot). Panel (**b**), schematics of the lake lab facility (source: https://www.lake-lab.de/index.php/Design.html, picture modified) and related sampling locations: central reservoir (green), experimental enclosure E1 (blue), experimental enclosure E13 (grey) and the adjacent open water (orange). Figure was created deploying R (v.3.3.1), Rstudio (v.1.0.153) and MS office software (v.365 ProPlus).*

Lake Stechlin has negligible river in-/outflow, small groundwater-feed (Kirillin et al. 2012a) and has been monitored for decades by the Leibniz Institute for Freshwater Ecology and Inland Fisheries (IGB) (Kirillin et al. 2013). Methane oversaturation in the lake's surface oxic layer has been observed since 2010 (Chapter 2, Chapter 4, Grossart et al. 2011, Tang et al. 2014, McGinnis et al. 2015). Throughout the years 2014, 2016 and 2018 a detailed data set was collected including dissolved methane concentration, surface methane emission and environmental parameters (temperature, dissolved oxygen, algal pigments, wind speed) at different sampling sites: Stechlin's Northeast and South basin and inside enclosures (data overview given by Table 6.1). This data set allowed to conduct a detailed methane mass balance analysis for the surface mixed layer, accounting for the different sources and sinks (Figure 6.3), including lateral methane input (2014 dataset) and oxic methane production (all datasets), under different seasonal conditions (2016 dataset, 1 repetition in 2018). Missing parameters making datasets collected before 2014 incompatible with mass balance analysis; however, the mass balance results were compared to earlier findings.

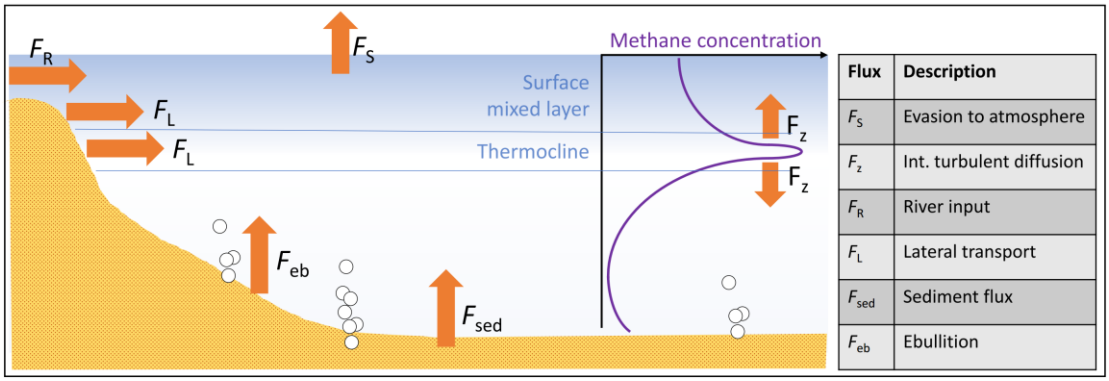

Figure 6.3: Transport fluxes affecting the methane inventory in the surface mixed layer. *The typical methane profile of the lake water column has a distinct peak within the thermocline. Methane is introduced into the surface mixed layer horizontally by lateral transport from peripheral water bodies and sediments (F_R, F_L) and vertically via (turbulent) diffusion (F_z) originating from bottom sediments (F_{eb}, F_{sed}). Methane is released to the atmosphere (F_S) across the water-air interface. Biological modulation accounts for additional methane sink and source: methane loss due to oxidation by methanotrophs is commonly acknowledged, whereas oxic methane production in the surface mixed layer represents an overlooked part of the global methane cycle (e.g. IPCC 2007, IPCC 2013). Picture was drafted according to Donis et al. (2017).*

Table 6.1: Sampling schedule throughout 2014 – 2018. *Detailed descriptions on how parameters were recorded can be found in the method section. Note, measurements in the experimental enclosures were done 2 weeks after the water had been exchanged with lake water; in contrast, the water in the central reservoir has never been exchanged since its installation in 2012.*

Year	Month	Location	Purpose	n[a]	WCP[b]	Surface emission[c]	Probe data[d]
2014	Aug	E1	quantify F_L	4 (SS)	yes	modelled	yes
2014	Aug	E13	quantify F_L	5 (SS)	yes	modelled	yes
2014	Aug	S	quantify F_L	4 (SS)	yes	modelled	yes
2016	Mar-Jul	NE	seasonal OMP, basin variation	6 (SS)	yes	measured (5/6)	yes
				13 (NS)	yes	measured (13/13)	yes
2016	Mar-Jul	S	seasonal OMP, basin variation	6 (SS)	yes	modelled	yes
				10 (NS)	yes	modelled	yes
2016	May, Jul	CR	seasonal OMP, isolated water	1 (SS)	yes	modelled	yes
				2 (NS)	yes	modelled	yes
2018	Jul	NE	seasonal OMP, basin variation	1 (SS)	yes	measured (1/1)	yes
2018	Jul	S	seasonal OMP, basin variation	1 (SS)	yes	measured (1/1)	yes

(**a**) n represents the repetition of methane measurements (each taken on a different day during day time) including water column profile (water samples transferred into glass bottles, crimp-closed, He head space replacement, GC/FID analysis) and surface emission (floating chamber measurements), recordings were done during the stratified season (SS) or non-stratified/intermediate season (NS); (**b**) WCP symbolizes water column methane profiles that were taken from the water surface down below the thermocline (at ca. 5-7 m depth) in 1 to 2 m steps; (**c**) surface emission was measured (see methods) using the floating chamber approach or estimated based on a wind based model developed from own floating chamber measurements and compared to literature models (using surface water temperature, surface water methane concentration, wind data); (**d**) probe data are environmental parameters including wind speed that were recorded in 10 m height by the Neuglobsow weather station next to Lake Stechlin and were provided by the Umweltbundesamt, water temperature was recorded by automatic YSI probes permanently mounted on the lake lab facility in the South basin (profiling the upper 20 m of the water column continuously in 60 min intervals); F_L symbolizes the lateral methane input and OMP is oxic methane production; in 2016 Lake Stechlin stratified ca. mid-May – the lake was not stratified throughout the months before and stratified afterwards – samplings in 2014 and 2018 were done while stratification. E1 – experimental enclosure 1; E13 – experimental enclosure 13; S – South basin; NE – Northeast basin; CR – Central reservoir.

Unlike the open ocean, oxic methane production in lake waters can be confounded by anoxic methane input from the littoral zone. To resolve this, concurrent measurements were made in 2014 in two experimental enclosures of the 'Lake Lab' facility (https://www.lake-lab.de; Figure 6.2b), which consists of a series of 'experimental enclosures' (with water exchange 2 weeks prior to this study; 1,200 m^3) and a 'central reservoir' in 2016 (a 14,000 m^3 enclosure, without any water exchange

since its installation in 2012), to examine the lake-water methane dynamics without the influence from the littoral zone.

Building upon the current knowledge of oxic methane production in lakes, here the local as well as the global relevance of oxic methane production was investigated: i) Using 2014 data from both enclosures and open water allowed to determine oxic methane production by excluding littoral methane input and quantify the relative contributions of the oxic and anoxic methane sources to the system-wide surface emission in two basins of Lake Stechlin. ii) With the high-resolution time series data (about weekly sampling scheme from March to July 2016, one repetition in July 2018), the seasonal variation of oxic methane production was resolved from the lake's mixed state in early spring to the strongly stratified state in summer. iii) Finally, combining own findings with literature data allowed developing a novel predictive model for oxic methane contribution in relation to lake morphology. The importance of corresponding predictions is discussed in a global context.

6.3 Methods

Study site. Lake Stechlin (Germany) is a meso-oligotrophic temperate glacial lake. This study focused on the Northeast and South basins. Typical of temperate lakes, the water column of Lake Stechlin is well mixed in winter, begins to stratify in May and remains stratified until September/October. Throughout the stratified period, the oxygen-rich surface mixed layer and thermocline are oversaturated with methane (Chapter 2, Chapter 4).

The 'Lake Lab' facility was installed in the South basin in 2011-2012, which consists of 24 experimental enclosures (each 9 m dia. x 20 m depth) and a central reservoir (30 m dia. x 20 m depth), all of which extend into the bottom sediment. Water in the experimental enclosures 1 and 13 of the lake lab facility was exchanged with open lake water 2 weeks prior to this study; the water in the central reservoir has never been changed since installation.

Mass balance analysis. The mass balance analysis examines the different processes leading to methane gains and losses within the surface mixed layer (Figure 6.3). The gains include horizontal transport from the shore, vertical diffusion from the

thermocline, river input and internal production (oxic methane production). The losses are methane oxidation and surface emission and river outflow.

The following mass balance equation was used and solved either for oxic methane production (P_{net}), or lateral methane input, (F_L) (Donis et al. 2017):

$$\frac{\partial C}{\partial t} * \forall = (Q_R * C_R) + (Q_C * C_C) + (A_{th} * F_z) + (A_{sed} * F_L) + (P_{net} * \forall) - (\mathrm{MOx} * \forall + A_{tot} * \mathrm{F}_S) \quad (6.1)$$

Here, $\frac{\partial C}{\partial t}$ describes the changing methane concentration over time [mol d^{-1}] (which under steady state condition is simplified to $\frac{\partial C}{\partial t}$ = 0), ∀ is the volume of the surface mixed layer [m^3]. (Q_R*C_R) and (Q_C*C_C) describes optional methane input and output by river in- and outflow where Q_R (Q_C) is the flowrate [m^3 d^{-1}] and C_R (C_C) is the methane concentration in inflowing (outflowing) water [mol m^{-3}]. The term (A_{th}*F_z) describes the vertical methane input from below via interior turbulent diffusion F_z [mol m^{-2} d^{-1}] (z is the depth in a 1-m resolution) multiplied by the thermocline area A_{th} [m^2]. The term (A_{sed}*F_L) describes lateral methane input from sediments with A_{sed} being the surface area of the littoral sediment [m^2] and F_L being the sediment methane flux [mol m^{-2} d^{-1}]. P_{net} is the local methane production rate per unit surface mixed layer volume [mol m^{-3} d^{-1}]. Methane loss terms include local oxidation rate (MOx; [mol m^{-3} d^{-1}]) and emission to the atmosphere (A_{tot}*F_S; where A_{tot} is the lakes' surface area [m^2] and F_S is the surface emission [mol m^{-2} d^{-1}]). Parameters of lake morphology, such as volume of the surface mixed layer (∀) and planar areas (A_{tot}, A_{th}, A_{sed}), were derived from thermocline depth data and bathymetry data. Supplementary Table S6.3 gives details of individual mass balance parametrisations for open-water and enclosures during the stratified (June – July 2016/2018; Aug 2014) and the non-stratified periods (March – April 2016).

Methane concentration. In two experimental enclosures (1, 13) and the adjacent open-water in the South basin, methane concentration within the top 18 m of the water column was sampled in a 1-m resolution 4–5 times over 10 days in August 2014. Weekly water column profile sampling was also carried out between 10:00 and 18:00 local time, from March to July in 2016 at the open-water sites in the Northeast basin (69.5 m deep) and in the South basin (20.5 m deep). In July 2018, one additional profile measurement was taken in both basins. Furthermore, the central reservoir was sampled on three occasions in 2016 (on 3rd and 10th May when stratification was developing, and on 7th July when the water was fully stratified). Water was collected from different depths by a

Limnos Water Sampler, and gently transferred to 50 ml serum bottles via a tubing. The bottles were fully flushed 3 times, filled and crimp-closed with PTFE-butyl septa (triplicates at the Northeast basin, duplicates elsewhere). Dissolved methane concentrations were measured in the lab by headspace displacement method and a GC/FID (Shimadzu) (Magen et al. 2014).

Methane emission to the atmosphere. Methane surface emission was captured by a 15 l-volume floating chamber. Trapped methane was quantified by withdrawing the gas from the chamber and measuring it by headspace analysis (GC/FID). Emission data were then used to derive gas transfer constant (k_{600}) as a function of wind speed at 10 m height (U_{10}): Using the general gas transfer formula, the measured surface methane emission (F_S) and surface water methane (c_{water}), gas transfer constants (k_{CH4}) were calculated (atmospheric methane content c_{air} = 1.88 ppm) as:

$$k_{CH4} = \frac{F_S}{(c_{water} - c_{air})}; \text{[cm h}^{-1}\text{]} \quad (6.2)$$

Subsequently, the k_{CH4} values were transformed into k_{600} values:

$$k_{600} = \frac{k_{CH4}}{\left(\frac{Sc_{CH4}}{600}\right)^{q}}; \text{[cm h}^{-1}\text{]} \quad (6.3)$$

Where Sc_{CH4} is the dimensionless Schmidt number (computed after Engle and Melack 2000) and q is a conversion factor with a value of (-1/2) for wind speeds ≥3.7 m s^{-1} and (-2/3) for wind speeds below (Jähne et al. 1987). The k_{600} values were plotted over wind speed (U_{10}) and the obtained linear relationship was then used to estimate missing methane surface emissions. Supplementary Table 6.3 illustrates measured and estimated surface emissions and related parameters using the established gas-transfer model. The conversion of methane surface fluxes to k_{600} values and plotting over U_{10} yielded the following relationship: k_{600} [cm h^{-1}] = 1.98 * U_{10} [m s^{-1}] + 0.94 (R^2 = 0.44, $p < 0.01$). For times when direct emission measurements were not available, the k_{600} relationship was used to estimate methane emissions based on wind speed. Surface methane emission rates for the South basin were additionally computed using alternative gas-transfer models from the literature (MacIntyre et al. 2010, Vachon and Prairie 2013, Donis et al. 2017).

Lateral methane input. To estimate how much methane was introduced from littoral sediments into the surface mixed layer during the stratified period, methane

measurements were taken inside mesocosm enclosures (2 weeks after the water was exchanged with open lake water) and in the open water adjacent to the enclosures in the South basin. As the enclosures were cut off from lateral transport, comparing the mass balance analysis results between inside and outside of the enclosures enabled an estimation of the lateral methane input.

The lateral methane input was neglected for the non-stratified season as sediment methanogenesis is highly temperature dependent (Duc et al. 2010, Marotta et al. 2014) and was observed to be zero or 1–2 orders of magnitude smaller under winter conditions compared to summer/autumn condition (Duc et al. 2010, Liu et al. 2017, Liikanen et al. 2003).

Vertical methane diffusion. The stratified period (June – July) was characterized by a distinct methane peak in the thermocline. Fick's First law was applied to estimate the transport of methane from the thermocline into the surface mixed layer via (turbulent) diffusion:

$$F_z = -K_z * \frac{\partial C}{\partial z}; \text{ [mol m}^{-2} \text{ d}^{-1}\text{]} \quad (6.4)$$

where F_z is the average vertical methane diffusion, z is depth [m], $\frac{\partial C}{\partial z}$ is the vertical methane gradient measured at 1-m depth resolution [mol m^{-4}], and K_z is the basin-scale diffusivity [m^2 s^{-1}] derived from temperature data based on heat-budget method (Supplementary Note 6.2).

To obtain a conservative estimate of oxic methane production in the surface mixed layer, maximum K_z values within the bottom 3 m of the surface mixed layer were used to compute F_z. Temperature and diffusivity profiles measured inside the mesocosms were very similar to the open-water profiles allowing to apply the same heat-budget estimates of open-water diffusivity values at depths >4 m to estimate the vertical flux in both open lake and mesocosm enclosures for the entire study period (Supplementary Figure S6.2).

Methane oxidation. Rates up to 103 nmol l^{-1} d^{-1} methane oxidation have been observed in Lake Stechlin, when water was spiked with high methane concentrations (Tang et al. 2014). However, methane oxidation rate in lake waters has been observed to differ by 1–2 orders of magnitude between winter and summer (Joye et al. 1999, Utsumi

et al. 2003, Carini et al. 2005). For a more conservative consideration (methane oxidation is a loss term in the mass balance) and to account for the seasonal difference and to simplify the mass balance analysis, methane oxidation during the non-stratified season was neglected, and methane oxidation was assumed to be 30 % of the internal production rate during the stratified season. This assumption was evaluated in a sensitivity analysis presented throughout the discussion section.

River in/- output and ebullition. Lake Stechlin is not connected to any river. Therefore, the corresponding mass balance terms (Q_R*C_R) and (Q_C*C_C) equal 0 (Equation 6.1). No methane ebullition was observed during the whole study period. Earlier studies reported generally low methanogenesis activity in Lake Stechlin sediments (Conrad et al. 2007, Casper et al. 2005, Casper et al. 2003), with the majority occurring below 20 cm sediment depth (Casper 1996). Tang et al. (2014) demonstrated that ebullition did not contribute methane to surface mixed layer waters for depths ≥ 20 m. This allowed to ignore ebullition in the mass balance analysis for Lake Stechlin (22.7 m mean depth).

Environmental parameters. Water depths were measured by a portable sounder gauge (Cole-Parmer). Temperature, dissolved oxygen and chlorophyll a fluorescence was measured using a YSI probe (Model 6600V2). Wind speed data (U_{10} recorded at 10 m height) were provided in 30 – 60 min resolution by the Umweltbundesamt weather station adjacent to the lake.

Monte Carlo simulation. To assess uncertainties, Monte Carlo simulation was used (9999 iterations) when solving the mass balance. For that, mass balance components were randomly picked within the normal distribution resulting from mean values and their standard deviations retrieved from field measurements.

Oxic methane contributions. The importance of oxic methane production relative to anoxic sources (lateral input, vertical diffusion) was examined by computing the oxic methane contribution (OMC):

$$OMC = \frac{(\mathrm{P}_{net}*\forall)}{(\mathrm{P}_{net}*\forall)+(A_{sed}*F_L)+(A_{th}*F_z)} * 100;\ [\%] \qquad (6.5)$$

The results were then compared with the literature data (Bogard et al. 2014, Donis et al. 2017) to examine the oxic methane contribution as a function of lake morphology. To

expand this analysis to larger lakes, oxic methane contribution was estimated for additional lakes based on the data in DelSontro et al. (2018) as described in the following section.

Estimating the oxic methane contribution for additional lakes. As indicated by the model for lateral transport alongside transects and actual transect measurements in DelSontro et al. (2018), methane concentrations of transect measurements reach a plateau phase at distances (corresponds to equivalent radius) ≥ 2 km (equivalent to lake surface areas > 12.6 km^2). Vertical diffusion from lower water layers into the surface mixed layer has been identified as a minor methane source; and therefore, lateral input and (oxic) internal production are the major sources of surface mixed layer methane. That is why, plateau concentrations in transect measurements can be assumed to be the result of internal production while concentrations above plateau concentration can be assumed to be the result of lateral transport. To estimate the dimension of both major methane sources, i) the plateau concentration was integrated over the lakes' equivalent radius (resembling a measure of the oxic methane source), ii) elevated methane concentrations were integrated over the distance of the gradient (resembling a measure of anoxic/lateral methane source) and iii) the oxic methane contribution ratio was formed as oxic measure divided by the sum of oxic and anoxic measure. The following table lists obtained oxic methane contribution estimations for lakes with equivalent radii above 2 km together.

Table 6.2: Estimations for oxic methane contribution for some lakes with equivalent radii > 2 km. *Transect data was extracted from the DelSontro et al. (2018) study. A graphical approach was used to compute estimates for the lateral and oxic methane source.*

Lake name	A_{tot} [km^2]	Ra [km]	z_{SML} [m]	A_{sed} [m^2]	V [m^3]	OMC [%]	TP [µg l^{-1}]
Beauchene (West basin)	17	2.3	5	1.0E+05	8.5E+07	97	3.5
Champlain	1269	20.1	10	1.3E+07	1.3E+10	100	15.2
Camichagama	26	2.9	7	1.8E+05	1.8E+08	100	7.1
Nominingue	22	2.7	5	1.2E+05	1.1E+08	84	8.5
Ontario	19009	77.8	12	2.0E+07	2.3E+11	90	3.7
Simard	170	7.3	10	6.5E+05	1.7E+09	82	21.4
St. Jean	1065	18.4	5	8.2E+05	5.3E+09	85	9.8

A_{tot} – lake surface area, *Ra* – equivalent radius, z_{SML} – depth of the surface mixed layer, A_{sed} – littoral sediment area, *V* – volume of the surface mixed layer, OMC – oxic methane contribution, TP – total phosphorus level indicating the trophic state: oligo- (0 – 12 µg l^{-1}), meso- (12 – 24 µg l^{-1}) or eutrophic (>24 µg l^{-1}). Note, equivalent radius assumes circular shape of lake surface. OMC calculation assumes a maximum lateral methane transport up to 2 km. Lake locations – Lake Beauchene West basin: 46°39'22.7"N, 78°56'53.2"W; Lake Champlain: 44°29'07.4"N, 73°19'08.8"W; Lake Camichagama: 47°49'54.1"N, 76°19'01.9"W; Lake Nominingue: 46°25'58.1"N, 74°59'33.0"W; Lake Ontario: 43°37'51.6"N, 77°11'06.4"W; Lake Simard: 47°37'37.9"N, 78°43'02.3"W; Lake St. Jean: 48°31'43.0"N, 71°54'27.4"W.

The equivalent radius Ra was determined to make lakes with different morphology comparable, by assuming the lakes' surface area (A_{tot}) to be of circular shape and solving the circle function $A_{tot} = \pi Ra^2$ after Ra. Values for A_{tot} were derived from DelSontro et al. (2018). Likewise, the volume of the surface mixed layer (V) was determined by multiplying lake surface area (A_{tot}) with depth of the surface mixed layer (z_{SML}). Both parameters were retrieved from Supplementary Information of DelSontro et al. 2018. The sediment area (A_{sed}) was estimated by computing the perimeter of the lake from lake surface area (A_{tot}) assuming circular lake shape. The perimeter was then multiplied by the average distance (d) littoral sediments reach into the surface mixed layer and into depth (z_{SML}). Assuming the sediments fall in a 45°-degree angle towards lake center, d was computed based on the depth of the surface mixed layer (z_{SML}) and Pythagorean theorem. Morphological lake parameters needed for these transformations were derived from DelSontro et al. 2018.

First-order estimation of oxic methane contribution in a global context. Global lake size data for lake size classes considering lakes ≥0.01 km^2 was extracted from Cael et al. (2017) (10^{4+i} to 10^{5+i} m^2 and $>10^{10}$ m^2 where i = 0 to 5): This includes the abundance (n) and total surface area (A_{class}; [km^2]) for all the 7 lake size classes (details in Table 6.6). The percentage contribution of each lake size class to the global surface area (γ_{class}; [%]) was computed where global lake surface area (A_{global}) is 5,128,000 km^2:

$$\gamma_{\text{class}} = \frac{A_{\text{class}} * 100\,\%}{A_{\text{global}}}\,;\,[\%] \tag{6.6}$$

The mean size of the lake size class (A_{mean}; [km^2]) which is the average of the upper and lower end of the size class was applied to the empirical model predicting oxic methane contribution based on lake size area (see result section) to compute the oxic methane contribution value for each lake size class (OMC_{class}; [%]):

$$\text{OMC}_{\text{class}} = \frac{90.87 * A_{\text{mean}}}{0.83 + A_{\text{mean}}}\,;\,[\%] \tag{6.7}$$

The oxic methane contribution values for the different lake size classes (OMC_{class}) was subsequently projected to the global lake inventory relative to the total surface area (γ_{global}; [%]) by multiplying OMC_{class} values by γ_{class}:

$$\gamma_{global} = \frac{\gamma_{class}}{100\,\%} * OMC_{class};\ [\%] \quad (6.8)$$

The oxic methane contribution estimate for the global lake inventory (OMC_{global}; [%]) was finally computed by summing up the γ_{global} of all lake size classes:

$$OMC_{global} = \sum \gamma_{global}\ ;\ [\%] \quad (6.9)$$

Data format. This study contains multiple field samplings done in the course of 2014, 2016 and 2018. Mean ± 1*standard deviations presented throughout the manuscript indicate temporal variation and were calculated separately for the stratified/non-stratified season for each basin or combined for the experimental enclosures or the central reservoir.

6.4 Results

Environmental conditions. Temperature and buoyancy frequency (N^2) profiles indicate that Lake Stechlin was completely mixed in 2016 until April (Figure 6.4a, b).

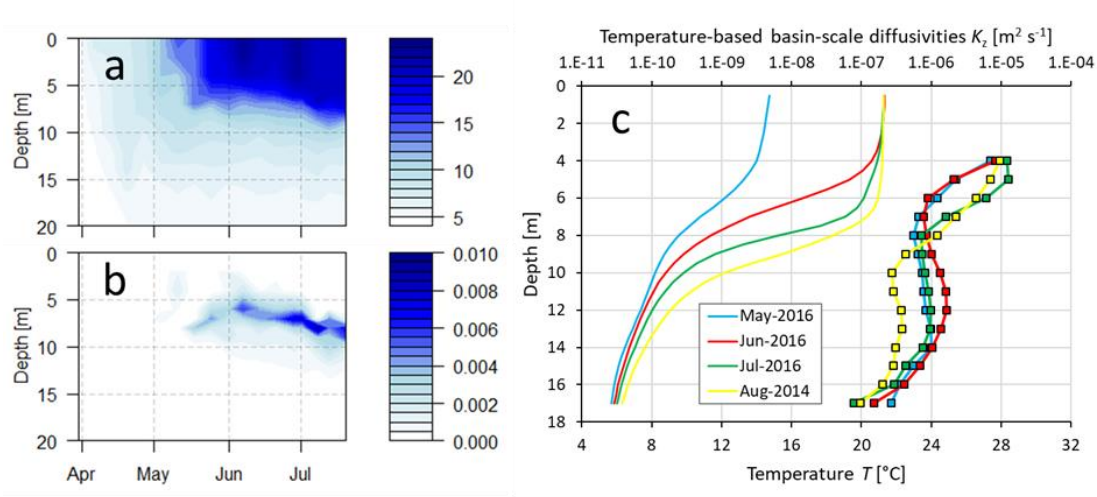

Figure 6.4: Physical characteristics of the water column. *Panel (**a**): Seasonal change of temperature [°C] in 2016 as recorded by a YSI probe. Panel (**b**): Seasonal development of buoyancy frequency N^2 [s^{-1}] in 2016, computed from temperature profiles using the R-package 'rLakeAnalyzer'. Panel (**c**): Temperature (T; lines) was recorded by automatized YSI probes profiling the water column continuously in a 30 min and 0.5 m interval and averaged monthly. Basin-scale diffusivities (K_z; squares) were calculated as after the heat-budget method from temperature data for stratified periods (monthly averages). Figure was created deploying R (v.3.3.1), Rstudio (v.1.0.153) and MS office software (v.365 ProPlus).*

In April 2016, the lake started to warm and thermal stratification established during May. From June to August, the lake was clearly stratified with temperatures ≥20 °C in the surface mixed layer. The stratified water column was mainly sampled during June and July; the term 'stratified period' refers to this period unless stated otherwise. The thickness of the surface mixed layer was about 5 m during June, and 6 m in July and August.

Throughout the study period, the lake water column never turned anoxic, with dissolved oxygen reaching up to ca. 17 mg l^{-1} (ca. 170 % saturation) typically 1 m below the methane peak (Figure 5.5).

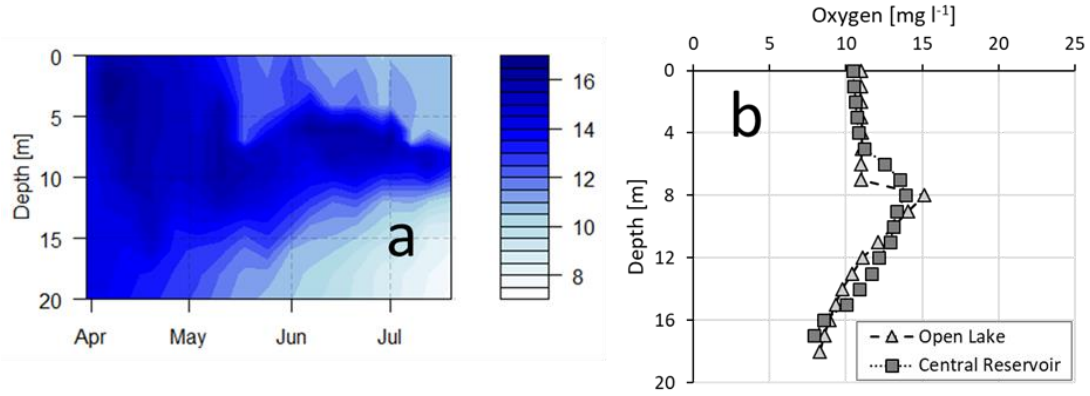

Figure 6.5: Oxygen measurements. *Panel (**a**): Seasonal change in oxygen concentration [mg l^{-1}] in the open lake (South basin, 2016). Panel (**b**): Discrete measurements taken on 7th July 2016 compare water-column oxygen content in the open lake and inside the central reservoir. Oxygen was measured using a YSI probe. Figure has been drafted using R (v.3.3.1), Rstudio (v.1.0.153) and MS office software (v.365 ProPlus).*

Methane concentrations. With the onset of stratification, methane concentrations in the oxic upper water column at both Northeast and South basins increased sharply, reaching up to 1400 nmol l^{-1} at thermocline depth (6 m). The surface mixed layer remained oversaturated (in relation to the atmosphere) with methane throughout the stratified season in both basins (400-900 nmol l^{-1}) while methane concentrations were less than 200 $nmol^{-1}$ l at >10 m depth (Figure 6.6a, b).

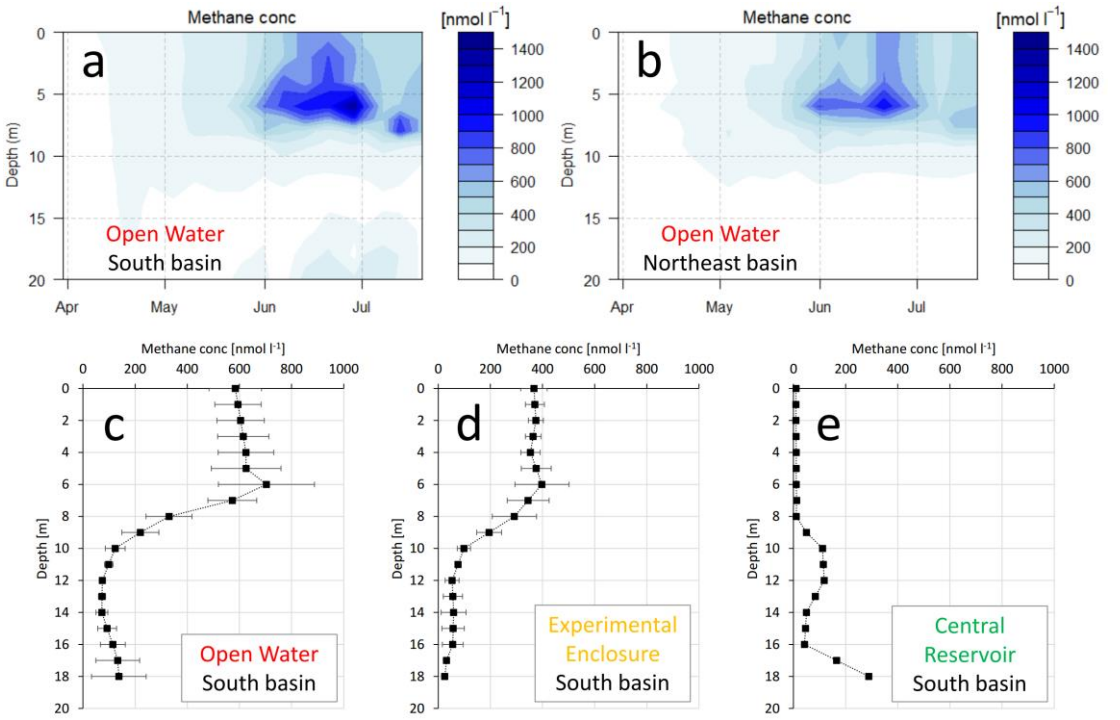

Figure 6.6: Methane accumulation in the water column of the open lake and enclosures. *Panel (**a**) shows the in-situ methane concentrations [nmol l^{-1} d^{-1}] recorded weekly in 2016 in the Northeast basin (53°09'20.2"N 13°01'51.5"E). Increasing concentrations indicate accumulation. Panel (**b**) shows the methane concentration [nmol l^{-1}] recorded weekly in 2016 in the South basin (53°08'36.6"N 13°01'42.8"E). Note, that panel (a) contains an additional data point compared to panel (b) in the end of June. Panel (**c**) shows the methane profile in the open Lake of the South basin (53°08'36.6"N 13°01'42.8"E; 20.5 m deep) as mean±SD of 4 profiles taken on 4 different days in August 2014. Panel (**d**) shows the methane profile inside experimental enclosure 1 (53°08'36.4"N 13°01'41.6"E; ca. 20 m deep) as mean±SD of 4 profiles taken on 4 different days in August 2014. Panel (**e**) illustrates the methane profile inside the central reservoir (53°08'35.8"N 13°01'41.1"E; ca. 18.5 m deep) as mean±SD of methodological duplicate measurement taken on 7th July. Figure was created deploying R (v.3.3.1), Rstudio (v.1.0.153) and MS office software (v.365 ProPlus).*

Inside the experimental enclosures (water exchanged with open-lake water 2 weeks prior to sampling), methane concentrations were also at over-saturation level in the surface mixed layer (300-400 nmol l^{-1}) with a profile similar to the open water, except for a smaller methane peak at the thermocline (Figure 6.6c, d). In contrast, the central reservoir (water never exchanged for 8 years) showed a completely different profile during the stratified period, with negligible amount of methane in the surface mixed layer (≤15 nmol l^{-1}) and higher concentration of methane below 16 m (300 nmol l^{-1}) (Figure 6.6e). The small peak (120 nmol l^{-1}) at 12 m depth in the central reservoir methane profile

appears to be the result of a different methane production-consumption balance at this depth, but has not been examined in detail.

Surface methane emission. The surface methane emission was either measured using a flux chamber (all Northeast basin values except on 20th June) or estimated from a wind-based model (all other values) that was developed from the flux chamber measurements and concurrent wind conditions: Emission data were transformed to gas transfer constants k_{600} as a linear function of wind speed (U_{10}, recorded at 10 m height), k_{600} [cm h^{-1}] = 1.98 * U_{10} [m s^{-1}] + 0.94 (R^2 = 0.44, $p < 0.01$) (Supplementary Table 6.3). This linear function was then used to estimate surface emissions in the South basin (enclosures and open lake) based on wind speed (details in the method section, Table 6.1).

In the Northeast basin the surface methane emission increased by an order of magnitude from the non-stratified period (March: mean±SD; 0.049±0.026 mmol m^{-2} d^{-1}) to the stratified period (0.47±0.27 mmol m^{-2} d^{-1}). Compared to the Northeast basin, higher surface emission was observed in the South basin during the stratified period (mean±SD; 0.71±0.24 mmol m^{-2} d^{-1}).

The experimental enclosures showed a surface methane flux of (mean±SD) 0.43±0.07 mmol m^{-2} d^{-1} in August 2014, which was about half of the flux measured in the adjacent open water (0.77 mmol m^{-2} d^{-1}) at the same time. In contrast, the central reservoir showed a much lower surface methane emission of 0.01 mmol m^{-2} d^{-1} (7th July).

Published gas emission models (MacIntyre et al. 2010, Vachon and Prairie et al. 2013, Donis et al. 2017) were used to validate emission predictions based on wind speed. Table 6.3 summarises the results (more details are given in the sensitivity analysis throughout the Discussion section).

Vertical methane diffusion. Diffusivity was high in the surface mixed layer, but it decreased to ca. 10^{-6} m^2 s^{-1} at the upper boundary of the thermocline in the stratified period (Figure 6.4c). Consequently, the diffusive methane input from the thermocline to the surface mixed layer during the stratified season was small for both the Northeast: (mean±SD) 0.032±0.031 mmol m^{-2} d^{-1} and the South basin: 0.050±0.065 mmol m^{-2} d^{-1}, and negligible in the central reservoir ($4.4*10^{-4}$ mmol m^{-2} d^{-1}).

Table 6.3: Summary of surface emission and mass balance results for Stechlins' South basin using June-July 2016/2018 data and different gas transfer models.

Type of model	F_S [mmol m^{-2} d^{-1}]	P_{net} [nmol l^{-1} d^{-1}]	OMC [%]
Stechlin relationship	0.772±0.186	109±61	55
Hallwil relationship	0.657±0.181	73±60	45
MacIntyre et al. (2010)			
- positive buoyancy flux	0.552±0.156	41±52	32
- negative buoyancy flux	0.925±0.201	155±64	64
- combined buoyancy fluxes	0.759±0.204	104±66	54
Vachon and Prairie (2013)			
- based on wind	1.027±0.243	185±77	68
- based on wind, lake area	0.813±0.160	120±53	58

F_S – surface methane emission; P_{net} – internal (oxic) methane production; OMC – contribution of internal (oxic) methane production to the system-wide surface emission. Stechlin relationship was developed based on flux chamber measurements: $k_{600} = 1.98 * U_{10} + 0.94$ (k_{600} – gas transfer constant [cm h^{-1}]; U_{10} – wind speed at 10 m height [m s^{-1}]). Donis et al. (2017)/Supplementary Note 6.1 - Hallwil relationship: $k_{600} = 2 * U_{10}$. MacIntyre et al. (2010) relationships: $k_{600} = 1.74 * U_{10} - 0.15$ (at buoyancy flux $\beta > 0$); $k_{600} = 2.04 * U_{10} + 2.0$ ($\beta < 0$); $k_{600} = 2.25 * U_{10} + 0.16$ (all β). Vachon and Prairie (2013) relationships: $k_{600} = 2.58 * U_{10} + 1.41$; $k_{600} = 1.48 * U_{10} + 0.39 * U_{10} * \log_{10}(LA) + 2.51$ where LA is lake area [km^2] (basin area was used instead of whole-lake area). Listed values as mean±SD of 6 replicates (2016 data).

When the diffusive methane input was compared between experimental enclosures and open water in August 2014, the experimental enclosures showed lower values (mean±SD; 0.007±0.009 mmol m^{-2} d^{-1}) than the adjacent open water (0.024 mmol m^{-2} d^{-1}).

Mass balance analysis – lateral input from the littoral zone. Methane measurements were done in the experimental enclosures and the adjacent open water (South basin) in August 2014. The experimental enclosures were shielded from the littoral zone (i.e. no lateral methane input), therefore oxic methane production in the surface mixed layer was estimated from Equation 6.1 (method section) – without the F_L term – to be (mean±SD) 101±17 nmol l^{-1} d^{-1}. By comparing the data from the experimental enclosures and those from the adjacent open water (both collected in the South basin), the transport of methane from littoral sediments within the surface mixed layer to the lake pelagic water was estimated to be 76±12 nmol l^{-1} d^{-1} (Table 6.4), which corresponds to an average littoral sediment methane flux of (mean±SD) 1.4±0.2 mmol m^{-2} d^{-1}.

Table 6.4: Mass balance components for estimating the lateral methane source. *Oxic production rates computed for the experimental enclosures were applied to the mass balance for the open water giving the average lateral methane input.*

Site	Mass Balance Component	Symbol	Whole System		Per Volume
			[mol d^{-1}]	[kg d^{-1}]	[nmol l^{-1} d^{-1}]
Exp. Enclosures	Surface emission	F_S	(2.7±0.5)E-2	(4.4±0.7)E-4	72.0±11.7
	Methane oxidation	MOx	1.2E-2	1.9E-4	30.3
	Lateral sediment input	F_L	0	0	0
	Diffusion from thermocline	F_z	(4.3±5.8)E-4	(6.9±9.3)E-6	1.1±1.5
	Internal (oxic) production	P_{net}	(3.9±0.6)E-2	(6.2±1.0)E-4	**101.1±16.8**
South basin	Surface emission	F_S	862.7	13.8	150.7
	Methane oxidation	MOx	173.7	2.8	30.3
	Lateral sediment input	F_L	437.1±67.2	7.0±1.1	**76.3±11.7**
	Diffusion from thermocline	F_z	19.1	0.3	3.3
	Internal (oxic) production	P_{net}	578.9±96.2	9.3±1.5	101.1±16.8

Measurements were taken inside enclosure 1 (20 m deep; 53°08'36.4"N 13°01'41.6"E) and enclosure 13 (20 m deep; 53°08'36.5"N 13°01'42.1"E), as well as in the open water adjacent to the enclosures (20.5 m deep; 53°08'36.6"N 13°01'42.8"E) in the South basin of Lake Stechlin. Measurements were done 4-5 times inside the enclosures and 4 times in the open lake on different days of the period 4-13th August 2014. Methane profiles and surface fluxes were averaged prior to the mass balance. Surface area: enclosures each 63.6 m^2, South basin 1,122,775 m^2. Standard deviation σ for surface emission/lateral sediment input/ diffusion from thermocline was computed as $\sqrt{[(\Sigma[x- \bar{x}])2/(n-1)]}$. Monte Carlo simulation (9999 iterations) was used to solve the mass balance after the target component (in bold) using the rnorm-function of R where normal distribution has the density f(x) = 1/(√(2 π) σ) e^-((x - μ)^2/(2 σ^2)) μ being the mean value. Values are presented as mean±1*σ.

Mass balance analysis – oxic methane production. Oxic methane production at high temporal resolution (approximately weekly) in the two open-water sites was estimated from Equation 6.1 using as F_L term (lateral methane input) the value obtained for August 2014 as described above. During the non-stratified season, oxic methane production rates were negligible and slowly increased in late April/May 2016 (Figure 6.7). As the water column became fully stratified, OMP rates averaged between the two basins ranged between 26 and 236 nmol l^{-1} d^{-1}, reaching the maximum for both basins (259 nmol l^{-1} d^{-1} in Northeast basin, 214 nmol l^{-1} d^{-1} in South basin) in late June (Figure 6.7).

Monte Carlo simulation was applied to assess uncertainties in the mass balance for the stratified period, and the resultant oxic methane production rates in the surface mixed layer were (mean±SD) 72±74 nmol l^{-1} d^{-1} (84 % probability of positive value) for the Northeast basin and 88±75 nmol l^{-1} d^{-1} for the South basin (Table 6.5). On average, oxic methane contributed 64 % of the surface methane emission in the Northeast basin, and 50 % in the South basin, with the remaining methane originating from anoxic sources. A sensitivity analysis (see discussion) examined the effect of variable mass balance components on the contribution pattern.

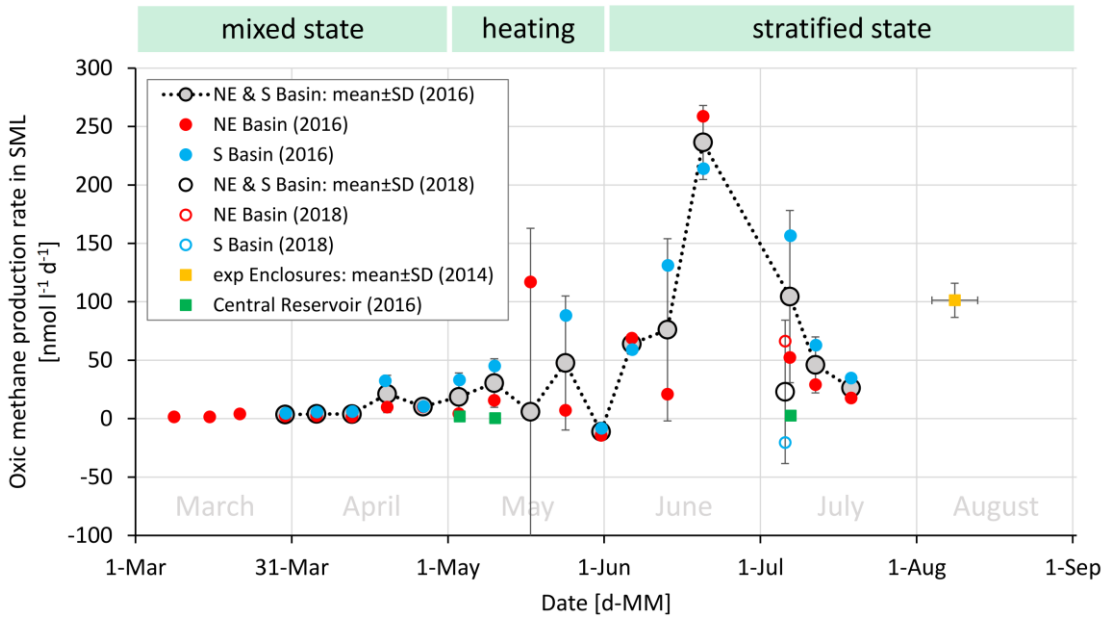

Figure 6.7: Oxic methane production rates in the surface mixed layer. *Production rates were computed using a mass balance approach. Red circles represent measurements in the open water of the Northeast basin (69.5 m deep; 53°09'20.2"N 13°01'51.5"E) and blue circles measurements in the open water of the South basin (20.5 m deep; 53°08'36.6"N 13°01'42.8"E). Grey circles are average values of both basins. Yellow square is the average values for the experimental enclosures (Enclosure 1 and 13 of the lake lab facility), and green squares are measurements in the central reservoir. Vertical error bars for illustrate standard deviation from mean values; and horizontal error bars (only experimental enclosures) depict the time frame of corresponding sampling. The mass balance was estimated for unstratified condition in March/April 2016 (negligible lateral methane flux, negligible methane oxidation) and for stratified condition June-August 2014/2016/2018 (lateral methane input from sediments: 1.4 mmol m^{-2} d^{-1}; 30 % of internally produced methane is oxidation). For May 2016, non-stratified parametrisation was used for the first half of the month and stratified parametrisation for the second half. Methane surface emission was measured in the Northeast basin (except on 20th June 2016) and on 6th July 2018 in the South basin, and was estimated for the other sites based on wind speed parametrisation. The sampling schedule for all field measurements are laid out in Table 6.1.*

Table 6.5: ***Mass balance components for estimating the oxic methane source.*** *Oxic production was computed by measuring/estimating surface emission, oxidation, lateral input, as well as vertical diffusion (Figure 6.3) and solving the mass balance for the missing component.*

Site	Mass Balance Component	Symbol	Whole System		Per Volume
			[mol d^{-1}]	[kg d^{-1}]	[nmol l^{-1} d^{-1}]
Northeast basin	Surface emission	F_S	942±538	15±9	90±52
	Methane oxidation	MOx	226	4	22
	Lateral sediment input	F_L	372±57	6±1	36±6
	Diffusion from thermocline	F_z	56±55	1±1	5±5
	Internal (oxic) production	P_{net}	752±771	12±12	**72±74**
South basin	Surface emission	F_S	795±268	13±4	148±50
	Methane oxidation	MOx	141	2	26
	Lateral sediment input	F_L	423±65	7±1	79±12
	Diffusion from thermocline	F_z	41±54	1±1	8±10
	Internal (oxic) production	P_{net}	470±400	8±6	**88±75**

Seven replicate measurements were taken in the open water of the Northeast and South basin (20.5 m deep; surface area 1,122,775 m^2; 53°08'36.6"N 13°01'42.8"E) of Lake Stechlin during the stratified period in 2016 (June-July). Standard deviation σ for surface emission/lateral sediment input/ diffusion from thermocline was computed as $\sqrt{[(\Sigma[x-\bar{x}])^2/(n-1)]}$. Note that Monte Carlo simulation (9999 iterations) was used to solve the mass balance after the target component (in bold) using the rnorm-function of R where normal distribution has the density f(x) = 1/(√(2π)σ)e^-((x-μ)^2/(2σ^2)) μ being the mean value (Supplementary Figure S5.3). Values are presented as mean±1*σ. If the Monte Carlo simulation were to be applied to whole lake data (combining South and Northeast basins data), oxic methane production rates P_{net} do not change: 78±80 nmol l^{-1} d^{-1} (F_S = 2503±1160, MOx = 496, F_L = 1198±185, F_z = 139±170, P_{net} = 1653±1703 mol d^{-1}).

Modelling the contribution of oxic methane to surface emission in relation to lake morphology. Own analysis showed that lateral input from the littoral zone and *in-situ* oxic methane contribution were the two major surface mixed layer methane sources, together accounting for ≥95 % of the surface emission in Lake Stechlin (Table 6.4 and 6.5). While the estimated oxic production rate was comparable between the two basins (Northeast: 72±74 versus South: 88±75 nmol l^{-1} d^{-1}), its relative importance, expressed as the percentage of oxic methane contribution to the system-wide emission, was considerably higher in the Northeast basin (64 %) than in the South basin (50 %). This difference was explained by the difference in geomorphology between the two basins: Lateral input is a function of littoral sediment area (A_{sed}), whereas oxic methane production is a function of the volume of surface mixed layer across the lake basin (∀). The relative importance between lateral input versus *in-situ* oxic methane production is therefore scaled to A_{sed}/∀, which decreases with increasing basin size.

While Stechlin's Northeast and South basin vary in surface area (Northeast: 2.01 km^2; South: 1.12 km^2) and surface mixed layer volume ∀ (Northeast: 11,200,000 m^3;

South: 5,700,000 m^3), their littoral sediment areas are comparable (Northeast: 0.28 km^2; South: 0.31 km^2) (values given for a 6 m deep surface mixed layer). As expected, oxic methane contribution to the system-wide surface emission was higher in the larger Northeast basin (64 %) compared to the smaller South basin (50 %) due to a smaller amount of A_{sed} per ∀ in the Northeast basin.

This scaling exercise was extended to other temperate oligo-to-mesotrophic lakes of various sizes extracted from the literature (DelSontro et al. 2018 – see methods, Bogard et al. 2014, Donis et al. 2017) in order to derive an empirical relationship between oxic methane contribution and lake morphology. The data showed that oxic methane contribution is a negative log-linear function of $A_{sed}/∀$ (Figure 6.8). Least square

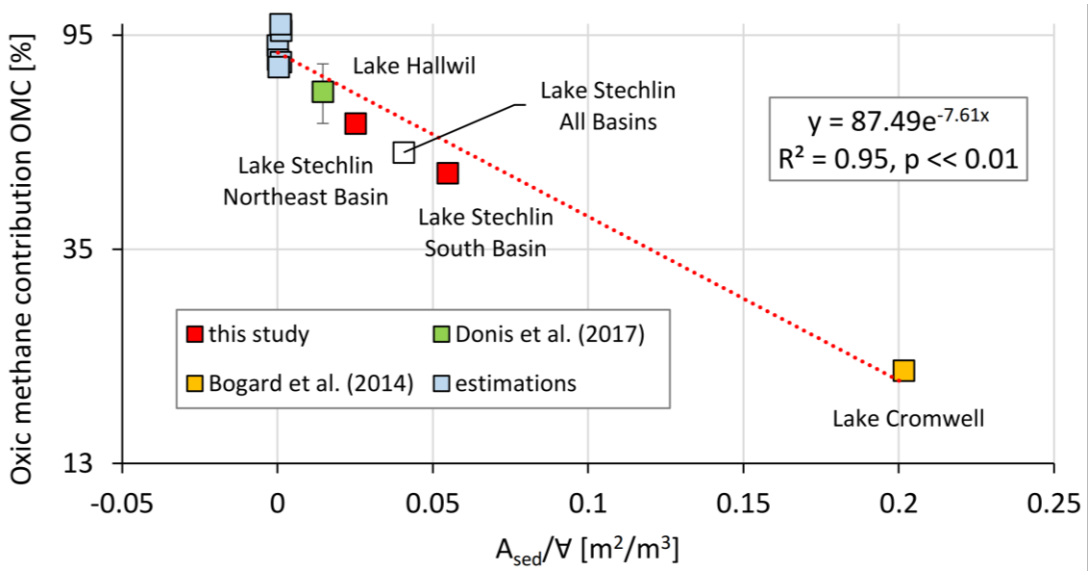

Figure 6.8: Oxic methane contribution to the system-wide surface emission (OMC) in relation with lake morphology of stratified meso-to-oligotrophic lakes in the temperate region. *The ratio of sediment area (A_{sed}) and surface mixed layer volume (∀) determines the oxic methane contribution to system-wide surface emission. The trend line (red line) follows the exponential function $y = 87.49e^{-7.61*x}$ ($R^2 = 0.95$, $p << 0.01$, standard error = 8.6 %). The y-axis is scaled to $log_{2.7}$ and the x-axis is linear. With increasing lake size, ∀ increases quicker than A_{sed} making oxic methane production the largest source of surface mixed layer methane in lakes with $A_{sed}/∀ \leq 0.07$ m^2/m^3. Lake Hallwil estimation (Donis et al. 2017) was updated as described in Supplementary Note 5.1; the lower and upper end (error bars) were used to compute the mean oxic methane contribution which was used for developing the trend line function. Estimations for other lakes were computed as defined in the method section. If whole-lake Stechlin data (combining South and Northeast basin data) was to be applied to this empirical modelling (empty symbol) the regression constants and statistics only changes minimally ($y = 88.48e^{-7.56*x}$; $R^2 = 0.96$, $p << 0.01$).*

regression after linearization gave a highly significant p-value (<< 0.01) and a high R^2 value (0.95). A significant relationship was also found between oxic methane contribution to system-wide surface emission and lake surface area (Figure 6.9). Both functions predicted that the importance of oxic methane production for surface mixed layer methane increases with lake size; for lakes with $A_{sed}/\forall \leq 0.07$ m^2/m^3 or surface area ≥ 1 km^2, oxic production is expected to be the main source (>50 %) of surface methane emissions.

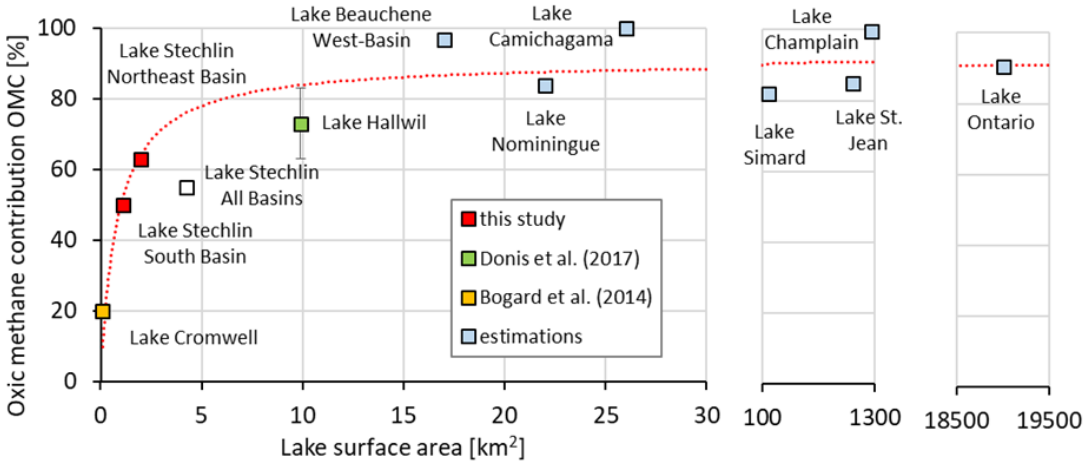

Figure 6.9: Oxic methane contribution (OMC) in relation with lake size. *Mass balance results, together with literature data and estimates (see methods), draw a function of the type y = (a * x) / (b + x). Deploying least standard error (SE) method gave the minimum standard error of 8.6 % when a = 90.87 and b = 0.83 (red line); indicating that the oxic source is the major surface mixed layer methane source in lakes sized larger than 1 km². Linear regression after double reciprocal transformation gives R^2 = 0.97 and p << 0.01. Note, the value for Lake Hallwil was updated as described in Supplementary Note 6.1; the upper and lower end estimation are here represented by error bars and the mean was used to establish the trend line function. The x- and y-axis are linearly scaled. If the datasets for Stechlin's basins alternatively were to be combined and the empirical model were to be solved using Stechlin as a single data point (empty symbol), the equation constants slightly change (a = 92.90, b = 1.92, SE = 10.7 %). In this case the empirical model predicts the oxic methane source to be the dominant source in lakes larger 2 km². Standard error was computed as* $SE = \sqrt{(\Sigma(\hat{x}-x)^2/(n-2))}$ *where* $\hat{x}$ *is the predicted value, x is the data point value and n is the number of data points.*

First-order estimation of oxic methane contribution in a global context. The established model of oxic methane contribution in relation with lake surface area (Figure 6.9) was used to get a first-order estimate of how much oxic methane production potentially contributes to the surface methane emission of lakes on a global scale. Note, that the model is based on temperate lakes with oligo-to-mesotrophic nutrient state.

Projecting obtained model to the global lake inventory does not account for environmental differences and purely serves the purpose of estimating whether oxic methane production is of global relevance. For accurate estimation, an appropriately sized cohort of lakes with global distribution needs to be surveyed including other lake types, such as eutrophic lakes or lakes in other climate zones (which might show deviation in the predictive function, especially for smaller lakes).

By accounting the different oxic methane contribution values of the lake size classes and the different contributions of these lake size classes to the global lake surface area, the first-order estimate for the global oxic methane contribution was computed to be 66 %. Table 6.6 summarises the parameters calculated for this estimation.

Table 6.6: First-order estimate of the global relevance of oxic methane contribution to the surface methane emission in lakes. *The global abundance of different lake size classes and the total surface area was extracted from Cael et al. (2017). The mean lake size was applied to the established model (oxic methane contribution~lake surface area; see result section) to estimate oxic methane contribution for different lake size classes. These oxic methane contribution values were then projected to the total surface area of the lake size classes.*

Literature values			Calc	Applying model		Global projection
Size class [m²]	***n*** **[#]**	A_{class} **[km²]**	γ_{class} **[%]**	A_{mean} **[km²]**	OMC_{class} **[%]**	γ_{global} **[%]**
$10^4 – 10^5$	23725071	683000	13.32	0.05	5.17	0.69
$10^5 – 10^6$	3813612	995000	19.40	0.5	34.21	6.64
$10^6 – 10^7$	331452	793000	15.46	5	77.96	12.06
$10^7 – 10^8$	24332	611000	11.91	50	89.39	10.65
$10^8 – 10^9$	1948	489000	9.54	500	90.72	8.65
$10^9 – 10^{10}$	211	537000	10.47	5000	90.85	9.51
$>10^{10}$	20	1020000	19.89	50000	90.86	18.07
Σ Global	**27896646**	**5128000**				**66.27**

n – lake abundance; A_{class} – total surface area; γ_{class} – total surface lake area expressed in percentage; A_{mean} – lake size mean; OMC_{class} – oxic methane contribution of Lake size class; γ_{class} – oxic methane contribution of a size class expressed in percentage

6.5 Discussion

In this study, the methane sources in two basins of the temperate meso-oligotrophic Lake Stechlin were balanced in high temporal resolution covering, for the first time, the shift from mixed to stratified water column conditions. Furthermore, this study analysed the methane budget in two different types of enclosures, both isolated from littoral methane input: in experimental enclosures (1,200 m^3) where water is periodically exchanged (last time 2 weeks prior to sampling) and in the central reservoir

(14,000 m^3) where water has not been exchanged for 8 years and is likely nutrient depleted. Comparing the methane budgets in the open water and enclosures allowed to demonstrate that: 1) stratification mainly disconnected surface mixed layer methane from bottom sediment methanogenesis; 2) the occurrence of oxic methane production irrespective of littoral influence; and 3) oxic methane production contributed substantially to the system-wide methane emission of Lake Stechlin's Northeast (64 %) and South basin (50 %) exceeding the littoral methane source contribution (32 % in the Northeast basin and 45 % in the South basin). Finally, combining the mass balance results for Lake Stechlin and literature data for other lakes allowed to develop a predictive model estimating the contribution of oxic methane production to the system-wide methane surface emission as a function of lake morphological parameters, and the model suggests that oxic methane production is globally important, especially in large stratified lakes.

Local implications. Mass balance approach has been successfully used by others to study methane dynamics in lakes, including oxic methane production (Bastviken et al. 2002, Bogard et al. 2014, Donis et al. 2017). However, this approach is sensitive to the accuracy of the individual components of the mass balance. Therefore, to assess the validity and robustness of the mass balance analysis, the different components were evaluated by comparing own measurements with literature values and examining how variabilities of the mass balance components may alter the overall conclusion.

Surface methane emission (F_S) – The average surface methane emission during the stratified period was 0.47 mmol m^{-2} d^{-1} (±57 % SD) in the Northeast basin and 0.71 mmol m^{-2} d^{-1} (±34 % SD) in the South basin (taken mainly during calm weather). The larger value in the South basin can be attributed to higher littoral sediment area per basin size versus Northeast basin. However, these emission values are comparable with the global estimate of 0.62 mmol m^{-2} d^{-1} for the region 25-54° latitude (Bastviken et al. 2011) and within the range reported earlier for Lake Stechlin (exceeding 4 mmol m^{-2} d^{-1} at strong wind; 2.6 mmol m^{-2} d^{-1} ±42 % SD) (McGinnis et al. 2015). Highly variable surface emission has been reported earlier, for some systems standard deviations exceed 100 % of mean emission values during summer (Sabrekov et al. 2017, Xiao et al. 2017). In case of the South basin the emission was estimated from wind speed data and the corresponding results are dependent on the gas transfer constant (k_{600}) value used. The retrieved k_{600}-wind speed relationship (k_{600}[cm h^{-1}] = 1.98*U_{10}[m s^{-1}] + 0.98) was very similar to an earlier report (e.g. Lake Hallwil: k_{600}[cm h^{-1}] = 2.0*U_{10}[m s^{-1}]; Donis et al.

2017). Applying six alternative emission models (based on wind or combined wind and lake size) presented by MacIntyre et al. 2010, Vachon and Prairie 2013, Donis et al. 2017 to this dataset resulted in an average emission rate between 0.55 and 1.03 mmol m^{-2} d^{-1}. Using these emission rates for mass balance analysis gave an oxic methane production rate between 41 and 185 nmol l^{-1} d^{-1}, which still translated to a substantial oxic methane contribution (32 – 68 %) to the surface methane emission (details in Table 6.3). Regardless of which method was used to estimate surface methane emission, oxic methane production was a major contributor to surface emission.

Lateral methane input (F_L) – Comparing the methane data inside the experimental enclosures with that of the open water gave an average lateral methane input of 1.4 mmol m^{-2} d^{-1} from the littoral sediment. It is within the range of fluxes reported for other temperate water bodies (i.e. Rzeszów Reservoir, Poland – Gruca-Rokosz and Tomaszek 2015: mean±SD 0.69±0.56 mmol m^{-2} d^{-1} in May-Sep; Lake Hallwil, Switzerland – Donis et al. 2017: 1.75±0.2 mmol m^{-2} d^{-1} in Sep (Supplementary Note 6.1); Arrhenius-Boltzmann equation at ca. 20°C – Peeters et al. 2019: ca. 2 mmol m^{-2} d^{-1}, including Lake Constance (Überlingen basin)/Lake Ammer/Lake Königsegg/Reservoir Schwarzbach in Germany with ca. 1.3 mmol m^{-2} d^{-1}). Even doubling the lateral methane input — an unlikely scenario for a meso-oligotrophic lake such as Lake Stechlin— still could not fully explain the observed surface mixed layer methane in the Northeast basin, and a substantial oxic methane production rate (19 nmol l^{-1} d^{-1}) would still be required to balance the methane budget. More importantly, within the experimental enclosures, which were isolated from lateral input, the estimated OMP was (mean±SD) 101±17 nmol l^{-1} d^{-1} (Aug 2014 dataset), which was very comparable to the estimated average oxic production in the open water for both basins (72 – 88 nmol l^{-1} d^{-1}) (June/July 2016 dataset).

Vertical methane diffusion (F_z) – The calculation of methane diffusive input from the lower water layers is dependent on the estimated K_z value. Own K_z values were comparable to an earlier report for the same lake (Kirillin et al. 2012b). Even in Lake Hallwil, which is 5 to 10 times larger than the investigated Lake Stechlin basins and is therefore exposed to stronger seiching effects, very similar K_z values were observed (thermocline minimum about 10^{-6} m^2 s^{-1}) (Donis et al. 2017). The surface mixed layer methane in Lake Stechlin was decoupled from bottom sediment methanogenesis during thermal stratification as it is indicated by the methane-depth profile of the central

reservoir (Figure 6.6e) where water has not been exchanged for 8 years. Accordingly, methane diffusion from Lake Stechlin's thermocline water accounted for only 2-5 % (likely overestimated) of the surface mixed layer methane in the open-water sites, and only 1 % in the experimental enclosures. Variability in the corresponding mass balance components, therefore, was negligible and would not affect the overall conclusion.

Methane oxidation (MOx) – The magnitude of methane oxidation varies between seasons (Joye et al. 1999, Utsumi et al. 2003, Carini et al. 2005) and between lakes (DelSontro et al. 2018). Oxygen concentration (Rudd 1976) and light (Dumestre et al. 1999, Murase and Sugimoto 2005) are important modulating factors for methane oxidation in lake surface waters. In other lakes, methane oxidation rates in oxic surface waters have been reported to range between 4 and 30 nmol l^{-1} d^{-1} (Bogard et al. 2014, Oswald et al. 2015, Donis et al. 2017). In this study, methane oxidation was assumed to be equivalent to a constant fraction (30 %) of the internal production during the stratified season (method section). The average oxic methane production rates for both basins were 70 – 88 nmol l^{-1} d^{-1}, giving a hypothetical methane oxidation rate of ca. 24 nmol l^{-1} d^{-1}, which is within this range of literature values. Because methane oxidation is a loss term in the mass balance analysis, higher methane oxidation would correspond to higher oxic methane production, and vice versa. If the extreme scenario was to be considered by completely ignoring methane oxidation (MOx = 0), the estimated average oxic methane production rate for the South basin would decrease to (mean±SD) 40±53 nmol l^{-1} d^{-1} and would remain an important surface mixed layer methane source (32 %).

Oxic methane production (P_{net}) – Comparing own measurements and assumptions against literature values shows that the own mass balance analysis is reasonably parametrised and robust. The system-wide methane emission from the surface mixed layer in the Northeast basin was estimated to be 942 mol d^{-1} in the stratified period, of which 32 % from lateral input (372 mol d^{-1}) and 5 % from vertical diffusion from the thermocline (56 mol d^{-1}) (Table 6.5). Similarly, methane emission from the surface mixed layer in the South basin was 795 mol d^{-1}, and only 45 % (423 mol d^{-1}) could be attributed to lateral input and 4 % (41 mol d^{-1}) to vertical input from the thermocline. The deficits (plus additional consumption via methanotrophy), therefore, must be compensated for by internal oxic methane production. The estimated oxic methane production rate averaged over the stratified period was (mean±SD) 72±74 nmol l^{-1} d^{-1} (Northeast basin) and 88±75 nmol l^{-1} d^{-1} (South basin). An earlier study (Grossart et al.

2011) using bottle incubations measured a net oxic methane production rate of up to 58 nmol l^{-1} d^{-1} for Lake Stechlin, which corresponds to a hypothetical gross production rate of 75 nmol l^{-1} d^{-1} when assuming 30 % oxidation. Similar oxic methane production rates have also been estimated for Lake Hallwil, between 76 and 138 nmol l^{-1} d^{-1} (Supplementary Note 6.1) (Donis et al. 2017). Particularly high production values, such as in Lake Stechlin during late June (mean±SD; 236±32 nmol l^{-1} d^{-1}), have also been reported by others (e.g. 230±10 nmol l^{-1} d^{-1} in Lake Cromwell, Canada) (Bogard et al. 2014).

Overall, accounting for the different methane sources and sinks in the surface mixed layer mass balance analysis showed that oxic methane production is a key contributor to system-wide surface emission in Lake Stechlin. This conclusion is consistent with previously reported oxic production rates obtained from bottle incubations (Grossart et al. 2011) and is not sensitive to inherent uncertainties in the mass balance approach as shown by the sensitivity analysis.

Global Context. In addition to known knowledge gaps in the global methane dynamics (Kirschke et al. 2013, Saunois et al 2016a,), oxic methane production has not been considered as source of uncertainty in global assessments (IPCC 2007, IPCC 2013, Kirschke et al. 2013, Saunois et al 2016a). The modelling approach indicated that OMP is an important contributor to surface methane emission in lakes. Especially in large lakes, oxic methane production can might be responsible for variability in atmospheric emission. Because both oxic and anoxic methane sources in lakes can be modulated by multiple factors and processes (Figure 6.10), some of which are still poorly understood, it would be premature to construct a mechanistic model to fully describe methane dynamics in lakes. Instead, empirical models were developed as useful tools to predict the contribution of oxic methane production to the system-wide emission in stratified meso-to-oligotrophic lakes in the temperate region based on a set of simple lake morphological parameters (Figure 6.8 and 6.9).

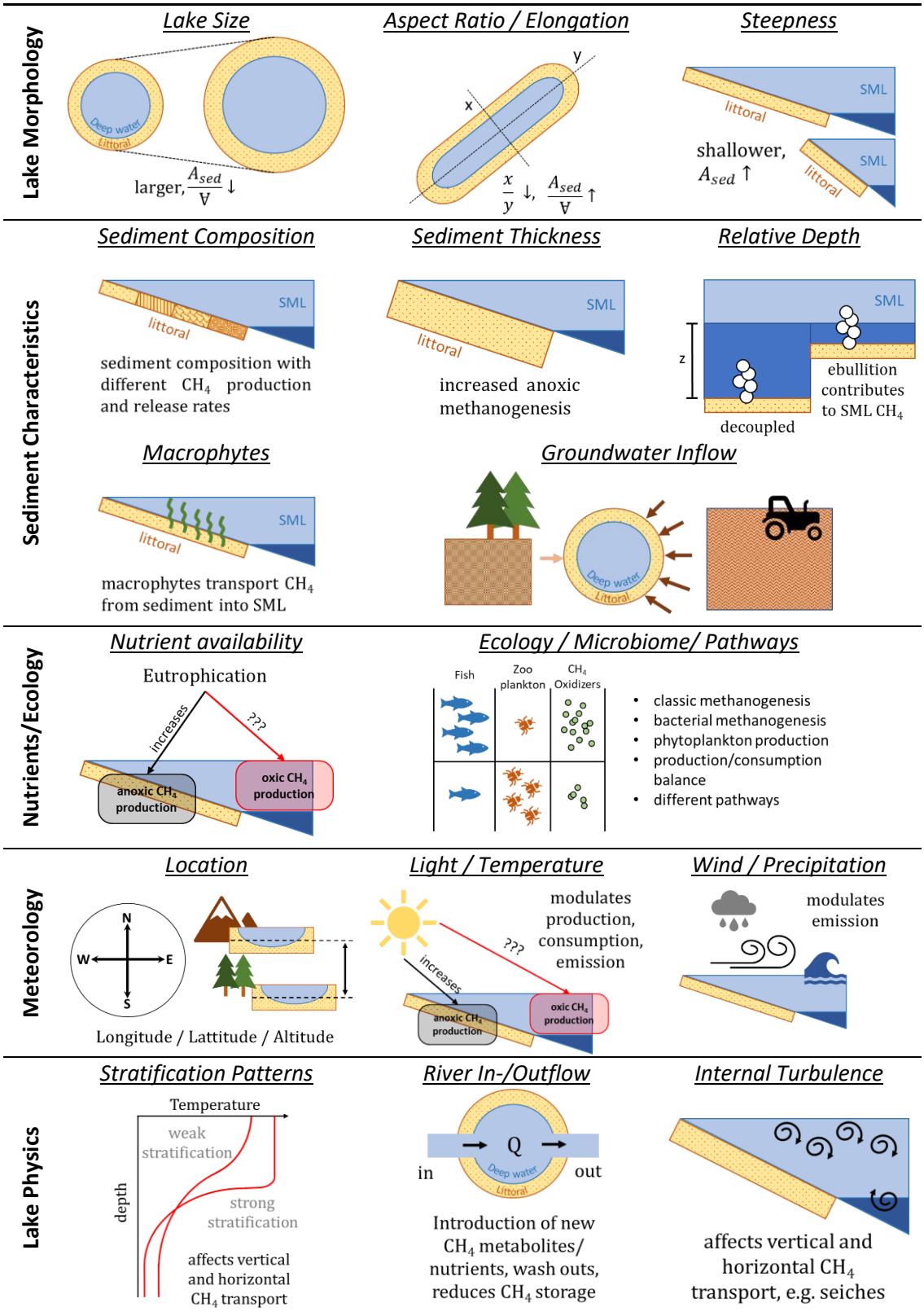

Figure 6.10: Selection of mechanistic factors affecting the contribution of oxic and anoxic methane sources to the system-wide surface emission. *Factors can be categorized into morphology, sediment characteristics, nutrient conditions/ecology, meteorology and lake physics. A_{sed} symbolizes littoral sediment area, SML is surface mixed layer, V refers to the volume of the surface mixed layer and Q is flow rate.*

The first model using littoral sediment area (A_{sed}) and surface mixed layer volume (∀) as proxy explains nearly the entire variance in the dataset (R^2 = 0.95, p << 0.01) making it a powerful predictive model to estimate oxic methane contribution from A_{sed} and ∀ (Figure 6.8). For cases where A_{sed} and ∀ data are unavailable, oxic methane contribution can be related to easily accessible lake surface area (Figure 6.9). With an average accuracy of 91.4 % (standard error = 8.6 %) also this model provides reliable estimates of oxic methane contribution. Both empirical models predict the importance of oxic methane production for atmospheric emission to increase together with lakes size.

The system-wide contribution of the anoxic methane sources is mainly controlled by the littoral sediment flux and the corresponding littoral sediment area. Trophic state (e.g. Adams 2005, Beaulieu et al. 2019) and temperature (Duc et al. 2010, Marotta et al. 2014, Aben et al. 2017, Peeters et al. 2019) are important drivers of the methane flux from sediments. Higher sediment fluxes in eutrophic systems and in warmer climate zones compared to the own dataset of stratified meso-to-oligotrophic lakes in the temperate region could shift the curve of the empirical models to the right (Figure 6.8 and 6.9). However, sediment methane fluxes vary in a rather narrow range by a factor of 26 for oligotrophic to eutrophic lakes (e.g. 0.2–5.2 mmol m^{-2} d^{-1}) (Adams 2005). Likewise, reported average oxic methane production rates varied by a factor of 6 in stratified lakes (40–230 nmol l^{-1} d^{-1}) (including this study, Grossart et al. 2011, Bogard et al. 2014, Donis et al. 2017,). In comparison, the presented predictive model covers lake surface area that varies by a factor of 190,000. The prediction of oxic methane contribution to the system-wide surface emission may vary mainly for small lakes which have been reported to cause less methane emission on a global scale compared to larger lakes (Bastviken et al. 2004) (<0.01 versus >1 km^2). It shall be noted that the model predictions based on A_{sed} and ∀ will be more reliable than based exclusively on lake surface area due to sediment steepness/aspect ratio and total depth modulating the littoral sediment area at constant lake surface area.

Methane emission from lakes has been identified as an important contributor of this powerful greenhouse gas to the atmosphere (Saunois et al. 2016a). It is therefore a legitimate question to ask: How important is oxic methane production in this context on a global scale? To get a first-order estimation, the empirical model was applied to the global lake size distributions based on satellite data, which covers lakes ≥0.01 km^2 (Cael et al. 2017). The result suggests that globally, an average of 66 % of lake methane

emission may have originated from oxic production (see method section for details, Table 6.6). Such a surprising finding justifies the need for further investigation of oxic methane production in lakes worldwide with different geological histories, trophic states, climates, and physical (e.g. lake colour, stratification patterns or with strong in-/ out flow) and chemical characteristics (e.g. alkaline versus acidic) (Figure 6.10). By increasing data resolution in the empirical models, the models can then be used to further improve the global methane emission assessments.

Unlike the anoxic methane production driven by anaerobic methanogens with enzymes that are oxygen-sensitive (Jarrell 1985), oxic methane production in lake waters has been attributed to novel biochemical pathways involving photoautotrophs (Chapter 3, Grossart et al. 2011, Lenhart et al. 2016, Teikari et al. 2018). The system-wide methane mass balance demonstrates that without oxic methane production a substantial methane source is missing when balancing Lake Stechlin's surface mixed layer methane sources and sinks. The estimated oxic production rates agree very well with earlier results from bottle incubation experiments (Grossart et al. 2011) and account for ≥50 % of the system-wide methane emission. Following the model, oxic methane contribution to system-wide surface emission is predicted to be the major methane source for the system-wide emission in lakes >1 km^2. In the light of global warming and wide-spread lake eutrophication, stratification periods will extend (De Stasio et al. 1996, Peeters et al. 2007) and phytoplankton production in the surface mixed layer is expected to increase worldwide (Visser et al. 2016), which may increase oxic methane production and its contribution to atmospheric methane emission. To understand and predict future climate change scenarios, it is crucial to consider lake-water oxic methane production in the global methane assessment and how it responds to environmental perturbations.

Chapter 7: General Discussion and Conclusion

Paradox reconsidered. Biological methane formation has been known for over 200 years (Volta 1777). It is commonly believed that biological methane formation is an anaerobic process exclusive to methanogenic Archaea in anoxic environments due to the reduced nature of methane and the oxygen-sensitivity of involved enzyme machinery (Schönheit et al. 1981, Jarrell 1985, Ragsdale and Kumar 1996). A recent assessment of the global methane budget and the latest IPCC report define biological methane production accordingly:

- "Biogenic methane is the final product of the decomposition of organic matter by Archaea in anaerobic environments…" (Saunois et al. 2016a)
- "Where oxygen is limited, as in waterlogged soils, some microbes also produce methane." (IPCC 2013)

In lakes, the frequently observed methane oversaturation in oxic surface-waters (Tang et al. 2016 and references therein), termed "the methane paradox," is often attributed to archaeal methane production in anoxic sediments coupled with horizontal or vertical physical transport processes (Murase et al. 2005, Hofmann et al. 2010, Fernandez et al. 2016, Peeters et al. 2019). Alternatively, micro-anoxic zones, such as the guts of zooplankton and fish (Sieburth 1987, de Angelis and Lee 1994, Schmale et al. 2017, Stawiarski et al. 2019) or faecal pellets (Karl and Tilbrook 1994, van der Maarel et al. 1999) are proposed to explain paradoxical oxic-water methane accumulation (Murase et al. 2005). The shape of the mid-water methane profile (Figure 1.3) with high methane content in epilimnic water, low methane in the hypolimnion and a distinct peak at the thermocline depth, is accordingly assumed to be associated with these anoxic methane sources, and surface emission, gas solubility gradients (Wilkinson et al. 2005) and variable methane oxidation at different water column-depths (e.g. inhibition by light; Murase and Sugimoto 2005) finally shape the profile.

The discovery of oxic methane production in marine (Karl et al. 2008) and freshwaters (Grossart et al. 2011) challenges the century-old dogma and indicates that our understanding of the global methane cycle needs to be re-evaluated. There are important questions such as: Who are the responsible microorganisms? What molecular pathways do they use for methane productions? What are the environmental driving forces? Moreover, is this phenomenon relevant on a global scale?

As oxic methane production goes against the prevailing dogma of exclusively anoxic methane production, there is scepticism about the existence and the contribution of an oxic methane source to surface-water methane (Fernandez et al. 2016, Peeters et al. 2019). This thesis produced clear evidence of oxic methane production in lake water (Lake Stechlin) and examined the environmental importance of this novel methane source.

This thesis deployed various methodological approaches to investigate the existence of methane production in the oxic water column of Lake Stechlin. These approaches included in-lab/in-field bottle incubation experiments (Chapters 2, 3, 4), balancing surface mixed layer methane sources and sinks (Chapters 4, 5), in-lab/in-field isotope labelling experiments (Chapters 2, 3, 4) and modelling methane concentration changes in the field based on ^{13}C-signatures (Chapter 2). All of these approaches came to the same result: Oxic methane production could and did occur in the oxic lake-water column.

The Oxic methane production. Since their discovery, paradoxical methane oversaturation and oxic methane production in Lake Stechlin have been observed in every stratified season (this thesis, Grossart et al. 2011, Tang et al. 2014, McGinnis et al. 2015, Bizic-Ionescu et al. 2018). In order to evaluate the importance of the oxic methane source, its contribution to the surface methane emission has been determined. In Lake Stechlin, the mass balance results showed that oxic methane production is the major (55 %) methane source during the stratified season (Chapter 5).

Freshwater methane emission accounts for a substantial contribution to the atmospheric methane burden (ca. 20 %). Demonstrating that oxically produced methane is emitted to the atmosphere in Lake Stechlin (this thesis, Grossart et al. 2011) and other Lakes (Bogard et al. 2014, Donis et al. 2017, DelSontro et al. 2018) identifies the oxic methane source as a yet unacknowledged contributor to the atmospheric methane burden. Global assessments are hampered by large uncertainty during upscaling freshwater methane emission (e.g. 122±60 Tg per year; Saunois et al. 2016a). Accordingly, the oxic methane source may be accountable for a large part of this uncertainty. The developed empirical models (Chapter 5) predict that the importance of oxic methane production for surface emission increases with increasing lake size. Large lakes are estimated to cause the majority of global freshwater methane emission (Bastviken et al. 2004, Saunois et al.

2016a). The first-order estimation reckons the contribution of the oxic methane production to mid-water methane emission to be 66 % (Chapter 5). Accordingly, the model predictions indicate that the oxic methane source is of global relevance. Acknowledging the oxic methane source in global methane budget assessments requires a proper distinction between the oxic and anoxic methane source and quantification of their individual contribution to system-wide atmospheric emission. So far, these individual contributions have only been investigated in a few stratified lakes with meso-to-oligotrophic nutrient state (this thesis, Grossart et al. 2011, Bogard et al. 2014, Donis et al. 2017, DelSontro et al. 2018). In the light of the large system-heterogeneity of lakes, the contribution patterns must be surveyed in different lake types (e.g. trophic state, different climate zones, morphological properties, physical/chemical/biological conditions) all around the globe. Only then, the entire global impact of the oxic methane source will be revealed.

Phytoplankton has been identified as a potential driving force of the oxic methane source: In-lab incubation experiments showed that Cyanobacteria, Green Algae, Diatoms, and Cryptophytes are able to produce methane, and corresponding phytoplankton pigments have been observed in the field to correlate with oxic water methane and ^{13}C-methane isotope signatures (Chapters 2, 3, 4). In Lake Stechlin, the average oxic methane production rate during the stratified season tripled during Cyanobacteria blooms at the end of June (78 versus 236 nmol l^{-1} d^{-1}). Accordingly, the contribution of the oxic methane source to surface emission in Lake Stechlin's South basin increased from ca. 50 % to over 90 % for a short period of time (Chapters 4, 5). These findings highlight the importance of understanding oxic methane production in relation to phytoplankton dynamics. Phytoplankton is ubiquitous to illuminated aquatic systems. In response to nutrient competition, light availability, temperature fluctuation, microbiome condition and food web-interactions (Aekanishi and Monsi 1976, Elser et al. 1990), phytoplankton exhibits strong dynamic growth affected by many environmental parameters. For instance, wind-induced mixing can stimulate nutrient migration into the surface mixed layer, promoting phytoplankton growth (Giling et al. 2017, Kasprzak et al. 2017). Oxic methane production, therefore, may mimic the highly dynamic nature of phytoplankton production (Chapter 2 and 4). Accordingly, fluctuation in the oxic methane source might be a key player for highly variable methane density fluxes within and across lake systems – a major challenge for upscaling freshwater

emissions (Natchimuthu et al. 2015, Wik et al. 2016a, Sabrekov et al. 2017, Xiao et al. 2017). In large lakes, phytoplankton dynamics could even be the sole driver for variable emission patterns due to the limitation of horizontal (DelSontro et al. 2018) and vertical methane transport mechanisms (Tang et al. 2014). A better understanding of phytoplankton methane production will help to reduce uncertainty (Saunois et al. 2016a) when upscaling freshwater methane emission in future studies.

Advancing our understanding of lake water methane cycling is associated with re-evaluating deployed methods in regard to their ability to account for the oxic methane source. For example, decreases in methane concentrations of oxic lake water incubated in bottles are usually attributed to methane oxidation without considering the entire production-consumption balance, and therefore, smaller methane decrease in the light has led to the hypothesis that oxidation can be inhibited by light (Murase and Sugimoto 2005). Acknowledging oxic methane production, however, allows an alternative explanation: increased methane production rates under sunlight exposure could have led to the same pattern of diurnally changing methane concentrations. Isotope labelling techniques recording methane production and consumption simultaneously are required in future studies to re-assess this hypothesis. In Chapter 2, for instance, methane production rates varied at different diel stages while oxidation remained stable. Correlative analysis of sediment methane fluxes and surface methane emission has led to the assumption that oxic methane production is not relevant for individual lake assessments (Fernandez et al. 2016, Peeters et al. 2019). Nevertheless, deploying detailed methane mass balance analyses of the surface mixed layer – the interface between deep waters and atmosphere – (Chapter 4, 5, Bogard et al. 2014, Donis et al. 2017) and bottle incubation experiments (Chapter 2, Grossart et al. 2011) clearly showed that oxic production does exist and contributes to lake methane cycling. In the light of the complex nature of methane cycling in lakes (including various oxic and anoxic production pathways, variable oxidation rates and different storage and transport mechanisms), future research will have to employ multi-prong approaches and high-resolution measurements to separate oxic versus anoxic methane sources and their variable character. The comparison of mesocosm enclosures with open lake methane proved useful for quantifying the lateral anoxic methane source (Chapter 5) compared to sediment core analysis (Chapter 4, Donis et al. 2017). Isotope discrimination is pathway-specific. Accordingly, isotope techniques that distinguish between different oxic

methane production pathways, in combination with mass balance, can be used to quantify pathway-related surface methane emission. Application of isotope techniques, however, require a comprehensive understanding of the isotope-signatures of methane-precursor molecules and pathway-specific ^{13}C-enrichment factors (Aelion et al. 2010). Mapping of multi-element isotope signatures (C, H, P, S, N) across the substrate and product pools of oxic methane production will additionally help to resolve the underlying biochemical pathways. During multiple field campaigns, methane samples were extracted from oxic waters and analysed with regard to the hydrogen isotope signature (data not shown). However, due to low methane content in the samples hydrogen isotope signatures could not be determined in this thesis. New extraction methods are required to obtain oxic water methane in sufficient quantity for further downstream analyses.

Also, methodological limitations during the upscaling of freshwater methane emissions can be a source of uncertainty. For example, the wind-based emission models developed by Cole and Caraco (1998) and Crusius and Wanninkhof (2003) are often applied to big datasets to estimate the water-air emission using only wind speed as proxy parameter (Bade 2009, Lopez Bellido et al. 2009, Takahashi et al. 2009, Lana et al. 2011, Wanninkhof 2014). As wind speed is not the only factor modulating the water-air gas transfer (Chapter 6), incorporation of additional proxy parameters such as lake area can lead to more reliable emission estimates (Vachon and Prairie 2013). The results presented in Chapter 6 suggest that using water- and air temperature as additional proxies will improve the gas transfer estimations. These temperature data are commonly recorded throughout routine measurements worldwide. Likewise, lake area data is easily accessible. Consecutive studies need to develop emission models using wind speed, lake area, water- and air temperature simultaneously for proxy modelling. Combining all of these parameters will allow to account for more system variability (heat flux, effective wind forcing; MacIntyre et al. 2010, Vachon and Prairie 2013) among earth's heterogeneous lake inventory (Cael et al. 2017) and lead to improved global emission estimates across climate zones.

While lake systems account for a substantial amount of freshwater methane emission, there are other systems such as reservoirs and rivers which have not been examined yet regarding the oxic methane source. Oxic methane production has been associated to a broad spectrum of aquatic organism including representants of all three Domains of life: Archaea, Prokaryotes (including Cyanobacteria – Chapter 3, Teikari et

al. 2018 and Proteobacteria – Yao et al. 2016), as well as Eukaryotes (including Green Algae, Diatoms, Cryptophytes – Chapter 4 and Haptophytes – Lenhart et al. 2016). Accordingly, it is expected that oxic methane production is prevalent in other aquatic systems than lakes. For estimating the contribution of oxically produced methane to surface emission in reservoirs, analogous techniques can be used as they have been deployed in lake systems. However, investigations in rivers will require new approaches suitable for flowing water conditions. The statistical analysis combined with modelling the oxic methane source in relation to flow rate in a pool of lakes with large size variability may be one possibility to examine oxic methane production in running waters. Oxic methane production, however, is not limited to the boundaries of aquatic systems. There is growing evidence that also terrestrial organisms can and do produce methane under oxic conditions. Plants (Keppler et al. 2006), fungi (Lenhart et al. 2012), methanogenic Archae (Angle et al. 2017) and desert crust Cyanobacteria (Chapter 3) have been so far identified as new terrestrial (oxic) methane sources. Similar to aquatic systems, the global impact of terrestrial oxic methane production remains obscure. When looking at the latest global methane budget by Saunois and colleagues (2016a) (Figure 1.2), land methane sources comprise a very high level of uncertainty (185±86 Tg yr^{-1} methane emission) similar to the freshwater methane sources (122±60 Tg yr^{-1} methane emission). The large uncertainty range for both freshwaters and inland methane sources concede that aquatic and terrestrial oxic methane production could be major contributors for the atmospheric methane burden. To resolve the scope of oxic methane production more research resources need to be invested and studies must use more systematic approaches: Future research should strategically screen banks of organisms with various taxonomic affiliations for oxic methane production. After identification of target organisms, corresponding ecosystems harbouring these target organisms should be examined in respect to atmospheric methane emission.

Environmental controls of oxic methane production. To understand how the oxic methane source will respond to environmental perturbations, comprehensive knowledge of involved organisms and molecular pathways is needed. Currently, research focusses on two types of methane formation in oxic waters: 1) methylphosphonate degradation, and 2) oxic methanogenesis. Degradation of methylphosphonates is an alternative way of phosphorus acquisition that produces methane as a by-product. The existence of such a pathway has been demonstrated for marine (Karl et al. 2008, Carini

et al. 2014) and freshwater Bacteria (Yao et al. 2016, Wang et al. 2017, Teikari et al. 2018) by observing methylphosphonate-triggered methane production and identifying the involved gene cassettes. The pathway of oxic methanogenesis, on the other hand, has not been resolved yet. Methane oversaturation in aquatic systems has been frequently observed to coincide with high oxygen content (Tang et al. 2014, Tang et al. 2016) and chlorophyll a (Tang et al. 2016 and references therein). These observations lead to the idea that photoautotrophic organisms could be responsible for oxic methane production. Indeed, oxic methane production has been associated with phototrophic organisms (Chapter 2, 3, 4, Lenhart et al. 2016) and primary production (Grossart et al. 2011, Bogard et al. 2014, Tang et al. 2014). Recognizing the two pathways and corresponding organisms suggests that nutrient (inorganic phosphorus) availability and light could be two key drivers of the oxic methane source. Chapter 2 established the first field evidence, that phosphor limitation should be acknowledged as a driving force: 1) the ^{13}C-methane isotope signature changed throughout incubation of lake water and modulating the inorganic phosphorus pool and soluble reactive phosphorus correlated with ^{13}C methane isotope signature, and 2) soluble reactive phosphorus concentration negatively correlated in a log-linear fashion with methane accumulation in surface waters, as well as with surface methane emission. It is not clear why these relations followed a log-linear fashion (probably associated with Michaelis-Menten kinetics; Cornish-Bowden 2015). Additionally, various in-lab and in-field incubation experiments (Chapter 2, 3, 4) showed all major phytoplankton types in Lake Stechlin are able to produce methane, suggesting this ability is widespread among phytoplankton types and likely prevalent in phytoplankton communities in lakes worldwide. Furthermore, the transformation of ^{13}C-labelled bicarbonate to methane (Chapter 2,3,4) as modulated by light exposure (Chapter 2) connects photosynthesis to oxic methane formation.

Eutrophication is a problem for many lakes all around the globe, and the communities started to counteract deploying bioremediation programs to reduce the nutrient loading in affected lakes (Smith et al. 1999). Lake methane has been studied in relation to the trophic state (Adams 2005, Beaulieu et al. 2019) and in relation to eutrophication (Aben et al. 2017). Higher nutrient loading in lakes enhances primary production and phytoplankton growth (Schindler 1977). Subsequently, sediments are fed with more organic matter substrate for the conversion to methane by anoxic sediment methanogenesis. Reducing nutrient loading in the frame of eutrophication management,

therefore, is assumed to reduce methane emission. However, the response of the oxic methane source to fighting eutrophication has not been considered yet. Potentially, there are two opposing effects on the oxic methane source, which could decrease or increase atmospheric emission: On the one hand, reduced primary production and phytoplankton growth could limit the oxic methanogenesis pathway. On the other hand, reducing the availability of inorganic phosphorus can trigger methane production by activating the methylphosphonate degradation (Yao et al. 2016, Teikari et al. 2018). Analysing ^{13}C-methane signatures and modelling using the Rayleigh equation showed that the oxic methane source was triggered by soluble reactive phosphorus concentrations below 4 µg l^{-1} (Chapter 2). It is unclear, however, which environmental conditions decide about the dominance of the single oxic production pathways. While methylphosphonate degradation is rather a short-term response to nutrient stress, reducing oxic methanogenesis is a long-term response. In the light of the opposing effects, the nature of deployed bioremediation program will decide about the oxic methane perturbation. In-depth studies are required to understand better the individual contribution of both oxic methane production pathways to surface emission and examining their relation to eutrophication and reducing the nutrient loading. Isotope labelling experiments may be useful for simultaneously resolving and quantifying both oxic production pathways. Phosphorus availability is seen as a major limiting factor for phytoplankton growth (Schindler 1977). However, nitrogen availability can also be a limiting factor (Schindler 1977, Sterner 2008). A recent study in Lake Stechlin (Bizic-Ionescu et al. 2018 with M. Günthel as co-author) showed that methylated amines (trimethylamine) can stimulate oxic water methane production suggesting this compound is a methane precursor molecule. The usage of methylated phosphonates and amines (and potentially sulphur compounds; Damm et al. 2010/2015, Althoff et al. 2014, Klintzsch et al. 2019) indicate that organisms producing methane oxically account for food web interactions that have not been studied yet. The response of the oxic methane source to altered nutrient availability must be subject to future studies, and eutrophication strategies should be re-evaluated accordingly.

Light availability is an essential factor for phytoplankton. Marine and lake water phytoplankton has been found to produce methane under oxic conditions (Teikari et al. 2018) even without inorganic phosphorus limitation (Chapter 3, 4). Accordingly, light will be a constant factor modulating oxic methane production and subsequently the

surface methane emission. During the stratified season, a positive correlation has been observed between surface water radiation and mid-water methane emission (Chapter 2). When the radiation increased by a factor of 3, the emission approximately doubled. Likewise, in the course of ^{13}C-labelling experiments, higher methane production was observed during light exposure at daytime (Chapter 2). On a global scale, lakes are exposed to a wide spectrum of sunlight radiation. This spectrum could lead to considerably different oxic methanogenesis activities with higher production rates closer to the equator. Furthermore, following the oxic methane production rates in Lake Stechlin from the mixed to the stratified period revealed that the oxic methane source is mainly relevant during the warm season. Lake systems with year-round warm surface water are expected to continuously contribute oxic methane to the atmosphere, while seasonal changes in temperate regions limit oxic methane emission to the warm season. Oxic methanogenesis has been observed under light and dark conditions throughout incubation experiments (Chapter 3) pointing to a pathway involving several reaction steps of which not all require light. A methane-precursor formed during a light reaction and its final conversion to methane in a dark reaction could explain the observed methane production with and without light (Chapter 2, 3). However, identification of the precise molecular pathway of oxic methanogenesis must be subject to ongoing research. This research should also investigate in which radiation spectrum oxic methanogenesis is thriving (minimum/maximum/optimum radiation levels).

Atmospheric methane emission is controlled by the balance of methane production and consumption. Accordingly, climate feedbacks of methane emission and global warming depend on how changing temperature will shift the production-consumption balance (Dean et al. 2018). The feedbacks of lake water methane emission with global warming are currently not well constrained. Generally, increased water temperatures are believed to increase lake methane emission (Aben et al. 2017, Sanches et al. 2019). Global warming will lead to rising lake water temperatures (Adrian et al. 2009), as well as extended ice-free seasons (Wik et al. 2016b) and stratification periods will extend (De Stasio et al. 1996, Peeters et al. 2007). That is why, sediment methanogenesis will accelerate and corresponding high-activity periods will prolong in, for examples, subarctic or temperate regions. Currently, the oxic methane source is not considered in future climate change predictions (IPCC 2014, Dean et al. 2018). As the oxic and anoxic methane source is associated with different microorganisms and

different pathways, they will react differently to environmental perturbations. The strength of the anoxic methane source is modulated by temperature (Duc et al. 2010, Marotta et al. 2014, Aben et al. 2017, Peeters et al. 2019), trophic state (e.g. Adams 2005, Beaulieu et al. 2019), organic matter quantity and quality, as well as competitive electron acceptors in the sediments (Strapoc 2017). The strength of the oxic methane source, on the other hand, is connected to phytoplankton dynamics, phosphorus availability and sunlight (see the previous section). In order to account the individual response of oxic and anoxic sources to environmental perturbations, both sources need to be considered separately in climate change predictions. In the light of globally increasing temperatures, primary production is expected to increase (McCornick and Fahnenstiel 1999, Livingston et al. 2003, Visser et al. 2006) which consequently could accelerate the oxic methane production. In analogy to anoxic methanogenesis, extended ice-free periods (e.g. subarctic regions) and stratified seasons (e.g. temperate regions) will also increase the timeframe for the oxic methane source to contribute to atmospheric methane. While the initial evidence (Chapter 2, 5) points to higher lake water methane emission due to higher oxic production rates at higher water temperatures, the methane production-consumption balance must be further assessed. As anoxic methane source is remote from the atmosphere and requires physical transportation prior to emission, the production-consumption balance for the oxic and anoxic sources should be separately considered.

Additional research focus. Studies about oxic methane production, so far, revolve around its existence, its relevance for atmospheric methane emission, and the two proposed pathways (methylphosphonate demethylation and oxic methanogenesis). However, there are other research questions that have yet not been addressed. Nitrogenase enzymes of the Alphaproteobacterium *Rhodopseudomonas palustris* have recently been discovered to produce methane (Fixen et al. 2016, Zheng et al. 2018). The reaction was triggered by light and could exhibit an alternative pathway for oxic water methane production. Furthermore, methyltransferase enzymes are involved in many cellular processes interacting with a wide range of molecules, including proteins, DNA/RNA, and metabolites. In proximity to proton pools methyltransferase enzymes of oxic water organisms could also lead to methane formation (Chen et al. 2014). These molecular mechanisms can be targeted in future studies researching alternative pathways of oxic-water methane formation.

All studies examining the relevance of oxic water methane production have used atmospheric emission as a measure for its importance. The ecological meaning of the oxic methane source has not been considered yet. In waters remote from shore (DelSontro et al. 2018) and bottom sediment methanogenesis (Chapter 5, Tang et al. 2014), oxic methane production is the main methane source and could be the base of a food chain (Devlin et al. 2015). In such waters, obligate methylotrophic organisms (methane oxidisers) using methane for their energy metabolism will rely on the oxic methane source. Zooplankton grazing on the methylotrophic community will subsequently form the food ground for higher organisms like fishes. Decomposition of organic material (fish, zooplankton, and methylotrophic community), in turn, could provide oxic methane producers with methane precursor molecules. The ecological meaning of the oxic methane source might be especially important for large lake systems and will be modified by phytoplankton dynamics.

Recent studies mainly focused on investigating single processes leading to datasets with anoxic methanogenesis, oxic methane production, methane oxidation, transport mechanisms and atmospheric emission being temporally and spatially separated. To advance our understanding of lake methane cycling, it is necessary that future studies contemplate more detailed network analyses accounting all the methane sources and sinks and the transport mechanisms at the same time.

Thesis merit. This thesis aimed for a better understanding of microbial methane production in oxic lake waters with a focus on the responsible organism(s), environmental driving forces, as well as local and global implications. In addition, wind-based and turbulence-based emission models were compared to flux chamber measurements to identify environmental conditions leading to a deviation between the models; and the temperature was tested as an additional proxy parameter for wind-based emission predictions. All major phytoplankton species in Lake Stechlin were shown to produce methane, and strong correlative evidence suggests that they were responsible for oxic methane production in Lake Stechlin. Several lines of evidence connected oxic methane production to photosynthesis/autotrophic carbon fixation. Accordingly, light and phosphorus availability were found to be critical driving forces for the oxic methane source on diurnal and seasonal scales. Balancing the system-wide methane sources and sinks in Lake Stechlin's surface mixed layer indicated that methane production in oxic waters was a major source for surface emission during the stratified season, especially

during Cyanobacteria blooms when the oxic methane source substantially outweighed the anoxic source. Comparing Lake Stechlin data with literature data led to the development of two empirical models predicting the contribution of oxic methane to surface emission in relation to lake size. Both models showed that the importance of the oxic methane source increases with lake size, indicating that oxic methane production has global implication. Finally, wind forcing was found to cause a discrepancy between wind-based/turbulence-based emission estimations and flux chamber measurements (wind speed substantially below and above 3 m s^{-1}), and wind-based emission estimates could be vastly improved by including the temperature gradient between water and air phases as additional proxies.

In contrast to the common belief of methanogenic Archaea being the only microbes capable of methane formation (e.g. Thauer et al. 1998, Ferry and Kastead 2007, IPCC 2013, Saunois et al. 2016a), numerous organisms including Archaea, Prokaryotes and Eukaryotes have been discovered to produce methane. Anoxia as a pre-requisite for biological methane production is outdated. Accordingly, the "methane paradox" in aquatic systems can be resolved by considering both oxic methane production and methane input from anoxic sources.

This thesis highlights that oxic methane production is an important part of lake methane cycling and a better understanding of methane production, consumption and distribution pathways is required to improve the global methane budget (Kirschke et al. 2013, Saunois et al. 2016a) and climate change predictions (IPCC 2007, IPCC 2014, Dean et al. 2018). Future work is required to uncover 1) importance of the oxic methane source in different lake types, 2) the precise molecular pathways of methane production and their individual contribution to surface emission, 3) its relation to phytoplankton dynamics, and 4) associated ecological impacts. Oxic-water methane production is a recent discovery (sea: Karl et al. 2008; lakes: Grossart et al. 2011). Accordingly, the amount of research on the oxic methane source pales when compared to the conventional anoxic methane source. To stimulate more studies on methane production in oxic waters, global assessments such as the upcoming IPCC Sixth Assessment Report (2021/22) should acknowledge the existence of oxic methane production and its potential role as uncertainty factor during upscaling.

Appendices

The appendix combines the supplementary information of all thesis chapters. Supplementary figures are listed first, followed by supplementary tables and supplementary notes, respectively.

Supplementary Figures

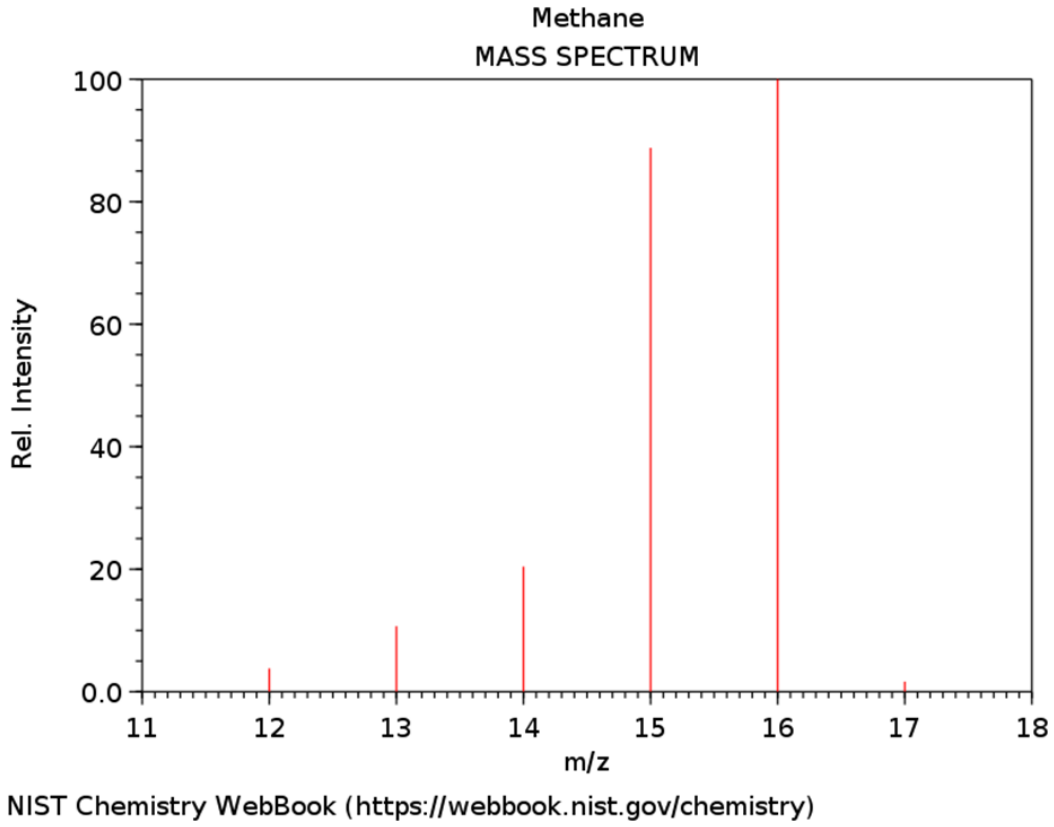

Supplementary Figure S3.1: Ionisation spectrum of methane during mass spectrometry. *The peak at m/z 15 was used for analyses with the Membrane Inlet Mass Spectrometer and resembles ca. 90 % of the main peak at m/z 16. This figure was drafted by collaborators and subsequently modified to fit thesis layout.*

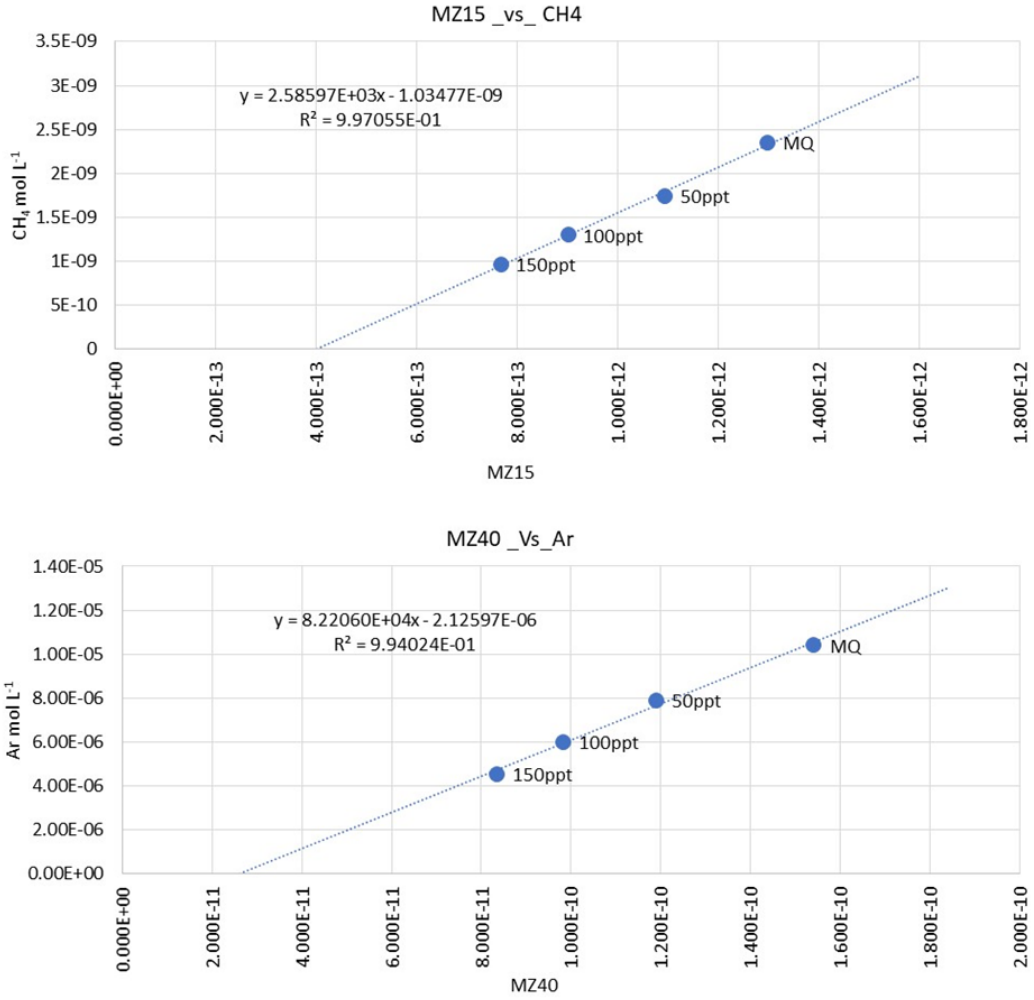

Supplementary Figure S3.2: MIMS signal in relation to solubility of gas analytes. *Raw signal obtained from mass 15 (methane) and mass 40 (argon) plotted against the calculated solubility at different salinities at 30 °C. The signal in both cases is linearly correlated to the concentration of the dissolved gas. The ratio between the two masses was extrapolated between 0 and 50 ppt and was used for calculating the methane concentration. This figure was drafted by collaborators and was modified to fit thesis layout.*

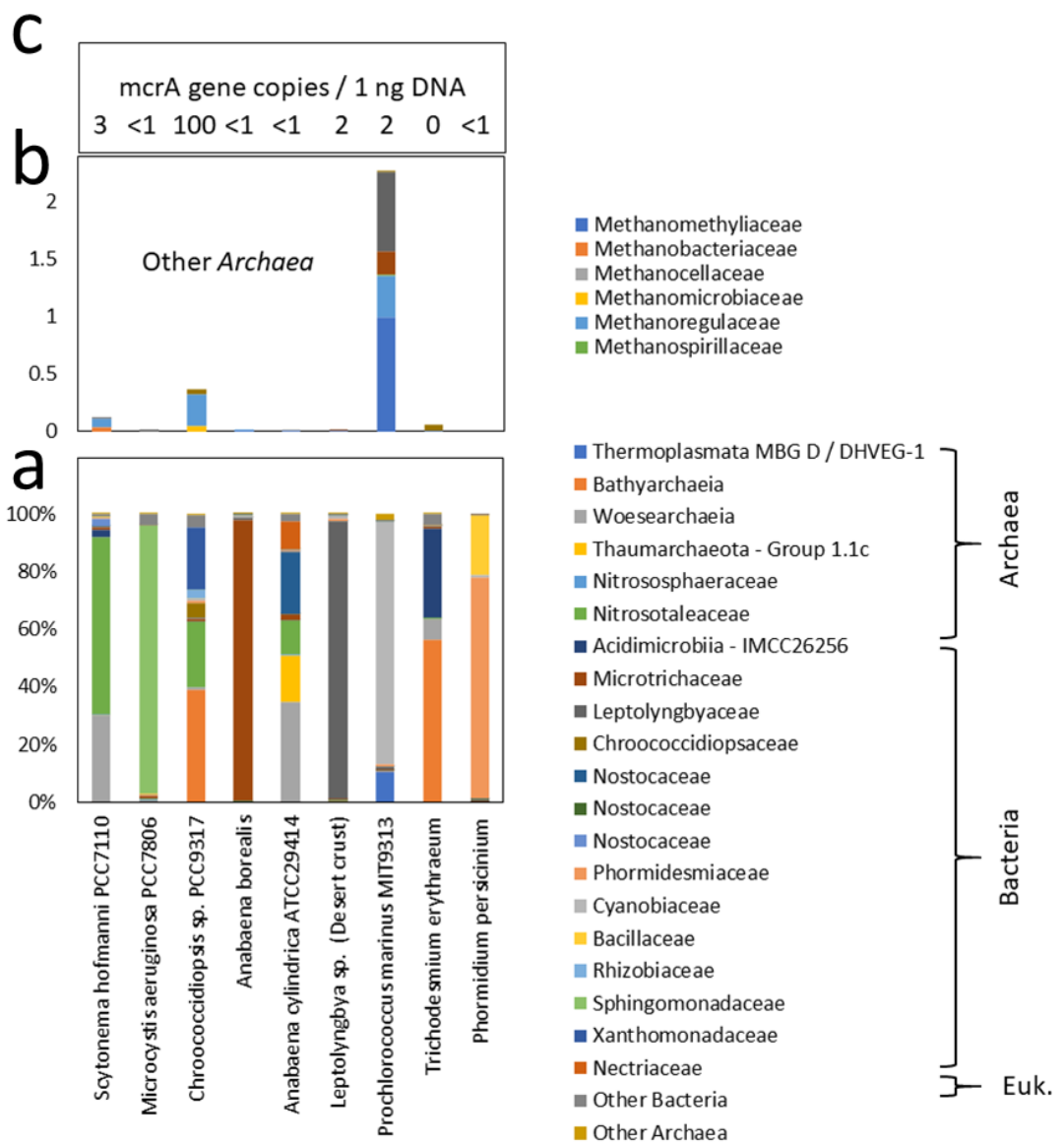

Supplementary Figure S3.3: Community composition of various cyanobacterial cultures. *Composition as obtained when sequenced using Archaea specific primers resulting in 71981 reads for PCC7110, 5442 reads for PCC 7806, 14,489 reads for PCC 9317, 91,105 reads for A. borealis, 13,173 reads for ATCC29414, 133,336 reads for Leptolyngbia sp., 172,112 reads for MIT9313, 35,257 for T. erythraeum and 82,190 reads for P. persicinum out of 200,000 commissioned reads. The variability in reads abundance alongside false positive results, suggest a low abundance of Archaea. Families of Archaea and false positive Bacteria making up more than 2 % of the reads are shown in panel (**a**). Low abundance Archaea, comprising of methanogens are shown in panel (**b**). The background presence or complete absence of methanogens was confirmed by qPCR of the mcrA gene (**c**). This figure was drafted by collaborators and was modified to fit thesis layout.*

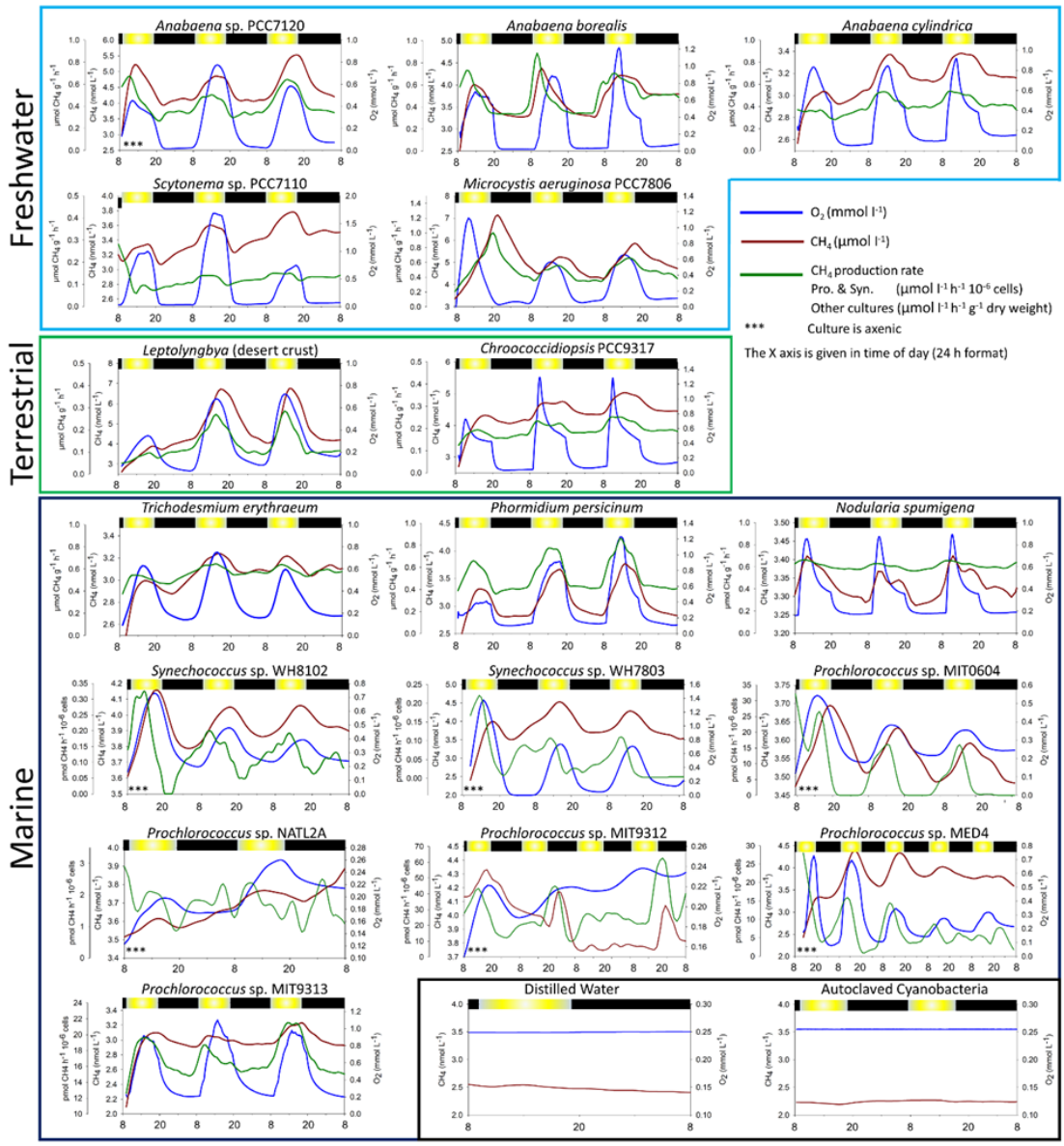

Supplementary Figure S3.4: MIMS results of all 17 different cyanobacterial cultures. *A decrease in methane concentration is a result of reduced (or no) production coupled with degassing from the supersaturated, continuously-mixing, semi-open incubation chamber towards equilibrium with atmospheric methane (2.5 nmol l^{-1} and 2.1 nmol l^{-1} for freshwater and seawater, respectively). Calculated methane production rates account for the continuous emission of methane from the incubation chamber for as long as the methane concentrations are supersaturated. The light regime for the experiments was as follows: dark (black bar) from 19:30 to 09:00 then light intensity (yellow bar) was programmed to increase to 60, 120, 180, 400 µmol photons m^{-2} s^{-1} with a hold time of 1.5 h at each intensity. After maximum light period the intensity was programmed to decrease in reverse order with the same hold times until complete darkness again at 19:30. Figure has been drafted by collaborators.*

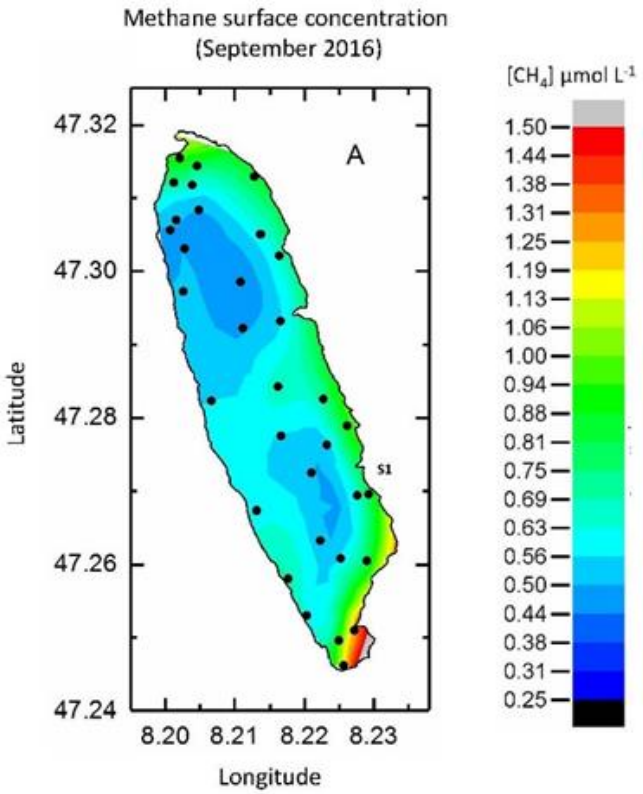

Supplementary Figure S6.1: Methane surface water concentrations in Lake Hallwil (9th September 2016). *Black dots represent the sampling points. S1 indicates the location of measured sediment fluxes - diffusive and ebullitive (see Methods in Donis et al. 2017). Figure was drafted by a collaborator.*

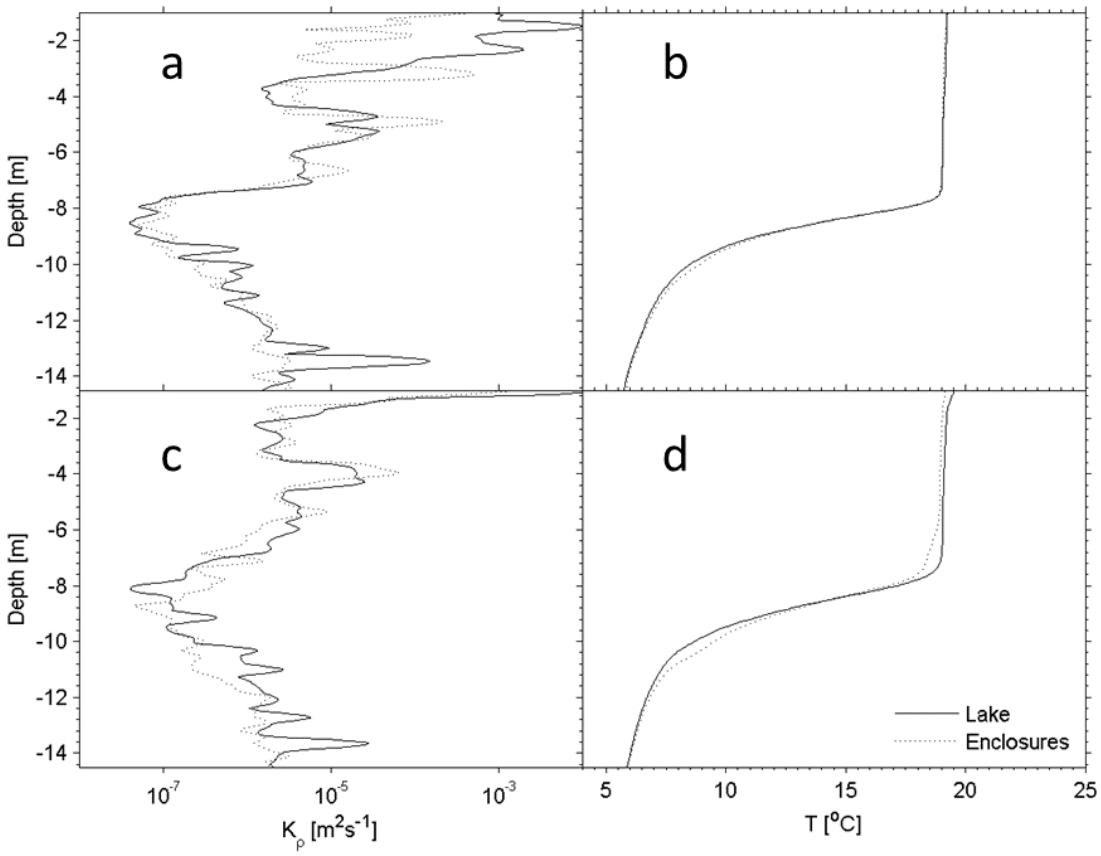

Supplementary Figure S6.2: Comparison of physical parameters inside enclosures and in the open lake. *Vertical turbulent diffusion coefficient (**a**, **c**) and vertical temperature distribution from the MSS profiling (**b**, **d**) in the mesocosm enclosures (dotted lines) and in the open lake (solid lines) at windy (Panels a-b, 3 Sep 2013, wind speeds 3-5 m s^{-1}) and calm (Panels c-d, 4 Sep 2013) conditions. Figure was created by a collaborator.*

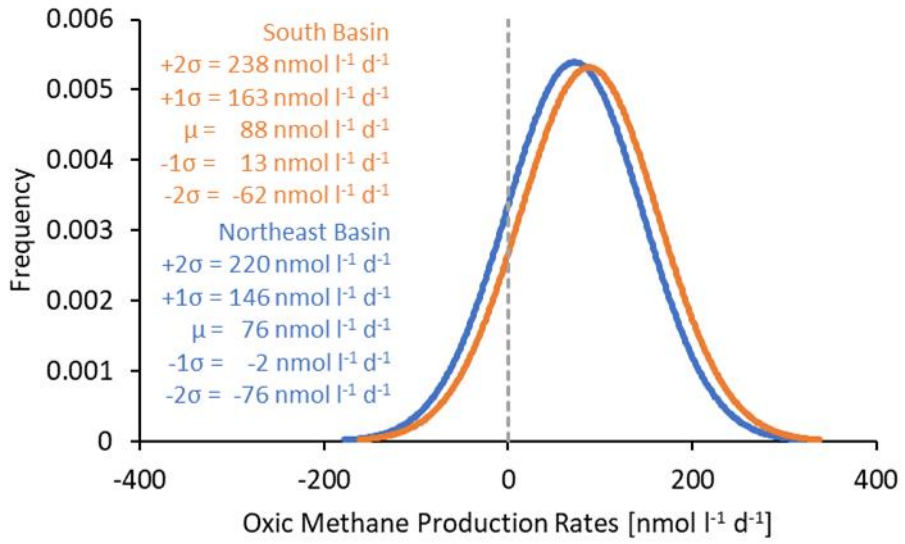

Supplementary Figure S6.3: Density curve of oxic methane production rates obtained from mass balancing. *Monte Carlo simulation was deployed to solve methane mass balances (9999 iterations). The density function was computed as f(x) = 1/(√(2 π) σ) e^-((x - μ)^2/(2 σ^2)). Here σ is the standard deviation and μ is the mean value.*

Supplementary Tables

Supplementary Table S2.1: Methane surface emission, parameters computed for estimating gas transfer constants, and environmental parameter in Lake Stechlin (2016 dataset).

Datetime	T_{water} @ surface	Solubility in surface water	Schmidt number	Wind speed u_{10}	CH_4 conc @ surface	Water-to-air CH_4 flux	k_{600}	Radiation	CH_4 acc in top 7 m	SRP conc in top 7 m
(dd-mm-yy hh:mm)	[°C]	[mol l^{-1} atm^{-1}]		[m s^{-1}]	[µmol l^{-1}]	[mmol m^{-2} d^{-1}]	[m d^{-1}]	[W m^{-2}]	[mmol]	[mg l^{-1}]
08-03-16 14:00	3.2	0.00235	1561	3.9	0.0222	0.0299	2.7	287	0.1524	n.a.
15-03-16 14:00	3.3	0.00234	1553	2.3	0.0313	0.0323	2.3	239	0.2193	n.a.
21-03-16 12:00	3.7	0.00232	1523	4.7	0.0452	0.0858	3.3	262	0.3101	n.a.
30-03-16 10:00	4.2	0.00228	1469	3.1	0.0449	0.0463	2.1	121	0.3081	0.0272
05-04-16 13:30	7.3	0.00209	1221	1.3	0.0680	0.0499	1.3	341	0.4285	0.0174
12-04-16 12:30	6.7	0.00213	1268	1.4	0.0785	0.0360	0.8	535	0.5927	0.0160
19-04-16 11:00	7.2	0.00210	1229	9.2	0.1278	0.2041	2.7	528	0.8047	0.0148
26-04-16 12:00	8.1	0.00205	1167	3.1	0.1366	0.2095	2.5	420	0.9809	0.0130
03-05-16 13:00	9.7	0.00197	1064	1.9	0.1174	0.0867	1.1	562	0.9306	0.0110
10-05-16 12:00	13.5	0.00179	858	3.8	0.1810	0.3286	2.2	844	1.4013	0.0088
17-05-16 15:00	13.0	0.00182	884	n.a.	0.1919	0.5592	3.8	72.8	1.4704	0.0090
24-05-16 12:00	16.9	0.00166	717	3.8	0.2658	0.3248	1.4	740	2.4595	0.0058
31-05-16 12:00	19.1	0.00159	645	0.6	0.3501	0.1574	0.5	337	3.5778	0.0044
06-06-16 13:00	22.0	0.00150	559	2.0	0.5729	0.4850	0.8	858	4.1635	0.0062
13-06-16 13:00	19.5	0.00157	632	1.4	0.4307	0.2683	0.6	388	3.4885	0.0070
07-07-16 14:30	20.1	0.00155	613	3.4	0.3638	0.4036	1.1	635	2.6514	0.0028
12-07-16 15:00	20.8	0.00153	592	4.1	0.4079	0.3395	0.8	445	3.0146	0.0028
19-07-16 15:00	20.0	0.00156	615	2.5	0.3877	0.2850	0.8	347	3.1526	0.0030

conc – concentration; k_{600} – gas transfer constant; acc – accumulation; SRP – soluble reactive phosphorus; n.a. – not available. Note, the water-to-air methane flux measurement on 19-04-16 was not accounted for when the linear k_{600}-wind speed relationship was established due to strong wind speed during measurement. Strong wind speeds have been found to cause deviations in the linear relationship (Wanninkhof 2014).

Supplementary Table S2.2: Methane production observed in different size fractions. *An integrated lake water sample (4-8 m depth) taken on 3rd July 2018 was filtered through a 20 µm net creating different size fractions, transferred to 50 ml serum bottles and incubated for 24 h in the laboratory under natural daylight exposure. Unfiltered lake water served as control. The water samples were saturated with atmospheric air by bubbling atmospheric air through a 0.2 µm filter for 10 min prior to incubation.*

Size Fraction	CH_4 production [nmol l^{-1} d^{-1}]
< 20 µm	4.3±0.3
> 20 µm	19.2±0.9
no filtration	5.4±0.3

mean ± SD of duplicate measurements

Supplementary Table S2.3: Raw data of the experiment investigating depth-specific methane production rates. *In situ parameters of the lake recorded on 13th June 2016 (methane concentration by GC/FID, chlorophyll a by YSI probe) and methane production measured in lake water collected same day. The lake water was incubated in the laboratory under natural day light exposure, and its methane content was measured on day 0, 14 and 21. The table lists production computed as changing methane concentration over time.*

	Lake parameters		**Laboratory parameters**	
			Incubation day 0-14	*Incubation day 0-21*
Depth [m]	**CH_4 conc [µmol l^{-1}]**	**Chl_a conc [µg l^{-1}]**	**CH_4 production [nmol l^{-1} d^{-1}]**	**CH_4 production [nmol l^{-1} d^{-1}]**
0	0.661±0.031	4.0	6.0±3.4	7.5±2.1
2	0.665±0.010	4.6	7.1±1.8	7.4±1.5
4	0.639±0.023	3.2	9.5±3.0	7.7±0.1
6	0.983±0.064	3.4	7.9±1.1	9.8±3.5
7	0.728±0.064	2.2	4.4±0.4	3.7±3.1
8	0.367±0.009	1.8	5.4±0.4	5.9±0.7
9	0.245±0.015	1.3	3.3±1.9	2.6±0.9
10	0.131±0.017	0.9	0.9±0.1	1.0±0.1
12	0.094±0.001	1.3	0.8±0.3	1.0±0.2
14	0.067±0.002	0.8	0.5±0.2	0.7±0.1
16	0.071±0.001	0.8	0.5±0.0	0.5±0.0
18	0.160±0.018	1.1	2.1±1.3	1.9±0.2
20	0.253±0.044	0.4	3.3±3.1	2.9±1.8

conc – concentration; Chl_a – chlorophyll a; linear regression shows significant correlations between the lakes' in situ concentration profile and the observed production (incubation day 0-14: $R^2 = 0.77$, $p < 0.001$; incubation day 0-21: $R^2 = 0.83$, $p < 0.001$), as well between chlorophyll a content during sampling and the observed production (incubation day 0-14: $R^2 = 0.68$, $p < 0.001$; incubation day 0-21: $R^2 = 0.75$, $p < 0.001$); mean ± SD of duplicate measurements

Supplementary Table S2.4: Observed ^{13}C atom % excess as part of the ^{13}C-labeling experiment. *Lake water was collected on 1st September 2016 from 7 m depth, transferred to exetainer vials without disturbing the gas condition, amended with ^{13}C-labeled substrate and incubated over a day-night cycle at 7 m in the lake. To measure methane oxidation, ^{13}C-methane was added to a final of 92.5 % of the total methane and the ^{13}C excess in the dissolved inorganic carbon product pool was measured over time. To measure methane production, ^{13}C-labeled bicarbonate was added to a final of 21 % of the total dissolved inorganic carbon and the increasing ^{13}C content in the methane product pool was measured. Methyl fluoride was added to the control (1.4 mmol l^{-1}) in addition to the labelled substrates. Concurrent PAR data are shown in the next supplementary table.*

Datetime	Measuring CH_4 Oxidation				Measuring CH_4 Production		
Treatment:		$+^{13}CH_4$	$+^{13}CH_4$ +MF		$+DI^{13}C$	$+DI^{13}C$ +MF	
	Incubation Time [h]	^{13}C atom % excess in DIC $*10^{-3}$ [%]	^{13}C atom % excess in DIC $*10^{-3}$ [%]	Avg CH_4 decrease [pmol l^{-1} h^{-1}]	^{13}C atom % excess in CH_4 $*10^{-3}$ [%]	^{13}C atom % excess in CH_4 $*10^{-3}$ [%]	Avg CH4 increase [pmol l^{-1} h^{-1}]
1-Sep 16:20	0.3	0.11±0.20	1.58±0.76		1.34±0.32	1.20±0.65	
1-Sep 22:30	6.5	1.20±0.20		2.3	0.62±0.62		0.5
2-Sep 07:30	15.5	1.99±0.83		1.9	0.91±0.57		2.3
2-Sep 12:20	20.3	3.05±0.52		1.7	3.65±1.50		8.9
2-Sep 17:30	25.5	4.06±0.74	1.93	1.9	3.11±0.09	0.62±0.23	0.7

DIC – dissolved inorganic carbon; MF – methyl fluoride; mean ± SD of triplicate measurements

Supplementary Table S2.5: Light condition during the ^{13}C-label experiment. *Photoactive radiation at 7 m depth of Lake Stechlin during the incubation experiments with ^{13}C-labeled substrates (previous supplementary table). PAR measurements were made using a YSI probe and ≤ 9 % of the PAR was absorbed by the experimental glass vials.*

Datetime [dd-mm-yy hh:mm]	PAR [µmol photons m^{-2} s^{-1}]	Datetime [dd-mm-yy hh:mm]	PAR [µmol photons m^{-2} s^{-1}]	Datetime [dd-mm-yy hh:mm]	PAR [µmol photons m^{-2} s^{-1}]
01-09-16 15:23	20	02-09-16 01:23	0	02-09-16 11:23	79
01-09-16 16:23	37	02-09-16 02:23	0	02-09-16 12:23	67
01-09-16 17:23	14	02-09-16 03:23	0	02-09-16 13:23	32
01-09-16 18:23	3	02-09-16 04:23	0	02-09-16 14:23	80
01-09-16 19:23	0	02-09-16 05:23	0	02-09-16 15:23	15
01-09-16 20:23	0	02-09-16 06:23	4	02-09-16 16:23	35
01-09-16 21:23	0	02-09-16 07:23	11	02-09-16 17:23	10
01-09-16 22:23	0	02-09-16 08:23	20	02-09-16 18:23	2
01-09-16 23:23	0	02-09-16 09:23	36	02-09-16 19:23	0
02-09-16 00:23	0	02-09-16 10:23	76		

PAR – photoactive radiation

Supplementary Table S2.6: Measurements for the light/dark incubation experiment. *An integrated lake water sample (from 4-8 m depth) was taken on 29th June 2018, filtered through a 100 µm net and incubated in serum bottles in the laboratory for 5 and 10 days under natural daylight or in the dark. Lake water remained untreated (Lake Water) or with inorganic phosphorus added (+K_2HPO_4). The $\delta^{13}C$ signature (mean ± methodological SD of 2-5 measurements), soluble reactive phosphorus (1 bottle killed per time point) and oxygen saturation (1 bottle killed per time point) were recorded on day 0, 5 and 10.*

Treatment	**Light**	**Time** [d]	**$\delta^{13}C$-CH_4** [‰]	**SRP conc** [mg l^{-1}]	**O_2 sat** [$\%_{sat}$]
Lake Water	light	0	-45.5±2.1	2	130.5
Lake Water	light	5	-41.4±2.0	3	126.2
Lake Water	light	10	-40.0±0.3	5	121.2
+K_2HPO_4	light	0	-40.9±1.3	1	130.7
+K_2HPO_4	light	5		7	122.8
+K_2HPO_4	light	10	-42.9±0.8	13	119.6
Lake Water	dark	0	-43.7±0.4	3	129.4
Lake Water	dark	5	-43.5±1.9	4	125.3
Lake Water	dark	10	-43.2±3.4	5	121.1
+K_2HPO_4	dark	0	-41.4±1.8	3	130.8
+K_2HPO_4	dark	5	-40.3±1.0	12	124.4
+K_2HPO_4	dark	10	-38.0±2.5	20	117.9

conc – concentration; $\delta^{13}C$ – isotope signature of CH_4; SRP – soluble reactive phosphorus; sat – saturation

Supplementary Table S4.1: Conservative mass balance parametrisation throughout sensitivity analysis.

Term	Floating Chamber		Donis et al. 2017	Vachon and Prairie 2013			MacIntyre et al. 2010		
	real	cons	U_{10}	U_{10}	U_{10}, LA	U_{10}, WF	U_{10}, all β	U_{10}, β<0	U_{10}, β>0
F_L	0.9	1.2	0.9	0.9	0.9	0.9	0.9	0.9	0.9
F_z	3.12 ±3.20	3.12 ±3.20	3.12 ±3.20	3.12 ±3.20	3.12 ±3.20	3.12 ±3.20	3.12 ±3.20	3.12 ±3.20	3.12 ±3.20
F_S	0.92 ±0.80	0.60 ±0.36	0.71 ±0.41	1.08 ±0.55	0.82 ±0.34	1.04 ±0.49	0.81 ±0.47	0.60 ±0.36	0.95 ±0.44
MOx	4.03 ±0.92	0 ±0	4.03 ±0.92	4.03 ±0.92	4.03 ±0.92	4.03 ±0.92	4.03 ±0.92	4.03 ±0.92	4.03 ±0.92
P_{net}	168 ±228	69 ±200	130 ±202	197 ±210	150 ±201	191 ±207	149 ±205	110 ±200	175 ±205

F_L – littoral sediment methane flux into the water [mmol m^{-3} d^{-1}], Fz – vertical methane diffusion from below the thermocline [µmol m^{-3} d^{-1}], FS – surface methane emission [mmol m^{-3} d^{-1}], MOx – methane oxidation [mmol m^{-3} d^{-1}], P_{net} – oxic methane production in the surface mixed layer [nmol l^{-1}], LA – lake area, WF – wind fetch, β – buoyancy flux

Supplementary Table S4.2: Methane emissions from Lake Stechlin estimated with floating chambers and wind-based models.

Date time	Wind speed U_{10} [m s^{-1}]	Floating chamber F [mmol m^{-2} d^{-1}]	Donis et al. 2017 F [mmol m^{-2} d^{-1}]	Vachon and Prairie 2013 (U_{10}) F [mmol m^{-2} d^{-1}]	Vachon and Prairie 2013 (U_{10}, LA) F [mmol m^{-2} d^{-1}]	Vachon and Prairie 2013 (U_{10}, WF) F [mmol m^{-2} d^{-1}]	MacIntyre et al. 2010 (U_{10}) β<0 F [mmol m^{-2} d^{-1}]	MacIntyre et al. 2010 (U_{10}) β<0 F [mmol m^{-2} d^{-1}]	MacIntyre et al. 2010 (U_{10}) all β F [mmol m^{-2} d^{-1}]
15.6.17 19:21	1.1	0.135	0.232	0.448	0.439	0.486	0.278	0.186	0.448
15.6.17 23:21	2.27	0.646	0.553	0.886	0.72	0.881	0.642	0.463	0.808
16.6.17 3:21	2.67	0.776	0.62	0.964	0.756	0.944	0.716	0.522	0.865
16.6.17 7:20	2.67	0.765	0.612	0.951	0.746	0.931	0.707	0.515	0.853
16.6.17 11:26	4.98	1.668	1.136	1.626	1.136	1.518	1.296	0.971	1.387
16.6.17 15:21	4.78	1.482	1.017	1.461	1.027	1.368	1.161	0.869	1.25
16.6.17 19:25	5.72	1.858	1.238	1.75	1.198	1.62	1.41	1.061	1.479
16.6.17 23:36	5.88	2.002	1.329	1.873	1.277	1.732	1.513	1.139	1.581
17.6.17 3:21	6.6	2.338	1.528	2.134	1.434	1.962	1.738	1.312	1.79
17.6.17 7:21	6.47	2.387	1.564	2.188	1.473	2.013	1.779	1.342	1.837
17.6.17 11:21	6.38	2.236	1.468	2.056	1.387	1.893	1.67	1.26	1.727
17.6.17 15:21	5.38	1.808	1.216	1.728	1.193	1.605	1.386	1.041	1.466
17.6.17 19:21	3.32	0.966	0.719	1.081	0.81	1.038	0.827	0.61	0.951
18.6.17 3:40	0.97	0.093	0.217	0.438	0.444	0.483	0.262	0.172	0.446
18.6.17 7:21	2.33	0.662	0.559	0.89	0.719	0.883	0.648	0.468	0.81
18.6.17 11:21	2.2	0.607	0.527	0.849	0.695	0.847	0.612	0.441	0.777
18.6.17 15:21	2.73	0.69	0.547	0.846	0.66	0.827	0.631	0.461	0.758
18.6.17 19:21	1.23	0.17	0.24	0.447	0.424	0.477	0.286	0.194	0.44
18.6.17 23:26	0.52	-0.071	0.102	0.27	0.323	0.323	0.13	0.074	0.3
19.6.17 3:21	0.4	-0.108	0.077	0.234	0.298	0.29	0.102	0.052	0.27
19.6.17 7:21	1.02	0.096	0.197	0.39	0.39	0.427	0.237	0.157	0.394
19.6.17 11:21	1.32	0.2	0.26	0.474	0.442	0.501	0.308	0.211	0.462
19.6.17 15:50	1.05	0.111	0.209	0.41	0.406	0.447	0.251	0.167	0.412
19.6.17 19:21	0.87	0.045	0.162	0.341	0.356	0.382	0.198	0.127	0.353
19.6.17 23:21	0.72	-0.004	0.143	0.325	0.357	0.373	0.177	0.109	0.345
20.6.17 3:21	0.65	-0.027	0.133	0.317	0.357	0.368	0.166	0.101	0.341
20.6.17 7:21	2.42	0.514	0.428	0.676	0.542	0.668	0.495	0.359	0.613
20.6.17 11:21	4.02	1.065	0.756	1.108	0.802	1.049	0.866	0.644	0.96
20.6.17 15:21	4.5	1.153	0.8	1.157	0.822	1.087	0.914	0.683	0.994
20.6.17 19:21	3.47	0.798	0.587	0.877	0.652	0.84	0.674	0.498	0.768
20.6.17 23:21	3.07	0.668	0.509	0.773	0.589	0.748	0.586	0.43	0.685
21.6.17 3:21	0.95	0.067	0.167	0.34	0.346	0.375	0.202	0.132	0.346
21.6.17 7:21	2.7	0.608	0.484	0.75	0.586	0.733	0.558	0.407	0.672
21.6.17 11:23	3.45	1.039	0.765	1.144	0.851	1.095	0.879	0.649	1.003
21.6.17 15:19	3.02	0.837	0.641	0.977	0.746	0.946	0.738	0.542	0.866
21.6.17 19:19	1.47	0.251	0.29	0.513	0.464	0.535	0.342	0.237	0.493

21.6.17 23:21	0.95	0.075	0.185	0.375	0.382	0.415	0.223	0.146	0.383
22.6.17 3:21	1.85	0.411	0.394	0.659	0.562	0.669	0.461	0.327	0.615
22.6.17 7:21	1.52	0.334	0.374	0.656	0.589	0.682	0.44	0.307	0.627
22.6.17 11:21	1.97	0.59	0.545	0.898	0.755	0.906	0.635	0.453	0.833
22.6.17 15:21	2.53	0.7	0.571	0.895	0.71	0.88	0.66	0.48	0.807
22.6.17 19:21	1.52	0.314	0.351	0.616	0.553	0.641	0.413	0.288	0.59
22.6.17 23:21	3.52	1.141	0.837	1.247	0.925	1.193	0.96	0.71	1.091
23.6.17 3:22	4.32	1.401	0.98	1.424	1.018	1.342	1.121	0.836	1.227
23.6.17 7:21	5.22	1.797	1.214	1.73	1.2	1.611	1.385	1.039	1.471
23.6.17 11:21	5.85	2.149	1.427	2.013	1.374	1.861	1.625	1.223	1.699
23.6.17 15:21	5.38	1.997	1.342	1.908	1.317	1.772	1.53	1.149	1.619
23.6.17 19:21	3.53	1.214	0.889	1.324	0.981	1.266	1.02	0.755	1.158
23.6.17 23:21	2.57	0.791	0.642	1.004	0.794	0.987	0.742	0.54	0.905
24.6.17 3:21	3.45	1.232	0.908	1.356	1.009	1.299	1.042	0.77	1.189
24.6.17 7:21	3.03	1.102	0.843	1.283	0.979	1.242	0.97	0.712	1.137
24.6.17 11:21	3.08	1.119	0.852	1.294	0.984	1.25	0.98	0.72	1.145
24.6.17 15:21	4.03	1.745	1.238	1.813	1.311	1.717	1.417	1.054	1.57
24.6.17 19:21	4.1	1.96	1.386	2.026	1.461	1.915	1.586	1.18	1.751
24.6.17 23:24	2.72	1.053	0.836	1.296	1.012	1.267	0.966	0.705	1.161
25.6.17 3:20	2.23	0.837	0.722	1.159	0.946	1.155	0.838	0.604	1.06
25.6.17 7:21	2.45	0.933	0.772	1.218	0.973	1.202	0.894	0.648	1.102
25.6.17 11:21	3.52	1.492	1.094	1.631	1.209	1.559	1.256	0.928	1.427
25.6.17 15:21	3.23	1.252	0.939	1.416	1.067	1.363	1.08	0.795	1.248

LA – lake area, WF – wind fetch, β – buoyancy flux, F – methane surface emission

Supplementary Table S4.3: Growth data of different phytoplankton cultures. *The rates presenting the biomass for of Algae and Cyanobacteria species based on dry weight (mean ± SD, n=4; $m(t_{start})$ at time point of inoculation; $m(t_{end})$ is end time point of incubation, the overall incubation period of Cyanobacteria and Algae were 4 days and 6 days, respectively).*

Phytoplankton		$m(t_{start})$ [mg_{dw} l^{-1}]	$m(t_{end})$ [mg_{dw} l^{-1}]	Yield Y [mg_{dw} l^{-1} d^{-1}]
Diatom	*Asterionella formosa*	1.0±0.0	23.2±3.0	3.7±0.5
Diatom	*Fragillaria crotonensis*	1.0±0.3	20.6±6.9	3.3±1.2
Diatom	*Synedra sp.*	2.6±0.3	14.5±1.9	2.0±0.3
Green Algae	*Scenedesmus quadricauda*	2.8±0.0	18.0±1.5	2.5±0.2
Green Algae	Green Alga (Stechlin StVis)	2.5±0.0	25.1±2.1	3.8±04
Cryptophyte	*Cryptomonas sp.*	26.3±1.9	29.3±1.5	0.5±0.3
Cyanobacterium	*Dolichospermum cylindrica* ATCC29414	2.9±0.3	17.3±0.7	2.4±0.1
Cyanobacterium	*Dolichospermum sp.* PCC7120	3.0±0.1	24.6±1.2	3.6±0.2

Supplementary Table S5.5: Parameters computed for estimating methane surface emission using literature models. *Methane concentration in surface water was determined deploying a M-CRDS unit and in the air using a Los Gatos GHG analyzer. Wind speed and wind angle was provided by the Umweltbundesamt (Neuglobsow weather station). The other parameters were estimated from empirical models and temperature data (see method section for details).*

Datetime [dd-mm-yy hh:mm]	$CH4_{water}$ [µmol l^{-1}]	$CH4_{air}$ [ppm]	Wind speed [m s^{-1}]	Wind angle [°]	Sc [ ]	T_{WS} [°C]	T_{air} [°C]	Solubility [mol l^{-1} atm^{-1}]
15-6-17 19:21	0.445	1.85	1.1	95.6	594.8	20.7	21.2	0.001535
15-6-17 23:21	0.506	1.89	2.3	197.1	610.3	20.2	17.9	0.001552
16-6-17 3:21	0.479	1.89	2.7	213.5	616.2	20.0	16.5	0.001558
16-6-17 11:26	0.471	1.87	5.0	260.4	617.5	19.9	19.3	0.001560
16-6-17 15:21	0.438	1.84	4.8	269.8	621.0	19.8	16.5	0.001563
16-6-17 19:25	0.445	1.86	5.7	263.0	625.0	19.7	16.4	0.001567
16-6-17 23:36	0.460	1.85	5.9	253.2	635.7	19.3	13.8	0.001579
17-6-17 3:21	0.469	1.85	6.6	263.8	642.7	19.1	13.6	0.001586
17-6-17 7:21	0.487	1.85	6.5	260.2	650.0	18.9	15.0	0.001594
17-6-17 11:21	0.466	1.85	6.4	273.4	641.9	19.1	19.2	0.001585
17-6-17 15:21	0.462	1.83	5.4	278.4	630.6	19.5	23.3	0.001573
17-6-17 19:21	0.440	1.84	3.3	305.0	630.3	19.5	20.8	0.001573
18-6-17 3:40	0.451	1.87	1.0	232.7	640.5	19.2	10.8	0.001584
18-6-17 7:21	0.481	1.89	2.3	252.7	640.1	19.2	14.9	0.001583

18-6-17 11:21	0.501	1.86	2.2	253.1	601.6	20.5	21.7	0.001543
18-6-17 15:21	0.430	1.81	2.7	285.1	578.4	21.3	26.0	0.001518
18-6-17 19:21	0.413	1.81	1.2	289.9	589.3	20.9	24.5	0.001529
18-6-17 23:26	0.416	1.83	0.5	253.4	591.9	20.8	16.3	0.001532
19-6-17 3:21	0.402	1.87	0.4	248.5	599.9	20.5	14.2	0.001541
19-6-17 7:21	0.409	1.84	1.0	248.1	594.5	20.7	19.2	0.001535
19-6-17 11:21	0.425	1.80	1.3	141.9	575.6	21.4	26.8	0.001515
19-6-17 15:50	0.440	1.79	1.1	248.0	553.6	22.2	30.1	0.001491
20-6-17 19:21	0.382	1.84	3.5	301.8	537.5	22.9	22.2	0.001473
20-6-17 23:21	0.370	1.85	3.1	307.7	548.2	22.5	15.5	0.001485
21-6-17 3:21	0.388	1.87	1.0	183.3	556.5	22.1	10.9	0.001494
21-6-17 7:21	0.395	1.85	2.7	297.1	557.2	22.1	16.7	0.001495
21-6-17 11:23	0.495	1.84	3.5	288.2	545.1	22.6	21.4	0.001481
21-6-17 15:19	0.479	1.84	3.0	295.7	536.8	22.9	23.7	0.001472
21-6-17 19:19	0.444	1.85	1.5	309.7	540.3	22.8	19.8	0.001476
21-6-17 23:21	0.435	1.85	1.0	87.7	545.1	22.6	14.6	0.001481
22-6-17 7:21	0.540	1.89	1.5	166.9	559.6	22.0	17.3	0.001497
22-6-17 11:21	0.613	1.85	2.0	164.2	550.8	22.3	26.2	0.001488
22-6-17 15:21	0.489	1.84	2.5	127.1	569.3	21.6	20.0	0.001508
22-6-17 19:21	0.509	1.86	1.5	163.4	557.5	22.1	21.0	0.001495
22-6-17 23:21	0.518	1.84	3.5	141.3	565.7	21.8	18.2	0.001504
23-6-17 3:22	0.486	1.88	4.3	232.1	575.9	21.4	17.6	0.001515
23-6-17 7:21	0.495	1.88	5.2	251.9	582.7	21.2	18.1	0.001522
23-6-17 11:21	0.516	1.87	5.9	247.3	588.0	21.0	18.5	0.001528
23-6-17 15:21	0.529	1.86	5.4	259.6	585.3	21.1	20.5	0.001525
23-6-17 19:21	0.532	1.86	3.5	253.1	591.5	20.8	20.8	0.001532
23-6-17 23:21	0.527	1.87	2.6	251.8	594.3	20.7	17.4	0.001535
24-6-17 3:21	0.552	1.87	3.5	230.8	598.7	20.6	16.3	0.001540
24-6-17 7:21	0.579	1.86	3.0	204.3	603.6	20.4	15.8	0.001545
24-6-17 11:21	0.575	1.91	3.1	200.6	605.1	20.4	16.7	0.001546
24-6-17 15:21	0.638	1.85	4.0	222.1	608.0	20.3	19.2	0.001549
24-6-17 19:21	0.701	1.87	4.1	227.4	610.9	20.2	19.7	0.001553
24-6-17 23:24	0.639	1.88	2.7	218.4	607.4	20.3	16.4	0.001549
25-6-17 3:20	0.667	1.89	2.2	166.3	612.6	20.1	16.0	0.001554
25-6-17 7:21	0.650	1.89	2.5	187.9	613.1	20.1	17.2	0.001555
25-6-17 11:21	0.640	1.84	3.5	231.9	615.0	20.0	17.4	0.001557
25-6-17 15:21	0.601	1.84	3.2	216.3	609.7	20.2	17.4	0.001551
25-6-17 19:21	0.611	1.84	2.2	189.0	615.3	20.0	17.4	0.001557

$CH4_{water}$ – methane concentration in surface water; $CH4_{air}$ – methane concentration at air saturation; Sc – Schmidt number; T_{WS} – temperature of surface water; T_{air} – temperature of the air.

Supplementary Table S6.1: Summary of surface methane fluxes measured and calculated for Lake Hallwil.

Type of model	**April – August [mmol m^{-2} d^{-1}]**	**June – August [mmol m^{-2} d^{-1}]**
Flux chamber	0.6±0.3	0.8±0.1
Hallwil relationship	0.8±0.5	0.8±0.2
MacIntyre et al. (2010)		
- positive buoyancy flux	0.7±0.4	1.0±0.2
- negative buoyancy flux	1.3±0.5	1.6±0.5
- combined buoyancy fluxes	1.0±0.5	1.1±0.6
Vachon and Prairie (2013)	1.4±0.5	1.7±0.2

Listed values as mean±SD

Supplementary Table S6.2: Lower and upper end of surface mixed layer methane mass balance in Lake Hallwil (June – August).

Mass balance component	**Symbol**	**Lower end [mol d^{-1}]**	**Upper end [mol d^{-1}]**
Surface emission	F_S	5969±2984	7958±1989
Methane oxidation	MOx	150±8	150±8
Littoral ebullition	$F_{L,eb}$	134±89	0
Littoral diffusion	$F_{L,sed}$	196±22	196±22
River input	F_R	0-207	0-207
Diffusion from thermocline	F_z	252±84	252±84
Internal (oxic) production	$P_{net,s}$	3738±3055	6629±2014
Oxic methane contribution	OMC	63 %	83 %

Note – symbols as in Dohnis et al. (2017) Values given as mean±SD

Supplementary Table S6.3: Mass Balance parametrisation for the stratified and non-stratified period.

		Open Lake		*Lake Lab Enclosures/Mesocosms (stratified)*	
Terminus	**Symbol**	**Stratified condition**	**Unstratified condition**	**Enclosure 1 & 13**	**Central Enclosure**
$\frac{\partial C}{\partial t} * \forall$		= 0 (steady state)	= 0 (steady state)	= 0 (steady state)	= 0 (steady state)
$(Q_R * C_R)$		= 0	= 0	= 0	= 0
$(A_{th} * F_z)$	A_{th}*(NE) A_{th}*(S) F_z	= 1,757,475 / 1,725,100 / 1,694,600 m^2 = 832,600 / 808,000 / 78,150 m^2 = K_z * C'	= 0 = 0 = K_z * C'	= 63.6 m^2 = K_z * C'	= 706.9 m^2 = K_z * C'
$(A_{sed} * F_L)$	A_{sed}*(NE) A_{sed}*(S) F_L	= 249,225 / 281,600 / 312,100 m^2 = 290,175 / 314,775 / 335,625 m^2 = 1.4±0.2 mmol m^{-2} d^{-1}	= 2,006,700 m^2 = 1,122,775 m^2 = 0 mmol m^{-2} d^{-1}	= 0 mmol m^{-2} d^{-1} = 0 mmol m^{-2} d^{-1}	= 0 mmol m^{-2} d^{-1} = 0 mmol m^{-2} d^{-1}
(MOx * ∀)	*MOx* ∀*(NE) ∀*(S)	= 0 * P_{net} = 9,439,750 / 11,197,225 / 12,922,325 m^3 = 4,893,575 / 5,726,175 / 6,534,175 m^3	= 0.3 * P_{net} = 59,843,550 m^3 = 16,857,425 m^3	= 0.3 * P_{net} = 318.1 / 381.7 / 445.3 m^3	= 0.3 * P_{net} = 3534.3 / 4241.2 / 4948.0 m^3
$(A_{tot} * F_S)$	A_{tot} F_S*	= 4,249,625 m^2 = measured (NE) / computed (S)	= 4,249,625 m^2 = measured (NE) / (S) computed	= 63.6 m^2 = computed	= 706.9 m^2 = computed
$(P_{net} * \forall)$	$P_{net,e}$ ∀*(NE) ∀*(S)	= target parameter; = 9,439,750 / 11,197,225 / 12,922,325 m^3 = 4,893,575 / 5,726,175 / 6,534,175 m^3	= target parameter = 59,843,550 m^3 = 16,857,425 m^3	= target parameter = 318.1 / 381.7 / 445.3 m^3	= target parameter = 3534.3 / 4241.2 / 4948.0 m^3

V - volume of the mixed layer [m^3]; ***C*** – methane concentration in the water column [mol m^{-3}]; ***t*** – time [d]; Q_R – inflow rate of river water [m^3 s^{-1}]; C_R – methane concentration in river water [mol m^{-3}]; A_{th} – planar area of thermocline [m^3]; A_{sed} – sediment area of the mixed layer; A_{tot} – total surface area of the lake [m^3]; F_z – internal turbulent diffusion from metalimnion to the surface mixed layer [mol m^{-2} d^{-1}]; F_L – lateral transported methane [mol m^{-2} d^{-1}]; F_S – water-to-air methane flux [mol m^{-2} d^{-1}]; **MOx** – methane oxidation rate [mol m^{-3} d^{-1}]; P_{net} – internal methane production [mol m^{-3} d^{-1}]; * depending on seasonal stage the mixed layer was either 5 (May/ June), 6 (July) or 7 m deep (August) leading to different dimensions of A_{th}, A_{sed} and ∀ while the whole water column was assumed to be mixed during the unstratified season; * methane emission at the surface was either measured using a combination of floating chamber and GC/FID unit (Northeast basin dataset; **NE**) or computed (South basin dataset; **S**) as after the linear relationship between gas transfer constants (**k**) and wind speed (U_{10}): k ~ U_{10}.

Supplementary Table S6.4 (part 1/2): Data summary of parameters related to estimating methane surface emission based on the k_{600} – wind relationship.

Date [dd/mm/yyyy]	**Site**	***t*** [hh:mm]	U_{10} [m s^{-1}]	T_{SW} [°C]	$C_{CH4\ SW}$ [µmol l^{-1}]	***L*** [mol l^{-1} atm^{-1}]	***Sc*** [ ]	Δ_{CH4}* [µmol l^{-1}]	k_{CH4} [cm h^{-1}]	k_{600} [cm h^{-1}]	***Fs*** [mmol m^{-2} d^{-1}]
08/03/2016	NE	14:00	3.9	3.2	0.02221	0.00235	1560.74	0.01779	7.012	11.309	0.030
15/03/2016	NE	14:00	2.3	3.3	0.03132	0.00234	1553.23	0.02691	5.000	9.427	0.032
21/03/2016	NE	12:00	4.7	3.7	0.04525	0.00232	1522.61	0.04089	8.743	13.927	0.086
30/03/2016	NE	10:00	3.1	4.2	0.04487	0.00228	1469.43	0.04059	4.749	8.629	0.046
05/04/2016	NE	13:30	1.3	7.3	0.06804	0.00209	1220.80	0.06410	3.246	5.212	0.050
12/04/2016	NE	12:30	1.4	6.7	0.07852	0.00213	1268.07	0.07452	2.015	3.319	0.036
26/04/2016	NE	12:00	3.1	8.1	0.13658	0.00205	1166.56	0.13272	6.578	10.248	0.210
03/05/2016	NE	13:00	1.9	9.7	0.11743	0.00197	1063.82	0.11373	3.175	4.651	0.087
10/05/2016	NE	12:00	3.8	13.5	0.18101	0.00179	858.09	0.17763	7.707	9.216	0.329
17/05/2016	NE	15:00	n. a.	13.0	0.19187	0.00182	884.33	0.18845	12.363	16.012	0.559
24/05/2016	NE	12:00	3.8	16.9	0.26583	0.00166	717.28	0.26271	5.152	5.633	0.325
31/05/2016	NE	12:00	0.6	19.1	0.35005	0.00159	644.75	0.34707	1.890	1.983	0.157
06/06/2016	NE	13:00	2.0	22.0	0.57289	0.00150	559.39	0.57008	3.545	3.383	0.485
13/06/2016	NE	13:00	1.4	19.5	0.43072	0.00157	632.03	0.42776	2.613	2.705	0.268
20/06/2016	NE	13:00	2.7	20.2	0.70184	0.00155	609.92	0.69892	6.247	6.299	1.048
07/07/2016	NE	14:30	3.4	20.1	0.36378	0.00155	613.14	0.36086	4.660	4.728	0.404
12/07/2016	NE	15:00	4.1	20.8	0.40794	0.00153	592.46	0.40506	3.493	3.471	0.340
19/07/2016	NE	15:00	2.5	20.0	0.38773	0.00156	614.61	0.38480	3.086	3.136	0.285
30/03/2016	S	12:30	3.3	4.7	0.04618	0.00225	1427.42	0.04195	4.855	7.489	0.049
05/04/2016	S	16:00	2.0	7.5	0.07498	0.00209	1212.91	0.07105	3.453	4.910	0.059

Site – sampling site (North-East basin – NE: 53°09'20.2"N 13°01'51.5"E / South basin – S: 53°08'35.8"N 13°01'43.2"E / Central Reservoir – CR: 53°08'35.8"N 13°01'41.1"E / Enclosure 1 – E1: 53°08'36.4"N 13°01'41.6"E / Enclosure 13 – E13: 53°08'36.5"N 13°01'42.1"E); *t* – time; U_{10} – wind speed recorded in 10 m height; T_{SW} – temperature of the surface water; $C_{CH4\ SW}$ – methane concentration in the surface water; *L* – methane solubility; *Sc* – Schmidt number; Δ_{CH4} – CH_4 gradient between surface water and air (= C_{water} – C_{air}; see Equation 6.2); *k* – wind dependent gas transfer constants; F_S – methane water-to-air flux; * assuming 1.88 ppm methane content in the atmosphere; □ corresponding parameters U_{10}, T_{SW} and $C_{CH4\ SW}$ were averaged for day times (06:00 – 21:00, local times) and given dates; n. a. – not available

Supplementary Table S6.4 (part 2/2): Data summary of parameters related to estimating methane surface emission based on the k_{600} – wind relationship.

Date [dd/mm/yyyy]	**Site**	***t*** [hh:mm]	U_{10} [m s^{-1}]	T_{SW} [°C]	$C_{CH4\,SW}$ [µmol l^{-1}]	***L*** [mol l^{-1} atm^{-1}]	***Sc*** [ ]	Δ_{CH4}* [µmol l^{-1}]	k_{CH4} [cm h^{-1}]	k_{600} [cm h^{-1}]	F_S [mmol m^{-2} d^{-1}]
12/04/2016	S	15:00	1.2	7.6	0.11609	0.00208	1202.91	0.11218	2.347	3.323	0.063
19/04/2016	S	13:30	9.3	7.9	0.11907	0.00206	1183.86	0.11519	12.327	19.392	0.341
26/04/2016	S	14:30	2.0	8.6	0.13230	0.00203	1135.32	0.12849	3.569	4.910	0.110
03/05/2016	S	15:30	6.4	11.0	0.15123	0.00190	986.56	0.14765	9.790	13.639	0.347
10/05/2016	S	14:30	3.6	14.7	0.28610	0.00174	803.93	0.28282	6.984	8.084	0.474
17/05/2016	S	17:30	0.0	13.6	0.21174	0.00179	854.36	0.20838	0.790	0.942	0.039
24/05/2016	S	14:30	5.0	18.4	0.26537	0.00161	665.19	0.26235	10.140	10.861	0.638
31/05/2016	S	14:30	1.4	20.4	0.39583	0.00155	604.04	0.39293	3.707	3.720	0.350
06/06/2016	S	15:30	2.2	23.0	0.50423	0.00147	534.33	0.50147	5.623	5.307	0.677
13/06/2016	S	15:30	2.0	20.6	0.66523	0.00154	598.11	0.66234	4.918	4.910	0.782
20/06/2016	S	15:30	2.9	20.6	0.63610	0.00154	599.96	0.63320	6.696	6.695	1.018
07/07/2016	S	17:00	4.1	20.1	0.44668	0.00155	611.97	0.44376	8.957	9.076	0.954
12/07/2016	S	17:30	2.6	20.8	0.46059	0.00153	591.90	0.45771	6.142	6.100	0.675
19/07/2016	S	17:30	1.9	20.4	0.46982	0.00155	605.54	0.46691	4.690	4.712	0.526
03/05/2016	CR	16:30	6.7	11.0	0.01316	0.00190	985.72	0.00958	10.152	14.135	0.023
10/05/2016	CR	15:30	3.2	16.3	0.00707	0.00168	740.05	0.00391	6.475	7.191	0.006
07/07/2016	CR	18:00	2.8	20.1	0.01001	0.00155	612.85	0.00709	6.429	6.497	0.011
04-13/08/2014□	S	6-21:00	2.1	23.7	0.58419	0.00145	517.76	0.58146	5.506	5.115	0.768
04-13/08/2014□	E1	6-21:00	2.1	23.7	0.36739	0.00145	517.76	0.58146	5.506	5.115	0.482
04-13/08/2014□	E13	6-21:00	2.1	23.7	0.29207	0.00145	517.76	0.58146	5.506	5.115	0.382

Site – sampling site (North-East basin – NE: 53°09'20.2"N 13°01'51.5"E / South basin – S: 53°08'35.8"N 13°01'43.2"E / Central Reservoir – CR: 53°08'35.8"N 13°01'41.1"E / Enclosure 1 – E1: 53°08'36.4"N 13°01'41.6"E / Enclosure 13 – E13: 53°08'36.5"N 13°01'42.1"E); *t* – time; U_{10} – wind speed recorded in 10 m height; T_{SW} – temperature of the surface water; $C_{CH4\,SW}$ – methane concentration in the surface water; *L* – methane solubility; *Sc* – Schmidt number; Δ_{CH4} – CH_4 gradient between surface water and air (= C_{water} – C_{air}; see Equation 6.2); *k* – wind dependent gas transfer constants; F_S – methane water-to-air flux; * assuming 1.88 ppm methane content in the atmosphere; □ corresponding parameters U_{10}, T_{SW} and $C_{CH4\,SW}$ were averaged for day times (06:00 – 21:00, local times) and given dates; n. a. – not available

Supplementary Notes

Supplementary Note 3.1: Molecular biological analyses to test for archaeal methanogenesis activity in Cyanobacteria cultures

Data analysis and illustration presented throughout this Supplementary Note 3.1 was done by the collaborators M. Bizic-Ionescu, D. Ionescu, A. M. Muro-Pastor and T. Urich.

Transcriptome experiment. Samples for transcriptome analyses were collected in triplicates at 5 time points during a 24 h experiment with *Dolichospermum sp.* PCC 7120 and *Microcystis aeruginosa* PCC 7806. For this experiment a non-axenic culture of *Dolichospermum sp.* PCC7120 was used. The cultures were divided into 16, 60 ml bottles. One of the bottles was connected to the MIMS as described above while the remaining fifteen were incubated under identical light and temperature conditions. The bottles were incubated for 24-36 h of acclimation before t_0 was collected on the day of the experiment. t_1 was sampled at 09:30, half an hour after the first light was turned on (60 µmol photons m^{-2} s^{-1}). t_2 was sampled at 12:30, half an hour after the third light was turned on (180 µmol photons m^{-2} s^{-1}). t_3 was sampled at 20:00, half an hour after all lights were turned off. t_4 was collected at 00:00. Collected samples were immediately filtered on polycarbonate filters (pore size 0.8 µm; Millipore) and frozen at -80 °C till further processing.

DNA and RNA extraction and sequencing. To evaluate the presence of methanogenic Archaea in non-axenic cultures DNA was extracted as described in Nercessian et al. (2005). The resulting DNA was sent for Illumina sequencing at MrDNA (Shallowater, TX, USA) on a Miseq platform (2x300 bp) using the Arch2A519F (CAG CMG CCG CGG TAA) and Arch1041R (GGC CAT GCA CCW CCT CTC) primers (Fischer et al. 2016). These primers with a barcode on the forward primer were used in a PCR applying the HotStarTaq Plus Master Mix Kit (Qiagen, USA) under the following conditions: 94 °C for 3 min, followed by 30 cycles of 94 °C for 30 s, 56 °C for 40 s and 72 °C for 1 min, after which a final elongation step at 72 °C for 5 min was performed. After amplification, PCR products were checked in 2 % agarose gel to determine the

success of amplification and the relative intensity of bands. The samples were pooled together in equal proportions based on their molecular weight and DNA concentrations. Pooled samples were purified using calibrated Ampure XP beads. Then the pooled and purified PCR product were used to prepare an Illumina DNA library. Sequencing was performed on a MiSeq following the manufacturer's guidelines. Archaeal community composition was analysed using the SILVA-NGS pipeline (Ionescu et al. 2012) (Supplementary Figure S3.3). After a standard PCR for the *mcrA* gene resulted in no visible products from any of the cultures, a qPCR assay was conducted as well.

For RNA extraction a similar protocol as above was used followed by DNA removal using the Turbo DNA Free kit (Cat: AM1907, Thermo Fisher Scientific). Ribosomal RNA was removed from the RNA samples using the Ribominus kit (Thermo Fisher Scientific) following the manufacturer's instructions. The mRNA enriched samples were sequenced at MrDNA (Shallowater, TX, USA). The RNA samples were resuspended in 25 ul of nuclease free water and further cleaned using RNeasy PowerClean Pro Cleanup Kit (Qiagen). The concentration of RNA was determined using the Qubit® RNA Assay Kit (Life Technologies). 60-500 ng of RNA was used to remove the DNA contamination using Baseline-ZERO™ DNase (Epicentre) following the manufacturer's instructions followed by purification using the RNA Clean & Concentrator columns (Zymo Research). DNA free RNA samples were used for library preparation using the KAPA mRNA HyperPrep Kits (Roche) by following the manufacturer's instructions. The concentration of double strand cDNA was evaluated using the Qubit dsDNA HS Assay Kit (Life Technologies). 25 ng DNA was used to prepare the libraries. The protocol starts with enzymatic fragmentation to produce dsDNA fragments followed by end repair and A-tailing to produce end-repaired, 5'-phosphorylated, 3'-dA-tailed dsDNA fragments. In the adapter ligation step, dsDNA adapters are ligated to 3'-dA-tailed molecules. The final step is library amplification, which employs high fidelity, low-bias PCR to amplify library fragments carrying appropriate adapter sequences on both ends. Following the library preparation, the final concentration of all the libraries was measured using the Qubit® dsDNA HS Assay Kit (Life Technologies), and the average library size was determined using the Agilent 2100 Bioanalyzer (Agilent Technologies). The libraries were then pooled in equimolar ratios of 2 nmol l^{-1}, and 8 pmol l^{-1} of the library pool was clustered using the cBot (Illumina) and sequenced paired end for 125 cycles using the HiSeq 2500 system (Illumina). The

resulting raw read data is deposited at the European Nucleotide Archive (ENA) under project number PRJEB32889.

Transcriptome analysis. The fifteen paired end libraries generated from each experiment were trimmed for quality and sequencing adapters using Trimommatic V 0.39 (Bolger et al. 2014). For purposes of annotation two strategies were used. For the first approach, all trimmed sequences from a single culture were co-assembled using Trinity V2.8.4 (Grabherr et al. 2011). The assembled transcripts were then annotated following the Trinotate pipeline (Bryant et al. 2017) replacing BLAST with Diamond V0.9.22 (Buchfink et al. 2015). For the second approach, the trimmed reads from each sample were mapped to the genes of either *Dolichospermum sp.* PCC 7120 (GCA_000009705.1) or *Microcystis aeruginosa* PCC 7806 (GCA_002095975.1). The full results of these experiments including differential expression will be eventually published separately.

Quantitative Real Time PCR assay. The abundance of methanogens was measured with quantitative PCR specific for the *mcrA* gene encoding the alpha subunit of methyl coenzyme M reductase, the key enzyme of archaeal methanogenesis. The primer pair mlas-mod for (GGY GGT GTM GGD TTC ACM CAR TA) / *mcrA*- rev (CGT TCA TBG CGT AGT TVG GRT AGT) (Steinberg and Regan 2009) was used. The assay was performed on a qTOWER 2.2 instrument (Analytic Jena, Germany). Assays were performed in 15 µl volume containing 7.5 µl of innuMIX qPCR MasterMix SyGreen (Analytic Jena), 0.75 µl of each primer (10 pmol/µl), 5 µl of ddH2O and 1 µl of template DNA. Assay conditions were 95°C initial denaturation 5 min, 35 cycles of denaturation (95 °C) 30 s, annealing (60 °C) 45 s and elongation (72 °C) 45 s, followed by melting curve analysis. Triplicate assays were performed for each sample, with template DNA concentrations of 10ng/µl. A parallel standard curve of *mcrA* genes was recorded. The standard curve DNA fragment consisted of the *mcrA* gene of a *Methanomassiliicoccus sp.* from cow rumen fluid cloned into the pGEM®-Teasy vector system (Promega, Mannheim, Germany), amplified with vector-specific primers sp6 and T7. The qPCR assay parameters were as follows: slope 3.55, efficiency 0.91, R2 > 0.99.

Supplementary Note 6.1: Re-analysis of Lake Hallwil surface mixed layer methane mass balance (June-August 2016)

Data analysis and illustration presented throughout this Supplementary Note 6.1 have been conducted by the collaborator D. Donis.

The Lake Hallwil methane mass balance (Donis et al. 2017) was re-analysed applying a bathymetry based on the Swiss topographic map of the lake, which was confirmed by a bathymetric survey (Bierlein et al. 2017). The analysis was performed reconsidering the key variables for the methane budget: (a) littoral methane flux contribution and (b) methane evasion to the atmosphere. The other budget components (methane oxidation, input from rivers and diffusion from the hypolimnion) play a minor role in this system and were applied as previously described (Donis et al. 2017):

Step 1: Re-calculation of Lake Hallwil bathymetry. The bathymetry of Lake Hallwil used in Donis et al. (2017) is the result of a seismic survey carried out in 2015 (Donis et al. 2017). These measurements lead to the estimation of the lake planar area and sediment area used for the methane mass balance of the surface mixed layer. When estimating these magnitudes based on a geometric extrapolation from the isolines of the topographic map of Lake Hallwil (https://www.swisstopo.admin.ch/en/home.html), the littoral area in Donis et al. (2017) was underestimated by a factor 7. According to the map-based calculations the surface lake area measures $9.9 * 10^6$ m^2 instead of $8.4 * 10^6$ m^2 as previously reported in Donis et al. (2017). The sediment area of the surface mixed layer (5 m deep) is $0.7 * 10^6$ m^2 instead of $0.1 * 10^6$ m^2 and consequently the surface mixed layer volume equals $48 * 10^6$ m^3 instead of $41 * 10^6$ m^3.

Step 2: Lake Hallwil littoral contribution to the surface mixed layer methane budget. As revealed from a survey of surface methane concentration carried out in September 2016, Lake Hallwil's littoral methane production is restricted to some areas of the lake sediments (Supplementary Figure S6.1).

Sediment methane diffusive fluxes were measured in one of the lake hotspots in September 2016 (S1 in Supplementary Figure S6 and Supplementary Figure 1 in Donis et al. 2017). The average diffusive flux value of 1.75 ± 0.2 (mean±SD) mmol m^{-2} d^{-1} was implemented in the surface mixed layer budget and assumed to be constant from June to September for the entire littoral sediment area. Similarly, a littoral methane ebullition rate of 1.2 ± 0.8 (mean±SD) mmol m^{-2} d^{-1}, as reported for the same site (S1) by Flury et

al. (2010), was applied to the entire sediment area assuming that bubbles contained 100 % methane that dissolved into the water column and homogeneously distributed in the surface mixed layer.

This conservative approach was adopted to compensate for the uncertainty intrinsic to a system-wide analysis based on discrete measurements. Applying the measured flux obtained from a hot spot to the entire littoral zone provides a conservative estimate of the littoral contribution to the methane concentration in the pelagic surface layer.

Step 3: Lake Hallwil – surface methane emission. Donis et al. (2017) determined the surface methane emission in Lake Hallwil in three ways: (a) in-situ measurements with floating chambers, (b) k_{600}-calculations based on own wind relationship ($k_{600} = 2 * U_{10}$), (c) k_{600}-calculations using wind relationships from MacIntyre et al. (2010) for heated water columns (positive buoyancy flux, $k_{600} = 1.74 * U_{10} - 0.15$). Three additional parametrisations were added: based on wind speed and lake size from Vachon and Prairie (2013) ($k_{600} = 2.51 + 1.48 * U_{10} + 0.39 * U_{10} * \log10[\text{lake Area}]$), and for cooling and mixing water column from MacIntyre et al. (2010) (negative buoyancy flux, $k_{600} = 2.04 * U_{10} + 2$, and all buoyancy fluxes combined, $k_{600} = 2.25 * U_{10} + 0.16$). Note, k600 is the standardized gas transfer constant for carbon dioxide at 20°C, and U_{10} refers to wind speed at 10 m height. The corresponding flux was solved by Fick's 1st Law with an average surface methane concentration of 0.3 μmol l^{-1} as reported in Donis et al. (2017). Results are summarised by Supplementary Table S6.1.

Step 4: Lake Hallwil surface mixed layer methane mass balance. Lake Hallwil methane mass balance for the surface mixed layer was recalculated (Eq. 3 in Donis et al. 2017) with the corrected: planar area (A_p), sediment area (A_s) and mixed layer volume (∀). In Supplementary Table S6.2, the lower end of the mass balance is represented by the most conservative approach, i.e. using chamber measurements for surface flux (April to August) and littoral sediment flux including methane ebullitive input. The upper end is represented by surface fluxes obtained by wind relationship from the study site and reasonably assuming ebullition as a negligible contribution to the pelagic surface methane concentrations.

With these inputs and assumptions, oxic methane production rates between 78±63 (lower) and 138±42 nmol l^{-1} d^{-1} (upper end) were obtained; this production rates

correspond to a minimum of 63 % to a maximum of 83 % contribution to total emissions to the atmosphere of Lake Hallwil.

Supplementary Note 6.2: Temperature-based basin scale vertical diffusivities (K_z) in the open lake and enclosures

Data analysis and illustration presented throughout this Supplementary Note 6.2 have been performed by collaborator G. Kirillin.

The open-water column temperature adjacent to the mesocosm enclosures was continuously recorded by an auto-profiler (30 min interval; between 0.5 and 20 m depth in 0.5 m steps) for the entire study period. The coefficient of the effective turbulent exchange K_{ZT} was estimated from temperature T within the water column of depth H = 20 m using the flux-gradient method (Powell and Jassby 1974, Dubovskaya et al. 2017):

$$K_{zT}(z) = -\frac{\int_H^z \frac{\partial T}{\partial t}}{\left(\frac{\partial T}{\partial z}\right)_z}\ ; [\mathrm{m^2\ s^{-1}}] \qquad \text{(S6.1)}$$

Additionally, vertical diffusivities in the enclosures and in the open lake were derived from measurements by a free-falling shear microstructure (MSS) profiler MSS-60 (ISW Wassermesstechnik) equipped with two airfoil velocity shear sensors for estimation of dissipation rate of the turbulence kinetic energy (TKE) ε, and a fast response thermistor for estimation of temperature and density fields (Prandke 2005). The instrument was allowed to fall through the water column at a speed of 0.5 m s^{-1} taking measurements at 1024 Hz. To compare the vertical diffusivities inside the mesocosm enclosures and the open lake, 12 profiles were taken in one mesocosm enclosures and another 12 profiles in the open lake on 3-4 Sep 2013 during daytime at an interval of 30 min to avoid previous mixing produced by the profiler itself. The TKE dissipation rate ε was then calculated from the measured velocity shearing $\frac{\partial U}{\partial z}$ as described by Hinze (1959):

$$\varepsilon = \frac{15}{2}\nu\left(\frac{\partial U}{\partial z}\right)^2\ ; [\mathrm{m^2\ s^{-3}}] \qquad \text{(S6.2)}$$

where $\nu \approx 10^{-6}$ $\mathrm{m^2\ s^{-1}}$ is the kinematic viscosity of water.

The mean profiles of the TKE dissipation rate were constructed by averaging over profile series in the open lake and in the enclosures and subsequent averaging over 0.25 m depth intervals. The values of ε were used for estimation of the coefficient of the vertical density exchange K_ρ using the procedure of Kirillin et al. (2012b):

$$K_\rho = \begin{cases} C_1 \varepsilon^{1/3} z^{4/3} & at \quad \varepsilon^{1/2} N^{-3/2} \geq \kappa z \quad \text{at the surface} \\ C_2 \varepsilon N^{-2} & at \quad \varepsilon^{1/2} N^{-3/2} < \kappa z \quad \text{in the thermocline} \end{cases} \tag{S6.3}$$

where N is the buoyancy frequency in the thermocline, $C_1 = 0.4^{4/3}$ and $C_2 = 0.2$ (Osborn 1980). Temperature and diffusivity profiles measured inside the mesocosms were very similar to the open-water profiles for the same period, except the upper several meters of the epilimnion, where wind mixing produced a stronger turbulence in the open lake (Supplementary Figure S6.2). This allowed to apply the same heat-budget estimates of open-water diffusivity values at depths >4 m to estimate the vertical flux in both open lake and mesocosm enclosures for the entire study period.

Glossary

Amictic	Permanently ice-covered lakes; never mix/circulate; inverse stratification, T ≤ 4°C (e.g. polar region)
Dimictic	Lakes with two overturns per year. Annual Cycle of spring heating leading to the stratified summer period and autumn cooling leading to inverse-stratified the winter period (e.g. cooler temperate region).
Epilimnion	Surface water with low density water at constant temperature, mixed by wind.
Eutrophic	Lakes with high primary production, high biomass, high nutrient content (e.g. total phosphorus > 24 µg l^{-1}).
Hypereutrophic	Lakes with extremely high primary production, extremely high biomass, extremely high nutrient content.
Hypolimnion	Deeper and colder water layer with high water density.
Mesotrophic	Lakes with intermediate primary production, intermediate biomass, intermediate nutrient content (e.g. total phosphorus 12-24 µg l^{-1}).
Metalimnion	Transition zone between epilimnion and hypolimnion, is defined as the water layer with the steepest temperature gradient. More commonly referred to as thermocline.
Monomictic	Cold-monomictic: Lakes never exceed 4°C; mostly ice-covered during winter stratification, annually one mixing event after melting (e.g. sub-polar regions); Warm-monomictic: Lakes never drop below 4°C; summer stratification, annually one mixing (e.g. sub-tropical regions).
Oligomictic	Irregularly/rarely mixed lakes; T > 4°C (e.g. tropical region)
Oligotrophic	Lakes with low primary production, low biomass, low nutrient content (e.g. total phosphorus < 12 µg l^{-1}).
Polymictic	Circulating lakes at ≤ 4°C (cold-polymictic) or at > 4°C (warm-polymictic) (e.g. shallow lakes).
Stratification	Process of layering waters of different densities. Typical layers (strata) are epilimnion, metalimnion and hypolimnion
Thermocline	Alternative terminology for metalimnion.

Bibliography

Aben, R. C. H., N., Barros, E., van Donk, T., Frenken, S., Hilt et al. 2017. Cross continental increase in methane ebullition under climate change. *Nat. Commun.* 8, 1682.

Abril, G., M.-V., Commarieu, A., Sottolichio, P., Bretel, and F., Guerin. 2009. Turbidity limits gas exchange in a macrotidal estuary. *Estuar. Coast Shelf Sci.* 83, 342-348.

Adams, D. D. 2005. Diffusive flux of greenhouse gases – methane and carbon dioxide – at the sediment water interface of some lakes and reservoirs of the world. In: Greenhouse gas emission – fluxes and processes. Hydroelectric reservoirs and natural environments, Tremply, A., L., Varfalvy, C., Roehm and M., Garneau (eds.), 129-153, Springer, Berlin Heidelberg.

Adrian, R., C. M., O'Reilly, H., Zagarese, S. B., Baines, D. O., Hessen et al. 2009. Lakes as sentinels of climate change. *Limnol. Oceanogr.* 54, 2283-2297.

Aekanishi, M. and M., Monsi. 1976. Factors that control the species composition of freshwater phytoplankton, with special attention to nutrient concentrations. *Int. Revue Ges. Hydrobiol.* 61, 439-470.

Aelion, M. C., P., Höhener, D., Hunkeler and R., Aravena (eds.). 2010. Environmental isotopes in biodegradation and bioremediation. CRC Press, Boca Raton, London, New York.

Allen, G. H. and T. M., Pavelsky. 2018. Global extent of rivers and streams. *Science* 361, 585-588.

Allen, M. R., K.P. Shine, J. S., Fuglestvedt, R. J., Millar, M., Cain et al. 2018. A solution to the misrepresentations of CO2-equivalent emissions of short-lived climate pollutants under ambitious mitigation. *npj Clim. Atmos. Sci.* 1, 16.

Althoff, F., K., Benzing, P., Comba, C., McRoberts, D. R., Boyd et al. 2014. Abiotic methanogenesis from organosulphur compounds under ambient conditions. *Nat. Commun.* 5, 4205.

Angel, R., D., Matthies and R., Conrad. 2011. Activation of methanogenesis in arid biological soil crusts despite the presence of oxygen. *PloS ONE* 6, e20453.

Angle, J. C., T. H., Morin, L. M., Solden, A. B., Narrowe, G. J., Smith et al. 2017. Methanogenesis in oxygenated soils is a substantial fraction of wetland methane emissions. *Nat. Commun.* 8, 1567.

Babenzien, H.-D. and C. Babenzien. 1985. Microbial activities at Lake Stechlin. In: Lake Stechlin: A temperate oligotrophic lake, S. J., Casper (ed.), 347-374, Junk Publishers, Dordrecht, Boston, Lancaster.

Bade, D. L. 2009. Gas exchange at the air-water interface. In: Encyclopedia of inland waters – Biogeochemistry of inland waters, Likens, G. E (ed.), 28-36, Academic Press,

Amsterdam, Boston, Heidelberg, London, New York, Oxford, Paris, San Diego, San Francisco, Singapore, Sydney, Tokyo.

Barker, J. F. and P., Fritz. 1981. Carbon isotope fractionation during microbial methane oxidation. *Nature* 293, 289-291.

Bastviken, D., J., Ejlertsson and L., Tranvik. 2002. Measurements of methane oxidation in lakes: A comparison of methods. *Environ. Sci. Technol.* 36, 3354-3361.

Bastviken, D., J., Cole, M., Pace and L., Tranvik. 2004. Methane emission from lakes: Dependence of lake characteristics, two regional assessments, and a global estimate. *Global Biogeochem. Cycles* 18, GB4009.

Bastviken, D., J. J., Cole, M. L., Pace and M. Van de Bogert. 2008. Fates of methane from different lake habitats: Connecting whole-lake budgets and CH4 emission. *J. Geophys. Res.-Biogeo.* 113, G02024.

Bastviken, D., A. L., Santoro, H., Marotta, L. Q., Pinho, D. F., Calheiros et al. 2010. Methane emission from Pantanal, South America, during the low water season: Toward more comprehensive sampling. *Environ. Sci. Technol.* 44, 5450-5455.

Bastviken, D., L. J., Tranvik, J. A., Downing, P. M., Crill and A., Enrich-Prast. 2011. Freshwater methane emission offset the continental carbon sink. *Science* 331, 50.

Beaulieu, J. J., T., DelSontro, J. A., Downing. 2019. Eutrophication will increase methane emissions from lakes and impoundments during the 21st century. *Nat. Commun.* 10, 1375.

Bedard, C. and R. Knowles. Some properties of methane oxidation in a thermally stratified lake. *Can. J. Fish. Aquat. Sci.* 54, 1639-1645.

Berg, A., P., Lindblad and B. H., Svensson. 2014. Cyanobacteria as a source of hydrogen for methane formation. *World J. Microbiol. Biotechnol.* 30, 539-545.

Beversdorf, L. J., A. E., White, K. M., Björkman, R. M., Letelier and D. M., Karl. 2010. Phosphonate metabolism by Trichodesmium IMS101 and the production of greenhouse gases. *Limnol. Oceanogr.* 55, 1768–1778.

Bierlein, K. A., M., Rezvani, S. A., Socolofsky, L. D., Bryant, A., Wüest et al. 2017. Increased sediment oxygen flux in lakes and reservoirs: The impact of hypolimnetic oxygenation. *Water Resour. Res.* 53, 4876-4890.

Bizic-Ionescu, M., R., Ammann and H.-P., Grossart. 2014. Massive regime shifts and high activity of heterotrophic Bacteria in an ice-covered lake. *PLoS ONE* 9, e113611.

Bizic-Ionescu, M., D., Ionescu, M., Günthel, K. W., Tang and H.-P., Grossart. 2018. Oxic methane cycling: New evidence for methane formation in oxic lake water. In: Biogenesis of hydrocarbons, Stams, A. J. M. and D., Sousa (eds.), 1-22, Springer, Cham.

Bizic-Ionescu, M., T., Klintzsch, D., Ionescu, M. Y., Hindiyeh, M., Günthel et al. 2019. Widespread methane formation by Cyanobacteria in aquatic and terrestrial ecosystems. Pre-print on bioRxiv, doi.org/10.1101/398958

Blair, C. C., S., D'Hondt, A. J., Spivack and R. H., Kingsley. 2007. Radiolytic hydrogen and microbial respiration in subsurface sediments. *Astrobiol.* 7, 951-970.

Blees, J., H., Niemann, M., Erne, J., Zopfi, C. J., Schubert et al. 2015. Spatial variation in surface water methane super-saturation and emission in Lake Lugano, southern Switzerland. *Aquat. Sci.* 77, 535-545.

Bogard, M. J., P. A., del Giorgio, L., Boutet, M. C. G., Chaves, Y. T., Prairie et al. 2014. Oxic water column methanogenesis as a major component of aquatic CH4 fluxes. *Nat. Commun.* 5, 5350.

Bolger, A. M., M., Lohse and B., Usadel. 2014. Trimmomatic: A flexible trimmer for Illumina sequence data. *Bioinformatics* 30, 2114-2120.

Borges, A. V., B., Delille, L.-S., Schiettecatte, F., Gazeau, G., Abril et al. 2004. Gas transfer velocities of CO2 in three European estuaries (Randers Fjord, Scheldt, and Thames). *Limnol. Oceanogr.* 49, 1630-1641.

Borges, A. V., G., Speeckaert, W., Champenois, M. I., Scranton and N., Gypens. 2018. Productivity and temperature as drivers of seasonal and spatial variations of dissolved methane in the southern bight of the North Sea. *Ecosystems* 21, 583-599.

Borrel, G., D., Jezequel, C., Biderre-Petit, N., Morel-Desrosiers, J.-P., Morel et al. 2011. Production and consumption of methane in freshwater lake ecosystems. *Res. Microbiol.* 162, 832-847.

Bosse, U., P., Frenzel and R., Conrad. 1993. Inhibition of methane oxidation by ammonium in the surface layer of a littoral sediment. *FEMS Microbiol. Ecol.* 13, 123-134.

Bothe, H., O., Schmitz, M., Geoffrey Yates and W. E., Newton. 2010. Nitrogen fixation and hydrogen metabolism in Cyanobacteria. *Microbiol. Mol. Biol. Rev.* 74, 529-551.

Boudreau, B. P. 1997. Diagenetic models and their implementation – Modelling transport and reactions in aquatic sediments. Springer, Berlin, Heidelberg, New York, Barcelona, Budapest, Hong Kong, London, Milan, Paris, Santa Clara, Singapore, Tokyo.

Bouffard, D. and A., Wüest. 2019. Convection in lakes. *Annu. Rev. Fluid Mech.* 51, 189-215.

Bousquet, P., P., Ciais, J. B., Miller, E. J., Dlugokencky, D. A., Hauglustaine et al. 2006. Contribution of anthropogenic and natural sources to atmospheric methane variability. *Nature* 443, 439–443.

Bowling, L. C., S., Blais and M., Sinotte. 2015. Heterogeneous spatial and temporal cyanobacterial distribution in Missisquoi Bay, Lake Champlain: An analysis of a 9 year data set. *J. Great Lakes Res.* 41, 164-179.

Broecker, W. S. and T.-H., Peng. 1974. Gas exchange rates between air and sea. *Tellus* 26, 21-35.

Brüggemann, N., R., Meier, D., Steigner, I., Zimmer, S., Louis et al. 2009. Nonmicrobial aerobic methane emission from popular shoot cultures under low-light conditions. *New Phytol.* 182, 912-918.

Brunskill, G. J. and D. W., Schindler. 1971. Geography and bathymetry of selected lake basins, experimental lakes area, Northwestern Ontario. *J. Fish. Res. Bd. Canada* 28, 139-155.

Bryant, D. M., K., Johnson, T., DiTommaso, T., Tickle, M. B., Couger et al. 2017. A tissue-mapped axolotl denovo transcriptome enables identification of limb regeneration factors. *Cell Rep.* 18, 762-776.

Buchfink, B., C., Xie and D. H., Huson. 2014. Fast and sensitive preotein alignment using DIAMOND. *Nat. Methods* 12, 59-60.

Buckel, W. and R. K., Thauer. 2013. Energy conservation via electron bifurcating ferredoxin reduction and proton/Na+ translocating ferredoxin oxidation. *Biochim. Biophys. Acta, Bioenerg.* 1872, 94-113

Buffett, B. and D., Archer. 2004. Global inventory of methane clathrate: Sensitivity to changes in the deep ocean. *Earth Planet. Sci. Lett.* 227, 185–199.

Burdige, D. F. 2011. Temperature dependence of organic matter remineralization in deeply-buried marine sediments. *Earth Planet. Sci. Lett.* 311, 396-410.

Bussmann, I. and E. Suess. 1998. Groundwater seapage in Eckernforde Bay (Western Baltic Sea): Effect on methane and salinity distribution of the water column. *Cont. Shelf Res.* 18, 1795-1806.

Cael, B. B., A. J., Heathcote and D. A., Seekell. 2017. The volume and mean depth of Earth's lakes. *Geophys. Res. Lett.* 44, 209–218.

Calleja, M. L., C. M., Duarte, Y. T., Prairie, S., Agusti and G. J., Herndl. 2009. Evidence for surface organic matter modulation of air-sea CO2 gas exchange. *Biogeosci.* 6, 1105-1114.

Callieri, C., S., Hernandez-Aviles, M. M., Salcher, D., Fontaneto and R., Bertoni. 2016. Distribution patterns and environmental correlates of Thaumarchaeota abundance in six deep subalpine lakes. *Aquat. Sci.* 78, 215-225.

Carini, S., N., Bano, G., LeCleir and S. B., Joye. 2005. Aerobic methane oxidation and methanotroph community composition during seasonal stratification in Mono Lake, California (USA). *Environ. Microbiol.* 7, 1127-1138.

Carini, P., A. E., White, E. O., Campbell and S. J., Giovannoni. 2014. Methane production by phosphate-starved SAR11 chemoheterotrophic marine bacteria. *Nat. Commun.* 5, 4346.

Carrick, H. J., F. J., Aldridge and C. L., Schleske. Wind influences phytoplankton biomass and composition in a shallow, productive lake. *Limnol. Oceanogr.* 38, 1179-1192.

Casper, S. J. 1985. Lake Stechlin. A temperate oligotrophic lake. Dr W. Junk Publisher, Dordrecht, Boston, Lancaster.

Casper, P. 1996. Methane production in littoral and profundal sediments of an oligotrophic and a eutrophic lake. *Arch. Hydrobiol. Spec. Issues Advanc. Limnol.* 48, 253-259.

Casper, P., A. L., Furtado and D. D. Adams. 2003. Biogeochemistry and diffuse fluxes of greenhouse gases (methane and carbon dioxide) and dinitrogen from the sediments of oligotrophic Lake Stechlin, northern Germany. *Arch. Hydrobiol. Spec. Issues Adv. Limnol.* 58, 53−71.

Casper, P., D.D., Adams, A. L. S., Furtado, O.-C., Chan, T., Gonsiorczyk et al. 2005. Greenhouse gas cycling in aquatic ecosystems – methane in temperate lakes across an environmental gradient in northeast Germany. *Verh. Internat. Verein. Limnol.* 29, 546-566.

Chan, A. S. K. and T. B., Parkin. 2000. Evaluation of potential inhibitors of methanogenesis and methane oxidation in a landfill cover soil. *Soil Biol. Biochem.* 32, 1581-1590.

Chen, Y.-B., J. P., Zehr and M., Mellon. 1996. Growth and nitrogen fixation of the diazotrophic filamentous nonheterocystous Cyanobacterium *Trichodesmium sp.* IMS 101 in defined media: evidence for a circadian rhythm. *J. Phycol.* 32, 916-923.

Chen, X., X., Wang, J., Feng., Y., Chen, Y., Fang et al. 2014. Structural insights into the catalytic mechanism of *Synechocystis* magnesium protoporphyrin IX O-methyltransferase (ChIM). *J. Biol. Chem.* 289, 25690-25698.

Cole, J. J. and N. F., Caraco. 1998. Atmospheric exchange of carbon dioxide in a low-wind oligotrophic lake measured by the addition of SF6. *Limnol. Oceanogr.* 43, 647-656.

Cole, J. J., Y. T., Prairie, N. F., Caraco, W. H., McDowell, L. J., Tranvik et al. 2007. Plumbing the global carbon cycle: Integrating inland waters into the terrestrial carbon budget. *Ecosystems* 10, 172–185.

Conrad, R. and W., Seiler. 1988. Methane and hydrogen in seawater (Atlantic Ocean). *Deep-Sea Res. Part A* 35, 1903-1917.

Conrad, R., O.-C., Chan, P., Claus and P. Casper. 2007. Characterization of methanogenic Archaea and stable isotope fractionation during methane production in the profundal sediment of an oligotrophic lake (Lake Stechlin, Germany). *Limnol. Oceanogr.* 52, 1393-1406.

Conrad, R. 2009. The global methane cycle: Recent advances in understanding the microbial processes involved. *Environ. Microbiol. Rep.* 1, 285–292.

Corbett, D. R., K., Dillon, W., Burnett and J., Chanton. 2000. Estimating the groundwater contribution into Florida Bay via natural tracers, 222Rn and CH4. *Limnol. Oceanogr.* 45, 1546-1557.

Cornish-Bowden, A. 2015. One hundred years of Michaelis-Menten kinetics. *Perspec. Sci.* 4, 3-9.

Crusius, J. and R., Wanninkhof. 2003. Gas transfer velocities measured at low wind speed over a lake. *Limnol. Oceanogr.* 48, 1010-1017.

Czernecki, B. and M., Ptak. 2018. The impact of global warming on lake surface water temperature in Poland – The application of empirical-statistical downscaling, 1971-2100. *J. Limnol.* 77, 330-348.

Damm, E., E., Helmke, S., Thoms, U., Schauer, E., Nöthig et al. 2010. Methane production in aerobic oligotrophic surface water in the central Arctic Ocean. *Biogeosci.* 7, 1099–1108.

Damm, E., B., Rudels, U., Schauer, S., Mau and G., Dieckmann. 2015. Methane excess in Arctic surface water- triggered by sea ice formation and melting. *Sci. Rep.* 5, 16179.

Dankwerts, P. V. 1951. Significance of liquid-film coefficients in gas absorption. *Ind. Eng. Chem.* 43, 1460-1467.

de Angelis, M. A. and C. Lee. 1994. Methane production during zooplankton grazing on marine phytoplankton. *Limnol. Oceanogr.* 39, 1298-1308.

Dean, J. F., J. J., Middelburg, T., Röckmann, R., Aerts, L. G., Blauw, et al. 2018. Methane feedbacks to the global climate system in a warmer world. *Rev. Geophysics.* 56, 207–250.

Dedysh, S. N., C., Knief and P.F., Dunfield. 2005. Methylocella species are facultatively methanotrophic. *J. Bacteriol.* 187, 4665-4670.

DelSontro, T., M. J., Kunz, T., Kempter, A., Wüest, B., Wehrli et al. 2011. Spatial heterogeneity of methane ebullition in a large tropical reservoir. *Environ. Sci. Technol.* 45, 9866-9873.

DelSontro, T., P. A., del Giorgio and Y. T., Prairie. 2018. No longer a paradox: The interaction between physical transport and biological processes explains the spatial distribution of surface water methane within and across lakes. *Ecosystems* 21, 1073-1087.

De Stasio Jr., B.T., D. K., Hill, J. M., Kleinhans, N. P., Nibbelink and J. J., Magnuson. 1996. Potential effects of global climate change on small north-temperate lakes: Physics, fish, and plankton. *Limnol. Oceanogr.* 41, 1136-1149.

Devlin, S. P., J., Saarenheimo, J., Syväranta and R. I., Jones. 2015. Top consumer abundance influences lake methane efflux. *Nat. Commun.* 6, 8787.

Donis, D., S., Flury, A., Stöckli, J. E., Spangenberg, D., Vachon et al. 2017. Full-scale evaluation of methane production under oxic conditions in a mesotrophic lake. *Nat. Commun.* 8, 1661.

Downing, J.A., Y. T., Prairie, J. J., Cole, C. M., Duarte, L. J., Tranvik et al. 2006. The global abundance and size distribution of lakes, ponds, and impoundments. *Limnol. Oceanogr.* 51, 2388-2397.

Dridi, B., M. L., Fardeau, B., Ollivier, D., Raoult and M., Drancourt. 2012. Methanomassiliicoccus luminyensis gen. nov., sp. nov.: A methanogenic archaeon isolated from human faeces. *Int. J. of Syst. Evol. Microbiol.* 62, 1902–1907.

Dubovskaya, O. P., A. P., Tolomeev, G., Kirillin, Z., Buseva, K. W., Tang et al. 2017. Effects of water column processes on the use of sediment traps to measure zooplankton non-predatory mortality: A mathematical and empirical assessment. *J. Plankton Res.* 40, 91-106.

Duc, N. T., P., Crill and D., Bastviken. 2010. Implication of temperature and sediment characteristics on methane formation and oxidation in lake sediments. *Biogeochemistry* 100, 185-196.

Duchemin, E., M., Lucotte and R., Canuel. 1999. Comparison of static chamber and thin boundary layer equation methods for measuring greenhouse gas emission from large water bodies. *Environ. Sci. Technol.* 33, 350-357.

Dueck, T. A., R., de Visser, H., Poorter, S., Persijn, A., Gorissen et al. 2007. No evidence for substantial aerobic methane emission by terrestrial plants: A 13C-labelling approach. *New Phytol.* 175, 29–35.

Dugan, H. A., R. I., Woolway, A. B., Santoso, J. R., Corman, A., Jaimes et al. 2015. Consequences of gas flux model choice on the interpretation of metabolic balance across 15 lakes. *Inland Waters* 6, 581-592.

Dyhrman, S. T., P. D., Chappell, S. T., Haley, J. W., Moffett, E. D., Orchard et al. 2006. Phosponate utilization by the globally important marine diazotroph *Trichodemsium*. *Nature* 439, 68-71.

Dyhrman, S. T., C. R., Benitez-Nelson, E. D., Orchard, S. T, Haley and P. J., Pellechia. A microbial source of phosphonates in oligotrophic marine systems. *Nat. Geosci.* 2, 696-699.

Dumestre, J. F., J., Guezennec, C., Galy-Lacaux, R., Delmas, S., Richard et al. 1999. Influence of light intensity on methanotrophic bacterial activity in Petit Reservoir, French Guiana. *Appl. Environ. Microbiol.* 65, 534-539.

Elser, J. J., H. J., Carney and C. R., Goldman. 1990. The zooplankton-phytoplankton interface in lakes of contrasting trophic status: an experimental comparison. In: Biomanipulation tool for water management, Gulati, R. D., E. H. R. R., Lammens, M. L., Meijer and E., van Donk (eds.), 69-82, Developments in Hydrobiologia, Springer, Dordrecht.

Engle, D. and J. M., Melack. 2000. Methane emission from an Amazon floodplain lake: Enhanced release during episodic mixing and during falling water. *Biogeochem.* 51, 71-90.

Erkkilä, K.-M., A., Ojala, D., Bastviken, T., Biermann, J. J., Heiskanen et al. 2018. Methane and carbon dioxide fluxes over a lake: Comparison between eddy covariance, floating chambers and boundary layer method. *Biogeosciences* 15, 429-445.

Eugster, W., G., Kling, T., Jonas, J. P., McFadden, A., Wüest et al. 2003. CO2 exchange between air and water in an Arctic Alaskan and midlatitude Swiss lake: Importance of convective mixing. *J. Geophys. Res.: Atmos.* 108, D12, 4362.

Eugster, W., T., DelSontro and S., Sobek. 2011. Eddy covariance flux measurements confirm extreme CH4 emissions from a Swiss hydropower reservoir and resolve their short-term variability. *Biogeosciences* 8, 2815-2831.

Evans, P. N., D. H., Parks, G. L., Chadwick, S. J., Robbins, V. J., Orphan et al. 2015. Methane metabolism in the archaeal phylum Bathyarchaeota revealed by genome-centric metagenomics. *Science* 350, 434–438.

Falcon, L. I., S., Magallon and A., Castillo. 2010. Dating the cyanobacterial ancestor of the chloroplast. *ISME J.* 4, 777-783.

Falkowski, P. G., T., Fenchel and E. F., Delong. 2008. The microbial engines that drive Earth's biogeochemical cycles. *Science* 320, 1034–1039.

Fernandez, J. E., F., Peeters and H. Hofmann. 2016. On the methane paradox: Transport from shallow water zones rather than in situ methanogenesis is the major source of CH4 in the open surface water of lakes. *J. Geophys. Res. Biogeosci.* 121, 2717-2726.

Ferry, J. G. 1999. Enzymology of one-carbon metabolism in methanogenic pathways. *FEMS Microbiol. Rev.* 23, 13–38.

Ferry, J. G. and K. A., Kastead. 2007. Methanogenesis. In: Archae: Molecular and cellular biology, Cavicchiolo, R. (ed.), 288-314, ASM Press, Washington, DC.

Fischer, M. A., S., Güllert, S. C., Neulinger, W. R., Streit and R. A., Schmitz. 2016. Evaluation of 16S rRNA gene primer pairs for monitoring microbial community structures showed high reproducibility within and low comparability between datasets generated with multiple archaeal and bacterial primer pairs. *Front. Microbiol.* 7, 1297.

Fixen, K. R., Y., Zheng, D. F., Harris, S., Shaw, Z.-Y., Yang et al. 2016. Light-driven carbon dioxide reduction to methane by nitrogenase in a photosynthetic bacterium. *Proc. Natl. Acad. Sci. U.S.A.* 113, 10163-10167.

Flaherty, B. L., F., Van Nieuwerburgh, S. R., Head and J. W., Golden. 2011. Directional RNA deep sequencing sheds new light on the transcriptional response of *Anabaena sp.* strain PCC 7120 to combined-nitrogen deprivation. *BMC Genomics* 12, 332.

Fletcher, S. E. and H., Schaefer. 2019. Rising methane: A new climate challenge. *Science* 364, 932-933.

Flury, S., D. F., McGinnis and M. O., Gessner. 2010. Methane emissions from a freshwater marsh in response to experimentally simulated global warming and nitrogen enrichment. *J. Geophys. Res.: Biogeosci.* 115, G01007.

Forster, G., R. C., Upstill-Goddard, N., Gist, C., Robinson, G., Uher et al. 2009. Nitrous oxide and methane in the Atlantic Ocean between 50°N and 52°S: Latitudinal distribution and sea-to-air flux. *Deap Sea Res. Pt. II* 56, 964-976.

Fuchs, A., E., Lyautey, B., Montuelle and P., Casper. 2016. Effect of increasing temperatures on methane concentration and methanogenesis during experimental incubation of sediments from oligotrophic and mesotrophic lakes. *J. Geophys. Res. Biogeosci.* 121, 1394-1406.

Frei, R., S.A., Crowe, M., Bau, A., Polat, D. A., Fowle et al. 2016. Oxidative elemental cycling under the low O2 Eoarchean atmosphere. *Sci. Rep.* 6, 21058.

Fricke, W. F., H., Seedorf, A., Henne, M., Kruer, H., Liesegang et al. 2006. The genome sequence of Methanosphaera stadtmanae reveals why this human intestinal archaeon is restricted to methanol and H_2 for methane formation and ATP synthesis. *J. Bacteriol.* 188, 642–658.

Frenzel, P., B., Thebrath and R., Conrad. 1990. Oxidation of methane in the oxic surface layer of a deep lake sediment (Lake Constance). *FEMS Microbiol. Lett.* 73, 149-158.

Frenzel, P. 2000. Plant-associated methane oxidation in rice fields and wetlands. In: B. Schink (ed.), Advances in Microbial Ecology, 85–114, Springer US, Boston, MA.

Frew, N. M., J. C., Goldman, M. R., Dennett and A. S., Johnson. 1990. Impact of phytoplankton-generated surfactants on air-sea gas exchange. *J. Geophys. Res.* 95, 3337-3352.

Frost, T. and R. C., Upstill-Goddard. 2002. Meteorological controls of gas exchange at a small English lake. *Limnol. Oceanogr*. 47, 1165-1174.

Garcia-Pichel, F., J, Belnap, S., Neuer and F., Schanz. 2003. Estimates of global cyanobacterial biomass and its distribution. *Algol. Stud.* 109, 213-227.

Gerhard, E., B. M., Butsch, I. W., Marison and U., von Stockar. 1993. Improved growth and methane production conditions for *Methanobacterium thermoautotrophicum*. *Appl. Microbiol. Biotechnol.* 40, 432-437.

Ghyczy, M., C., Torday and M., Boros. 2003. Simultaneous generation of methane, carbon dioxide, and carbon monoxide from choline and ascorbic acid: a defensive mechanism against reductive stress? *FASEB J.* 17, 1124-1126.

Ghyczy, M., C., Torday, J., Kaszaki, A., Szabo, M., Czobel et al. 2008. Hypoxia-induced generation of methane in mitochondria and eukaryotic cells: an alternative approach to methanogenesis. *Cell Physiol. Biochem.* 21, 251-258.

Giling, D. P., J. C., Nejstgaard, S. A., Berger, H.-P., Grossart, G., Kirillin et al. 2017. Thermocline deepening boosts ecosystem metabolism: Evidence from a large-scale lake enclosure experiment simulating a summer storm. *Global Change Biol.* 23, 1448-1462.

Glibert, P. M., R., Maranger, D. J., Sobota and L., Bouwman. 2014. The Haber Bosch-harmful algal bloom (HB-HAB) link. *Environ. Res. Lett.* 9, 105001.

Gomez-Garcia, M. R., M., Davison, M., Blain-Hartnung, A. R., Grossman and D., Bhaya. 2011. Alternative pathways for phosphonate metabolism in thermophilic Cyanobacteria from microbial mats. *ISME J.* 5, 141-149.

Grabherr, M. G., B. J., Haas, M., Yassour, J. Z., Levin, D. A., Thompson et al. 2011. Full-length transcriptome assembly from RNA-Seq data without a reference genome. *Nat. Biotech.* 29, 644-652.

Grilli, R., J., Triest, J., Chappellaz, M., Calzas, T., Desbois et al. 2018. Sub-Ocean: Subsea dissolved methane measurements using anembedded laser spectrometer technology. *Environ. Sci. Technol.* 52, 10543-10551.

Grossart, H.-P., K., Frindte, C., Dziallas, W., Eckert and K. W., Tang. 2011. Microbial methane production in oxygenated water column of an oligotrophic lake. *Proc. Natl. Acad. Sci. USA* 108, 19657-19661.

Gruca-Rokosz, R. and J. A., Tomaszek. 2015. Methane and carbon dioxide in the sediment of a eutrophic reservoir: Production pathways and diffusion fluxes at the sediment-water interphase. *Water Air Soil Pollut.* 226, 16.

Guerin, F., G., Abril, D., Serca, C., Delon, S., Richard et al. 2007. Gas transfer velocities of CO2 and CH4 in a tropical reservoir and its river downstream. *J. Mar. Syst.* 66, 161-172.

Guillard, R. R. L. and J. H., Ryther. 1962. Studies of marine planktonic Diatoms. *Canad. J. Microbiol.* 8, 229-239.

Guillard, R. R. L. and C. J., Lorenzen. 1972. Yellow-green Algae with chlorophyllide C12. *J. Phycol.* 8, 10-14.

Guillard, R. R. L. 1975. Culture of phytoplankton for feeding marine invertebrates. In: *Culture of marine invertebrate animals*, Smith W. L. and M. H., Chanley (eds.), 29-60, Springer, Boston, MA

Gumsley, A. P., K. R., Chamberlain, W., Bleeker, U., Söderlund, M. O., de Kock et al. 2017. Timing and tempo of the Great Oxidation Event. *Proc. Natl. Acad. Sci. U.S.A.* 114, 1811-1816.

Hakanson, L. and M. Jansson. 1983. Principles of lake sedimentology, 5-31, Springer, Berlin Heidelberg, New York, Tokyo.

Hanson, R. S. and T. E., Hanson. 1996. Methanotrophic Bacteria. *Microbiol. Rev.* 60, 439–471.

Hao, W. M, D., Scharffe, P. J., Crutzen and E., Sanhueza. 1988. Production of N2O, CH4, and CO2 from soils in the tropical savanna during the dry season. *J. Atmos. Chem.* 7, 93-105.

Haroon, M. F., S., Hu, Y., Shi, M., Imelfort, J., Keller et al. 2013. Anaerobic oxidation of methane coupled to nitrate reduction in a novel archaeal lineage. *Nature* 500, 567–570.

Hartmann, J. F., T., Gentz, A., Schiller, M., Greule, H.-P., Grossart et al. 2018. A fast and sensitive method for the continuous in situ determination of dissolved methane and its δ13C-isotope ratio in surface waters. *Limnol. Oceanogr.: Methods* 16, 273-285.

Haußecker, H., B., Jähne and S., Reinelt. 1995. Heat as proxy tracer for gas exchange measurements in the field: principles and technical realization. In: Air water gas transfer, Jähne, B., E. C., Monahan (eds.), 405-413, Aeon publisher, Hanau.

Haußecker, H., B., Jähne and S., Reinelt. 1995. Heat as proxy tracer for gas exchange measurements in the field: principles and technical realization. In: Air water gas transfer, Jähne, B., E. C., Monahan (eds.), 405-413, Aeon publisher, Hanau.

Hemschemeier, A. and T., Happe. 2011. Alternative photosynthetic electron transport pathways during anaerobiosis in the Green Alga *Chlamydomonas reinhardtii*. *Biochim. Biophys. Acta.* 1807, 919-926.

Hester, K. C. and P. G, Brewer. 2009. Clathrate hydrates in nature. *Annu. Rev. Mar. Sci.* 1, 303–327.

Hinze, J. O. 1959. Turbulence. McGraw Hill, New York.

Ho, D. T., L. F., Bliven, R., Wanninkhof and P., Schlosser. 1997. The effect of rain on air-water gas exchange. *Tellus B* 49, 149-158.

Ho, D. T., F., Veron, E., Harrison, L. F., Bliven, N., Scott and W. R., McGillis. 2007. The combined effect of rain and wind on air-water gas exchange: A feasibility study. *J. Marine Syst.* 66, 150-160.

Hofmann, H., L., Federwisch and F. Peeters. 2010. Wave-induced release of methane: Littoral zones as source of methane in lakes. *Limnol. Oceanogr.* 55, 1990-2000.

Holzbecher, E., G., Nützmann and G., Ginzel. 1999. Water and component mass balances in the catchment of Lake Stechlin. *Proc. Int. Assoc. Hydrol. Sci.* 258, 37-46.

Horita, J. and M. E., Berndt. 1999. Abiogenic methane formation and isotopic fractionation under hydrothermal conditions. *Science* 285, 1055-1057.

Hubalek, V., X., Wu, A., Eiler, M., Buck, C., Heim et al. 2016. Connectivity to the surface determines diversity patterns in subsurface aquifers of the Fennoscandian shield. *ISME J.* 10, 2447-2458.

Huisman, J., G. A., Codd, H. W., Paerl, B. W., Ibelings, J. M. H., Verspagen et al. 2018. Cyanobacterial blooms. *Nat. Rev. Microbiol.* 16, 471-483.

Huntsman, S. A. and R. T., Barber. 1977. Primary production off northwest Africa: the relationship to wind and nutrient conditions. *Deep Sea. Res.* 24, 25-33.

Imberger, J., 1985. Thermal characteristics of standing waters: An illustration of dynamic processes. *Hydrobiol.* 125, 7-29.

Ionescu, D., C., Siebert, L., Polerecky, Y. Y., Munwes, C., Lott et al. 2012. Microbial and chemical charcaterization of underwater fresh water springs in the Dead Sea. *PLOS One* 7, e38319.

IPCC, Intergovernmental Panel on Climate Change, Climate Change – The IPCC Scientific Assessment 1990. Report Prepared for IPCC by Working group 1. Houghton, J. T., G. J., Jenkins and J. J., Ephramus (eds.), Cambridge University Press, Cambridge, New York, Port Chester, Melbourne, Sydney.

IPCC, Summary for Policymakers. In: Climate Change 2007: The Physical Science Basis. Contribution of Working Group I to the Fourth Assessment Report of the Intergovernmental Panel on Climate Change [Solomon, S., D. Qin, M. Manning, Chen, M. Marquis, K.B. Averyt, M.Tignor and H.L. Miller (eds.)]. Cambridge University Press, Cambridge, United Kingdom and New York, NY, USA.

IPCC, Summary for Policymakers. In: Climate Change 2013: The Physical Science Basis. Contribution of Working Group I to the Fifth Assessment Report of the Intergovernmental Panel on Climate Change (IPCC) [Stocker, T.F., D. Qin, G.-K. Plattner, M. Tignor, S.K. Allen, J. Boschung, A. Nauels, Y. Xia, V. Bex and P.M. Midgley (eds.)]. Cambridge University Press, Cambridge, United Kingdom and New York, NY, USA, 1535 pp.

IPCC, 2014: Climate Change 2014: Synthesis Report. Contribution of Working Groups I, II and III to the Fifth Assessment Report of the Intergovernmental Panel on Climate Change [Core Writing Team, R.K. Pachauri and L.A. Meyer (eds.)]. IPCC, Geneva, Switzerland, 151 pp.

Jähne, B., K. O., Münnich, R., Bösinger, A., Dutzi, W., Huber et al. 1987. On the parameters influencing air-water gas exchange. *Limnol. Oceanogr.* 92, 1937-1949.

Jarrell, K. F. 1985. Extreme oxygen sensitivity in methanogenic Archaebacteria. *Bioscience* 35, 298-302.

Jayakumar, D. A., A. W. A., Naqvi, P. V., Narvekar and M. D., George. 2001. Methane in coastal and offshore waters of the Arabian Sea. *Mar. Chem.* 74, 1-13.

Johnsson, A., J., Aberg, A., Lindroth and M., Jansson. 2008. Gas transfer rate and CO2 flux between an unproductive lake and the atmosphere in northern Sweden. *J. Geophys. Res.: Biogeosci.* 113, G04006.

Joye, S. B., T. L., Connell, L. G., Miller, R. S., Oremland and R. S., Jellison. 1999. Oxidation of ammonia and methane in an alkaline, saline lake. *Limnol. Oceanogr.* 44, 178-188.

Ju, K. S., J., Gao, J. R., Doroghazi, K. K., Wang, C. J., Thibodeaux et al. 2015. Discovery of phosphonic acid natural products by mining the genomes of 10,000 actinomycetes. *Proc. Natl. Acad. Sci. U.S.A.* 112, 12175-12180.

Jugold, A., F., Althoff, M. Hurkuck, M., Greule, K., Lenhart et al. 2012. Non-microbial methane formation in oxic soils. *Biogeosciences* 9, 5291-5301.

Juutinen, S., M., Rantakari, P., Kortelainen, J. T., Huttunen, T. Larmola et al. 2009. Methane dynamics in different boreal lake types. Biogeosci. 6, 209-223.

Kammamm, C., S., Hepp, K., Lenhart and C., Müller. 2009. Stimulation of methane consumption by endogenous CH4 production in aerobic grassland soil. *Soil Biol. Biochem.* 41, 622-629.

Kana, T. M., J. C., Cornwell and L., Zhong. 2006 Determination of denitrification in the Chesapeake Bay from measurements of nitrogen accumulation in bottom water. *Estuaries and Coasts* 29, 222-231.

Karl, D. M. and B. D., Tilbrook. 1994. Production and transport of methane in oceanic particulate organic matter. *Nature* 368, 737-734.

Karl, D. M., L., Beversdorf, K. M., Björkman, M. J., Church, A., Martinez et al. 2008. Aerobic production of methane in the sea. *Nat. Geosci.* 1, 473–478.

Kasprzak, P., T., Shatwell, M. O., Gessner, T., Gonsiorczyk, G., Kirillin et al. 2017. Extreme weather event triggers cascade towards extreme turbidity in a clear-water lake. *Ecosystems* 20, 1407-1420.

Kendall, M. M. and D. R., Boone. 2006. The order methanosarcinales. In: Dworkin, M., S., Falkow, E., Rosenberg, K. H., Schleifer and E., Stackebrandt (eds.) The Prokaryotes. Springer, New York, NY.

Keppler, F., J. T. G., Hamilton, M., Braß and T., Röckmann. 2006. Methane emissions from terrestrial plants under aerobic conditions. *Nature* 439, 187–191.

Keppler, F., M., Boros, C., Frankenberg, J., Lelieveld, A., McLeod et al. 2009. Methane formation in aerobic environments. *Environ. Chem.* 6, 459–465.

Keppler, F., A., Schiller, R., Ehehalt, M., Greule, J., Hartmann et al. 2016. Stable isotope and high precision concentration measurements confirm that all humans produce and exhale methane. *J. Breath Res.* 10, 016003

Kirillin, G., C., Engelhardt and S., Golosov. 2008. A mesoscale vortex in a small stratified lake. *Environ. Fluid Mech.* 8, 349-366.

Kirillin, G., W., Phillip, C., Engelhardt and G., Nützmnn. 2012a. Net groundwater inflow in an enclosed lake: From synoptic variations to climate projections. *Hydrol. Process.* 27, 347-359.

Kirillin, G., H.-P., Grossart and K. W., Tang. 2012b. Modeling sinking rate of zooplankton carcasses: Effects of stratification and mixing. *Limnol. Oceanogr.* 57, 881-894.

Kirillin, G., T., Shatwell and P., Kasprzak. 2013. Consequences of thermal pollution from a nuclear plant on lake temperature and mixing regime. *J. Hydrol.* 496, 47-56.

Kirillin, G., M. S., Lorang, T. C., Lippmann, C. C., Gotschalk and S., Schimmelpfennig. 2015. Surface seiches in flathead lake. *Hydrol. Earth Syst. Sci.* 19, 2605-2615.

Kirschke, S., P., Bousquet, P., Ciais, M., Saunois, J. G., Canadell et al. 2013. Three decades of global methane sources and sinks. *Nat. Geosci.* 6, 813–823.

Klintzsch, T., G., Langer, G., Nehrke, A., Wieland, K., Lenhart et al. 2019. Methane production by three widespread marine phytoplankton species: release rates, precursor compounds, and relevance for the environment. *Biogeosci. Discuss.* preprint. https://doi.org/10.5194/bg-2019-245

Knapp, A. N. 2012. The sensitivity of marine N2 fixation to dissolved inorganic nitrogen. *Front. Microbiol.* 3, 374.

Koschel, R. and S. J., Casper. 1986. Die ökologische Bedeutung des Kernkraftwerkes I der DDR „Rheinsberg“ für Stechlin. In: Biologische Rundschau 24, 179-195, VEB Gustav Fischer Verlag Jena.

Kouzuma, A., S., Kato and K., Watanabe. 2015. Microbial intersecies interactions: Recent findings in syntrophic consortia. *Front. Microbiol.* 6, 477

Kremer, J. N., S. W., Nixon, B., Buckley and P., Roques. 2003a. Technical note: Conditions for using the floating chamber method to estimate air-water gas exchange. *Estuaries* 26, 985-990.

Kremer, J. N., A., Reischauer and C., D'Avanzo. 2003b. Estuary-specific variation in the air-water gas exchange coefficient for oxygen. *Estuaries* 26, 829-836.

Kröninger, L., J., Gottschling and U., Deppenmeier. 2017. Growth characteristics of *Methanomassiliicoccus luminyensis* and expression of methyltransferase encoding genes. *Archaea* 2017, 2756573.

Krüger, M., A., Meyerdierks, F. O., Glöckner, R., Amann, F., Widdel et al. 2003. A conspicuous nickel protein in microbial mats that oxidize methane anaerobically. *Nature* 426, 878–881.

Kundzewicz, Z.W., L.J. Mata, N.W. Arnell, P. Döll, P. Kabat, B. Jiménez, K.A. Miller, T. Oki, Z. Sen and I.A. Shiklomanov, 2007: Freshwater resources and their management. Climate Change 2007: Impacts, Adaptation and Vulnerability. Contribution of Working Group II to the Fourth Assessment Report of the Intergovernmental Panel on Climate Change, M.L. Parry, O.F. Canziani, J.P. Palutikof, P.J. van der Linden and C.E. Hanson, Eds., Cambridge University Press, Cambridge, UK, 173-210.

Kutovaya, O. A., R. M. L., McKay and G. S., Bullerjahn. 2013. Detection and expression of genes for phosphorus metabolism in picocyanobacterial from the Laurentian Great Lakes. *J. Great Lakes Res.* 39, 612-621.

Lambert, M. and J.-L., Frechette. 2005. Analytical techniques for measuring fluxes of CO2 and CH4 from hydroelectric reservoirs and natural water bodies. In: Greenhouse gas emission – fluxes and processes, Tremblay, A., L., Varfalvy, C., Roehm and M., Garneau (eds.), 37-60, Springer, Berlin Heidelberg.

Lamont, J. C. and D. S., Scott. 1970. An eddy cell model of mass transfer into the surface of a turbulent liquid. *AIChE J.* 16, 513-519.

Lana, A., T. G., Bell, R., Simo, S. M., Vallina, J., Ballabrera-Poy et al. 2011. An updated climatology of surface dimethylsulfide concentrations and emission fluxes in the global ocean. *Global Biogeochem. Cy.* 25, GB1004.

Lang, K., J., Schuldes, A., Klingl, A., Poehlein, R., Daniel et al. 2015. New mode of energy metabolism in the seventh order of methanogens as revealed by comparative genome analysis of "Candidatus Methanoplasma termitum". *Appl. Environ. Microbiol.* 81, 1338–1352.

Lange, P. K., R. J. W., Brewin, G., Dall'Olmo, G. A., Tarran, S., Sathyendranath et al. 2018. Scratching beneath the surface: A model to predict the vertical distribution of *Prochlorococcus* using remote sensing. *Remote Sens.* 10, 847.

Langer, G., K., Oetjen and T., Brenneis. 2013. Coccolithophores do not increase particulate carbon production under nutrient limitation: A case study using *Emiliania huxleyi* (PML B92/11). *J. Exp. Mar. Biol. Ecol.* 443, 155-161.

Lenhart, K., M., Bunge, S., Ratering, T. R., Neu, I., Schüttmann et al. 2012. Evidence for methane production by saprotrophic fungi. *Nat. Commun.* 3, 1046.

Lenhart, K., B., Weber, W., Elbert, J., Steinkamp, T., Clough et al. 2015. Nitrous oxide and methane emissions from cryptogamic covers. *Glob. Change Biol.* 21, 3889-3900.

Lenhart, K., T., Klintzsch, G., Langer, G., Nehrke, M., Bunge et al. 2016. Evidence for methane production by the marine algae *Emiliania huxleyi*. *Biogeosci.* 13, 3163-3174.

Lidstrom, M. E. and L., Somers. 1984. Seasonal study of methane oxidation in Lake Washington. *Appl. Environ. Microbiol.* 47, 1255-1260.

Lien, R.-C. and E. A., D'Asaro. 2002. The Kolmogorov constant for the Lagrangian velocity spectrum and structure function. *Phys. Fluids* 14, 4456.

Liikanen, A., J. T., Huttunen, K., Valli and P., Martikainen. 2002. Methane cycling in the sediment and water column of mid-boreal hyper-eutrophic Lake Kevätön, Finland. *Arch. Hydrobiol.* 154, 585-603.

Liikanen, A., J. T., Huttunen, T. Murtoniemi, H., Tanskanen, T., Väisänen et al. 2003. Spatial and seasonal variation in greenhouse gas and nutrient dynamcs and their interactions in the sediments of a boreal eutrophic lake. *Biogeochemistry* 65, 83-103.

Liu, J., H., Chen, Q., Zhu, Y., Shen, X., Wang et al. 2015. A novel pathway of direct methane production and emission by eukaryotes including plants, animals and fungi: An overview. *Atmos. Environ.* 115, 26–35.

Liu, L., J., Wilkinson, K., Koca, C., Buchmann and A. Lorke. 2016. The role of sediment structure in gas bubble storage and release. *J. Geophys. Res. Biogeosci.* 121, 1992-2005.

Liu, X., Y., Gao, Z., Zhang, J., Luo and S., Yan. 2017. Sediment-water methane flux in a eutrophic pond and primary influential factors at different time scales. *Water* 9, 601.

Livingstone, D. M. Impact of secular climate change on the thermal structure of a large temperate central European lake. *Clim. Change* 57, 205-225.

Lopez Bellido, J., T., Tulonen, P., Kankaala and A., Ojala. 2009. CO2 and CH4 fluxes during spring and autumn mixing periods in a boreal lake (Pääjärvi, southern Finland). *J. Geophys Res.* 114, G04007.

Lorke, A., P., Bodmer, C., Noss, Z., Alshboul, M., Koschorreck et al. 2015. Technical note: Drifting versus anchored flux chambers for measuring greenhouse gas emissions from running waters. *Biogeosciences* 12, 7013-7024.

Luo, C. and K. T., Konstantinidis. 2011. Phosphorus-related gene content is similar in Prochlorococcus populations from the North Pacific and North Atlantic Oceans. *Proc. Natl. Acad. Sci. U.S.A.* 108, E62-E63.

van der Maarel, M. J. E. C., W., Sprenger, R., Haanstra and L. J., Forney. 1999. Detection of methanogenetic Archaea in seawater particles and the digestive tract of a marine fish species. *FEMS Microbiol. Lett.* 173, 189-194.

MacIntyre, S., R., Wanninkhof and J., Chanton. 1995. Trace gas exchange across the air-water interface in freshwater and coastal marine environments. In: Biogenic trace gases: measuring emission from soil and water, Matson, P. A. and C., Harriss (eds.), 52-97, Wiley-Blackwell.

MacIntyre, S. 1998. Turbulent mixing and resource supply to phytoplankton. In: Physical processes in lakes and oceans, J., Imberger (ed.), 561-590, American Geophysical Union, Washington, DC.

MacIntyre, S. and M., Melack. 2009. Mixing Dynamics in Lakes across climate zones. In: Encyclopedia of Inland Waters, Likens., G. E. (ed.), 603-612, Elsevier, Amsterdam.

MacIntyre, S., J. P., Fram, P. J., Kushner, N. D., Bettez, W. J., O'Brien et al. 2009. Climate-related variations in mixing dynamics in an Alaskan artic lake. *Limnol. Oceanogr.* 54, 2401-2417.

MacIntyre, S., A., Jonsson, M., Jonsson, J., Aberg, D. E., Tunrey et al. 2010. Buoyancy flux, turbulence, and the gas transfer coefficient in a stratified lake. *Geophys. Res. Lett.* 37, L24604.

Maeck, A., T., DelSontro, D. F., McGinnis, H., Fischer, S., Flury et al. 2013. Sediment trapping by dams creates methane emission hot spots. *Environ. Sci. Technol.* 47, 8130-8137.

Maeck, A., H., Hofmann and A., Lorke. 2014. Pumping methane out of aquatic sediments – ebullition forcing mechanisms in an impounded river. *Biogeosciences* 11, 2925-2938.

Magen, C., L. L., Lapham, J. W., Pohlman, K., Marshall, S., Bosman et al. 2014. A simple headspace equilibration method for measuring dissolved methane. *Limnol. Oceanogr.* 12, 637-650.

Mahieu, K., A., De Visscher,P. A., Vanrolleghem and O., Van Cleemput. 2006. Carbon and hydrogen isotope fractionation by microbial methane oxidation: Improved determination. *Waste Manage.* 389-398.

Marino, R. and R. W., Howarth. 1993. Atmospheric oxygen exchange in the Hudson River: Dome measurements and comparison with other natural waters. *Estuaries* 16, 433-445.

Marotta, H., L., Pinho, C., Gudasz, D., Bastviken, L. J., Tranvik et al. 2014. Greenhouse gas production in low-latitude lake sediments responds strongly to warming. *Nat. Clim. Chang.* 4, 467-470.

Martinez-Cruz, K., A., Sepulveda-Jauregui, K., Walter Anthony and F., Thalasso. 2015. Geographic and seasonal variation of dissolved methane and aerobic methane oxidation in Alaskan lakes. *Biogeosciences* 12, 4595-4606.

Matthews, C. J. D., V. L., St. Louis and R. H., Hesslein. 2003. Comparison of three techniques to measure diffusive gas exchange from sheltered aquatic surfaces. *Environ. Sci. Technol.* 37, 772-780.

Mayhew, L. E., E. T., Ellison, T. M., McCollom, T. P., Trainor and A. S., Templeton. 2013. Hydrogen generation from low-temperature water-rock reactions. *Nat. Geosci.* 6, 478-484.

Mayumi, D., H., Mochimaru, H., Tamaki, K., Yamamoto, H., Yoshioka et al. 2016. Methane production from coal by a single methanogen. *Science*, 354, 222–225.

McAullife, C. K. 1971. Gas chromatographic determination of solutes by multiple phase equilibrium. *Chem. Technol.* 1, 46-51.

McCormick, M. J. and G. L., Fahnenstiel. 1999. Recent climatic trends in nearshore water temperatures in the St. Lawrence Great Lakes. *Limnol. Oceanogr.* 44, 530-540.

McFadden, G. I. and M., Melkonian. 1986. Use of Hepes buffer for microalgal culture media and fixation for electron microscopy. *Phylologia* 15, 551-557.

McGillis, W. R., J. B., Edson, C. J., Zappa, J. D., Ware, S. P., McKenna et al. 2004. Air-sea CO2 exchange in the equatorial Pacific. *J. Geophys. Res.: Oceans* 109, C08S02.

McGinnis, D. F., A., Lorke, A., Wüest, A., Stöckli and J. C., Little. Interaction between a bubble plume and the near field in a stratified lake. *Water Resour. Res.* 40, W10206.

McGinnis, D. F., J., Greinert, Y., Artemov, S. E., Beaubien and A., Wüest. 2006. Fate of rising bubbles in stratified waters: How much methane reaches the atmosphere? *J. Geophys. Res.-Oceans* 111, C09007.

McGinnis, D. F., G., Kirillin, K. W., Tang, S., Flury, P., Bodmer et al. 2015. Enhancing surface methane fluxes from an oligotrophic lake: Exploring the microbubble hypothesis. *Environ. Sci Technol.* 49, 873-880.

McKay, M. D., P. J., Neale, C. D., Arp, L. N., De Senerpont Domis, X., Fang et al. 2009. Modelling lakes and reservoirs in the climate system. *Limnol. Oceanogr*. 54, 2315-2329.

McKenna, S. P. and W. R., McGillis. 2004. The role of free-surface turbulence and surfactants in air-water gas transfer. *Int. J. Heat Mass Transf.* 47, 539-553.

McLeod, A. R., S. C., Fry, G. J., Loake, D. J., Messenger, D. S., Reay et al. 2008. Ultraviolet radiation drives methane emission from terrestrial plant pectins. *New Phytol.* 180, 124-132.

Messenger, D. J., A. R., McLeod and S. C., Fry. 2009. The role of ultraviolet radiation, photosensitizer, reactive oxygen species and ester groups in mechanisms of methane formation from pectin. *Plant Cell Environ.* 32, 1-9.

Metcalf, W. W., B. M., Griffin, R. M., Cicchillo, J., Gao, S. C., Janga et al. 2012. Synthesis of methylphosphonic acid by marine microbes: A source for methane in the aerobic ocean. *Science* 337, 1104-1107.

Meybeck, M. 1995. Global distribution of lakes. In: Physics and chemistry of lakes (Lerman, A., D., Imboden, J., Gat eds.), 1-32, Springer, Berlin Heidelberg 1995 (2nd edition).

Milberg, P., L., Törnqvist, L. M., Westerberg and D., Bastviken. 2017. Temporal variation in methane emission from emergent aquatic macrophytes in two boreonemoral lakes. *AoB Plants* 9, plx029.

Mitschke, J., A., Vioque, F., Haas, W. R., Hess and A. M., Muro-Pastor. 2011. Dynamics of transcriptional start site selection during nitrogen stress-induced cell differentiation in *Anabaena* sp. PCC7120. *Proc. Natl. Acad. Sci. U.S.A.* 108, 20130-20135.

Monks, P. S. 2003. Tropospheric photochemistry. In: Handbook of atmospheric sciences: Principles and applications, Hewitt, C. N. and A. V., Jackson (eds.), 156-187, Blackwell Publishing, Malden, Oxford, Victoria.

Moore, L. R., A., Coe, E. R., Zinser, M. A., Saito, M. B., Sullivan et al. 2007. Culturing the marine Cyanobacterium *Prochlorococcus*. *Limnol. Oceanogr.: Methods* 5, 353-362.

Moran, J. J., C. H., House, J. M., Vrentas and K. H., Freeman. 2008. Methyl sulfide production by a novel monoxide metabolism in Methanosarcina acetivorans. *Appl. Environ. Microbiol.* 74, 540-542.

Mountfort, D. O. and R. A., Asher. 1979. Effect of inorganic sulfide on the growth and metabolism of *Methanosarcina barkeri* strain DM. *Appl. Environ. Microbiol.* 37, 670-675.

Müller, B. L. D., Bryant, A., Matzinger and A., Wüest. 2012. Hypolimnetic oxygen depletion in eutrophic lakes. *Eniron. Sci. Technol.* 46, 9964-9971.

Murase, J. and A., Sugimoto. 2001. Spatial distribution of methane in the Lake Biwa sediments and its carbon isotopic composition. *Geochem. J.* 35, 257-263.

Murase, J. and A., Sugimoto. 2002. Seasonal and spatial variation of methane production in mesotrophic lake sediments (Lake Biwa, Japan). *Verh. Int. Verein. Limnol.* 28, 971-974.

Murase, J. and A., Sugimoto. 2005. Inhibitory effect of light on methane oxidation in the pelagic water column of a mesotrophic lake (Lake Biwa, Japan). *Limnol. Oceanogr.* 50, 1339-1343.

Murase, J., Y., Sakai, A., Kametani and A., Sugimoto. 2005. Dynamics of methane in mesotrophic Lake Biwa, Japan. *Ecol. Res.* 20, 377-385.

Myhre, G., D. Shindell, F.-M., Bréon, W., Collins, J., Fuglestvedt, et al. 2013. Anthropogenic and natural radiative forcing. In: Climate Change 2013: The Physical Science Basis. Contribution of Working Group I to the Fifth Assessment Report of the Intergovernmental Panel on Climate Change, 659–740, Cambridge University Press, Cambridge.

Natchimuthu, S., I., Sundgren, M., Galfalk, L., Klemedtsson, P., Crill et al. 2015. Spatio-temporal variability of lake CH4 fluxes and its influence on annual whole lake emission estimates. *Limnol. Oceanogr.* 61, S13-S26.

Nercessian, O., E., Noyes, M. G., Kalyuzhnaya, M. E., Lidstrom and L., Chistoserdova. 2005. Bacterial populations active in metabolism of C1 compounds in the sediment of Lake Washington, a freshwater lake. *Appl. Environ. Microbiol.* 71, 6885-6899.

Nisbet, R. E. R., R., Fisher, R. H., Nimmo, D. S., Bendall, P. M., Crill et al. 2009. Emission of methane from plants. *P. Roy. Soc. B-Biol. Sci.* 276, 1347–1354.

Nisbet, E. G., M. R., Manning, E. J., Dlugokencky, R. E., Fisher, D. Lowry et al. 2019. Very strong atmospheric methane growth in the 4 years 2014-2017: Implication for the Paris Agreement. *Global Biogeochem. Cy.* 33, 318-342.

NOAA/ESRL, Ed Dlugokencky, NOAA/ESRL (National Oceanic and Atmospheric Administration/Earth System Research Laboratory/Global Monitoring Division). Accessed on 23rd June 2019. (www.esrl.noaa.gov/)

Oremland, R. S. 1979. Methanogenic activity in plankton samples and fish intenstines: A mechanism for in situ methanogenesis in oceanic surface waters. *Limnol. Oceanogr.* 24, 1136-1141.

Osborn, T. R. 1980. Estimates of the local rate of vertical diffusion from dissipation measurements. *J. Phys. Oceanogr.* 10, 83-89.

Ostrovsky, I., D. F., McGinnis, L., Lapidus and W., Eckert. 2008.. Quantifying gas ebullition with echosounder: The role of methane transport by bubbles in a medium-sized lake. *Limnol. Oceanogr.: Methods* 6, 105-118.

Oswald, K., J., Milucka, A., Brand, S., Littmann, B., Wehrli et al. 2015. Light-dependent aerobic methane oxidation reduces methane emission from seasonally stratified lakes. *PLoS ONE* 10, e0132574.

Pace, N. R. 2009. Mapping the tree of life: Progress and prospects. Microbiol. Mol. Biol. Rev. 73, 565-576.

Paerl, H. W. and J., Huisman. 2009. Climate change: A catalyst for global expansion of harmful cyanobacterial blooms. *Environ. Microbio. Rep.* 1, 27-37.

Panganiban, A. T., T. E., Patt, W., Hart and R. S., Hanson. 1979. Oxidation of methane in the absence of oxygen in lake water samples. Appl. *Environ. Microbiol.* 37, 303–309.

Paterek, J. R. and P. H., Smith. 1988. Methanohalophilus mahii gen. nov., sp. nov., a methylotrophic halophilic methanogen. *Int. J. Syst. Bacteriol.* 38, 122-123.

Peeters, F., D., Straile, A., Lorke and D. M., Livingstone. 2007. Earlier onset of the spring phytoplankton bloom in lakes of the temperate zone in a warmer climate. *Glob. Chang. Biol.* 13, 1898-1909.

Peeters, F. and H., Hofmann. Length-scale dependence of horizontal dispersion in the surface water of lakes. *Limnol. Oceanogr.* 60, 1917-1934.

Peeters, F., J. E., Fernandez and H. Hofmann. 2019. Sediment fluxes rather than oxic methanogenesis explain diffusive CH4 emission from lakes and reservoirs. *Sci. Rep.* 9, 243.

Peters, V. and R., Conrad. 1995. Methanogenic and other strictly anaerobic Bacteria in desert soil and other oxic soils. *Appl. Environ. Microbiol.* 61, 1673-1676.

Pfreundt, U., M., Kopf, N., Belkin, I., Berman-Frank and W. R., Hess. The primary transcriptome of the marine diazotroph *Trichodesmium erythraeum* IMS101. *Sci. Rep.* 4, 6187.

Podgrajsek, E., E., Sahlee and A., Rutgersson. 2014. Diurnal cycle of lake methane flux. *J. Geophys. Res.: Biogeosci.* 119, 236-248.

Powell, R., 1972. Solubility of 16 gases in heptacosafluorotributylamine and carbon disulphide. *J. Chem. Eng. Data* 17, 302-304.

Powell, T. and A., Jassby. 1974. The estimation of vertical eddy diffusivities below the thermocline in lakes. *Water Resour. Res.* 10, 191-198.

Prandke, H. 2005. Microstructure sensors. In: Marine turbulence: theories, observations, and models, Baumert, H., J., Simpson and J., Sündermann (eds.), 101-109,

Cambridge University Press, Cambridge, New York, Port Melbourne, Madrid, Cape Town.

Puente-Sanchez, F., A., Arce-Rodriguez, M., Oggerin, M., Garcia-Villadangos, M., Moreno-Paz et a. 2018. Viable Cyanobacteria in the deep continental subsurface. *Proc. Natl. Acad. Sci. U.S.A.* 115, 10702-10707.

Qaderi, M. M. and D. M., Reid. 2009. Methane emission from six crop species exposed to three components of global climate change: Temperature, ultraviolet-B radiation and water stress. *Physiol. Plant.* 137, 139-147.

Ragsdale, S. W. and M., Kumar. 1996. Nickel-containing carbon monoxide dehydrogenase/acetyl-CoA Synthase. *Chem. Rev.* 96, 2515-2540.

Rao, H., L. C., Schmidt, J., Bonin and M., Robert. 2017. Visible-light-driven methane formation from CO2 with a molecular iron catalyst. *Nature*, 548, 74-77.

Ratkowsky, D. A., J., Olley, T. A., McMeekin and A. Ball. 1982. Relationship between temperature and growth rate of bacterial cultures. *J. Bacteriol.* 149, 1-5.

Raymond, P. A., C. J., Zappa, D., Butman, T. L., Bott, J., Potter, et al. 2012. Scaling the gas transfer velocity and hydraulic geometry in streams and small rivers. *Limnol Oceanogr. Fluids Environ.* 2, 41-53.

Razmi, A. M., D. A., Barry, U., Lemmin, F., Bonvin, T., Kohn et al. 2014. Direct effects of dominant winds on residence and travel times in the wide and open lacustrine embayment: Vidy Bay (Lake Geneva, Switzerland). *Aquat. Sci.* 76, 59-71.

Read, J. S., D. P., Hamilton, A. R., Desai, K. C., Rose, S. MacIntyre et al. 2012. Lake-size dependency of wind shear and convection as controls on gas exchange. *Geophys. Res. Lett.* 39, L09405.

Reeburgh, W. S. 1976. Methane consumption in Cariaco Trench waters and sediments. *Earth Planet. Sci. Lett.* 28, 337–344.

Reeburgh, W. S. 2007. Oceanic methane biogeochemistry. *Chem. Rev.* 107, 486-513.

Repeta, D. J., S., Ferron, O. A.., Sosa, C. G., Johnson, L. D., Repeta et al. 2016. Marine methane paradox explained by bacterial degradation of dissolved organic matter. *Nat. Geosci.* 9, 884–887.

Repo, E., T., Huttunen, A. V., Naumov, A. V., Chichulin, E. D., Lapshina et al. 2007. Release of CO2 and CH4 from small wetland lakes in western Siberia. *Tellus B: Chem. Phys. Meteorol.* 59, 788-796

Ribalet, F., J., Swalwell, S., Clayton, V., Jimenez, S., Sudek et al. 2015, Light-driven synchrony of Prochlorococcus growth and mortality in the subtropical Pacific gyre. *Proc. Natl. Acad. Sci. U.S.A.* 112, 8008-8012.

Rippka, R., J., Deruelles, J. B., Waterbury, M., Herdman and R. Y., Stanier. 1979. Generic assignments, strain histories and properties of pure cultures of Cyanobacteria. *Microbiol.* 111, 1-61.

Rotaru, A.-E., P. M,. Shrestha, F., Liu, B., Markovaite, S., Chen et al. 2014.Direct interspecies electron transfer between *Geobacter metallireducens* and *Methanosarcina barkeri Appl. Environ. Microbiol.* 80, 4599-4605.

Rudd, J. W. M., A., Furutani, R. J., Flett and R. D., Hamilton. 1976. Factors controlling methane oxidation in shield lakes: The role of nitrogen fixation and oxygen concentration. Limnol. Oceanogr. 21, 357-364.

Sabrekov, A. F., B. R. K., Runkle, M. V., Glagolev, I. E., Terentieva, V. M., Stepanenko et al. 2017. Variability in methane emission from West Siberia's shallow boreal lakes on a regional scale and its environmental controls. *Biogeosciences*, 14, 3715-3742.

Sanches, L. F., B., Guenet, C. C. Marinho, N., Barros and F. de Assis Esteves. (2019). Global regulation of methane emission from natural lakes. *Sci. Rep.* 9, 255.

Sasakawa, M., U., Tsunogai, S., Kameyama, F., Nakagawa, Y., Nojiri et al. 2008. Carbon isotope characterization for the origin of excess methane in subsurface seawater. *J. Geophts. Res.-Oceans* 113, C03012.

Saunois, M., P., Bousquet, B., Poulter, A., Peregon, P., Ciais et al. 2016a. The global methane budget 2000–2012. *Earth Syst. Sci. Data* 8, 697–751.

Saunois, M., R. B., Jackson, P., Bousquet, B., Poulter and J. G., Canadell. 2016b. The growing role of methane in anthropogenic climate change. *Environ. Res. Lett.* 11, 120207.

Savitzky, A. and M. J. E., Golay. 1964. Smoothing and differentiation of data by simplified least square procedures. *Anal. Chem.* 36, 1627-1639.

Schilder, J., D., Bastviken, M., van Hardenbroek, P., Kankaala, P., Rinta et al. 2013. Spatial heterogeneity and morphology affect diffusive greenhouse gas emission estimates of lakes. *Geophys. Res. Lett.* 40, 5752-5756.

Schindler, D. W. 1977. Evolution of phosphorus limitation in lakes. *Science* 195, 4275, 260-262.

Schladow, G. S., M., Lee, B. E., Hürzeler and P. B., Kelly. 2002. Oxygen transfer across the air-water interface by natural convection in lakes. *Limnol. Oceanogr.* 47, 1394-1404.

Schlüter, M. and T., Gentz. 2008. Application of Membrane Inlet Mass Spectrometry for online and in situ analysis of methane in aquatic environments. *J. Am. Soc. Mass Spectr.* 19, 1395-1402.

Schmale, O., J., Wage, V., Mohrholz, N., Wasmund, U., Gräwe et al. 2017. The contribution of zooplankton to methane supersaturation in the oxygenated upper waters of the central Baltic Sea. *Limnol. Oceanogr.* 63, 412–430.

Schönheit, P., H., Keweloh and R. K., Thauer. 1981. Factor F420 degradation in *Methanobacterium thermoautotrophicum* during exposure to oxygen. *FEMS Microbiol. Lett.* 12, 347-349.

Schubert, C. J., T., Diem and W., Eugster. 2012. Methane emission from a small wind shielded lake determined by eddy covariance, flux chambers, anchored funnels, and boundary model calculations: A comparison. *Environ. Sci. Technol.* 46, 4515-4522.

Scranton, M. I. and P. G., Brewer. 1977. Occurrence of methane in the near-surface waters of the western subtropical North-Atlantic. *Deep Sea Res.* 24, 127-138.

Scranton, M. I. and J. W. Farrington. 1977. Methane production in the waters off Walvis Bay. *J. Geophys. Res.* (1896-1977) 82, 4947-4953.

Semrau, J. D., A. A., DiSpirito and S., Yoon. 2010. Methanotrophs and copper. *FEMS Microbiol. Rev.* 34, 496-531.

Shannon, R. D., J. R., White, J. E., Lawson and B. S., Gilmour. 1996. Methane efflux from emergent vegetation in peatlands. *J. Ecol.* 84, 239-246.

Sherwood Lollar, B., S. K., Frape, S. M., Weise, P., Fritz, S. A., Macko et al. 1993. Abiogenic methanogenesis in crystalline rocks. *Geochim. Cosmochim. Acta* 57, 5087-5097.

Sieburth, J. M. 1987. Contrary habitats for redox-specific processes: Methanogenesis in oxic waters and oxidation in anoxic waters. In: Microbes in the sea, Sleigh, M. A. (ed.), Ellis Horwood, Chichester, UK.

Sleep, N. H., A., Meibom, T., Fridriksson, R. G., Coleman and D. K., Bird. 2004. H2-rich fluids from serpentinization: Geochemical and biotic implications. *Proc. Nat. Acad. Sci. U.S.A.* 101, 12818-12823.

Smith, V. H., G. D., Tilman and J. C., Nekola. 1999. Eutrophication: Impacts of excess nutrient inputs on freshwater, marine, and terrestrial ecosystems. *Environ. Pollut.* 100, 179-196.

Söhngen, N. L. 1906. Über Bakterien, welche Methan als Kohlenstoffnahrung und Energiequelle gebrauchen. *Z. Bakteriol. Parasitenk.* 15, 513–517.

Sosa, O. A., J. R., Casey and D. M., Karl. Methylphosphonate oxidation in Prochlorococcus supports phosphate acquisition, formate excretion, and carbon assimilation into purines. *Appl. Environ. Microbiol.* in press, doi:10.1128/AEM.00289-19

Sparrow, K. J., J. D. Kessler, J. R., Southon, F., Garcia-Tigeros, K. M., Schreiner et al. 2018. Limited contribution of ancient methane to surface waters of the U.S. Beaufort Sea shelf. *Sci. Adv.* 4, eaao4842.

Staehr, P. A., J. P. A., Christensen, R. D., Batt and J. S., Read. 2012. Ecosystem metabolism in a stratified lake. *Limnol. Oceanogr.* 57, 1317-1330.

Stal, L. J. and R., Moezelaar. 1997. Fermentation in Cyanobacteria. *FEMS Microbiol. Rev.* 21, 179-211.

Stawiarski, B., S., Otto, V., Thiel, U., Gräwe, N., Loick-Wilde et al. 2019. Controls on zooplankton methane production in the central Baltic Sea. *Biogeosci.* 16, 1-16.

Teikari, J. E., D. P., Fewer, R., Shrestha, S., Hou, N., Leikoski et al. 2018. Strains of the toxic bloom-forming Nodularia spumigena (Cyanobateria) can degrade methylphosphonate and release methane. *ISME* 12, 1619-1630.

Steinberg, L. M. and J. M., Regan. 2009. mcrA-targeted real-time quantitative PCR method to examine Methanogen communities. *Appl. Environ. Microbiol.* 75, 4435-4442.

Strapoc, D. 2017. Biogenic methane. In: Encyclopedia of geochemistry - Encyclopedia of earth sciences series, White, W. (ed.), Springer, Cham.

Takahashi, T., S. C., Sutherland, R., Wanninkhof, C., Sweeney, R.A., Feely et al. 2009. Climatological mean and decaldal change in surface ocean pCO2, and net sea-air CO2 flux over the global oceans. *Deep-Sea Res. Pt. II* 56, 554-577.

Takai, K., K., Nakamura, T., Toki, U., Tsunogai, M. Miyazaki et al. 2008. Cell proliferation and isotopically heavy CH4 production by a hyperthermophilic methanogen under high-pressure cultivation. *Proc. Nat. Acad. Sci. U.S.A.* 105, 10949-10954.

Tang, K. W., D. F., McGinnis, K., Frindte, V., Brüchert and H.-P., Grossart. 2014. Paradox reconsidered: Methane oversaturation in well-oxygenated lake waters. *Limnol. Oceanogr.* 59, 275-284.

Tang, K. W., D. F., McGinnis, D., Ionescu and H.-P., Grossart. 2016, Methane production in oxic lake waters potentially increases aquatic methane flux to air. *Environ. Sci. Technol. Lett.* 3, 6, 227-233.

Taniguchi, M. 2001. Evaluation of the groundwater capture zone for modelling of nutrient discharge. *Hydrol. Process.* 15, 1939-1949.

Thauer, R. K. 1998. Biochemistry of methanogenesis: a tribute to Marjory Stephenson: 1998 Marjory Stephenson Prize Lecture. *Microbiol.* 144, 2377-2406.

Thauer, R. K., A.-K., Kaster, H., Seedorf, W., Buckel and R., Hedderich. 2008. Methanogenic Archaea: Ecologically relevant differences in energy conservation. *Nat. Rev. Microbiol.* 6, 579–591.

Thomas, R., M., Meybeck and A., Beim. 1996. Lakes. In: Water quality assessments – a guide to use of biota, sediments and water in environmental monitoring, D. Chapman (ed.), 325-422, Cambridge University Press (2nd edition).

Thompson, A. M. 1992. The oxidizing capacity of the earth's atmosphere: Probable past and future changes. *Science* 256, 1157-1165.

Thornton, B. F., M., Wik and P. M., Crill. 2016. Double-counting challenges the accuracy of high-latitude methane inventories. *Geophys. Res. Lett.* 43, 12569-12577.

Tokoro, T., H., Kayanne, A., Watanabe, K., Nadaoka, H., Tamura et al. 2008. High gas-transfer velocity in coastal regions with high energy-dissipation rates. *J. Geophys. Res.: Oceans* 113, C11006.

Tuboly, E., A., Szabo, D., Garab, G., Bartha, A., Janovszky et al. 2013. Methane biogenesis during sodium azide-induced chemical hypoxia in rats. *Am. J. Physiol-Cell Physiol.* 304, C207-C214.

Utsumi, M., Y., Nojiri, T., Nakamua, N., Takeshi, A., Otsuki et al. 2003. Oxidation of dissolved methane in a eutrophic, shallow lake: Lake Kasumigaura, Japan. *Limnol. Oceanogr.* 43, 471-480.

Vachon, D., Y. T., Prarie and J. J., Cole. 2010. The relationship between near-surface turbulence and gas transfer velocity in freshwater systems and its implications for floating chamber measurements of gas exchange. *Limnol. Oceanogr.* 55, 1723-1732.

Vachon, D. and Y., Prairie. 2013. The ecosystem size and shape dependence of gas transfer velocity versus wind speed relationships in lakes. *Can. J. Fish. Aquat. Sci.* 70, 1757-1764.

Vagle, S., J., Hume, F., McLaughlin, E., MacIsaac and K., Shortreed. 2010. A methane bubble curtain in meromictic Sakinaw Lake, British Columbia. *Limnol. Oceanogr.* 55, 1313-1326.

Vanwonterghem, I., P. N., Evans, D. H., Parks, P. D., Jensen, B. J., Woodcroft et al. 2016. Methylotrophic methanogenesis discovered in the archaeal phylum Verstraetearchaeota. *Nat. Microbiol.* 1, 16170.

Visser, P. M., J. M. H., Verspagen, G., Sandrini, L. J., Stal, H. C. P., Matthijs, et al. 2016. How rising CO2 and global warming may stimulate harmful cyanobacterial blooms. *Harmful Algae* 54, 145-159.

Volta, D. A. 1777. Sull' Aria Inflammabile Native Delle Paludi. In: Milano M. DCC. LXXVII. Nella Stamperia Di Guiseppe Marelli. Con licenza de' Superiori. Attilio Sampietro Editore Menaggio.

Wang, Z.-P., S. X., Chang, H., Chen and X.-G. Han. 2013. Widespread non-microbial methane production by organic compounds and the impact of environmental stresses. *Earth-Sci. Rev.* 127, 193-202.

Wang, J., C., Liu, X., Gong, Y., Liu and C., Chen. 2016. Trimethylamine stimulated and dissolved organic matter inhibited methane production in sediment from the Poyang Lake, China. *Environ. Technol.* 37, 2545-2554.

Wang, Q., J. E., Dore and T. R., McDermott. 2017. Methylphosphonate metabolism by Pseudomonas sp. populations contributes to the methane oversaturation paradox in an oxic freshwater lake. *Environ. Microbiol.* 19, 2366–2378.

Wanninkhof, R., J. R., Ledwell, W. S., Broecker and M., Hamilton. 1987. Gas exchange on Mono Lake and Crowley Lake, California. *J. Geophys. Res.: Oceans* 92, 14567-14580.

Wanninkhof, R. 1992. Relationship between wind speed and gas exchange over the ocean. *J. Geophys. Res.: Oceans* 97, 7373-7382.

Wanninkhof, R. 2014. Relationship between wind speed and gas exchange over the ocean revisited. *Limnol. Oceanogr.: Methods* 12, 351-362.

Watanabe, S., N., Higashitani, N., Tsurushima and S., Tsunogai. 1995. Methane in the western North Pacific. *J. Oceanogr.* 51, 39-60.

Weiss, R. F. 1974. Carbon dioxide in water and seawater: The solubility of a non-ideal gas. *Mar. Chem.* 2, 203—215.

Whiteman, W. B., T. L., Bowen and D. R., Boone. 2014. The methanogenic Bacteria. In: The Prokaryotes, E., Rosenberg, E. F., DeLong, S., Lory, E., Stackebrandt and F., Thompson (eds.), 123-163, Springer, Berlin, Heidelberg.

Whiticar, M., E., Faber and M., Schoell. 1986. Biogenic methane formation in marine and freshwater environments: CO2 reduction vs. acetate fermentation—Isotope evidence. *Geochim. Cosmochim. Acta* 50, 693–709.

Whiticar, M. J. 1999. Carbon and hydrogen isotope systematics of bacterial formation and oxidation of methane. *Chem. Geol.* 161, 291-314.

Wiesenburg, D. A. and N. L., Guinasso Jr. 1979. Equilibrium solubilities of methane, carbon monoxide, and hydrogen in water and sea water. *J. Chem. Eng. Data* 24, 356-360.

Wik, M., B. F., Thornton, D., Bastviken, J., Uhlbäck and P. M., Crill. 2016a. Biased sampling of methane release from northern lakes: A problem for extrapolation. *Geophys. Res. Lett.* 43, 1256-1262.

Wik, M., R. K., Varner, K. W., Anthony, S., MacIntyre and D., Bastviken. Climate-sensitive northern lakes and ponds are critical components of methane release. *Nat. Geosci*. 9, 99-105.

Wiles, P. J., T. P., Rippeth, J. H., Simpson and P. J., Hendricks. 2006. A novel technique for measuring the rate of turbulent dissipation in the marine environment. *Geophys. Res. Lett.* 33, L21608.

Wilke, C. R. and P., Chang. 1955. Correlation of diffusion coefficients in dilute solutions. *AIChE J.* 1, 264-270.

Wilkerson, F. P., A. M., Lassiter, R. C., Dugdale, A., Marchi and V. E., Hogue. 2006. The phytoplankton bloom response to wind events and upwelled nutrients during the CoOP West study. *Deep-Sea Res. PT II* 53, 3023-3048.

Wilkinson, G. M., J. J., Cole, M. L., Pace, R. A., Johnson and M. J., Kleinhans. 2015. Physical and biological contributions to metalimnic oxygen maxima in lakes. *Limnol. Oceanogr.* 60, 242-251

Wishkerman, A., S., Greiner, M., Ghyczy, M., Boros, T., Rausch et al. 2010. Enhanced formation of methane in plant cell cultures by inhibition of cytochrome c oxidase. *Plant Cell Environ.* 34, 457-464.

Wood, A. M., R. C., Everroad and L. A., Wingard. 2005. Measuring growth rates in microalgal cultures. In: Algal Culturing Techniques, R. A. Andersen (ed.), 269-285, Elsevier Academic Press, Amsterdam, Boston, Heidelberg, Lodon, New York, Oxford, Paris, San Diego, San Francisco, Singapore, Sydney, Tokyo.

Xiao, Q., M., Zhang, Z., Hu, Y., Gao, C., Hu et al. 2017. Spatial variations of methane emission in a large shallow eutrophic lake in subtropical climate. *J. Geophys. Res.: Biogeosi.* 122, 1597-1614.

Yamamoto, S., J. B., Alcauskas and T. E., Crozier. 1976. Solubility of methane in distilled water and seawater. *J. Chem. Eng. Data* 21, 78-80.

Yao, M., C., Henny, C. and J. A. Maresca. 2016. Freshwater Bacteria release methane as a by-product of phosphorus acquisition. *J. Appl. Environ. Microbiol.* 82, 6994–7003.

Young, I. R., S., Zieger and A. V., Babanin. 2011. Global trends in wind speed and wave height. *Science* 332, 451-455.

Yu, X., J. R., Doroghazi, J. K., Zhang, B., Circello, B. M., Griffin et al. 2013. Diversity and abundance of phosphonate biosynthetic genes in nature. *Proc. Natl. Acad. Sci. U.S.A.* 110, 20759-20764.

Zappa, C. J., W. E., Asher, A. T., Jessup, J., Klinke and S. R., Long. 2004. Microbreaking and the enhancement of air-water transfer velocity. *J. Geophys. Res.-Oceans* 109, C08S16.

Zappa, C. J., W. R., McGillis, P. A., Raymond, J. B., Edson, E. J., Hintsa et al. 2007. Environmental turbulent mixing controls on air-water gas exchange in marine and aquatic systems. *Geophys. Res. Lett.* 34, L10601.

Zhang, X., X., Li, D., Zhang, N. Q., Su, W., Yang et al. 2017. Product selectivity in plasmonic photocatalysis for carbon dioxide hydrogenation. *Nat. Commun.* 8, 14542.

Zheng, Y., D. F., Harris, Z., Yu, Y., Fu, S., Poudel et al. 2018. A pathway for biological methane production using bacterial iron-only nitrogenase. *Nat. Microbiol.* 3, 281-286.

Zhu, C. J. and Y. K., Lee. 1997. Determination of biomass dry weight of marine microalgae. *J. Appl. Phycol.* 9, 189-194.